SIMULTANEOUS TWO-PHOTON ABSORPTION OF TETRAPYRROLIC MOLECULES: FROM FEMTOSECOND COHERENCE EXPERIMENTS TO PHOTODYNAMIC THERAPY

by

Aliaksandr Karotki

A dissertation submitted in partial fulfillment
of the requirements for the degree

of

Doctor of Philosophy

in

Physics

MONTANA STATE UNIVERSITY
Bozeman, Montana

December 2003

©COPYRIGHT

by

Aliaksandr Karotki

2003

All Rights Reserved

APPROVAL

of a dissertation submitted by

Aliaksandr Karotki

This dissertation has been read by each member of the dissertation committee and has been found to be satisfactory regarding content, English usage, format, citations, bibliographic style, and consistency, and is ready for submission to the College of Graduate Studies.

Aleksander Rebane

Approved for the Department of Physics

William A. Hiscock

Approved for the College of Graduate Studies

Bruce R. McLeod

STATEMENT OF PERMISSION TO USE

In presenting this dissertation in partial fulfillment of the requirements for a doctoral degree at Montana State University, I agree that the Library shall make it available to borrowers under rules of the Library. I further agree that copying of this dissertation is allowable only for scholarly purposes, consistent with "fair use" as described in the U.S. Copyright Law. Requests for extensive copying or reproduction of this dissertation should be referred to Bell & Howell Information and Learning, 300 North Zeeb Road, Ann Arbor, Michigan 48106, to whom I have granted "the exclusive right to reproduce and distribute my dissertation in and from microform along with the non-exclusive right to reproduce and distribute my abstract in any format in whole or in part."

ACKNOWLEDGEMENTS

This thesis is the result of four years of work whereby I have been accompanied and supported by many people. It is a pleasant aspect that I have now the opportunity to express my gratitude to all of them.

First, let me thank my advisor, Prof. Aleksander Rebane, for giving me an opportunity to be a part of this challenging research project. His advices and constant help kept me moving forward. Aleks's overall enthusiasm and integral view on research and his mission for providing 'only high-quality work and not less', have made a deep impression on me. I owe him lots of gratitude for having shown me this way of research.

I would like to thank Dr. Mikhail Drobizhev, the Research Assistant Professor in our group, who kept an eye on the progress of my work, participated in many of the experiments described here, and always was available when I needed an advice. Mikhail's ability to come up with theoretical explanation for about anything that we encountered in our experiments proved to be crucially important. Without his encouragement, instruction, and leadership this thesis would not exist.

My thanks are also to Dr. Mikalai Kruk. He was my scientific adviser back in Belarus when I was an undergraduate student and as such he started my career in science. During his visits to Dr. A. Rebane lab, Mikalai participated in many experiments described in the thesis.

I also would like to thank many people from different chemistry departments around the world, who contributed to this work by synthesizing molecules with unique

properties that we investigated. My special thanks are to Prof. Charles W. Spangler, Dr. Fanquing Meng, and Dr. Erik Nickel from Department of Chemistry and Biochemistry, Montana State University, Bozeman, USA, Prof. Harry L. Anderson and Dr. Peter N. Taylor from Chemistry Department, University of Oxford, Oxford UK, Dr. Nugzar Mamardashvili from Institute of Solution Chemistry, Ivanovo, Russia.

My thanks are also to Prof. Rufus Cone for his kind loan of IR-detector whenever we needed it. Without this detector, the Chapter 5 of this thesis would never be written.

Finally, the person that I am grateful the most is my wife Yuliya Dzenis. She participated in many experiments described here and provided support for simulations and quantum-chemical calculations with Hyperchem. But most of all I am grateful to her for her love and patience that allowed me to finish this work.

TABLE OF CONTENTS

TABLE OF CONTENTS - CONTINUED

LIST OF TABLES

LIST OF FIGURES

LIST OF FIGURES - CONTINUED

LIST OF FIGURES - CONTINUED

LIST OF FIGURES - CONTINUED

ABSTRACT

Simultaneous two-photon absorption (TPA) in tetrapyrrolic molecules is studied and its applications to two-photon coherence gratings and singlet oxygen generation for photodynamic therapy are demonstrated in this thesis.

First ever comprehensive study of TPA properties of tetrapyrrolic molecules is conducted in this work. Two-photon transitions in two key spectral regions, red to green and blue to near-UV (transition wavelengths) are investigated. Physical mechanisms leading to enhancement of TPA cross section in tetrapyrroles are elucidated. Porphyrin molecules with greatly enhanced two-photon cross sections are obtained.

Spectral coherence interference gratings are created by means of two-photon excitation with pairs of phase-locked femtosecond pulses in tetrapyrrolic molecules. First, gratings are detected by means of persistent spectral hole burning, which constitutes the first ever demonstration of spectral hole burning by simultaneous absorption of two photons. Next, the gratings are detected in fluorescence spectrum, which we use to study zero-phonon lines and phonon sidebands in two-photon transitions.

Application of tetrapyrrolic molecules to two-photon photosensitization of singlet molecular oxygen is investigated. First, TPA properties of some known one-photon photosensitizers are investigated. Then, a new class of TPA based photosensitizers with greatly enhanced two-photon cross sections is developed. The generation of singlet molecular oxygen upon two-photon excitation of the new photosensitizers demonstrated for the first time, which opens up new perspectives for two-photon photodynamic therapy.

CHAPTER 1

INTRODUCTION

Introduction to Research Topic

First observations of two-photon absorption (TPA) [1], second harmonic generation [2], stimulated Raman scattering [3], and other similar phenomena in the early 1960's marked the beginning of nonlinear optics. The effect of TPA immediately established itself as a particularly useful spectroscopic technique and, eventually, became a unique source of information about atomic and molecular structure [4-6]. In the years to follow, several practical applications of TPA were put forward, such as ultrashort pulse characterization [7-19], frequency upconversion lasing [20-22], two-photon excitation microscopy [23-29], three-dimensional (3D) ultrahigh density optical data storage [30-42], 3D microfabrication [43-52], optical power limiting [53-56], and photodynamic therapy (PDT) [57-62].

Today, some 40 years later, two-photon spectroscopy of organic molecules received a new impact because of two main factors. First, development of mode-locked ultrafast lasers in the 1990-s provided a source of extremely high peak intensity light pulses that facilitate instantaneous two-photon processes. Second, there appeared an increasing demand for efficient two-photon absorbers, especially chromophores that are compatible with new technological and biological applications.

An advantage of TPA as a spectroscopic tool arises from the different from one-photon absorption (OPA) parity selection rules in centrosymmetrical molecules. While one-photon transitions are allowed only between the states of different parity, i.e.

ungerade ↔ *gerade*, two-photon transitions are allowed between the states of the same parity, i.e. *gerade* ↔ *gerade* and *ungerade* ↔ *ungerade* (see Appendix A for details). Since the ground level is usually of *gerade* parity, TPA facilitates investigation of excited *gerade* parity levels that are usually very difficult to access for ordinary linear absorption spectroscopy. As a result, TPA spectroscopy greatly increases our understanding of molecular properties.

While one- and two-photon electronic transitions in the gas phase are well resolved and either allowed or forbidden according to parity selection rules, the nature of electronic transitions in solids is often masked by large inhomogeneous broadening and electron-phonon coupling. The absorption spectrum of a single molecule in a solid at low temperature consists of a spectrally narrow pure electronic transition (zero-phonon line (ZPL)) and, accompanying it, a much broader phonon wing (PW) emerging because of interaction of the molecule with phonon modes. The spectral width of the ZPL in organic molecules is of the order of 10 MHz – 1 GHz, while the overall inhomogeneous width can be 10^4 times larger. The ZPL is a remarkable feature of low temperature absorption spectrum. At room temperature interaction with phonons is so strong that only the PW is observable.

Persistent spectral hole burning (SHB) is a process whereby normally smooth inhomogeneously broadened absorption bands in solids at low temperature can be spectrally modified for time periods longer than the lifetime of any excited state [63-69]. It is based on high spectral resolution provided by the ZPL. The SHB allows for high-resolution spectral measurements to be performed without limitations set by

inhomogeneous broadening. In addition, SHB can be used to provide a frequency dimension for optical data storage, ultimately increasing density of the data storage by a factor of 10^4 and more.

Time-and-space domain holography is a coherent optical effect based on the SHB that allows one to manipulate, in addition to spatial waveforms, also temporal characteristics of optical wave amplitude [70-77]. The SHB of a frequency comb created by reference and object beams in some frequency selective material allows one to store and later retrieve the time profile of the object pulse. This unique property allows for holographic recording of ultrafast events and for information processing.

Until recently, most frequency-selective experiments in organic solids used ZPLs originating in one-photon transitions. In particular, SHB and time-and-space-domain holography have been previously demonstrated only using one-photon transitions. It may be expected that by using two-photon SHB new important information can be obtained about molecular properties and guest-host interactions in solids. Incorporation of two-photon coherent processes into time-and-space-domain holography can greatly increase the variety of nonlinear optical effects useful for optical storage and processing of information.

There is a whole list of unique properties that make TPA attractive for several practical applications in addition to those mentioned above:

1. quadratic dependence of absorption rate on the excitation intensity ($\sim I^2$);
2. instantaneous response time;
3. possibility to selectively excite molecules in a small volume $\sim \lambda^3$;

4. large difference between excitation wavelength and resulting fluorescence wavelengths
5. deeper penetration of near-IR light, typically used for two-photon excitation, into tissues;

The quadratic dependence on the excitation light intensity can be used for optical power limiting. An ideal power limiter allows low intensity light to propagate practically without absorption, whereas high intensity light is strongly attenuated. Furthermore, the instantaneous response of TPA can provide for efficient cutoff even on the femtosecond time scale. Quadratic dependence of TPA on the excitation intensity allows one to measure second order intensity autocorrelation or cross-correlation functions and is used for short laser pulse characterization.

By focusing laser light in a two-photon absorbing medium, one effectively confines two-photon excitation to the small focal volume, providing for diffraction-limited 3D resolution. This is particularly important for high-density 3D optical data storage, 3D microfabrication, and two-photon fluorescence microscopy.

Since in a two-photon transition the energies of two photons are added up, the excitation wavelength is typically much longer and well separated from the fluorescence wavelength. This greatly simplifies registration of two-photon excited fluorescence, because excitation and fluorescence photons are easily separated by filters and/or monochromator. Apart from being useful in laboratory experiments, this fact also makes two-photon fluorescence microscopy advantageous over its one-photon counterpart. Two-photon excited fluorescence is also employed for readout in high density 3D optical

data storage. Upconverted fluorescence permits lasing at new wavelengths where one-photon pumping is inefficient.

Finally, near-IR light, which is typically used for two-photon excitation, is much less absorbed and scattered by human tissues than visible light. This enables increased penetration of exciting light into a human body and can be used for two-photon excitation of biologically relevant molecules deep inside of the tissues. As a result, TPA-based fluorescence microscopy, which employs near-IR light for excitation, provides imaging of the tissues an order of magnitude deeper than one-photon confocal fluorescence microscopy using visible light. Similar advantage can be gained by TPA-based PDT, which uses excitation by light of a drug (photosensitizer) inside of the body as a first step of photophysical and photochemical processes leading to tumor destruction. Currently, only tumors either sitting close to the surface or accessible by endoscope can be treated by OPA-based PDT. The use of near-IR light for two-photon excitation of photosensitizers can greatly increase the efficiency of PDT.

The ultimate success of any of the two-photon-based applications critically depends on the efficiency of TPA, in particular, on the value of intrinsic nonlinear cross section, σ_2. So far, TPA properties of only a limited number of molecules have been known in sufficient detail. Lack of reliable spectroscopic data has been holding back the search for new efficient two-photon absorbers. In particular, almost no information has been available on TPA properties of biologically relevant tetrapyrrolic molecules.

In this respect, study of the TPA properties of organic molecules, especially those compatible with biological and medical applications, is of great importance. Tetrapyrrolic

molecules perform several crucial functions in nature, such as oxygen transportation (breathing), photosynthesis, etc. They are widely used in OPA-based PDT. Moreover, tetrapyrrolic molecules are well-known to possess ZPL. They are, probably, the most often used organic molecules in OPA-based SHB experiments. For these reasons, a comprehensive spectroscopic investigation of the TPA properties of tetrapyrroles is in order.

Overview of Thesis

This thesis investigates TPA properties of tetrapyrrolic molecules and their applications for two-photon-based coherence experiments and two-photon-induced singlet oxygen generation.

Chapter 2 of the thesis introduces the main concepts of TPA and gives a theoretical background of this phenomenon in the framework of the semiclassical approximation. The three-level model is introduced that is used throughout the thesis. The general expression for the two-photon cross section is analyzed in terms of this model leading to its simplification. The influence of molecular symmetry on TPA is considered.

Chapter 3 starts by introducing basic spectroscopic features of tetrapyrrolic molecules. Their TPA properties are investigated in great detail for the first time. Several different mechanisms leading to TPA enhancement are identified and analyzed quantitatively. As a result, practical guidelines for design of tetrapyrrolic molecules with strongly enhanced TPA are established.

Chapter 4 uses information obtained in the previous chapter to study TPA-based SHB and coherent phenomena in tetrapyrrolic molecules. A spectral coherence interference grating is created by two consecutive phase locked femtosecond pulses. A brief, theoretical treatment of the formation of spectral grating in relation to TPA is given. Next, experiments are discussed where we study TPA-based spectral gratings in the profile of persistent spectral hole and in the fluorescence spectrum of tetrapyrrolic molecules at low temperature. A new method to study the homogeneous TPA spectra by means of spectral gratings in centrosymmetrical and non-centrosymmetrical molecules is demonstrated.

Chapter 5 uses information obtained in the Chapter 3 to show the feasibility of TPA-based photosensitization of singlet molecular oxygen. First, TPA properties of some photosensitizers currently used for one-photon PDT are investigated. Next, a new class of specially developed porphyrin photosensitizers with greatly enhanced two-photon cross sections in near-IR is developed. Generation of singlet molecular oxygen upon two-photon excitation of the new photosensitizers is demonstrated.

Chapter 6 presents a summary of the work done in the thesis together with conclusions. An outline of possible future research directions is also given.

CHAPTER 2

TWO-PHOTON ABSORPTION: THE MAIN CONCEPTS AND THEORETICAL CONSIDERATIONS

This chapter starts by introducing the main concepts of TPA. Next, a general expression for two-photon cross section is derived using semiclassical approximation, i.e. molecules are treated quantum mechanically and light is treated classically. Finally, a particular case of three-level model, which is often used throughout the thesis, is considered in detail.

The Main Concepts of TPA

TPA is a nonlinear optical process in which two photons are absorbed simultaneously, such that energy of the photons adds up to the energy of the excited atom or molecule:

$$h\nu_1 + h\nu_2 = E\,, \tag{2.1}$$

where h is the Plank constant, ν_i is the frequency of the i-th absorbed photon, E is the transition energy. The absorption of all the photons is simultaneous in the sense that there are no real intermediate energy levels that are populated in this process. The absorption takes place through so-called virtual levels (Figure 2.1a), whose existence is allowed by quantum mechanics. Note, that this effect is completely different from stepwise absorption, in which case there are real intermediate levels involved into absorption that are populated at some point (Figure 2.1b).

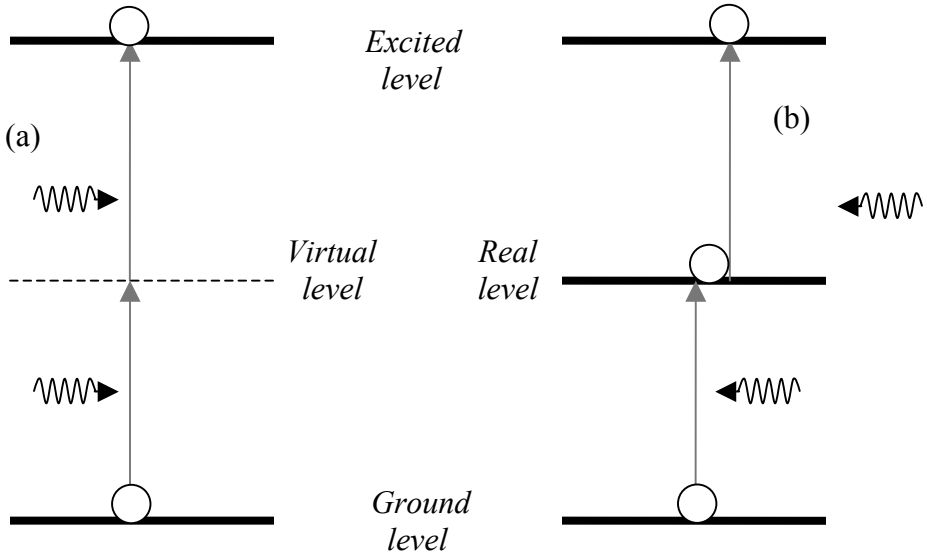

Figure 2.1 Graphic representation of simultaneous and stepwise TPA. (a) Simultaneous TPA. There is no real intermediate level populated in this process. Both photons are absorbed simultaneously through virtual level. (b) Stepwise TPA. The stepwise TPA can be divided into two distinctive OPA processes. Every level is physically populated, which can be registered by means of transient spectroscopy. The next level in the sequence is populated only after the previous one.

TPA was predicted theoretically by M. Göppert-Mayer [78] in 1931 for transitions between discrete energy states and was later applied for transitions between band states in dielectrics and semiconductors. The probability of multiphoton absorption on excitation light intensity follows the power law:

$$P \propto I_1^{n_1} I_2^{n_2} ... I_k^{n_k}, \tag{2.2}$$

where P is the probability of multiphoton excitation, I_k is the intensity of k-th source of light, and n_k is the number of photons from the k-th source of light participating in a single act of simultaneous multiphoton absorption so that the sum $\sum_k n_k$ is equal to the total number of absorbed photons. In the case of one excitation source (laser), expression (2.2) simplifies to:

$$P = \frac{1}{n}\sigma_n I^n, \tag{2.3}$$

where σ_n is the n-photon absorption cross section, i.e. σ_2 is the two-photon cross section. Coefficient $1/n$ takes into account the fact that n photons are required for n-photon excitation of one atom (molecule). The values of σ_n for multiphoton absorption are so small, that if linear absorption is present it usually dominates. Simple numerical estimations show that the typical two-photon cross section of a molecule should be of the order of $\sigma_2 \sim 10^{-50} \div 10^{-48}$ cm^4·s/photon or 1 ÷ 100 GM, where 1 GM = 10^{-50} cm^4·s/photon. This value is called Göppert-Mayer to honor the woman who theoretically predicted TPA. The values of one-photon cross section are around $\sigma_1 \sim 10^{-17} \div 10^{-15}$ cm^2. Because the probability of TPA grows faster with intensity than that of the OPA at some intensity they should equalize. Based on the cross sections presented above, the required excitation light intensity can be estimated:

$$\begin{aligned} &\frac{1}{2}\sigma_2 I^2 = \sigma_1 I \\ &I = 2\sigma_1/\sigma_2 = 2\cdot 10^{31}\, photon/(cm^2\cdot s) \approx 6\cdot 10^{12} W/cm^2 \end{aligned}, \tag{2.4}$$

where the lowest value ($\sigma_1 = 10^{-17}$ cm^2) for one-photon cross section and the largest value for two-photon cross section are used ($\sigma_2 = 10^{-48}$ cm^4·s/photon). Transition from photons to watts is made using energy of ruby laser photons (λ = 694 nm, $E = 2.9\cdot 10^{-19}$ J/photon). The estimated intensity is large. It shows how really small the probability of TPA is.

The qualitative explanation for such a low probability can be given in terms of the short lifetime of the virtual intermediate levels. It can be estimated from quantum mechanics uncertainty relation:

$$\begin{aligned} &\Delta E \Delta \tau \le h/(2\pi) \\ &\Delta \tau \sim 7 \cdot 10^{-16} s \end{aligned}, \tag{2.5}$$

where ΔE is the energy detuning of the virtual level from the real one, $\Delta \tau$ is the virtual level lifetime. The expression (2.5) gives a lifetime estimate for ΔE = 1 eV. The probability of the second photon hitting the molecule after it was raised to its virtual level by the first photon in the timeframe determined by (2.5) is extremely small.

Note, that one does not need the light intensity estimated in (2.4) to detect TPA. The fluorescence signal from a two-photon excited sample with excitation intensity several orders of magnitude lower is easily detectable. Nevertheless the required intensities are extremely large making high power pulsed lasers a favorite excitation source for TPA studies.

Theoretical Treatment of TPA

Let us consider a molecule which interaction with electromagnetic field is described by the following Hamiltonian $\widehat{H}$ [79]:

$$\widehat{H} = \widehat{H}_0 + \widehat{V}(t), \tag{2.6}$$

where $\widehat{H}_0$ is the Hamiltonian of the unperturbed molecule and $\widehat{V}(t)$ is the interaction energy with the applied electromagnetic field:

$$\widehat{V}(t) = -\boldsymbol{\mu} \boldsymbol{e} \widetilde{E}(t), \tag{2.7}$$

where $\boldsymbol{\mu}$ is a molecular dipole moment, $\widetilde{E}(t)$ is electric field of the electromagnetic wave, and $\boldsymbol{e}$ is the direction of polarization of the electromagnetic wave. It is supposed

that the wave is linearly polarized. For simplicity, the monochromatic wave is considered:

$$\widetilde{E}(t) = \frac{E}{2}(e^{-i\omega t} + e^{i\omega t}), \tag{2.8}$$

where E is the amplitude of the electric field. The electromagnetic field is switched on suddenly at time $t = 0$. Let us suppose that $u_l(\boldsymbol{r})$ are the energy eigenfunctions of unperturbed molecule with the corresponding energy eigenvalues equal to $E_l = \hbar\omega_l$. The ω_l is the angular frequency of the transition from the ground state to the l-th energy eigenstate. Since functions $u_l(\boldsymbol{r})$ form a complete set, the wavefunction $\psi(\boldsymbol{r},t)$ describing the molecule interacting with the electromagnetic field can be represented as a linear combination of them:

$$\psi(\boldsymbol{r},t) = \sum_l a_l(t)u_l(\boldsymbol{r})e^{-i\omega_l t}, \tag{2.9}$$

where the value of $|a_l(t)|^2$ is equal to the probability of finding the molecule at the l-th energy level at the time t.

According to the time-dependent perturbation theory, the coefficients $a_l(t)$ can be represented as the following expansion series:

$$a_l(t) = a_l^{(0)}(t) + a_l^{(1)}(t) + a_l^{(2)}(t) + \ldots. \tag{2.10}$$

The first term of this series corresponds to the *0*-th approximation, the second term corresponds to the first approximation and so on. The first and the second approximations describe OPA and TPA, respectively. The values of the terms can be found by solving the following set of differential equations [79]:

$$\frac{da_m^{(N)}(t)}{dt} = \frac{1}{i\hbar}\sum_l a_l^{(N-1)} V_{ml} e^{-i\omega_{ml}t}, \tag{2.11}$$

where N is the integer number, N = 1, 2, 3, 4 …, and $\omega_{ml} = (E_m - E_l)/\hbar$. Let us assume that in the absence of the electromagnetic field the molecule is in its ground state, g, so that:

$$\begin{cases} a_l^{(0)}(t) = 1, & l = g \\ a_l^{(0)}(t) = 0, & l \neq g. \end{cases} \tag{2.12}$$

By substituting equations (2.7) and (2.8) into equation (2.11) and taking into account initial conditions (2.12), the following differential equation for $a_m^{(1)}(t)$ is obtained:

$$\begin{aligned} &\frac{da_m^{(1)}(t)}{dt} = \frac{1}{i\hbar} V_{mg} e^{-i\omega_{gm}t} = -\frac{1}{i\hbar}\boldsymbol{\mu}_{mg}\boldsymbol{e}\frac{E}{2}(e^{-i\omega t} + e^{i\omega t})e^{-i\omega_{gm}t} = \\ &= -\frac{1}{i\hbar}\frac{\boldsymbol{\mu}_{mg}\boldsymbol{e}E}{2}(e^{i(\omega_{mg}-\omega)t} + e^{i(\omega_{mg}+\omega)t}) \end{aligned}, \tag{2.13}$$

where $\boldsymbol{\mu}_{mg}$ is the transition dipole moment between levels m and g.

$$\boldsymbol{\mu}_{mg} = < m|\boldsymbol{er}|g >, \tag{2.14}$$

where e is the electron charge and $\boldsymbol{r}$ is the distance. The solution of the differential equation (2.13) is rather straightforward:

$$a_m^{(1)}(t) = \frac{\boldsymbol{\mu}_{mg}\boldsymbol{e}E}{2\hbar(\omega_{mg}-\omega)}(e^{i(\omega_{mg}-\omega)t} - 1) + \frac{\boldsymbol{\mu}_{mg}\boldsymbol{e}E^*}{2\hbar(\omega_{mg}+\omega)}(e^{i(\omega_{mg}+\omega)t} - 1), \tag{2.15}$$

where symbol * means complex conjugation. The first term corresponds to the one-photon absorption and the second term corresponds to the stimulated one-photon emission. Now, when expression for the $a_m^{(1)}(t)$ is known, it is possible to calculate the

second order contribution $a^{(2)}(t)$ to the $a(t)$, which eventually leads to the TPA. We neglect the second term in equation (2.15) because it does not result in TPA.

$$\begin{aligned}
&\frac{da_f^{(2)}(t)}{dt} = \frac{1}{i\hbar}\sum_m a_m^{(1)} V_{fm} e^{-i\omega_{mf}t} = \\
&= -\frac{1}{i\hbar}\sum_m \frac{\boldsymbol{\mu}_{mg}\boldsymbol{e}E}{2\hbar(\omega_{mg}-\omega)}(e^{i(\omega_{mg}-\omega)t}-1)\boldsymbol{\mu}_{fm}\boldsymbol{e}\frac{E}{2}(e^{-i\omega t}+e^{i\omega t})e^{-i\omega_{mf}t} = \\
&= -\frac{1}{i\hbar}\sum_m \frac{(\boldsymbol{\mu}_{fm}\boldsymbol{e})(\boldsymbol{\mu}_{mg}\boldsymbol{e})E^2}{4\hbar(\omega_{mg}-\omega)}(e^{i(\omega_{fg}-2\omega)t}-e^{i(\omega_{fm}-\omega)t}+e^{i\omega_{fg}t}-e^{i(\omega_{fm}+\omega)t}) \approx \\
&\approx -\frac{1}{i\hbar}\sum_m \frac{(\boldsymbol{\mu}_{fm}\boldsymbol{e})(\boldsymbol{\mu}_{mg}\boldsymbol{e})E^2}{4\hbar(\omega_{mg}-\omega)}e^{i(\omega_{fg}-2\omega)t}
\end{aligned} \qquad (2.16)$$

All the terms that are obviously not related to the TPA are dropped. The physical meaning of the subscripts *f*, *m*, and *g* is excited (final) level, intermediate level, and ground level (Figure 2.2).

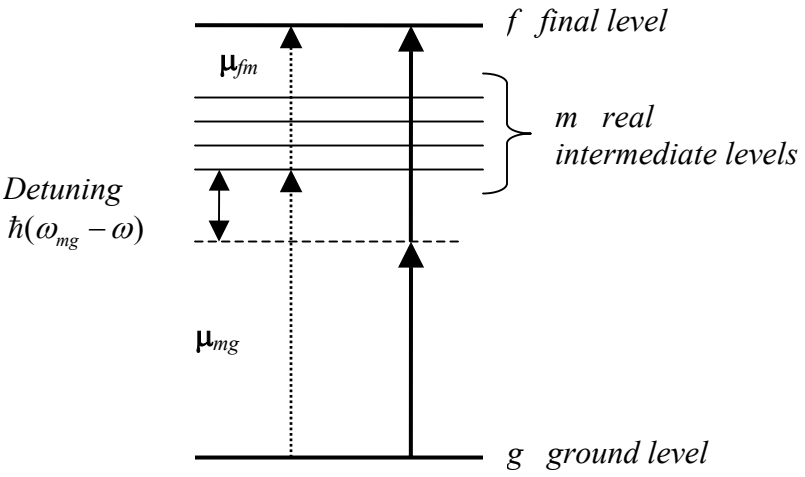

Figure 2.2 Schematic diagram of energy levels in molecule. The number of intermediate levels *m* is infinite. The contribution of every intermediate level is determined by the detuning between excitation photon energy end the energy of the level. Dotted arrows show transition dipole moments $\boldsymbol{\mu}_{mg}$ and $\boldsymbol{\mu}_{fm}$.

The obtained differential equation is analogous to the equation (2.13). The solution is:

$$a_f^{(2)}(t) = \sum_m \frac{(\boldsymbol{\mu}_{fm}\boldsymbol{e})(\boldsymbol{\mu}_{mg}\boldsymbol{e})E^2}{4\hbar(\omega_{mg}-\omega)} \times \frac{e^{i(\omega_{fg}-2\omega)t}-1}{\omega_{fg}-2\omega}. \tag{2.17}$$

The probability $p_f^{(2)}(t)$ of finding the molecule at the level *f* is:

$$p_f^{(2)}(t) = \left|a_f^{(2)}(t)\right|^2 = \left|\sum_m \frac{(\boldsymbol{\mu}_{fm}\boldsymbol{e})(\boldsymbol{\mu}_{mg}\boldsymbol{e})E^2}{4\hbar(\omega_{mg}-\omega)}\right|^2 \left|\frac{e^{i(\omega_{fg}-2\omega)t}-1}{\omega_{fg}-2\omega}\right|^2. \tag{2.18}$$

The time dependence of the probability is given by the second multiplier:

$$\left|\frac{e^{i(\omega_{fg}-2\omega)t}-1}{\omega_{fg}-2\omega}\right|^2 = \frac{4\sin^2[(\omega_{fg}-2\omega)t/2]}{(\omega_{fg}-2\omega)^2}. \tag{2.19}$$

The limit of the function (2.19) when *t* goes to infinity is:

$$\lim_{t\to\infty} \frac{4\sin^2[(\omega_{fg}-2\omega)t/2]}{(\omega_{fg}-2\omega)^2} = 2\pi t\delta(\omega_{fg}-2\omega). \tag{2.20}$$

Combining together (2.18) and (2.20), we get:

$$p_f^{(2)}(t) = \left|\sum_m \frac{(\boldsymbol{\mu}_{fm}\boldsymbol{e})(\boldsymbol{\mu}_{mg}\boldsymbol{e})E^2}{4\hbar(\omega_{mg}-\omega)}\right|^2 2\pi t\delta(\omega_{fg}-2\omega). \tag{2.21}$$

The delta function $\delta(\omega_{fg}-2\omega)$ indicates that transitions are possible only if the combined energy of the two photons is in resonance with the transition energy. The probability of the two-photon transition from the level *g* to the level *f* per unit time (transition rate) is:

$$R_{fg}^{(2)} = \left|\sum_m \frac{(\boldsymbol{\mu}_{fm}\boldsymbol{e})(\boldsymbol{\mu}_{mg}\boldsymbol{e})E^2}{4\hbar(\omega_{mg}-\omega)}\right|^2 2\pi\delta(\omega_{fg}-2\omega). \tag{2.22}$$

The two-photon cross section is defined in the following way:

$$R_{fg}^{(2)} = \frac{1}{2}\sigma_{fg}^{(2)}(\omega)I^2. \tag{2.23}$$

Here I is the excitation light intensity and coefficient ½ takes into account the fact that two photons are required for one transition. The two-photon cross section is typically quoted with intensities measured in $photons/(cm^2 s)$. The intensity in these units is equal to:

$$I = \frac{nc}{8\pi\hbar\omega}|E|^2. \tag{2.24}$$

Here n is the refractive index and c is the speed of light. The following expression for the two-photon cross section is found from equations (2.22) –(2.24)*:

$$\sigma_{fg}^{(2)}(\omega) = 2\frac{(2\pi)^3\omega^2}{\hbar^2 n^2 c^2}\left|\sum_m \frac{(\boldsymbol{\mu}_{fm}\boldsymbol{e})(\boldsymbol{\mu}_{mg}\boldsymbol{e})}{(\omega_{mg}-\omega)}\right|^2 \delta(\omega_{fg}-2\omega). \tag{2.25}$$

Usually, the local field factor $L = (n^2+2)/3$ is also introduced to take into account the effect of media [80]. Equation (2.25) leads to nonphysical behavior when $\omega_{mg} = \omega$, i.e. two-photon cross section is infinitely large, which can be avoided by introducing a phenomenological damping factor, $\Gamma_m(\omega)$.

$$\sigma_{fg}^{(2)}(\omega) = 2\frac{(2\pi)^3\omega^2 L^4}{\hbar^2 n^2 c^2}\left|\sum_m \frac{(\boldsymbol{\mu}_{fm}\boldsymbol{e})(\boldsymbol{\mu}_{mg}\boldsymbol{e})}{(\omega_{mg}-\omega)+i\Gamma_m(\omega)}\right|^2 \delta(\omega_{fg}-2\omega). \tag{2.26}$$

The damping factor is equal to the full width at half maximum of the OPA band $m \leftarrow g$. The damping effects can be properly taken into account using density matrix formalism

---

* It is supposed here that $\langle I^2(t)\rangle = \langle I(t)\rangle^2$, which is not always true. In general, $\langle I^2(t)\rangle = g^{(2)}\langle I(t)\rangle^2$, where $g^{(2)}$ describes second-order temporal coherence of the excitation source. Everywhere in this thesis we suppose that $g^{(2)} = 1$.

(see for example [81]). Finally, expression (2.26) is only true if the two-photon transition $f \leftarrow g$ is infinitely narrow, which is also nonphysical. To account for the finite width of the real electronic transitions, we introduce a line shape function, $g(2\omega)$:

$$\begin{cases} \sigma_{fg}^{(2)}(\omega) = 2\dfrac{(2\pi)^3 \omega^2 L^4}{\hbar^2 n^2 c^2} \left| \sum_m \dfrac{(\boldsymbol{\mu}_{fm}\boldsymbol{e})(\boldsymbol{\mu}_{mg}\boldsymbol{e})}{(\omega_{mg} - \omega) + i\Gamma_m(\omega)} \right|^2 g(2\omega) \\ \int_0^\infty g(2\omega)d(2\omega) = 1 \end{cases}. \tag{2.27}$$

The line shape function is normalized so that its integral over all the frequency range is unity. Since broad structurless absorption bands in organic molecules typically exhibit Gaussian line shape [82,83], we write*:

$$g(2\omega_p) = \sqrt{\frac{4\ln(2)}{\pi(\Delta\omega)^2}} \exp[-\frac{4\ln(2)}{(\Delta\omega)^2}(2\omega - \omega_{fg})^2], \tag{2.28}$$

where $\Delta\omega$ is the full width at the half maximum of the two-photon transition absorption band measured at the transition frequencies, i.e. twice the excitation laser frequency.

Three-Level Model

Since equation (2.26) represents a sum consisting of infinite number of terms it is not easily applicable for a practical calculation of the two-photon cross section. In some cases, the excitation photon frequency ω is close to some real intermediate one-photon transition. Then, because of the resonance factor, $1/(\omega_{mg} - \omega + i\Gamma_m(\omega))$, the term

* The Gaussian line shape function is usually used for description of the inhomogeneous broadening. Expression (2.28) corresponds to TPA averaged over inhomogeneous distribution of the molecules. The line shape function of a single molecule can be considerably different from Gaussian. It, typically, consists of a zero-phonon line and a phonon wing. The relative weight of these two factors depends on temperature, so that the line shape function of single molecule also depends on temperature.

corresponding to this particular transition may become much larger than all the other terms combined. To estimate two-photon cross section in such near-resonance case, one can use a three-level approximation. In this approximation only three energy levels are taken into account, namely initial (ground), *g*, final, *f*, and resonance intermediate, *m* ones. The sum in equation (2.26) then reduces to only three terms:

$$\sigma_{fg}^{(2)}(\omega) = 2\frac{(2\pi)^3\omega^2 L^4}{\hbar^2 n^2 c^2}\left|\sum_{m=g,m,f}\frac{(\boldsymbol{\mu}_{fm}\boldsymbol{e})(\boldsymbol{\mu}_{mg}\boldsymbol{e})}{(\omega_{mg}-\omega)+i\Gamma_m(\omega)}\right|^2 g(2\omega)\,. \tag{2.29}$$

Although this model does not always give quantitative agreement with the experimentally observed values of TPA cross section, it still greatly simplifies the analysis of the experimental data. The three-level model is used many times throughout this thesis. The rest of the chapter deals with its more detailed description.

Three-Level Model for a Centrosymmetrical Molecule

Many molecules, including most of those studied in this thesis, possess a center of inversion. The inverse symmetry leads to two important properties which profoundly influence TPA behavior (a) electronic transition between energy levels follow parity selection rules (see Appendix A); (b) the static dipole moment of centrosymmetrical molecules is equal to zero. In the framework of the three-level model the expression for two-photon cross section of centrosymmetrical molecules reads:

$$\begin{aligned}\sigma_{fg}^{(2)}(\omega) &= 2\frac{(2\pi)^3\omega^2 L^4}{\hbar^2 n^2 c^2}\left|\frac{(\boldsymbol{\mu}_{fm}\boldsymbol{e})(\boldsymbol{\mu}_{mg}\boldsymbol{e})}{(\omega_{mg}-\omega)+i\Gamma_m(\omega)}\right|^2 g(2\omega) = \\ &= 2\frac{(2\pi)^3\omega^2 L^4}{\hbar^2 n^2 c^2}\frac{(\boldsymbol{\mu}_{fm}\boldsymbol{e})^2(\boldsymbol{\mu}_{mg}\boldsymbol{e})^2}{(\omega_{mg}-\omega)^2+\Gamma_m^2(\omega)}g(2\omega)\end{aligned}\,, \tag{2.30}$$

where, we have taken into account that since static dipole moments are equal to zero, only one term in the equation (2.29) differs from zero. The TPA cross section depends on the relative direction of the polarization of the excitation light and the two transition dipole moment vectors. In isotropic medium such as a solution or polymer host spatial averaging over all possible polarization directions leads to relation [84]:

$$<(\boldsymbol{\mu}_{fm}\boldsymbol{e})^2(\boldsymbol{\mu}_{mg}\boldsymbol{e})^2>=\frac{[2\cos^2(\alpha)+1]}{15}\left|\boldsymbol{\mu}_{fm}\right|^2\left|\boldsymbol{\mu}_{mg}\right|^2, \tag{2.31}$$

where α is the angle between transition dipole moments $\boldsymbol{\mu}_{fm}$ and $\boldsymbol{\mu}_{mg}$, <…> means isotropic average. Therefore, in isotropic medium expression (2.30) modifies to:

$$\sigma_{fg}^{(2)}(\omega)=2\frac{[2\cos^2(\alpha)+1]}{15}\frac{(2\pi)^3\omega^2L^4}{\hbar^2n^2c^2}\frac{\left|\boldsymbol{\mu}_{fm}\right|^2\left|\boldsymbol{\mu}_{mg}\right|^2}{(\omega_{mg}-\omega)^2+\Gamma_m^2(\omega)}g(2\omega). \tag{2.32}$$

If the dipole moments are parallel to each other then:

$$\sigma_{fg}^{(2)}(\omega)=\frac{2}{5}\frac{(2\pi)^3\omega^2L^4}{\hbar^2n^2c^2}\frac{\left|\boldsymbol{\mu}_{fm}\right|^2\left|\boldsymbol{\mu}_{mg}\right|^2}{(\omega_{mg}-\omega)^2+\Gamma_m^2(\omega)}g(2\omega). \tag{2.33}$$

In many cases two-photon cross section is defined not as a function of angular frequency ω but rather as a function of ν, where $\nu=\omega/2\pi$. By substituting ω with ν the following expression is obtained for $\sigma_{fg}^{(2)}(\nu)$:

$$\sigma_{fg}^{(2)}(\nu)=2\frac{[2\cos^2(\alpha)+1]}{15}\frac{(2\pi)^5L^4\nu^2}{h^2c^2n^2}\frac{\left|\boldsymbol{\mu}_{fi}\right|^2\left|\boldsymbol{\mu}_{i0}\right|^2}{(\nu-\nu_{mg})^2+\Gamma_m^2(\nu)}g(2(2\pi\nu)), \tag{2.34}$$

where $\Gamma_m(\nu)$ is the full width at half maximum of the absorption band $m \leftarrow g$ represented as a function of frequency ν. The line shape function (see equation(2.28)) transforms in the following way:

$$g(2(2\pi\nu)) = \frac{1}{2\pi}\sqrt{\frac{4\ln(2)}{\pi(\Delta\nu)^2}}\exp[-\frac{4\ln(2)}{(\Delta\nu)^2}(2\nu-\nu_{fg})^2] = \frac{1}{2\pi}g(2\nu). \tag{2.35}$$

Combining equations (2.34) and (2.35), the final expression for $\sigma_2(\nu)$ can be obtained:

$$\sigma_{fg}^{(2)}(\nu) = 2\frac{[2\cos^2(\alpha)+1]}{15}\frac{(2\pi)^4\nu^2L^4}{h^2n^2c^2}\frac{\left|\boldsymbol{\mu}_{fm}\right|^2\left|\boldsymbol{\mu}_{mg}\right|^2}{(\nu_{mg}-\nu)^2+\Gamma_m^2(\nu)}g(2\nu). \tag{2.36}$$

If dipole moments are parallel to each other, then:

$$\sigma_{fg}^{(2)}(\nu) = \frac{2}{5}\frac{(2\pi)^4\nu^2L^4}{h^2n^2c^2}\frac{\left|\boldsymbol{\mu}_{fm}\right|^2\left|\boldsymbol{\mu}_{mg}\right|^2}{(\nu_{mg}-\nu)^2+\Gamma_m^2(\nu)}g(2\nu). \tag{2.37}$$

At this point one can perform a numerical estimate of two-photon cross section that can be expected in centrosymmetrical organic molecules. First we estimate the maximum possible two-photon cross section that can be achieved. We suppose that the molecule is excited under double resonance conditions, i.e. the frequency of the excitation photons, ν, is equal to the frequency of the intermediate one-photon transition, ν_{mg}, and the maximum of the two-photon transition (line shape maximum) corresponds to twice the frequency of the excitation photons, so that $g(2\nu) = \sqrt{4\ln(2)/\pi(\Delta\nu)^2}$. Then,

$$\sigma_{fg}^{(2)}(\max) = \frac{2}{5}\frac{(2\pi)^4\nu^2L^4}{h^2n^2c^2}\frac{\left|\boldsymbol{\mu}_{fm}\right|^2\left|\boldsymbol{\mu}_{mg}\right|^2}{\Gamma_m^2(\nu)}\sqrt{\frac{4\ln(2)}{\pi(\Delta\nu)^2}}. \tag{2.38}$$

We also suppose that both intermediate one-photon transitions are strongly allowed, so that the corresponding transition dipole moments are equal to 10 D (1 Debye = $3.336 \cdot 10^{-30}$ C·m). Using typical values for the rest of the parameters, n =1, L = 1, $\nu = 4\cdot10^{14}$ Hz (~ 800 nm), $\Gamma = \Delta\nu = 10^{13}$ Hz, the following value for TPA cross section is obtained,

$\sigma_{fg}^{(2)}(\max) = 2 \cdot 10^{-44}$ cm^{4}s/photon = $2 \cdot 10^6$ GM. The largest two-photon cross section measured so far is equal to 11 000 GM [85], which is two orders of magnitude lower than the estimate. Thus, considerable enhancement of the TPA cross sections is possible if the "right" molecule is designed.

Typically, the molecules, which TPA cross section is measured, are far from intermediate one-photon resonance, so that $\nu_{mg} - \nu \approx 5 \cdot 10^{13}$ Hz (~ 100 nm in the red part of the visible spectrum). Also, the intermediate one-photon transitions are not as strong as supposed above. If one supposes that transition dipole moments are equal to 5 D, and TPA band maximum still coincides with twice the excitation laser frequency, then two-photon cross section is equal to ~ $5 \cdot 10^3$ GM, which is close to the maximum values measured experimentally so far [85,86]. If excitation photons are detuned from the two-photon resonance by only 10^{13} Hz, the TPA cross section drops to 300 GM, which is typically observed in experiments.

The above estimations unambiguously demonstrate that strong enhancement of TPA cross section is possible amounting to as much as 10^4 - 10^6 GM. To obtain such large two-photon cross sections, one must look for the molecules with nearly double resonance condition.

Three-Level Model for a Non-Centrosymmetrical Molecule

If a molecule does not possess the center of inversion, then both initial and final levels have a static dipole moment. In such case they also need to be taken into account as intermediate levels (see equation (2.29)),

$$\sigma_{fg}^{(2)}(\omega) = 2\frac{(2\pi)^3\omega^2 L^4}{\hbar^2 n^2 c^2}\left|\frac{(\boldsymbol{e}\cdot\boldsymbol{\mu}_{fm})(\boldsymbol{e}\cdot\boldsymbol{\mu}_{mg})}{\omega_{mg}-\omega+i\Gamma_m(\omega)}+\frac{(\boldsymbol{e}\cdot\boldsymbol{\mu}_{fg})(\boldsymbol{e}\cdot\boldsymbol{\mu}_{gg})}{-\omega}+\right.$$
$$\left.+\frac{(\boldsymbol{e}\cdot\boldsymbol{\mu}_{ff})(\boldsymbol{e}\cdot\boldsymbol{\mu}_{fg})}{\omega_{fg}-\omega+i\Gamma_f(\omega)}\right|^2 g(2\omega), \qquad (2.39)$$

where $\boldsymbol{\mu}_{gg}$ and $\boldsymbol{\mu}_{ff}$ are permanent dipole moments of the initial and final states, respectively. The first, second, and third terms employ *m*, *g*, and *f* levels as the intermediate ones. In the case of a non-centrosymmetrical molecule, both one- and two-photon transitions are allowed between any energy levels so that $\boldsymbol{\mu}_{fg} \neq 0$ [*]. The following parameters are obviously equal to zero: $\omega_{gg} = \omega_{ff} = 0$, $\Gamma_g = 0$. An additional simplification, $\omega_{fg} - \omega \gg \Gamma_f$, can also be made because the final energy level is never in close resonance with excitation photons in degenerate TPA. Taking into account that $\omega_{fg} - \omega = \omega$, equation (2.39) can be rewritten in the following form:

$$\sigma_{fg}^{(2)}(\omega) = 2\frac{(2\pi)^3\omega^2 L^4}{\hbar^2 n^2 c^2}\left|\frac{(\boldsymbol{e}\cdot\boldsymbol{\mu}_{fm})(\boldsymbol{e}\cdot\boldsymbol{\mu}_{mg})}{\omega_{mg}-\omega+i\Gamma_m(\omega)}+\frac{(\boldsymbol{e}\cdot\boldsymbol{\mu}_{fg})(\boldsymbol{e}\cdot\boldsymbol{\Delta\mu}_{fg})}{\omega}\right|^2 g(2\omega). \qquad (2.40)$$

where $\boldsymbol{\Delta\mu}_{fg}$ is the difference between static dipole moments in the excited and ground levels, $\boldsymbol{\Delta\mu}_{fg} = \boldsymbol{\mu}_{ff} - \boldsymbol{\mu}_{gg}$. Therefore,

$$\sigma_{fg}^{(2)}(\omega) = 2\frac{(2\pi)^3\omega^2 L^4}{\hbar^2 n^2 c^2}\left[\frac{(\boldsymbol{e}\cdot\boldsymbol{\mu}_{fm})^2(\boldsymbol{e}\cdot\boldsymbol{\mu}_{mg})^2}{(\omega-\omega_{fg})^2+\Gamma_i^2(\omega)}+\frac{(\boldsymbol{e}\cdot\boldsymbol{\mu}_{fg})^2(\boldsymbol{e}\cdot\boldsymbol{\Delta\mu}_{fg})^2}{\omega^2}+\right.$$
$$\left.+2\frac{(\boldsymbol{e}\cdot\boldsymbol{\mu}_{fm})(\boldsymbol{e}\cdot\boldsymbol{\mu}_{mg})(\boldsymbol{e}\cdot\boldsymbol{\mu}_{fg})(\boldsymbol{e}\cdot\boldsymbol{\Delta\mu}_{fg})}{\omega[(\omega_{mg}-\omega)^2+\Gamma_i^2(\omega)]}(\omega_{mg}-\omega)\right]g(2\omega) \qquad (2.41)$$

---

[*] Note that in case of centrosymmetrical molecule not only static dipole moments $\boldsymbol{\mu}_{gg}$ and $\boldsymbol{\mu}_{ff}$ are equal to zero but also transition dipole moment between ground and excited states $\boldsymbol{\mu}_{fg}$ is also zero. It is because one-photon transition between initial and final states $f \leftarrow g$ is parity forbidden.

The three terms correspond to the contribution of the (1) transition in a three-level system with the real intermediate state, *m*, (2) transition in a two-level system with a change of permanent dipole moment, and (3) interference term between the first two contributions. Note that, depending on the sign, the last term can either increase or decrease $\sigma_{fg}^{(2)}(\omega)$. If the real intermediate transition is exactly halfway to the final excited state then contribution of the interference term zeros out.

An important case of equation (2.41) is when intermediate level can be neglected. It is possible if change of the static dipole moment $\Delta\boldsymbol{\mu}_{fg}$ is very large in comparison to the transition dipole moments $\boldsymbol{\mu}_{mg}$ and $\boldsymbol{\mu}_{fm}$ and excitation photons are far from the resonance with intermediate level. In such case, equation (2.41) turns into a simple expression for two-photon cross section:

$$\sigma_{fg}^{(2)}(\omega) = 2\frac{(2\pi)^3 L^4}{\hbar^2 n^2 c^2}(\boldsymbol{e}\cdot\boldsymbol{\mu}_{fg})^2(\boldsymbol{e}\cdot\Delta\boldsymbol{\mu}_{fg})^2 g(2\omega)\,. \tag{2.42}$$

An averaging over space coordinates similar to the equation (2.31) can be performed [84] yielding the following expression for TPA cross section:

$$\sigma_{fg}^{(2)}(\omega) = 2\frac{[2\cos^2(\beta)+1]}{15}\frac{(2\pi)^3 L^4}{\hbar^2 n^2 c^2}\left|\boldsymbol{\mu}_{fg}\right|^2\left|\Delta\boldsymbol{\mu}_{fg}\right|^2 g(2\omega)\,, \tag{2.43}$$

where β is an angle between vectors $\boldsymbol{\mu}_{fg}$ and $\Delta\boldsymbol{\mu}_{fg}$. If the vectors are parallel then:

$$\sigma_{fg}^{(2)}(\omega) = \frac{2}{5}\frac{(2\pi)^3 L^4}{\hbar^2 n^2 c^2}\left|\boldsymbol{\mu}_{fg}\right|^2\left|\Delta\boldsymbol{\mu}_{fg}\right|^2 g(2\omega)\,. \tag{2.44}$$

In terms of ν, an expression for the two-photon cross section has the following form in general case:

$$\sigma_{fg}^{(2)}(\nu) = 2\frac{[2\cos^2(\beta)+1]}{15}\frac{(2\pi)^4 L^4}{h^2 n^2 c^2}\left|\boldsymbol{\mu}_{fg}\right|^2\left|\Delta\boldsymbol{\mu}_{fg}\right|^2 g(2\nu)\,. \tag{2.45}$$

If $\beta = 0$ then

$$\sigma_{fg}^{(2)}(\nu) = \frac{2}{5}\frac{(2\pi)^4 L^4}{h^2 n^2 c^2}\left|\boldsymbol{\mu}_{fg}\right|^2\left|\Delta\boldsymbol{\mu}_{fg}\right|^2 g(2\nu)\,. \tag{2.46}$$

An order of magnitude estimate of two-photon cross section, similar to that done in the previous section, can also be performed for a non-centrosymmetrical molecule. Using the same values for the parameters as in the previous section, i.e. n =1, L = 1, $\Delta\nu$ = 10^{13} Hz, $\boldsymbol{\mu}_{fg} = \Delta\boldsymbol{\mu}_{fg}$ = 10 D, gives for the maximum TPA cross section 1300 GM. Although the estimated value is larger than most of the experimentally measured TPA cross sections it is two orders of magnitude lower than estimate for the three-level centrosymmetrical molecule in double resonance condition. It is explained by the fact that equation (2.46) corresponds to the case when one-photon intermediate resonance is far off the excitation laser frequency, so that change of the static dipole moment is the main factor contributing to the two-photon cross section. The estimate does not imply that TPA cross sections of non-centrosymmetrical molecules are naturally lower than TPA cross sections of centrosymmetrical molecules. By coming close to some intermediate resonance, so that approximations made upon derivation of equation (2.46) are no longer valid, the two-photon cross section of non-centrosymmetrical molecule can skyrocket to much larger values.

CHAPTER 3

TPA PROPERTIES OF TETRAPYRROLIC COMPOUNDS AND METHODS OF ENHANCEMENT OF TWO-PHOTON CROSS SECTION

Tetrapyrrolic compounds (porphyrins, chlorins, bacteriochlorins, and so on) occur widely in nature and play very important role in different biological processes. For example, porphyrin-type molecules are the critical part of hemoglobin and myoglobin, which are the proteins transporting and storing oxygen in all animals. Chlorophyll, a derivative of chlorin, is found in green plants. It plays the central role in plant photosynthesis. Bacteriochlorophyll is used for the same purpose in photosynthetic bacteria. Owing to the great importance of the tetrapyrrolic molecules in biological processes, a great deal of attention has been paid to the study of their spectroscopic, physical, chemical, and biophysical properties.

Tetrapyrrolic molecules have attracted attention also from a rather different direction, due to their potential applications in various areas of technology including photonics. For example, particular spectroscopic and linear absorption properties of tetrapyrroles have inspired research in the area of synthetic light harvesting antenna-systems [87-89], holographic data storage [70,71,73-77], molecular scale electronic components [90-93], and PDT [94-96].

Recently, growing interest to the nonlinear optical properties of organic materials has prompted a new wave of investigation of tetrapyrrolic molecules. In particular, tetrapyrroles are of great interest to nonlinear optics applications like electrooptical signal processing, power limiting, molecular scale electronic components, and PDT [61,62,97-

102]. On the other hand, investigations of the TPA properties of tetrapyrroles have been very few and far between. Lack of reliable data on TPA properties of tetrapyrroles is in a stark contrast with variety of proposed multiphoton-based applications. Moreover, if one wants to increase efficiency of two-photon excitation, almost total lack of data about TPA properties of tetrapyrrolic molecules makes it exceedingly difficult to judge what values of TPA cross sections can be expected after their modification. Therefore, a systematic study of TPA properties of the tetrapyrroles leading to the guidelines defining steps necessary for their TPA enhancement is of great practical importance.

The main objectives of experiments described in this chapter are:

1. Measure TPA cross section in a broad wavelength range for a number of tetrapyrrolic compounds.
2. Investigate different physical mechanisms that contribute to the enhancement of TPA cross section.
3. Find tetrapyrrolic molecules with strongly increased TPA cross sections, which can be viable for practical applications.

The chapter starts by giving basic information about tetrapyrrolic molecules, their structure and one-photon spectroscopic features, followed by an overview of previous studies of TPA properties of tetrapyrroles. Next, our results on TPA spectral measurements of different types of tetrapyrrolic molecules are presented and several physical mechanisms leading to the TPA enhancement in tetrapyrroles are analyzed. Finally, we propose a new method of TPA cross section measurement.

The work presented in this chapter was reported in the following publications [103-113].

Porphyrins and their Derivatives

This section gives a brief description of the porphyrins and related compounds [114]. Strong interest to the porphyrins and related compounds (tetrapyrrolic molecules) is caused first by their importance for life on earth and second by their technological applications. The influence of these molecules on our life is fundamental. Tetrapyrrolic molecules play crucial role in the processes like photosynthesis by plants and bacteria and oxygen transportation and storage inside animals (including humans). Needless to say that without these compounds the Earth would be devoid of life as we know it.

Figure 3.1a presents the structure of porphine, which is a basic building block of tetrapyrrolic molecules. Porphine consist of four pyrrole rings linked by methine bridges forming a so-called porphyrin macrocycle. The porphyrin macrocycle is a heteroaromatic system containing 22 π-electrons, 18 of which form a conjugated ring. It means that these electrons are not bound to some specific atom in the porphine but rather delocalized throughout the macrocycle. The macrocycle is very stable and, as a result, it was chosen by nature to perform various important functions. By adding different substituents to periphery of the basic macrocycle and/or by introducing metals into the center of the macrocycle one can obtain different kinds of porphyrins. For example, porphyrins containing iron in the center of their macrocycle are called hemes and are found extensively in biophysics.

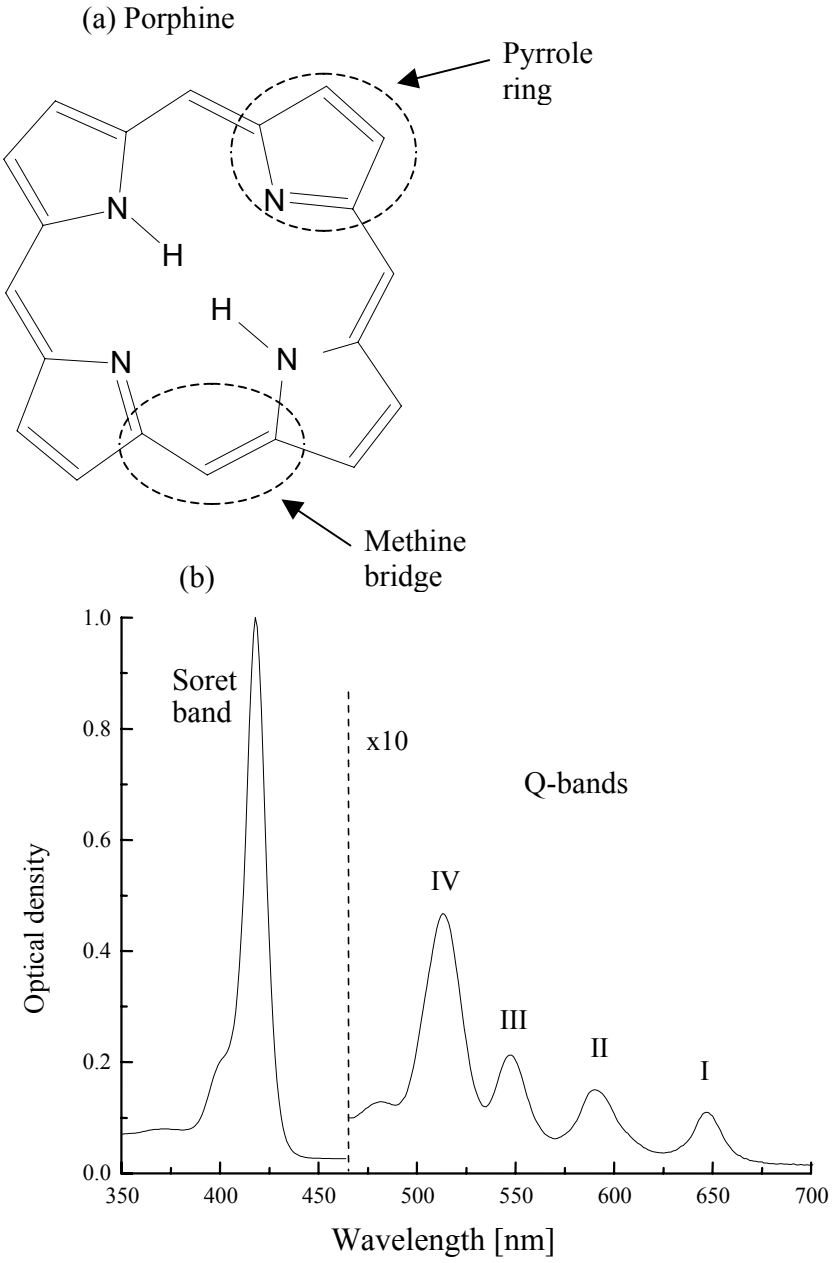

Figure 3.1 (a) Chemical structure of porphine. Pyrrole ring and methine bridge constituting main elements of the porphine macrocyle are highlighted with dashed ovals. (b) Typical absorption spectrum of porphyrin molecules. The right part of the spectrum is multiplied by 10 to make Soret band and Q-bands of about the same height.

Typical UV-visible absorption spectrum of a porphyrin shows intense absorption near 400 nm (Soret band) accompanied by weaker absorption bands (Q-bands) in the visible (Figure 3.1b). The Q-bands are denoted I, II, III, and IV, starting from the most redshifted one. Figure 3.2 represents Jablonski diagram of the photophysical processes in organic molecules, including porphyrins. The solid and wavy arrows represent radiation and radiationless transitions, respectively. The numbers I, II, III, and IV show transitions responsible for the Q-bands in the porphyrin absorption spectrum (Figure 3.1b). The Q-bands are attributed to the lowest-energy spin-allowed electronic transitions, namely, $S_1 \leftarrow S_0$ transition and its vibronic satellite correspond to the I-st and II-nd Q-bands. Second spin-allowed electronic transition from the ground state $S_2 \leftarrow S_0$ and its vibronic satellite correspond to the III-rd and IV-th Q-bands.

If the center of the macrocycle is protonated with two additional protons (hydrogen atoms), so that every nitrogen atom in the macrocycle has a hydrogen atom or if a metal is introduced into the center, then the symmetry of the macrocycle increases, changing from D_{2h} to D_{4h} point group. This leads to degeneracy of the S_1 and S_2 (Figure 3.2) electronic levels decreasing number of Q-bands from four to two. Rich visible absorption spectrum of the porphyrins leads to their strong coloration. Solutions of many porphyrin molecules have intense red color. For example, the color of the blood is conditioned by the oxygen-transporting porphyrins. In fact, the word porphyrin is derived from the Greek word “porphyra”, meaning purple.

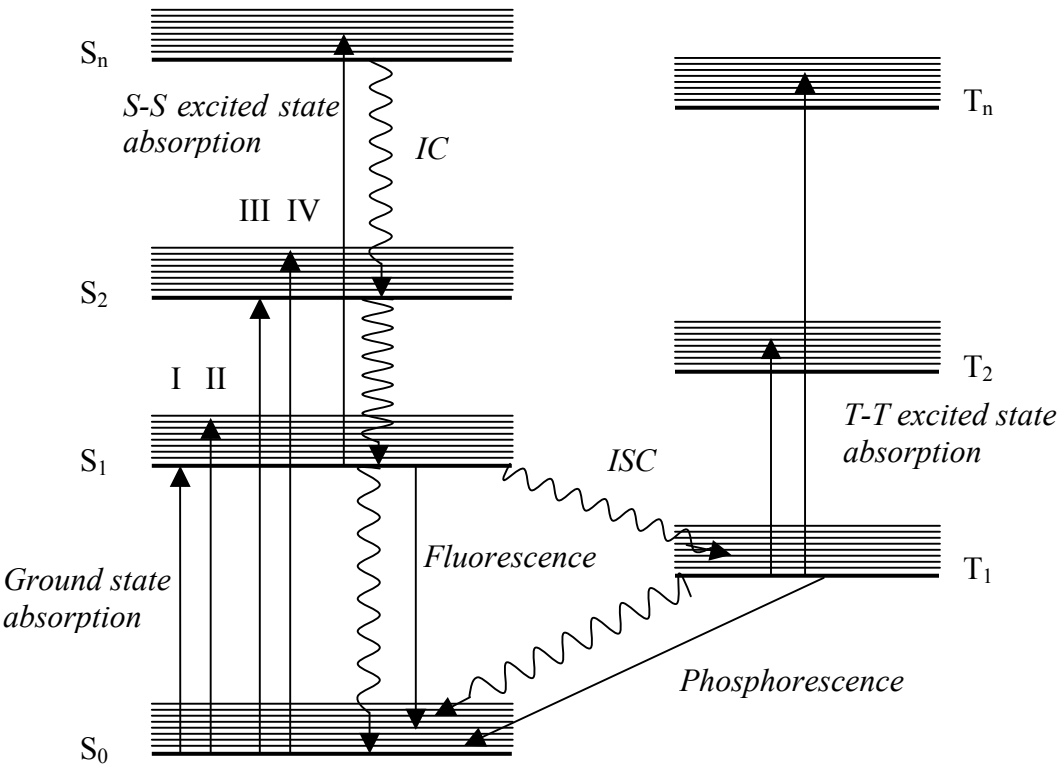

Figure 3.2 Jablonski diagram describing photophysical processes in organic molecules. S_0, S_1, S_2, and S_n are singlet electronic levels, T_1, T_2, and T_n are triplet electronic levels (thick solid lines). The ground electronic level is typically singlet and denoted S_0. The vibrational structure of every electronic level is shown with thin solid lines. Solid arrows represent radiation transitions between energy levels. Arrows on the left correspond to ordinary linear ground state absorption. Numbers I, II, III, and IV correspond to the Q-bands of the porphyrins. Excited state absorption is possible from both singlet and triplet levels. In this figure the following examples of excited state absorption are presented: $S_n \leftarrow S_1$, $T_2 \leftarrow T_1$, and $T_n \leftarrow T_1$. Radiation transitions from upper to lower electronic levels include fluorescence and phosphorescence. Fluorescence takes place between levels with the same multiplicity, i.e. $S \rightarrow S$ or $T \rightarrow T$, phosphorescence takes place between levels with different multiplicity, i.e. $T \rightarrow S$ or $S \rightarrow T$. Since radiation transition between levels with different multiplicity is forbidden, the efficiency of the phosphorescence is lower than efficiency of the fluorescence. The efficiency of radiationless processes between excited energy levels is very high so that fluorescence usually takes place only from the first excited singlet level $S_1 \rightarrow S_0$, phosphorescence takes place from the first triplet level $T_1 \rightarrow S_0$. Examples of fluorescence and phosphorescence between other energy levels are extremely rare and even if they do occur, the quantum yield of such processes is very small. Wavy arrows represent radiationless transitions in organic molecules. They are: internal conversion (IC) – radiationless transition between electronic levels with the same multiplicity and intersystem crossing (ISC) – radiationless transition between levels with different multiplicity.

The first Q-band of the tetrapyrrolic molecules is known to possess ZPL at low temperature, which explains their widespread use in the site selective spectroscopy and coherence-based experiments. This prompted us to investigate TPA properties of tetrapyrroles in the Q-bands region of the spectrum, so that better understanding of the application of TPA to such experiments could be achieved.

Apart from pure porphyrins there are several other classes of tetrapyrrolic molecules that have a modified structure of the macrocycle[*]. Tetrapyrroles from four different classes have been studied in this work. Following is a brief description of their chemical structures. Reduction of one of the pyrrole units in the porphyrin ring leads to a class of porphyrin derivatives called chlorins (Figure 3.3a). Magnesium-containing chlorins are called chlorophylls. They are the central photosensitive pigments in chloroplasts in plants and are responsible for photosynthesis. Green color of chlorins provides for the color of plants. Azaporphyrins have the same structure as porphine, but with nitrogen atoms in the *meso*-positions instead of carbon (Figure 3.3b). Tetrabenzoporphyrins are formed by adding benzene rings to the pyrrole rings (Figure 3.3c). Finally, naphthalocyanines are made by adding napthalenes to the tetraazaporphine (Figure 3.3d)[†].

---

[*] Sometimes all such molecules (tetrapyrroles) are called porphyrins.

[†] Note, that it is not description of the chemical reactions leading to synthesis of these compounds. It just highlights the difference in their structures.

(a) Chlorin

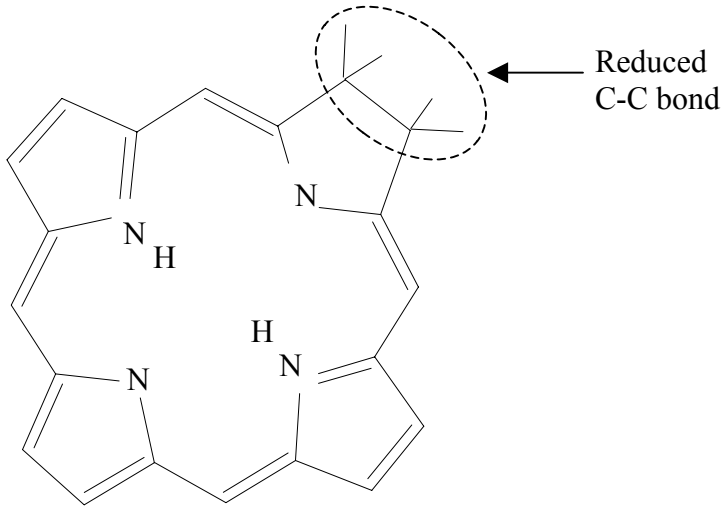

(b) Tetraazaporphine

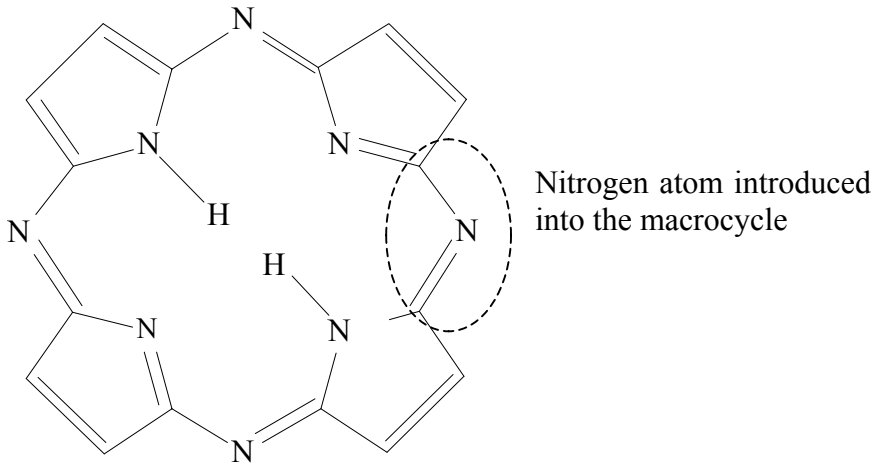

Figure 3.3 (a,b) Chemical structures of (a) chlorin and (b) tetraazaporphine. Dashed ovals are used to highlight structural differencies between the porphine and the rest of the molecules.

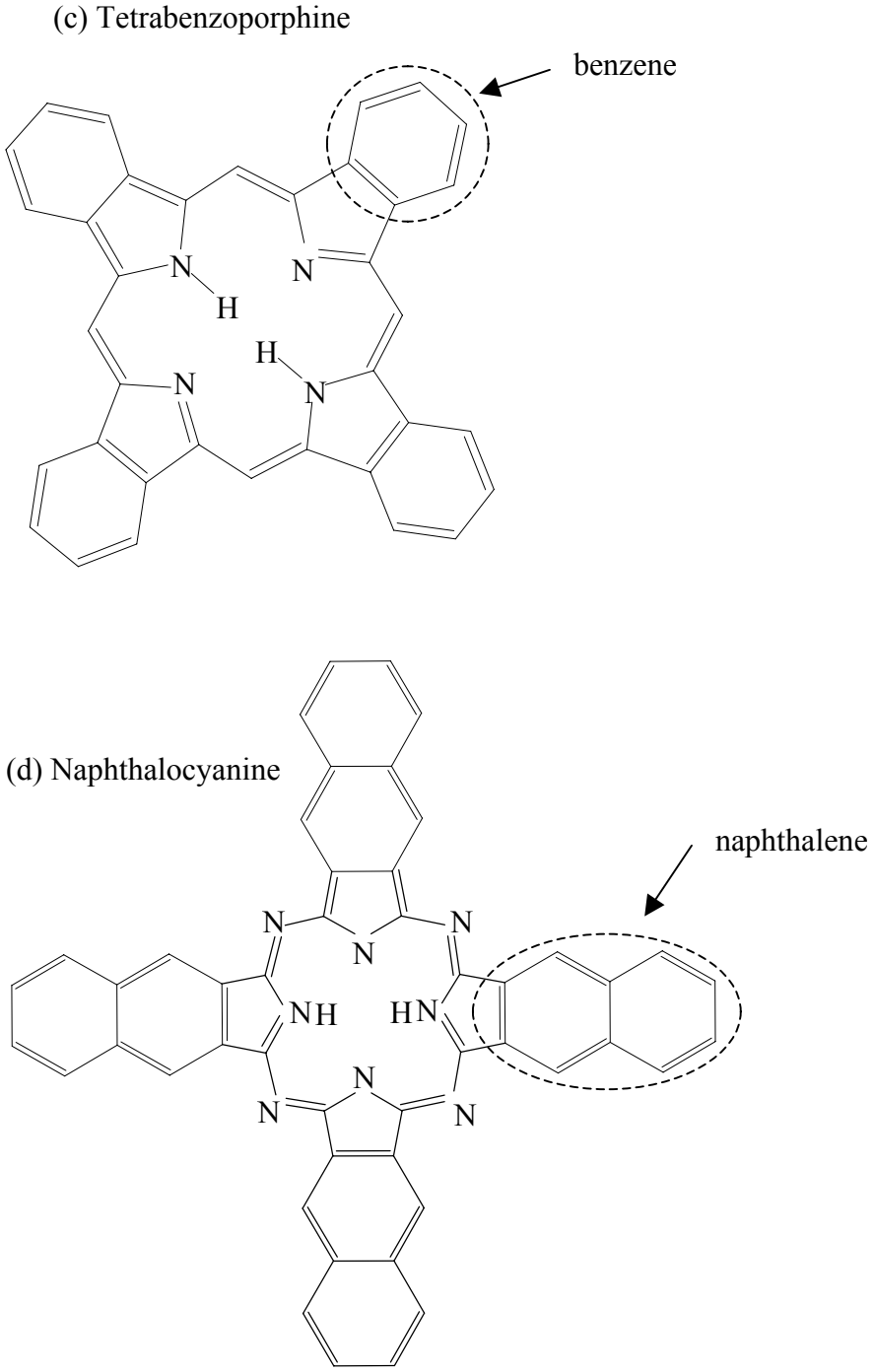

Figure 3.3 (c,d) Chemical structures of (c) tetrabenzopoprhin and (d) naphthalocyanine. Dashed ovals are used to highlight structural differencies between the porphine and the rest of the molecules.

Previous Work on Nonlinear Absorption of Tetrapyrrolic Molecules

There are two main processes that can lead to nonlinear absorption: (1) simultaneous TPA and (2) excited state absorption. We are interested in simultaneous TPA, which has instantaneous response in comparison to excited state absorption and can be used for a number of practical applications. Nevertheless, excited state absorption experiments are supplementary to direct TPA studies in that they allow probing position of the *g*-parity levels, which are involved in simultaneous TPA. In addition, one can use quantum mechanical calculations to predict position and intensity of the TPA bands. But for such large molecules as tetrapyrroles it is exceedingly difficult. This kind of calculations can be considered only as a guide that supplements experimental work.

Taking into account significance of the tetrapyrrolic molecules, there is a surprisingly limited number of prior studies of their intrinsic TPA. So far, only a few measurements of TPA cross sections in tetrapyrrolic molecules have been performed. In particular, it was found that two-photon cross sections of chlorophyll *a* and aluminum phthalocyanine at λ_{ex} = 1064 nm are σ_2 = 8 GM [62] and σ_2 = 12.7 GM [61], respectively. For protoporphyrin IX the following values were reported: σ_2 = 0.7 GM (λ_{ex} = 760 nm), σ_2 = 0.9 GM (λ_{ex} = 770 nm), σ_2 = 0.6 GM (λ_{ex} = 780 nm), σ_2 = 2.0 GM (λ_{ex} = 790 nm) [115]. More recently, a number of TPA cross section measurements were performed for several metalloporphyrins doped into boric acid glass [116]. The measured cross sections were in the range 25 – 114 GM. Ref. [117,118] reported relative TPA spectra of several tetrapyrroles, but without giving absolute values of σ_2.

One conclusion, that can be made from these experimental studies, is that two-photon cross sections of tetrapyrroles are rather small, typically less than 100 GM. Larger cross sections ($\sigma_2 \sim 10^3 - 10^4$ GM) are required to advance TPA applications of tetrapyrrolic molecules.

It is possible to understand these early results if we consider that most of the studied molecules are either centrosymmetrical or near-centrosymmetrical, so that parity selection rules for TPA can be applied to them (see Appendix A). This means that large σ_2 requires transitions into *g*-parity excited states. Location of these states in tetrapyrroles is not well known and it may be that they have never been probed. Quantum-mechanical calculations support this interpretation.

A number of quantum-mechanical calculations have been carried out by semiempirical and *ab initio* methods [107,119-133], and the main conclusion is that the lowest *g*-parity electronic states are located in the blue part of the spectrum near Soret band and above. The calculations also predict a large value of $\sigma_2 = 590$ GM (transition wavelength 325 nm) for free base porphyrins [124] and carbaporphyrins $\sigma_2 \sim 10^3$ GM (transition wavelength 400 nm) [133] for transitions into *g*-parity levels. One of the goals of our experiments is to probe experimentally *g*-*g* transitions in a rigorous manner.

Another way to probe *g*-parity levels is to study excited state OPA (transient absorption) from the first excited singlet level S_1 (see Figure 3.2). Since the S_1 has *u*-parity, the OPA from this energy level is allowed to *g*-parity levels. The OPA spectra from the first singlet excited state can be obtained by means of pump-probe technique. Two consecutive pulses, pump and probe, are used for excitation. The pump pulse

populates the S_1 state, while the probe pulse, applied with some time delay, leads to excited state absorption $S_n \leftarrow S_1$ (Figure 3.2). The measured transmittance of the probe pulse allows calculating excited state absorption.

Singlet-singlet excited state absorption of porphyrins shows an increase of the absorption towards higher energies, above the Soret band. J. Rodriguez et al. [134] studied excited state absorption of a large group of porphyrins. All the molecules show considerable increase of singlet-singlet excited state absorption when scaning the probe frequency from near-IR to the blue part of the spectrum, with maxima of the differential absorption lying near $\lambda_{max} \sim 450$ nm. Note that since singlet-singlet excited state absorption $S_n \leftarrow S_1$ sits on top of the first allowed electronic transition from the ground state $S_1 \leftarrow S_0$ (see Figure 3.2), one must add up energy of this transition to the energy of the probe pulse photons to determine position of the *g*-parity levels relative to the ground state. The wavelength of the $S_1 \leftarrow S_0$ transition in porphyrins is roughly 600 nm. Correspondingly, maxima of the *g*-parity levels of the studied porphyrins lie near $\lambda_{max} \sim$ 260 nm relatively to the ground level with long absorption tails going almost to the Soret band.

H. Gratz and A. Penzkofer [135] investigated $S_n \leftarrow S_1$ excited state absorption of meso-tetraphenylporphyrin in the wavelength range $\lambda = 250 – 450$ nm with respect to the ground state. Again strong increase of $S_n \leftarrow S_1$ absorption was revealed when going to shorter wavelengths. To summarize, singlet-singlet excited state absorption studies indicate that *g*-parity levels could be present in the near-UV part of the spectrum in the tetrapyrrolic compounds. This implies that two-photon cross sections of porphyrin

molecules in the near-UV transition wavelengths region could be considerably larger than the data obtained before this work. This prompted us to conduct a rigorous investigation of the TPA properties of the tetrapyrroles in the near-UV spectral region.

Experimental

Figure 3.4 shows chemical structures of 16 compounds studied in this chapter. The origin of the compounds was as following. 2,3,7,8,12,13,17,18-Octaethylporphine Zinc (II) (ZnOEP), 5,10,15,20-Tetraphenylporphine (H_2TPP), and 2,7,12,17-Tetra-*tert*-butyl-tetraazaporphine (Bu_4TAP) were purchased from Aldrich. Tetrabenzoporphine (H_2TBP) was purchased from Porphyrin Products (Logan, UT). 5-Monophenyl-tetrabenzoporphine Zinc (II) (ZnMPTBP), 5,15-Diphenyltetrabenzoporphine Zinc (II) (ZnDiPTBP), 5,10,15-Triphenyltetrabenzoporphine Zinc (II) (ZnTriPTBP), and 5,10,15,20-Tetraphenyltetrabenzoporphine Zinc (II) (ZnTPTBP) were synthesized and purified by A.M. Shul'ga (Minsk, Belarus)[*]. 2,3,7,8,12,13,17,18-(4-bromophenyl)-tetraazaporphine ($(BrPh)_8$TAP) and 2,3,7,8,12,13,17,18-(4-nitrophenyl)-tetraazaporphine ($((NO_2)Ph)_8$TAP) were synthesized by Dr. N. Mamardashvili group[†] [136,137]. H_2TMPyP and H_2TSPP were obtained from Dr. M. Kruk[‡]. [5,15-bis(3,5-bi-tert-butylphenyl)-10,20-bis(trihexylsilylethynyl)porphyrinato]zinc(II) (monomer),

---

[*] A. M. Shul'ga, senior staff researcher, Laboratory of Molecular Photonics, Institute of Molecular and Atomic Physic of National Academy of Sciences, 70 F. Skaryna Avenue, 220072 Minsk, Belarus.
[†] Dr. N. Mamardashvili, Institute of Solution Chemistry, Russian Academy of Sciences, Akademicheskaya St. 1, 153045 Ivanovo, Russia.
[‡] Dr. M. Kruk, Laboratory of Molecular Photonics, Institute of Molecular and Atomic Physic of National Academy of Sciences, 70 F. Skaryna Avenue, 220072 Minsk, Belarus.

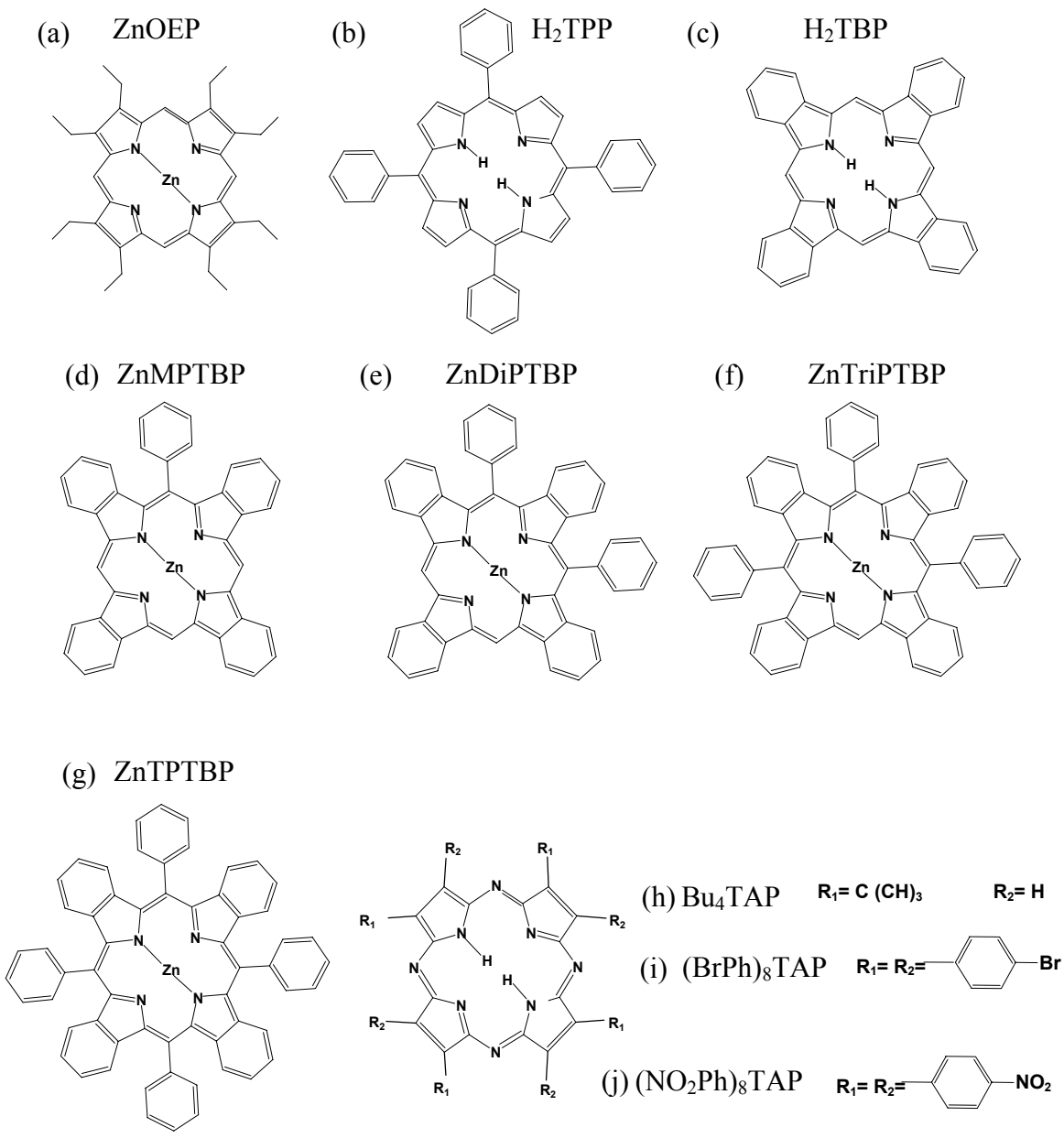

Figure 3.4 (a-j) Chemical structures of the molecules studied in this chapter: (a) 2,3,7,8,12,13,17,18- Octaethylporphine Zinc (II) (ZnOEP); (b) 5,10,15,20-Tetraphenylporphine (H_2TPP); (c) Tetrabenzoporphine (H_2TBP); (d) 5-Monophenyltetrabenzoporphine Zinc (II) (ZnMPTBP); (e) 5,15-Diphenyltetrabenzoporphine Zinc (II) (ZnDiPTBP); (f) 5,10,15-Triphenyltetrabenzoporphine Zinc (II) (ZnTriPTBP); (g) 5,10,15,20-Tetraphenyltetrabenzoporphine Zinc (II) (ZnTPTBP); (h) 2,7,12,17-Tetra-*tert*-butyl-tetraazaporphine (Bu_4TAP); (i) 2,3,7,8,12,13,17,18-(4-bromophenyl)-tetraazaporphine (($BrPh)_8$TAP); (j) 2,3,7,8,12,13,17,18-(4-nitrophenyl)-tetraazaporphine (($NO_2Ph)_8$TAP).

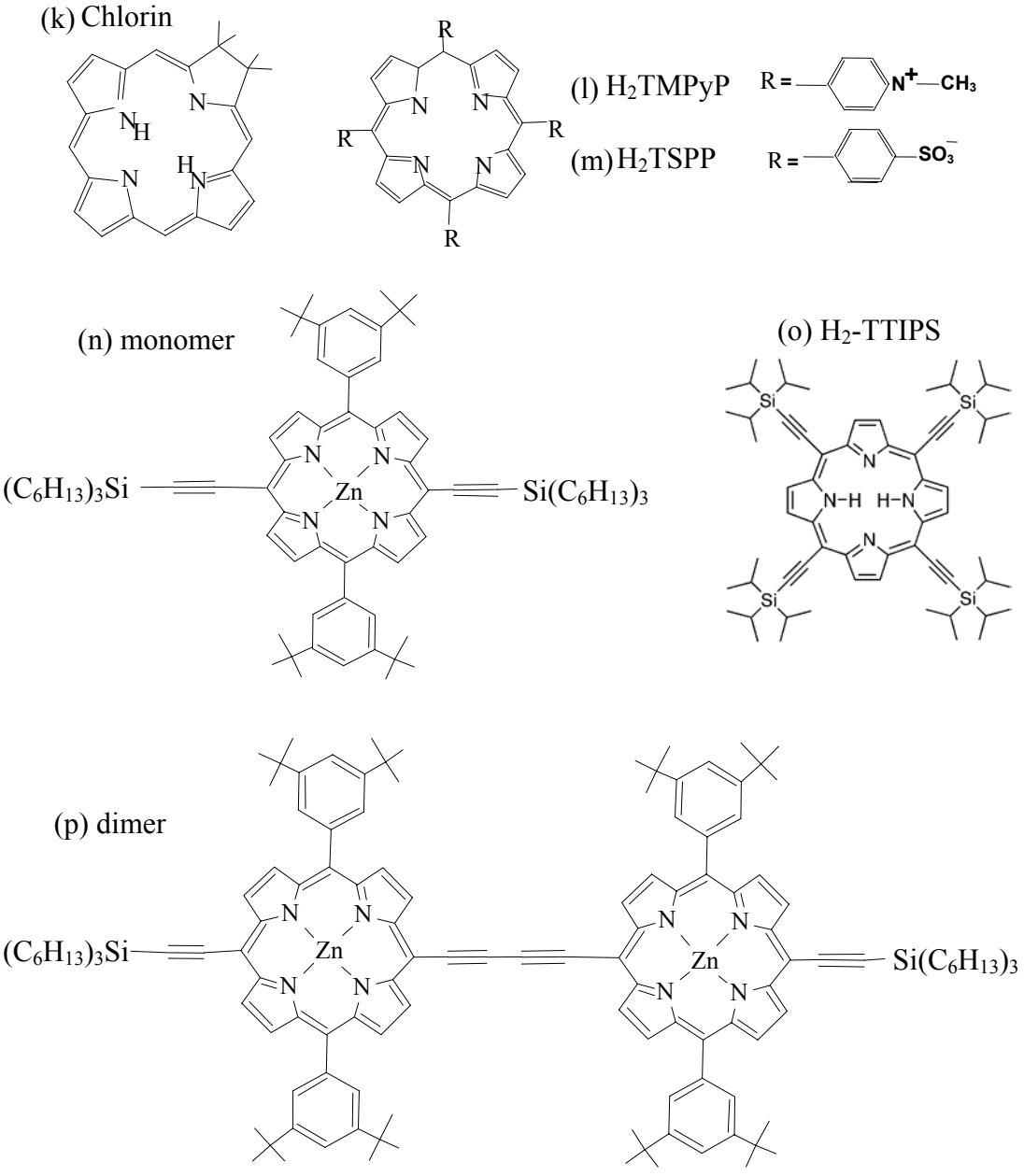

Figure 3.4 (k-o) Chemical structures of the molecules studied in this chapter. (k) 7,8-dihydroporphine (chlorin) (l) 5,10,15,20-Tetrakis(4-*N*-methylpyridyl)-porphine (H_2TMPyP); (m) 5,10,15,20-Tetrakis(4-sulfonatophenyl)-porphine (H_2TSPP); (m) [5,15-bis(3,5-bi-tert-butylphenyl)-10,20-bis(trihexylsilylethynyl)porphyrinato]zinc(II) (monomer), (o) H_2-TTIPS (p) 5,5′-(1,3-butadiyne-1,4diyl)bis[10,20-bis(3,5-bi-tert-butylphenyl)-15-(trihexylsilylethynyl)porphyrinato]zinc(II) (dimer).

5,5′-(1,3-butadiyne-1,4-diyl)bis[[10,20-bis(3,5-bi-tert-butylphenyl)-15-(trihexylsilylethynyl)porphyrinato]zinc(II) (dimer), and H_2TTIPS were synthesized by the Prof. H. L. Anderson group* [138,139].

For experiments at room temperature all the samples except chlorin were dissolved in dichloromethane (CH_2Cl_2), toluene (C_7H_8), pyridine (C_5H_5N) or water (H_2O) at concentration 10^{-5} – 10^{-4} M. For experiments with chlorin at room temperature and H_2TTIPS at low temperature the compounds were embedded into polyvinylbutyral (PVB) (Aldrich) polymeric film.

In case of H_2TTIPS the sample was prepared by mixing a dichloromethane-pyridine (95:5) solution of dye with dichloromethane solution of PVB powder and casting the mixture on a glass substrate overnight. The resulting films were removed from the glass substrate after evaporation of the dichloromethane and pyridine. Linear absorption spectra were measured with Lambda 900 Perkin Elmer spectrophotometer.

The experimental setup is shown in Figure 3.5. The laser system comprised a Ti:sapphire regenerative amplifier (CPA-1000, Clark, MXR), which was operated at 1 kHz repetition rate and produced 150-fs duration pulses (FWHM) of 0.8 mJ energy per pulse at wavelength λ = 770 - 815 nm. Both fundamental wavelength and second harmonic of the regenerative amplifier (λ = 385 - 405 nm) were used for two-photon cross section measurements. Figure 3.6 shows typical spectra of the first (a) and second (b) harmonics and autocorrelation function (c) of the first harmonic.

---

*Prof. H. L. Anderson, University of Oxford, Chemistry Department, Dyson Perrins Laboratory, South Parks Road, Oxford, OX1 3QY U.K.

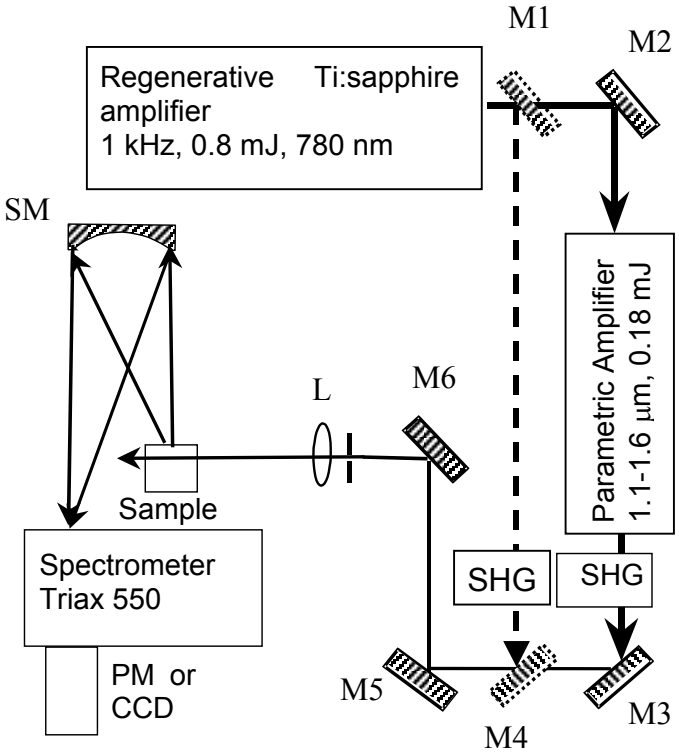

Figure 3.5 Schematic of experimental setup: SHG – second harmonic generator; PM – photomultiplier; M1 – M6 – mirrors; SM – spherical mirror, L – lens.

The fundamental pulses from the regenerative amplifier were parametrically down-converted in an optical parametric amplifier (TOPAS, Quantronix), which yielded 100-fs long pulses (FWHM) continuously tunable in the wavelength range from 1.1 to 1.6 μm with energy 100-200 μJ per pulse (signal) or 1.6 – 2.6 μm with energy 50 μJ per pulse (idler). Again, both fundamental wavelength and second harmonic were used for TPA cross section and spectral measurements. Figure 3.7 shows typical spectra of the first (a) and second (b) harmonics and autocorrelation function (c) of the first harmonic.

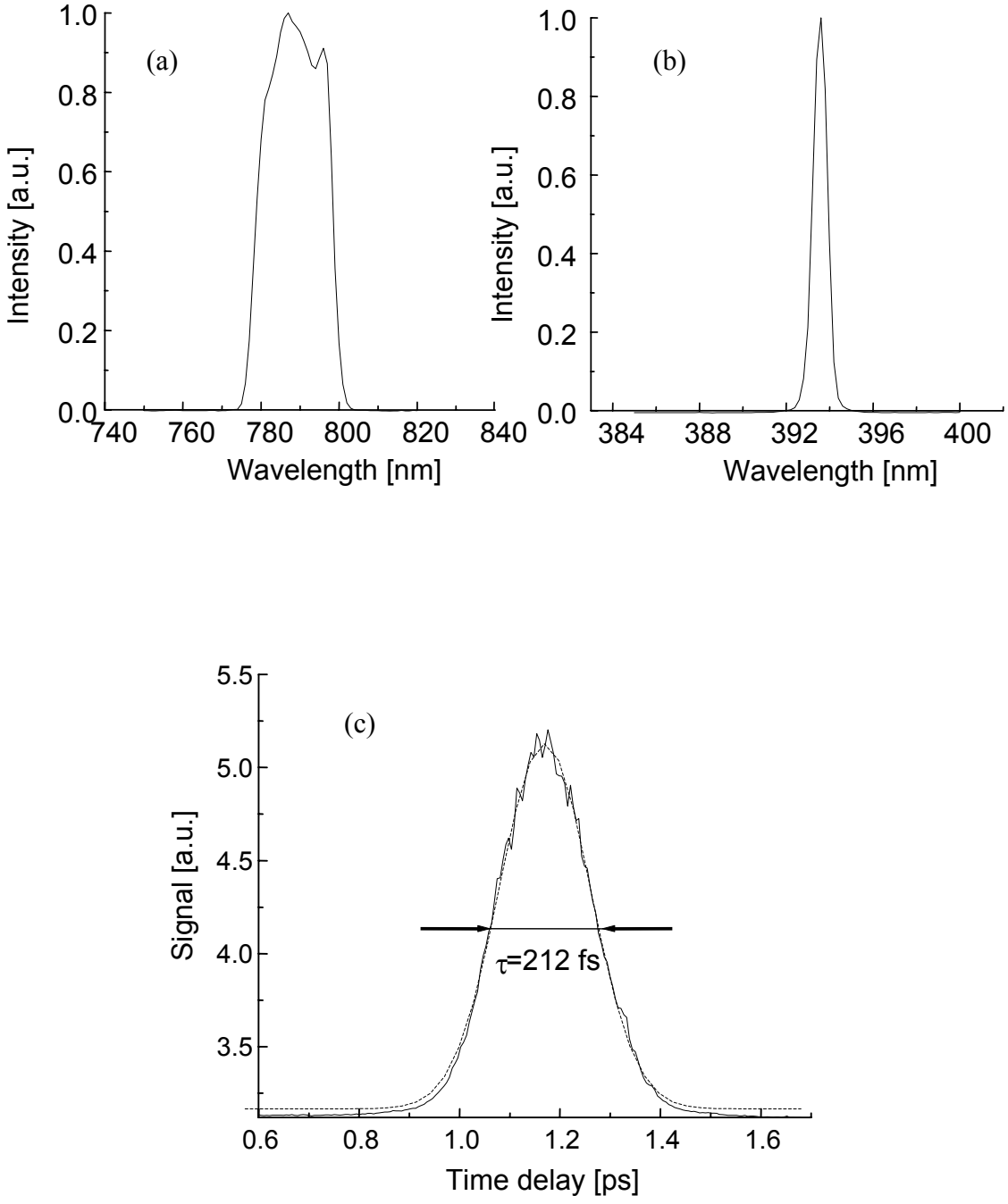

Figure 3.6 Typical laser spectra and autocorrelation function of regenerative amplifier: (a) fundamental harmonic; (b) second harmonic; (c) autocorrelation function (solid) and Gaussian fit (dashed)

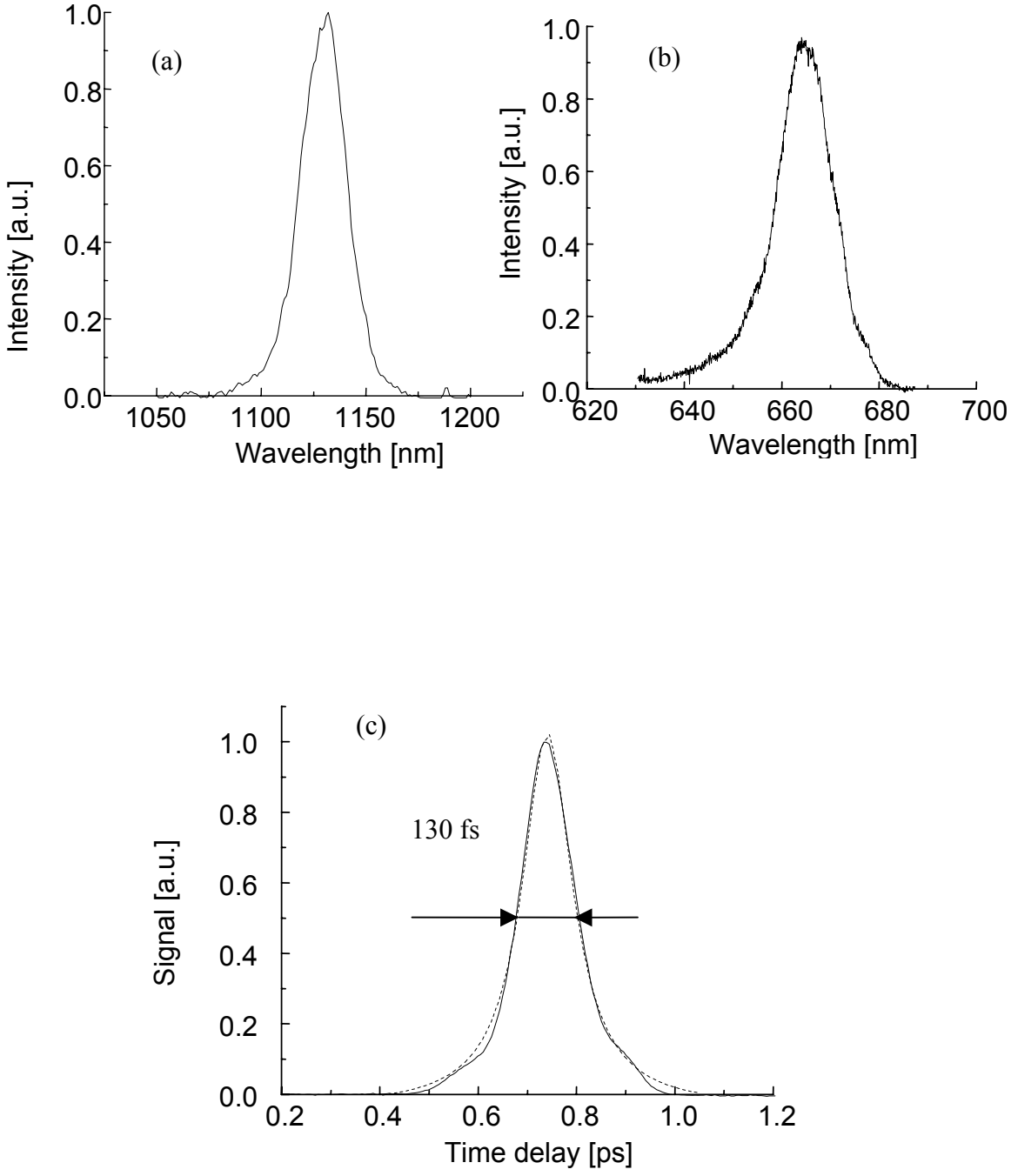

Figure 3.7 Typical laser spectra and autocorrelation function of optical parametric amplifier: (a) fundamental harmonic; (b) second harmonic; (c) autocorrelation function (solid) and Lorentzian fit (dashed)

The laser spectrum was recorded with either a Lambda 900 Perkin Elmer spectrophotometer coupled with a light-collecting fiber or with TRIAX 550 Jobin Yvon/Spex spectrometer. The duration and temporal profile of the femtosecond pulses were measured with an auto-correlator (Clark-MXR, AC-150). The laser power was measured with (1) Coherent, Fieldmaster, LM10, 1mW – 300 mW, (2) Molectron, EPM 2000, J3-02, 0.249 mW – 249 mW, and (3) ILX Lightwave OMM 6810, power below 0.249 mW. Since ILX Lightwave powermeter is not designed to measure energy of the femtosecond pulses, it was calibrated using Molectron, EPM 2000, J3-02 and a set of neutral density filters. Figure 3.8 shows the calibration curve for the near-UV (λ = 390 – 400 nm) femtosecond ($\tau \approx 150$ fs) pulses.

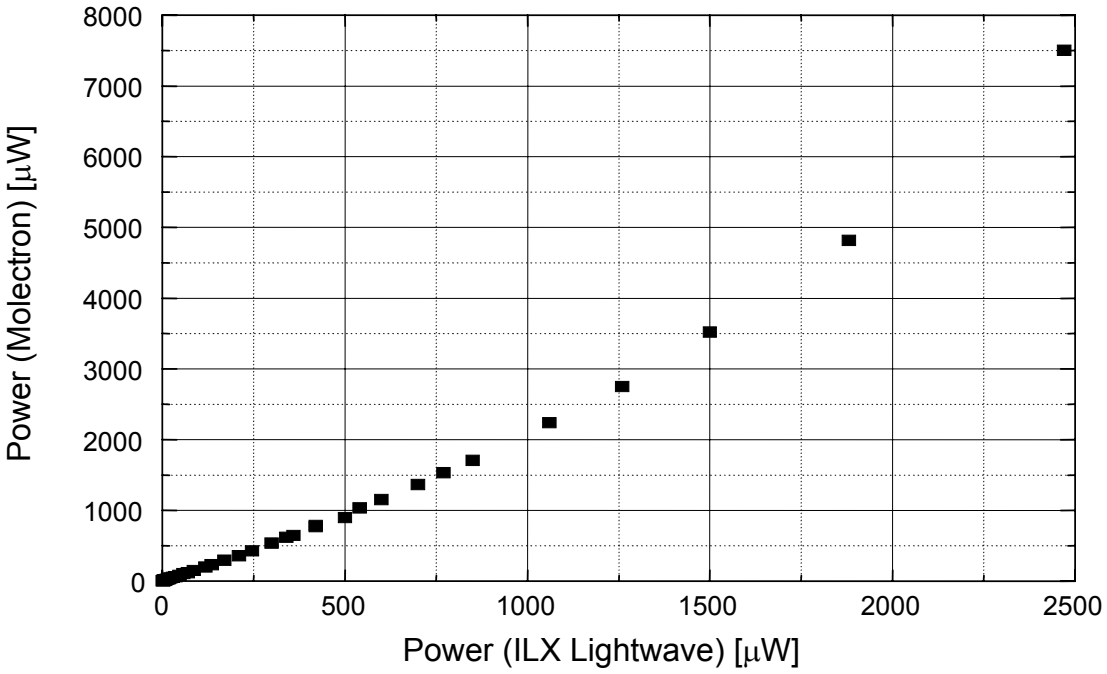

Figure 3.8 Calibration data for ILX Lightwave powermeter. The ILX powermeter is not designed to measure energy of the femtosecond pulses. It was calibrated with Molectron powermeter and a set of neutral density filters with known transmittance. The x-axis shows power measured with ILX powermeter, the y-axis shows the real power, measured with Molectron powermeter.

The curve was used to measure power of the second harmonic of regenerative amplifier, when it was used for one-photon excitation of the samples in two-photon cross section measurements (see below).

At low power ($I^{(ILX)}$ < 1000 μW) the following empirical expression was used to calculate the real power:

$$I^{(laser)} = kI^{(ILX)}, \tag{3.1}$$

where $I^{(laser)}$ is the power of the laser, $I^{(ILX)}$ is the power measured by ILX powermeter, and k is the coefficient determined from the Figure 3.8:

$$k = 1.43 + 0.00073I^{(ILX)}, \tag{3.2}$$

where $I^{(ILX)}$ must be substituted in [μW].

The fluorescence signal was collected with a spherical mirror (f = 50 cm) and focused on the entrance slit of TRIAX 550 Jobin Yvon/Spex spectrometer. The intensity of the fluorescence was measured either with a photomultiplier (Hamamatsu, HC120-05) or with a liquid nitrogen cooled CCD array (Jobin Yvon/Spex CCD-3000). In case of the photomultiplier, the signal was further amplified by a lock-in amplifier (Stanford Research Systems, SR830 DSP).

Some measurements with H_2TTIPS were performed at low temperature (T = 4.2 – 300 K). In this case the compound was doped into (PVB) polymer film and placed into a variable-temperature cryostat A-240 (Institute of Physics, Kyiv, Ukraine), which was cooled either with liquid nitrogen or liquid nitrogen and liquid helium. The temperature was stabilized (ΔT = ± 1K) by temperature regulator UTRECS K.41 (Institute of Physics, Kyiv, Ukraine).

TPA by the samples is established by the appearance of fluorescence quadratically dependent on the pumping power. Note, that because of nonlinear nature of TPA (see equation (2.3)), what is important for efficient two-photon excitation is not the total energy emitted by the laser but its peak intensity. It is straightforward to show, using pulses with rectangular time profile, that for pulsed lasers with the same average but different instantaneous power the total fluorescence signal emitted by the two-photon excited molecules is inverse proportional to the laser duty circle. TPA-induced fluorescence signal excited by the laser system in our laboratory is about $7 \cdot 10^9$ (Ti:sapphire amplifier, 1 kHz, 150 fs) times larger than the signal excited by cw laser with the same average power, which explains the use of femtosecond laser system for TPA studies. The average energy output of the Ti-sapphire amplifier is 0.8 W, which can easily be beaten by any household lamp. Nevertheless, the high peak intensity of the pulsed femtosecond laser allows detecting TPA, which is definitely impossible if one uses a lamp as an excitation source. In contrast, the efficiency of OPA does not depend on the light intensity if a sample is far from saturation. The total amount of one-photon absorbed photons is determined only by the total energy applied to the sample, no matter what excitation source is used.

Although TPA was first observed more than forty years ago, reliable and accurate measurement of absolute value of two-photon cross section still represents a technically challenging problem. Different methods developed for σ_2 measurements can generally be divided into two categories: (a) nonlinear transmittance-based and (b) fluorescence-based. The transmittance-based methods (the main such method is called Z-scan [140])

measure excitation laser light transmittance through the sample. Fluorescence-based methods use two-photon excited fluorescence signal as a measure of the TPA efficiency. In the last case, two-photon excited fluorescence is often compared to some reference compound or to the one-photon excited fluorescence of the same compound. Often the results obtained by different methods disagree with each other. Table 3.1 compares pros and cons of the two approaches.

Table 3.1 Comparison of the two main experimental techniques used for two-photon cross section measurements, fluorescence-based and Z-scan. The signs "+" and "-" mark advantages and disadvantages.

Comparison parameter	Fluorescence method	Nonlinear Transmittance (Z-scan)
Pulse duration dependence	+ weak	- strong, value of the measured TPA cross section changes by several orders of magnitude when going from nanosecond to femtosecond laser pulses
Required excitation intensity	+ < 20 GW/cm^2, can be further reduced	- 40 – 180 GW/cm^2, TPA is masked by other nonlinear effects like white light generation, stimulated emission, etc.
Background	+ background free method	- weak signal on top of the strong background
Required concentration of the studied compound	+ 10^{-5} – 10^{-4} M	- 10^{-2} M such large concentration leads to the aggregation of studied molecules, changing their photophysical properties
Fluorescence	- studied compound must fluoresce	+ fluorescence is not required

One of the many problems encountered in two-photon cross section measurements is strong dependence of measured σ_2 on the duration of the laser pulses

used for two-photon excitation. It is generally agreed that this dependence is caused by one-photon excited state absorption, for example $S_n \leftarrow S_1$ (see Figure 3.2) [141]. If the excitation pulses are in the nanosecond range, then the molecules excited by means of TPA by the front of the pulse can participate in OPA of the rest of the pulse from their excited states. Since the efficiency of one-photon excitation is usually much larger than the efficiency of two-photon excitation it may lead to large overestimation of the two-photon cross section. Excited state absorption is particularly critical for nonlinear transmittance-based methods, because then OPA from the excited state contributes to the decrease of the transmittance signal.

Fluorescence-based methods are less affected by excited state absorption because one-photon excitation from the first singlet excited state is followed by internal conversion back to the first excited singlet state (Figure 3.2). When a molecule fluoresces, it produces only one photon for the fluorescence signal no matter how many times it was recycled through one-photon excited state absorption process. This is because fluorescence from the higher excited states, $S_n \rightarrow S_o$, where $n>1$, is highly unlikely (Figure 3.2).

The only reliable way to overcome excited state absorption is to use sufficiently short laser pulses of few picoseconds or less. It is generally agreed among the experimental groups in this area that excited state absorption does not pose a problem only if two-photon excitation is performed by femtosecond laser pulses.

Another type of encountered experimental difficulties is that large excitation light intensities, required for TPA, may lead to undesired side-effect such as stimulated

emission, Raman scattering, self-phase modulation, plasma and white light continuum generation and others. Strong side-effects can easily mask the TPA. Again, nonlinear transmittance methods are plagued by this problem much more than fluorescence-based methods.

The fluorescence-based techniques typically belong to zero-background type of experiments. Modern photomultipliers and CCD are very sensitive instruments, so that single-photon counting level of registration is possible. Moreover, one can accumulate a weak signal using a cooled CCD. As a result, much lower excitation light intensity is required in fluorescence-based experiments (see Table 3.1). Typically, unwanted side-effects can be eliminated by decreasing the intensity. In contrast, nonlinear transmittance experiments require high intensity (see Table 3.1) and have strong background signal, therefore often making interpretation of the data somewhat ambiguous [142].

Since nonlinear transmittance-based methods are much less sensitive by their nature, a large concentration of the studied molecules is required to obtain signal from the strong background. Typically, concentration on the order of 10^{-2} M is used, which is 100-1000 times larger as compared to the fluorescence measurements. At so high concentrations, many molecules start to aggregate changing their photophysical properties. As a result, sometimes it is not clear two-photon cross section of what material has been measured.

The main disadvantage of fluorescence-based methods is that the molecules must fluoresce. In our experiments we found that we can easily detect two-photon excited fluorescence of molecules with moderate two-photon cross sections and with quantum

yield of fluorescence below 1% at concentration around 10^{-5} – 10^{-4} M. It means that the fluorescence method is suitable for all of the compounds studied in this work.

Surprisingly, nonlinear transmittance methods, in particular Z-scan, are very popular for two-photon cross section measurements. In our opinion, it is mainly because of its simplicity. We have chosen to use fluorescence-based method in our experiments. In particular, we use a method consisting in comparison of the efficiency of one- and two-photon excitation of fluorescence. An important advantage of this method is that it is absolute by its nature, i.e. we do not need to use a reference compound. Taking into account disagreement between two-photon cross sections measured by different authors, it seems extremely important. The method was first proposed by M. D. Galanin and Z. A. Chizhikova [143] and latter used with some modifications in a number of studies [83,144,145].

We obtained the following expression for evaluation the two-photon cross section (see Appendix B for details):

$$\sigma_2 = \sqrt{\frac{2\pi^3}{\ln(2)}} \frac{F_{TPA} h \nu_{TPA}^2 g \tau r_0^2 \left\langle I_{OPA} \right\rangle}{p F_{OPA} \nu_{OPA} \left\langle I_{TPA} \right\rangle^2} \sigma_1 . \tag{3.3}$$

Here F_{TPA} and F_{OPA} are the intensities of two- and one-photon excited fluorescence, ν_{TPA} and $\left\langle I_{TPA} \right\rangle$ are the frequency and average intensity of the laser light used for two-photon excitation, ν_{OPA} and $\left\langle I_{OPA} \right\rangle$ are the frequency and average intensity of the laser light used for one-photon excitation, g is the repetition rate of the laser used for two-photon excitation, τ is the pulse duration (FWHM) of the laser used for two-photon excitation, σ_1 is the extinction coefficient at the wavelength of one-photon excitation, r_0 is the pinhole

radius, p is equal to the ratio of the concentrations of the sample used for two-photon excitation and the sample used for one-photon excitation.

The following experimental procedure is followed. Initially, a sample is excited by means of two-photon excitation. Depending on the required wavelength, either Ti:sapphire regenerative amplifier or optical parametric amplifier (first or second harmonic) is used (Figure 3.5). The diameter of the laser beam is about 1 cm and 0.5 cm for the regenerative amplifier and the optical parametric amplifier, respectively. A 1.6 mm pinhole is used in front of the sample. The pinhole cuts off only the central part of the beam, which gives nearly constant intensity over the whole cross section. In this case, in addition to beam radius, the only parameters of the laser excitation light that are required are excitation wavelength, pulse duration (FWHM) (we suppose that temporal profile of the laser pulses is Gaussian), average intensity of the excitation light, repetition rate of the laser pulses, and intensity of the TPA- excited fluorescence.

The next step consists in one-photon excitation of the sample in the same geometry. The optical density of the samples used for one-photon excitation is less than 0.1 at the one-photon excitation wavelength and provides for constant excitation along the entire length of the cuvette. Typically, second harmonic of the Ti:sapphire regenerative amplifier is used ($\lambda_{ex} \sim 390$ nm). The fundamental wavelength of the amplifier is cut off from the excitation beam by a UV-filter. Note that the one-photon excitation of the sample is possible by any laser source because quantum yield of fluorescence of organic molecules does not depend on the excitation wavelength. We do not have to reach exactly the same electronic transition that was populated in the two-

photon excitation. The only parameters that one has to know in case of one-photon excitation are excitation laser wavelength, intensity of the excitation light, one-photon extinction coefficient at the one-photon excitation wavelength, and OPA-excited fluorescence intensity. This method allows to easily overcome problems related to excitation light scattering. Many one-photon fluorescence-based experiments are plagued by strong scattering of the excitation light which is spectrally close to the fluorescence. In our case one can choose any one-photon excitation wavelength. In particular we use λ_{ex} ~ 390 nm which is spectrally separated from the fluorescence spectra of all the studied molecules (λ_{fl} – 500 – 800 nm). By employing filters and/or monochromator one can easily cut off any scattering light. In case of TPA, the excitation scattered light is also easily separated from the fluorescence in the same way.

Note that if a monochromator is used, then integration of the fluorescence spectrum is not required. Since fluorescence spectrum is the same in both modes of excitation, it is enough to use signal at any particular wavelength. This considerably simplifies calculations because spectral response of the photomultiplier or CCD must not be taken into account. Moreover, if the sample with the same concentration is used for both one- and two-photon excitation then one does not have to worry about fluorescence reabsorption effects, because their influence on the detected fluorescence signal is exactly the same in both cases.

To obtain the TPA spectra in the 700 – 820 nm excitation wavelength region, the second harmonic of the optical parametric amplifier was used (Figure 3.5). In case of low fluorescence signal, the laser beam was focused with f = 25 - 200 cm lens on the sample.

The fundamental harmonic was cut off by dichroic mirrors with reflectance in the 700 – 900 nm or 600 - 800 nm wavelength range. Variable neutral density filter was used to equalize excitation photon flux at different wavelengths. The intensity of the fluorescence was measured as a function of the excitation wavelength. Since for large organic molecules, including tetrapyrroles, the quantum yield of fluorescence is independent of the excitation wavelength, the resulting fluorescence excitation spectrum, in effect, represents two-photon absorption spectrum in some arbitrary units. To calibrate the TPA spectra in absolute units of two-photon cross section we used the following procedure. We measured the absolute value of σ_2 at one particular wavelength, usually in a separate experiment, and then scaled the whole spectrum according to this value.

Our spectral range was limited from the long wavelength side to 820 nm by the longest wavelength of the signal that the optical parametric amplifier can generate, λ = 1640 nm. From the short wavelength side the limit was set by OPA of the molecules. The probability of one-photon excitation is usually much larger than the probability of two-photon excitation. As a result, if OPA is present, then TPA contribution into the resulting fluorescence signal is difficult to deduce. Note, that even small residual OPA by the long wavelength tail of the first absorption band (I-st Q band in tetrapyrroles) can be stronger than TPA[*]. For every point of the TPA spectrum we attested that the fluorescence intensity follows the square law, rather than linear dependence, to confirm that the fluorescence is excited by means of TPA. At shorter wavelengths (< 700 nm, depends on

[*] A detailed discussion of linear vs. quadratic absorption is given in the end of this chapter (see New Method for Measuring Absolute TPA Cross Section). It is shown there that the residual OPA by the long wavelength tail can be turned to our advantage and used in the new method of TPA cross section measurement.

the molecule) the power dependence gradually turns into linearone, preventing us from measuring TPA spectra.

In the 1.1 – 1.4 μm excitation wavelength region, the experimental procedure was the same as described above, except that fundamental wavelengths of the optical parametric amplifier were used for the excitation. In this case, the wavelength range of the TPA spectra was limited by the optical parametric amplifier from the short wavelength side (1100 nm is the shortest wavelength that it can generate). For the excitation wavelengths longer than 1400 nm (depends on the molecule) the signal practically disappeared because of the lack of TPA.

TPA Properties of Tetrapyrrolic Molecules in the Transitions Spectral Region Corresponding to the Q-bands.

Figure 3.9 shows the measured absolute TPA spectra of H_2TMPyP, H_2TSPP, H_2TPP, Bu_4TAP, $(NO_2Ph)_8$TAP, and Chlorin, in the laser excitation wavelength region λ_{ex} = 1100 – 1400 nm, along with OPA spectra in the corresponding transition wavelengths region (λ_{tr} = 550 – 700 nm). The solid lines and squares correspond to the OPA and TPA spectra. Note that the studied molecules belong to three different classes of tetrapyrrolic compounds, i.e. porphyrins: H_2TMPyP, H_2TSPP, H_2TPP, azaporphyrins: Bu_4TAP, $(NO_2Ph)_8$TAP, and one representative of chlorins. The linear absorption spectra of H_2TMPyP, H_2TSPP, and H_2TPP show four distinctive bands that are specific for porphyrins (see Figure 3.1b).

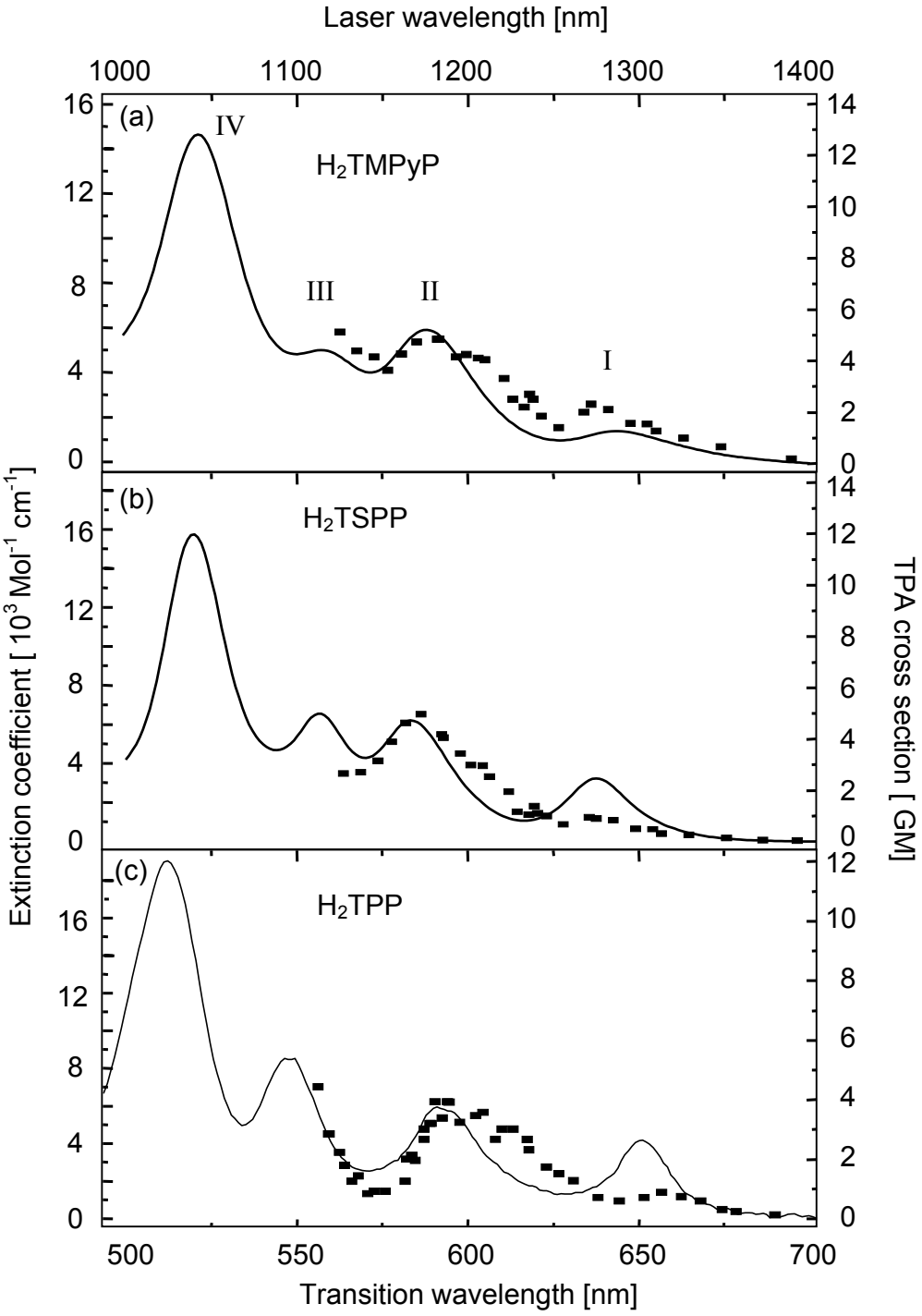

Figure 3.9 (a-c) TPA spectra in the Q bands spectral region. Squares – TPA spectrum; Solid line - linear absorption spectrum. (a) H_2TMPyP in water; (b) H_2TSPP in water; (c) H_2TPP in toluene.

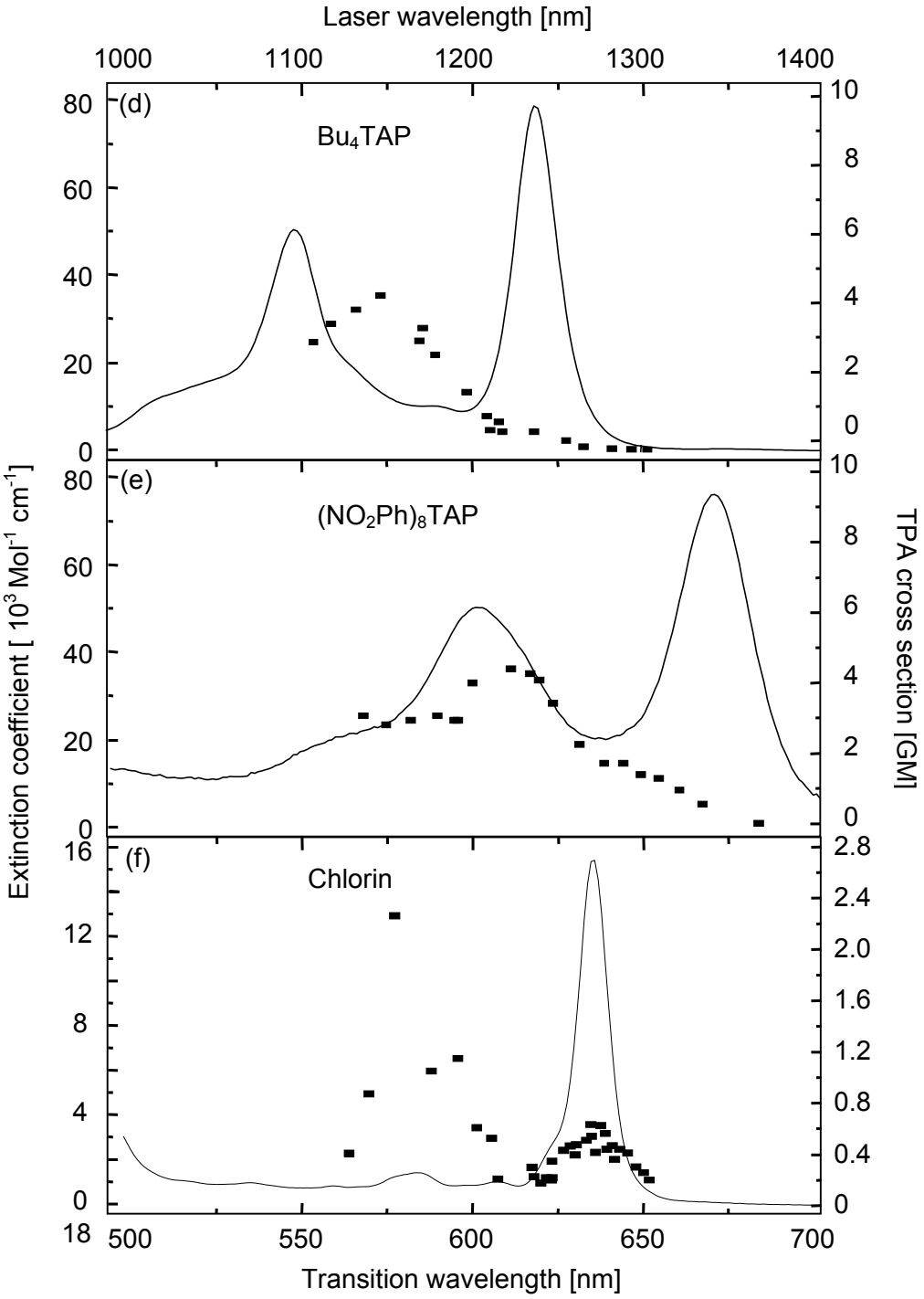

Figure 3.9 (d-f) TPA spectra in the Q bands spectral region. Squares – TPA spectrum; Solid line - linear absorption spectrum. (d) Bu_4TAP in dichloromethane; (e) $(NO_2Ph)_8TAP$ in dichloromethane; (f) chlorin in PVB film.

The linear spectra of azaporphyrins and chlorin are also typical for these kinds of tetrapyrrolic compounds with linear Q-bands stronger than in the porphyrins. The TPA spectra of the H_2TMPyP, H_2TSPP, H_2TPP and chlorin (Figure 3.9(a-c,f)) strongly resemble their linear absorption spectra. In contrast, TPA of tetraazaporphyrins, Bu_4TAP and $(NO_2Ph)_8$TAP (Figure 3.9(d,e)), shows only the vibronic satellite, while the Q(0-0) transition is missing.

At first glance, such different behavior may appear puzzling, especially in view of the parity selection rules (see Appendix A). Since all the molecules (except chlorin) possess a centrosymmetrical chemical structure (Figure 3.4(b,h,j-m)), one may expect that one- and two-photon spectra should be substantially different. Accidental degeneracy between one- and two-photon transitions can be ruled out, first, because several different porphyrins show similar coincidence of one- and two-photon transitions, and, second, because theoretical calculations place the first parity-allowed two-photon $g \leftarrow g$ transitions at a much higher energy, namely, near Soret band [107,119-133]. This means that we observe $u \leftarrow g$ type two-photon transitions making it even more puzzling.

Similar situation was encountered earlier upon investigation of TPA in several organic molecules. Anthracene represents a classical example. It is the first molecule in which this kind of behavior was observed and meticulously studied. When TPA of anthracene, which is a centrally-symmetrical organic molecule, was observed for the first time [146,147] at a single wavelength corresponding to the ruby laser frequency (14 400 cm^{-1}) it was supposed that there was a *gerade* parity level in the vicinity of twice the ruby laser frequency (28 800 cm^{-1}) so that the observed TPA corresponds to some $g \leftarrow g$

transition. However, theoretical calculations strongly contradicted this interpretation indicating that *gerade* parity levels in anthracene should be located at higher energies around 40 000 cm^{-1} [148]. It was also well known from linear spectroscopy that there are *ungerade* parity energy states originating around 25 300 cm^{-1}, which obviously implied that, in fact, one dealt with $u \leftarrow g$ type two-photon transition. Soon it became clear that the same effect takes place in a number of other organic molecules. Following are several explanations that were put forward at the time to resolve the apparent controversy.

I) The Hamiltonian describing an interaction of electrons with monochromatic light in semiclassical form is [149,150]:

$$H = -(e/mc)(\boldsymbol{P}\cdot\boldsymbol{A}) + (e^2/2mc^2)A^2, \tag{3.4}$$

where $\boldsymbol{A}$ is the vector potential of the radiation field, $\boldsymbol{P}$ is the momentum operator, c is the speed of light, m and e are the mass and charge of electron. When the transition probability is expended in terms of a power series in the electric charge, double-photon transitions can take place in first order by means of the A^2 term or in second order by ($\boldsymbol{P}\cdot\boldsymbol{A}$) term. Two-photon transition through ($\boldsymbol{P}\cdot\boldsymbol{A}$) term corresponds to the "classical" case of simultaneous TPA absorption considered by Göppert-Mayer in 1931 [78]. This kind of transition is prohibited between states of different parity in electric dipole approximation by symmetry considerations. The ability of A^2 term to cause TPA was first suggested by M. Iannuzzi [151,152], who showed that this kind of transition can take place between levels of different parity. Fortunately, a simple experiment can resolve if it is really A^2 absorption. The matrix element of the A^2 term vanishes for circularly polarized light so that if this term is important, the relative intensity of the fluorescence induced by the

linearly polarized light should be much larger than that from circularly polarized light. Another possibility is to measure polarization of the two-photon excited fluorescence, which should be very different for A^2- and ($\boldsymbol{P}\cdot\boldsymbol{A}$)-type processes [153]. Experiments showed that the intensity of the two-photon excited fluorescence in anthracene does not depend appreciably on polarization of excitation light [154]. The polarization dependence turned out to be much closer to the value corresponding to the ($\boldsymbol{P}\cdot\boldsymbol{A}$) term in TPA [153] thus ruling out the A^2 term as being responsible for two-photon $g \rightarrow u$ transitions in organic molecules. Further theoretical investigation also indicated that the contribution of this term should be negligible [150,155].

II) Another possibility to satisfy the parity selection rules is to consider ($\boldsymbol{P}\cdot\boldsymbol{A}$) term but suppose that one of the virtual transitions is a dipole transition and the other is either an electric quadrupole or magnetic dipole transition. However, the probability of such multipole transitions is smaller than that of the pure dipole transitions by a factor of $(a/\lambda)^2$, where a is the size of the molecule and λ is the wavelength. In optical region, this ratio is $10^{-6} - 10^{-7}$. An estimation suggests that the expected values of two-photon cross section for this type of transitions, $\sigma_2 \sim 10^{-2} - 10^{-3}$ GM, are too small to explain experimental results [4,149,155,156].

III) The final explanation, that turned out to be the right one, is that coupling between electronic and vibrational levels might partially allow two-photon transition between levels with different parity (Herzberg-Teller effect). If the final state comprises a superposition of odd parity electronic state together with odd parity vibration, the resulting state effectively has *gerade* parity thus partially lifting the prohibition for TPA.

An estimate shows that two-photon cross section of such transitions should be on the order of 1 GM (see for example [4]). The subsequent measurement of the TPA spectrum of anthracene confirmed vibronic nature of the observed two-photon transitions [157,158]. Further theoretical investigation showed that the observed two-photon transition in anthracene was indeed due to electronic-vibrational coupling and that this mechanism has rather general nature being responsible for observed TPA in a number of organic molecules [150,156-159].

To explain the experimentally observed similarity of the OPA and TPA spectra in some tetrapyrrolic molecules we note the following: 1) all tetrapyrroles have a wide set of vibrational modes of various degree of symmetry in the frequency range 300-3000 cm^{-1}, including non-centrosymmetrical vibrations; 2) two-photon cross sections of the studied tetrapyrroles are in the range of 1 – 10 GM. Similarly to the anthracene case we conclude that TPA of tetrapyrrolic molecules in the visible region results from the Herzberg-Teller effect. Different types of vibrations showing up in one- and two-photon bands can result in dissimilar shape of the II-nd linear Q-band and corresponding TPA band.

Vibrations, though, should not influence the pure electronic transition, and one still expects the TPA at the wavelength of the I-st Q band to be minimal. Both tetraazaporphyrins obey this rule quite well (Figure 3.9(d,e)), which is not the case for the rest of the molecules (Figure 3.9(a-c,f)). While for non-centrosymmetrical chlorin this kind of behavior is expected, for porphyrins it is rather surprising. The explanation that the TPA into pure electronic transition occurs either through electric quadrupole or magnetic dipole transitions is ruled out because the measured two-photon cross section σ_2

~ 1 GM is several orders of magnitude larger than expected for such processes. This leads us to the conclusion that non-azasubstituted porphyrins are not entirely centrosymmetrical. The lowering of electronic symmetry may occur because of substituents and also because of solvent effects (or both). This conclusion is further strengthened by the fact that in chlorin, which is a distinctly non-centrosymmetrical molecule, the 0-0 band is especially well pronounced in the TPA spectrum. Also, a slightly broken symmetry of porphyrins can explain why the vibronic satellites tend to be stronger than the pure electronic band. Absence of an exact center of symmetry allows weak TPA in both bands, however, a coupling between electronic and vibronic motion significantly enhances the II-nd Q band. In fact, by comparing the relative TPA intensities of the II-nd and I-st Q bands, one can qualitatively estimate to what degree the molecule's symmetry is preserved.

In conclusion, TPA spectra of tetrapyrrolic molecules in the visible part of spectrum are obtained for the first time. Measured two-photon cross sections are rather weak. This is explained by the lack of strong two-photon allowed $g \leftarrow g$ transitions in this spectral region. Weak TPA into one-photon Q-states is observed because of breaking of central symmetry by substituents and/or by solvent effects and because of vibronic coupling.

Resonance Enhancement of TPA in the Spectral Region Corresponding to One-Photon Soret Transition

Figure 3.10 presents TPA spectra of ZnTPTBP, H_2TBP, Bu_4TAP, $(NO_2Ph)_8$TAP, H_2TPP, and ZnOEP in the region of Soret transition (~ 350 – 410 nm transition wavelength). The data shows that the characteristic value of two-photon cross section in this region is considerably larger than that in the Q-bands region. The maximum σ_2 values in Soret region are in the range ~ 20 – 1600 GM as compared to ~ 1 – 7 GM in the Q-bands region. The most significant increase of TPA cross section takes place in $(NO_2Ph)_8$TAP (Figure 3.10d) resulting in σ_2 = 1600 GM which is one of the largest two-photon cross sections ever obtained for tetrapyrrolic molecules. In all cases the TPA increases monotonically towards shorter wavelengths. In tetraazaporphyrins it qualitatively follows the linear absorption, whereas in all the other porphyrins the behavior of the TPA spectrum is completely different from that of the linear absorption. Strong OPA into first linear absorption band $S_1 \leftarrow S_0$ prevented us from measuring TPA spectra further into near-UV.

To explain the strong increase of σ_2 in Soret region one has to take into account that, if the laser excitation frequency ω is close to the frequency of some real intermediate transition ω_{mg}, then strong resonance enhancement of TPA takes place (see Chapter 2 Theoretical Treatment of TPA for details). The following equation demonstrates the resonance nature of the TPA:

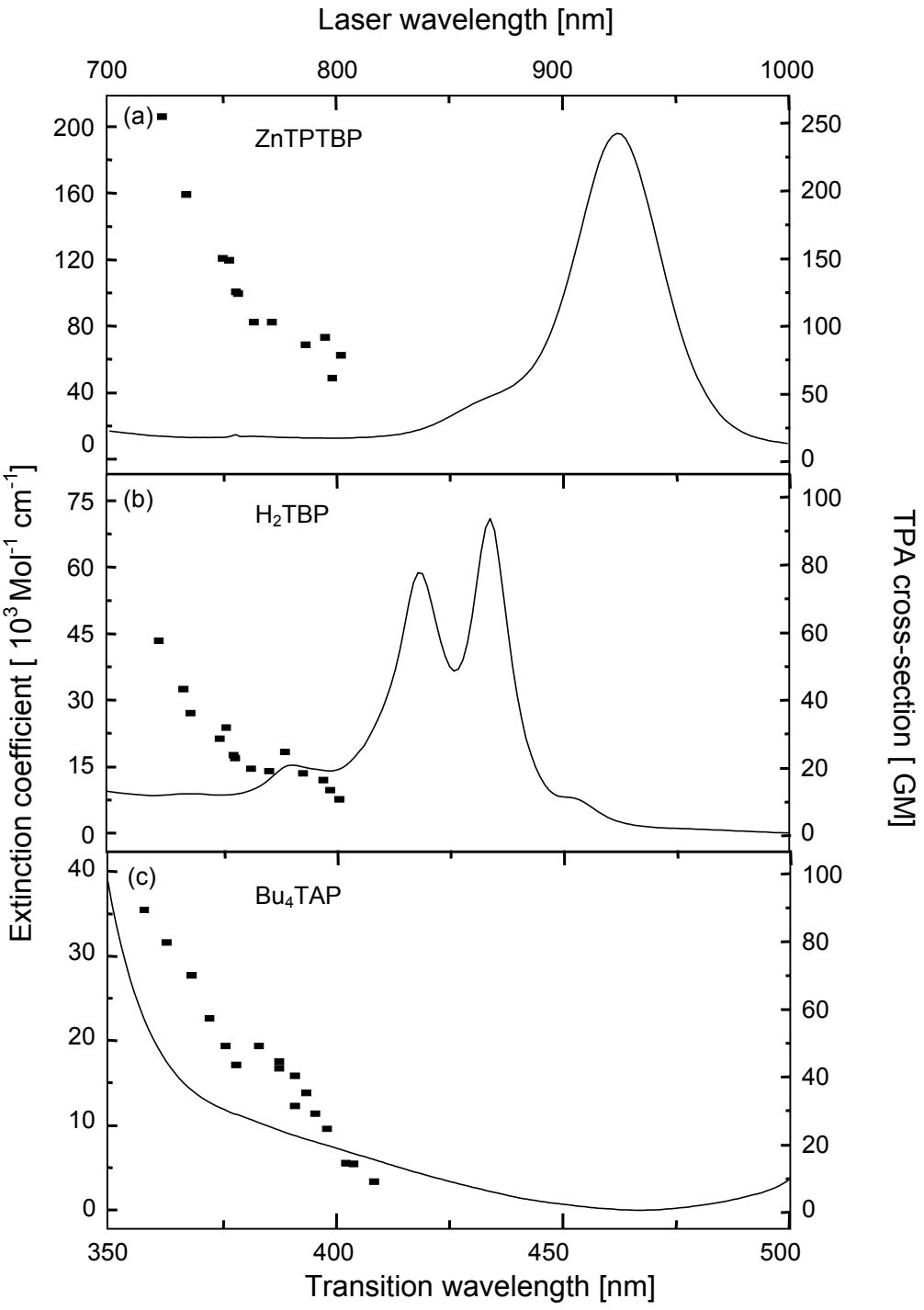

Figure 3.10 (a-c) TPA spectra in the Soret band spectral region as a function of transition wavelength. Squares – TPA spectrum; Solid line – linear absorption spectrum. (a) ZnTPTBP in toluene; (b) H_2TBP in pyridine; (c) Bu_4TAP in dichloromethane.

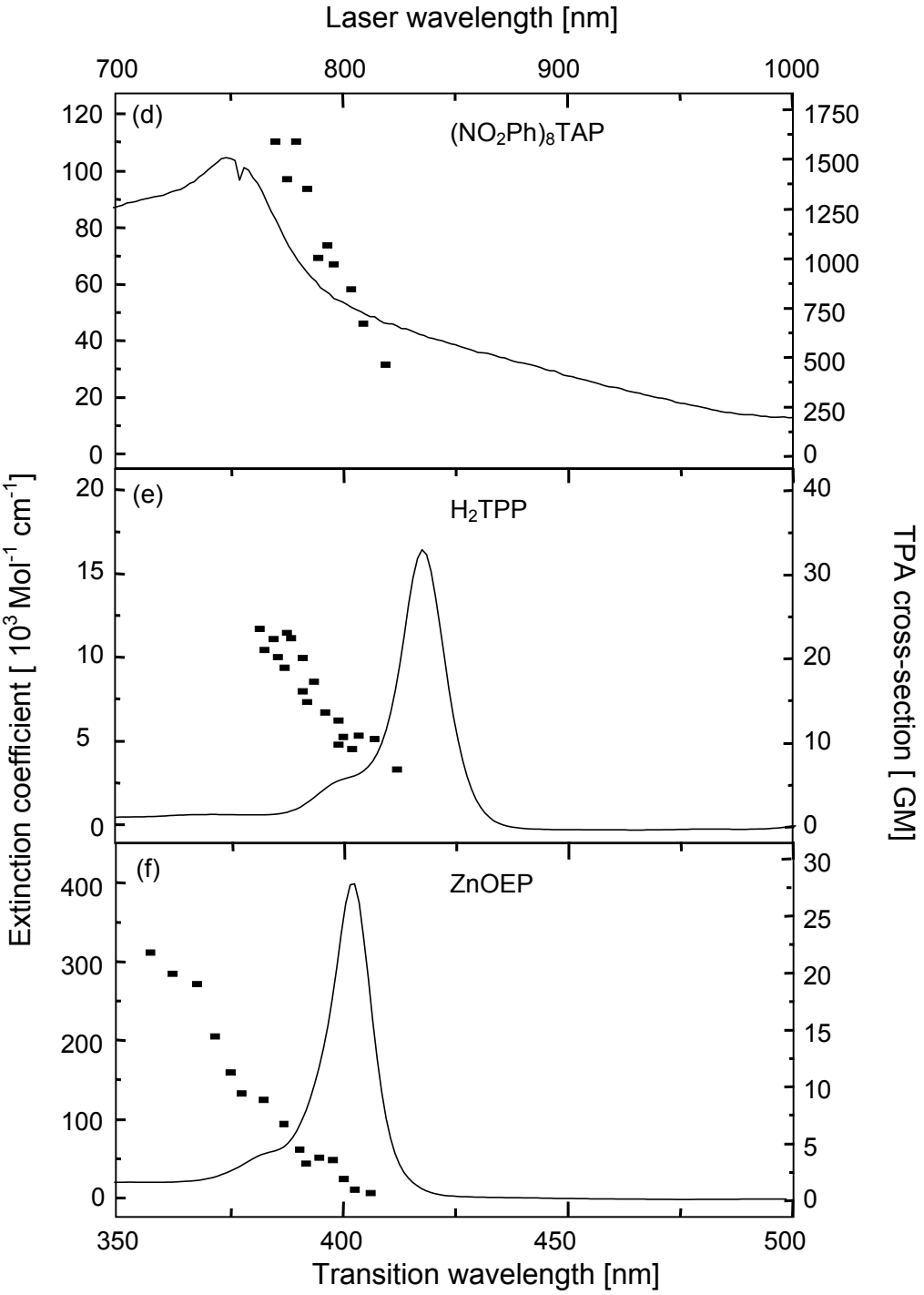

Figure 3.10 (d-f) TPA spectra in the Soret band spectral region as a function of transition wavelength. Squares – TPA spectrum; Solid line – linear absorption spectrum. (d) $(NO_2Ph)_8TAP$ in dichloromethane; (e) H_2TPP in toluene; (f) ZnOEP in dichloromethane.

$$\sigma_2(\omega) \sim \left| \sum_m \frac{(\boldsymbol{\mu}_{fm}\boldsymbol{e})(\boldsymbol{\mu}_{mg}\boldsymbol{e})}{(\omega_{mg} - \omega) + i\Gamma_m(\omega)} \right|^2 . \tag{3.5}$$

Note that the enhancement occurs without actually populating the intermediate level ω_{mg}. This would result in a step-wise absorption, which is a different process.

Due to selection rules (see Appendix A) the intermediate energy levels contributing to TPA should have *u*-parity and must be clearly distinct in linear absorption spectrum because $u \leftarrow g$ transitions are one-photon allowed (ground state has *g*-parity). For two-photon excitation into Q-bands, described in the previous section, the laser excitation frequency is far off from any intermediate level thus excluding any resonance enhancement. On the other hand two-photon excitation into near-UV region of spectrum makes use of photons with frequency being very close to the first Q-band. It is clear that the first Q-band represents the first intermediate energy level in equation (3.5) that can contribute to TPA. Indeed, the enhancement is observed in our experiments and described in what follows.

We verified that for every experimental point presented in Figure 3.9 and Figure 3.10, fluorescence intensity followed the quadratic dependence on the laser power. This is especially important for short-wavelength data points in Figure 3.10, where we made sure that OPA due to nearby I-st Q-band is insignificant. At even shorter wavelengths (not shown), the quadratic law gradually changes into linear one.

If the frequency detuning between laser and intermediate transition becomes small, then the resonance term may dominate over the contribution of all the other levels combined. In this case, the three-level model can be used to describe TPA. In this model

only three energy levels of a molecule are considered, namely ground level, two-photon excited level, and single intermediate level (see Chapter 2 Three-Level Model). For centrosymmetrical molecules, the sum in equation (3.5) then reduces to just one term corresponding to the resonance intermediate level (equation (2.36)):

$$\sigma_{fg}^{(2)}(\omega) = 2\frac{[2\cos^2(\alpha)+1]}{15}\frac{(2\pi)^4 \nu^2 L^4}{h^2 n^2 c^2}\frac{\left|\boldsymbol{\mu}_{fm}\right|^2 \left|\boldsymbol{\mu}_{mg}\right|^2}{(\nu_{mg}-\nu)^2+\Gamma_m^2(\nu)} g(2\nu)\,. \tag{2.36}$$

To obtain better quantitative picture of the resonance enhancement effect, we plot the TPA data points as a function of the laser frequency (rather than the transition frequency), along with the corresponding OPA in the Q-region (Figure 3.11) and apply three-level model to analyze the data. For ZnTPTBP, H_2TBP, and Bu_4TAP (Figure 3.11(a-c)) the laser frequency is rather close to the Q-resonance. For the rest of the molecules (Figure 3.11(d-f)) the detuning is larger and association with the resonance is less obvious. To perform quantitative analysis, we note that all the molecules in Figure 3.11 are centrosymmetrical. Correspondingly, three-level model for centrosymmetrical molecules can be applied to describe TPA spectra, i.e. we turn to equation (2.36). By assuming that line shape function $g(2\nu)$ is constant (the validity of this assumption in the spectral region of interest will be discussed below), and by differentiating equation (2.36) with respect to the laser frequency ν, the following relation between the normalized derivative of TPA spectrum and resonance frequency is obtained:

$$\alpha = \frac{1}{\sigma_2}\frac{d\sigma_2}{d\nu} = \frac{2}{\nu} + \frac{2(\nu_{mg}-\nu)}{(\nu_{mg}-\nu)^2+\Gamma_{mg}^2(\nu)}\,. \tag{3.6}$$

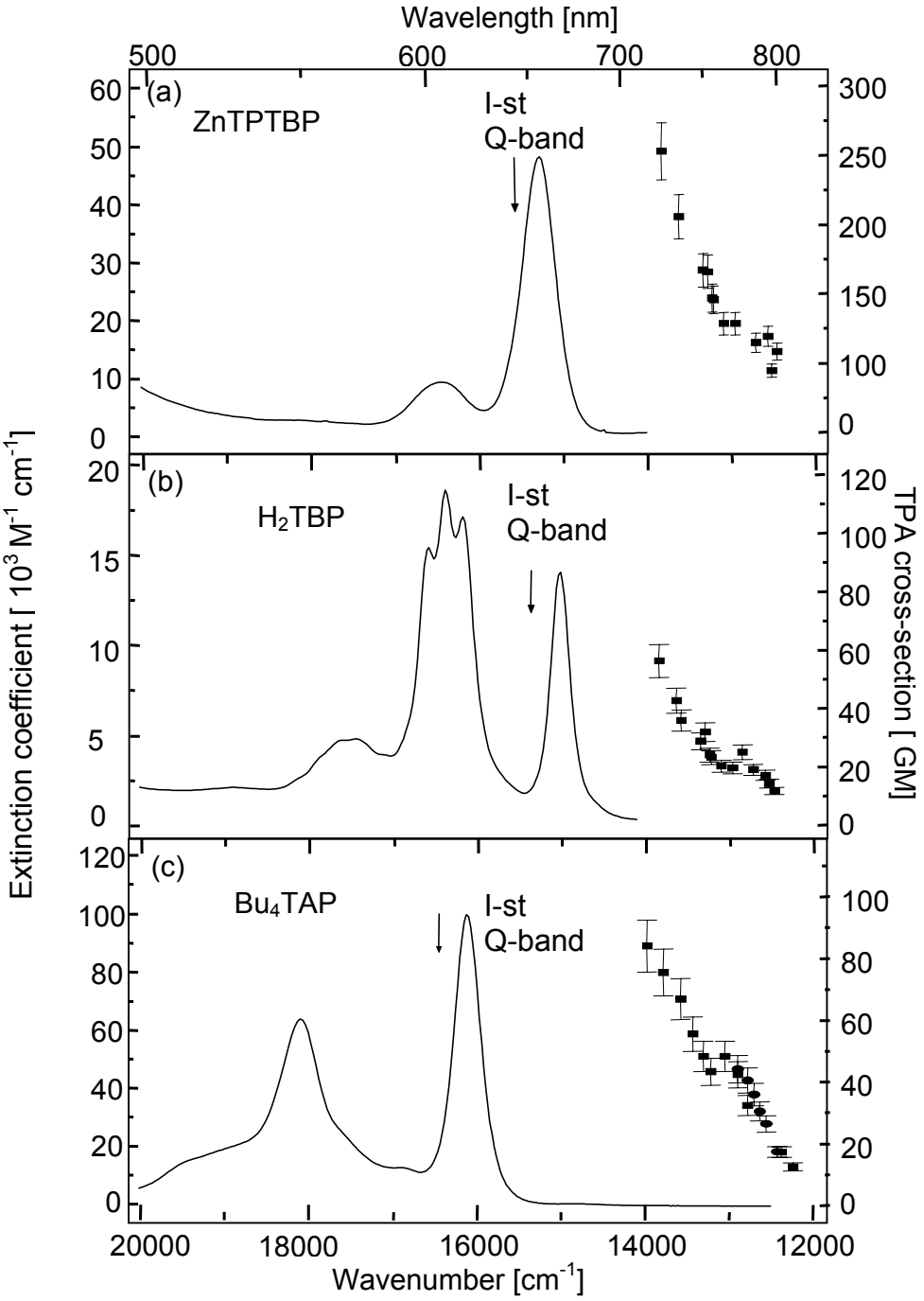

Figure 3.11 (a-c) Two-photon absorption cross section as a function of excitation photon frequency (one-half of the transition frequency) for the same molecules as in Figure 3.10. Squares – TPA spectrum; Solid line – linear absorption spectrum. Vertical arrows indicate frequency of the intermediate transition calculated according to equation (3.7).

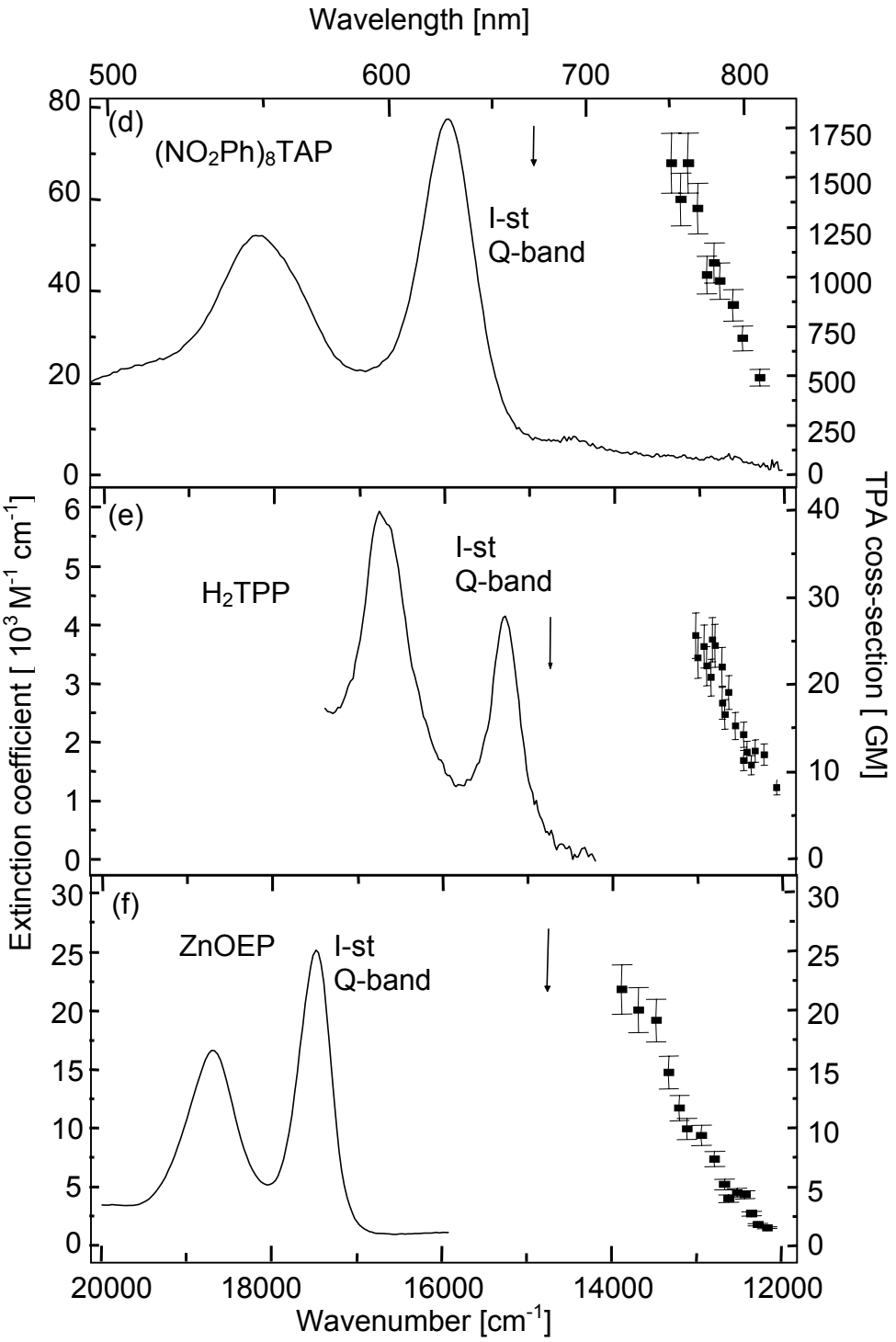

Figure 3.11 (d-f) Two-photon absorption cross section as a function of excitation photon frequency (one-half of the transition frequency) for the same molecules as in Figure 3.10. Squares – TPA spectrum; Solid line – linear absorption spectrum. Vertical arrows indicate frequency of the intermediate transition calculated according to equation (3.7).

By rearranging this relation, one can express the resonance frequency, ν_{mg}, as a function of experimentally measured parameters:

$$\nu_{mg} = \nu + \frac{\nu + [\nu^2 - \Gamma_{mg}^2 (\nu\alpha - 2)^2]^{1/2}}{\nu\alpha - 2}. \tag{3.7}$$

Vertical arrows in Figure 3.11 indicate effective ν_{mg} calculated according to the equation (3.7) and experimental data. We can use the deviation of the calculated frequency from the actual resonance frequency as a quantitative measure of the validity of the three-level approximation. From experimental point of view, this approach is rather reasonable because we have in our disposal only a relatively narrow section of TPA spectrum, which would hardly allow a good fit to full spectral line shape function, but is nevertheless sufficient for estimation of derivative at a particular frequency. An advantage of this approach consists also in using only relative values of TPA (one does not need absolute cross sections). Although the value of Γ_{mg} (homogeneous linewidth) is known only approximately, we can take it to be equal to the inhomogeneous line width of the first Q-band. In any case, if $\nu_{mg} - \nu \gg \Gamma_{mg}$, then the result is not very sensitive to the value of Γ_{mg}. For ZnTPTBP, H_2TBP, and Bu_4TAP we find a good agreement between the ν_{mg} and the actual first Q-band transition frequency (Figure 3.11(a-c)). The fact, that the actual resonance frequency is slightly lower than the estimated one, is easily explained by the contribution from the rest of the absorption bands, lying above the first Q-band, which are not accounted for in the three-level model.

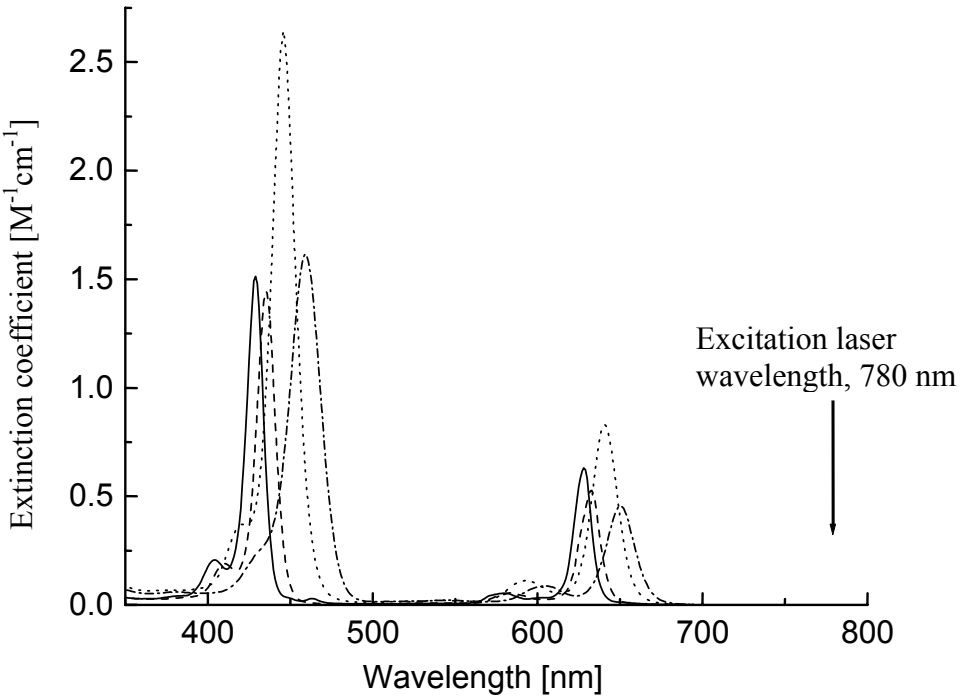

Figure 3.12 Linear absorption spectra of a series of phenyl-substituted Zn-tetrabenzoporphyrins. solid – ZnMPTBP, dash – ZnDiPTBP, dot – ZnTriPTBP, dash dot – ZnTPTBP. All the compounds are dissolved in toluene.

To confirm the role of the resonance enhancement by the first Q-transition even further, we compare the two-photon cross-section of closely related tetrabenzoporphyrins, namely H_2TBP, ZnMPTBP, ZnDiPTBP, ZnTriPTBP and ZnTPTBP (Figure 3.4(c-f)) at 780 nm (12821 cm^{-1}). The linear absorption spectra of Zn-substituted porphyrins are similar to that of ZnTPTBP, with the only difference that the intensity of the first Q-band slightly changes and it shifts to the red with increasing number of the phenyl substituents (Figure 3.12). As it was already shown above the TPA of H_2TBP and ZnTPTBP in near-UV is strongly dominated by resonance enhancement mechanism. If we suppose that the TPA cross-sections at 780 nm for the rest of the porphyrins, presented in Figure 3.12, are also mainly determined by the resonance enhancement mechanism, then the equation (2.36) predicts that TPA cross section should

be proportional to the linear transition dipole moment squared over frequency detuning squared:

$$\sigma_2 \sim \frac{\left|\boldsymbol{\mu}_{mg}\right|^2}{(\nu_{mg}-\nu)^2}, \tag{3.8}$$

provided that $\left|\boldsymbol{\mu}_{fm}\right|^2 g(2\nu)$ does not vary much from one molecule to another.

The following relation holds between the product $\left|\boldsymbol{\mu}_{fm}\right|^2 g(2\nu)$ and extinction coefficient $\varepsilon_{fm}(2\bar{\nu}-\bar{\nu}_{mg})$ of one-photon transition $f \leftarrow m$ from the intermediate state m to the final excited state f (see Appendix C for details):

$$\left|\boldsymbol{\mu}_{fm}\right|^2 g_{TPA}(2\nu) = \frac{\varepsilon_{fm}(2\bar{\nu}-\bar{\nu}_{mg})}{1.07\cdot 10^{38}\bar{\nu}_{fm}c}, \tag{C.10}$$

where the bar on top of the ν means that wavenumbers [cm^{-1}] are used instead of frequencies [Hz], $\bar{\nu}$ is the laser wavenumber [cm^{-1}], $\bar{\nu}_{mg}$ is the wavenumber of the $m \leftarrow g$ transition, $\bar{\nu}_{fm}$ is the wavenumber of the $f \leftarrow m$ transition, $\boldsymbol{\mu}_{fm}$ is the transition dipole moment of the $f \leftarrow m$ transition [e.s.u.], and c is the speed of light. Thus, one can use $\varepsilon_{fm}(2\bar{\nu}-\bar{\nu}_{mg})$ as a measure of variation of $\left|\boldsymbol{\mu}_{fm}\right|^2 g(2\nu)$ from one molecule to another. Indirect evidence that $\left|\boldsymbol{\mu}_{fm}\right|^2 g(2\nu)$ indeed does not vary too much is found in picosecond transient absorption data. These data are collected in Table 3.2, which shows the literature values of singlet excited state extinction, ε_{fm}, at λ_{fm} = 532 nm [134,160-162].

It is evident that the value of extinction coefficient does not vary more than 25% upon transition from a free base tetraphenylporphine (H_2TPP) to metallo-

tetraphenylporphyrins (ZnTPP and MgTPP) and to tetrabenzo-substituted porphyrins, (MgTBP and ZnTPTBP). Furthermore, it has been shown for various porphyrins that the transient singlet-singlet absorption spectra consist of a characteristic broad peak centered at approximately 440 – 510 nm, accompanied by a smooth tail in the region of 800 – 900 nm [134]. Whereas it is true that in our experiment we are probing a slightly different spectral region, corresponding to λ_{fm} ~ 790 - 1100 nm, we still can assume that for all the porphyrins in current series, the excited state absorption will be similar.

Table 3.2 Summary of one- and two photon absorption properties of tetraphenyl- and tetrabenzoporphyrins and ZnOEP.

Porphyrin	solvent	λ_{max}, nm	$\bar{\nu}_{mg}$, cm^{-1}	ε_{mg}(max), $mM^{-1}cm^{-1}$	$\Delta\bar{\nu}$, cm^{-1}	ε_{fm}(532nm) $mM^{-1}cm^{-1}$	σ_2, GM
H_2TPP	toluene toluene	647	15500	3.4	470	15[b] 16[c]	15
ZnTPP	CH_2Cl_2 toluene					16[b] 18[c]	
H_2TBP	Pyridine	666	15015	13	310		20
MgTBP	EP[a]			79		15[d]	
ZnMPTBP	toluene	628	15924	66	325		67
ZnDiPTBP	toluene	632	15810	56	370		50
ZnTriPTBP	toluene	641	15600	86	460		130
ZnTPTBP	toluene benzene	650	15385	49	510	19[e]	90
ZnOEP	CH_2Cl_2	571	17510	13	550	8[b]	4.4

[a] Diethyl ether/iso-propanol mixture (3/1, *v/v*).
[b] Ref. [134], [c] Ref. [160], [d] Ref. [161], [e] Ref. [162].

To make the plot of σ_2 as a function of $\left|\boldsymbol{\mu}_{fm}\right|^2 g(2\nu)$, we note that (see Appendix C for details):

$$\frac{\left|\boldsymbol{\mu}_{fm}\right|^2}{(\nu_{mg}-\nu)^2} \sim \frac{\varepsilon_{\max}(\overline{\nu}_{mg})\Delta\overline{\nu}_{mg}}{\overline{\nu}_{mg}(\overline{\nu}_{mg}-\overline{\nu})^2}, \tag{C.14}$$

where $\varepsilon_{\max}(\overline{\nu}_{mg})$ and $\Delta\overline{\nu}_{mg}$ are the maximum extinction coefficient [$M^{-1}cm^{-1}$] and halfwidth [cm^{-1}] of the transition $m \leftarrow g$, respectively.

Figure 3.13 shows the TPA cross-section of a series of tetrabenzoporphyrins, measured at 780 nm plotted as a function of linear absorption parameters $\varepsilon_{\max}(\overline{\nu}_{mg})\Delta\overline{\nu}_{mg} / \overline{\nu}_{mg}(\overline{\nu}_{mg}-\overline{\nu})^2$, taken from Table 3.2.

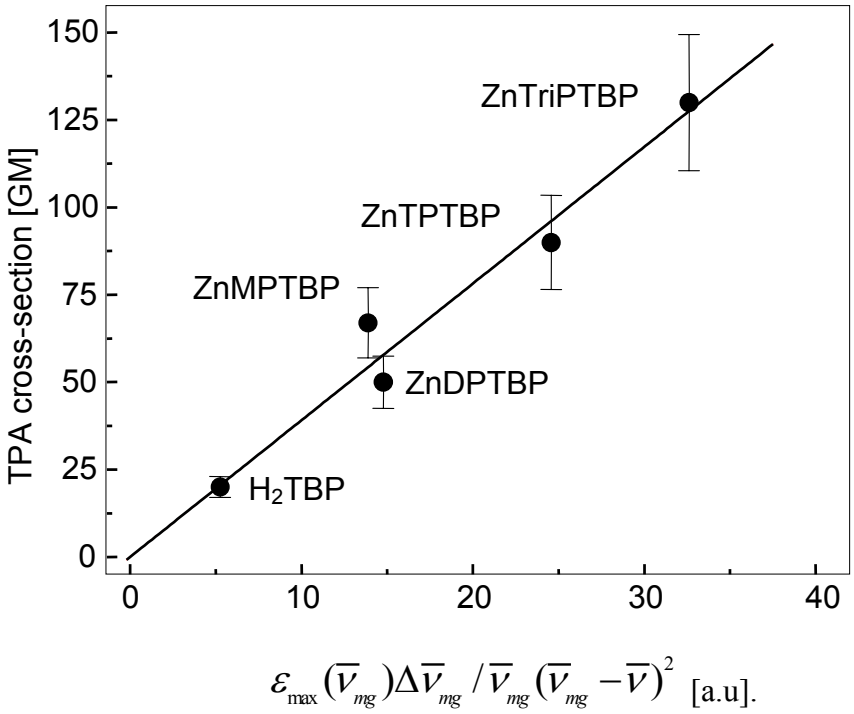

Figure 3.13 Correlation between two-photon absorption cross-section and a combination of linear absorption parameters for a series of tetrabenzoporphyrins. The plot clearly shows linear dependence of TPA cross section on the resonance factor confirming presence of strong resonance enhancement and validity of the three-level model.

The dependence is well fitted to a straight line. This result substantiates our earlier conclusion that there is indeed a quantitative relation between TPA cross section and resonance enhancement factor, $\left|\boldsymbol{\mu}_{mg}\right|^2/(\nu_{mg}-\nu)^2$. On the other hand, this fact also supports our conclusion about small variations of $\left|\boldsymbol{\mu}_{fm}\right|^2 g(2\nu)$ for studied molecules. Very illustrative in this sense is a behavior in a series of four phenyl-substituted tetrabenzoporphyrins. As the number of the phenyl substituents increases from one to four, the lowest absorption Q-band shifts to the red thus improving resonance condition with the laser frequency. The intensity of the first Q-band changes slightly when going from one porphyrin to another peaking for ZnTriPTBP. The resulting TPA cross section of ZnTriPTBP is the largest among tetrabenzoporphyrins. It is evident from Figure 3.13 that both effects, the improved resonance conditions as well as the change of the intensity of the first Q-band, contribute to the resulting two-photon cross-section increase. The presence of strong resonance enhancement and validity of the three-level model for benzoporphyrins is established.

Since the experimental measurement of two-photon cross section is often a time consuming and tedious process prone to experimental uncertainties, it is highly desirable to find some way to estimate σ_2 from easily obtainable linear absorption data. Simple theoretical estimate of TPA cross section is always a problem because expression describing σ_2 consists of infinite number of terms (see equation (2.27)). Moreover, not all parameters entering the expression (2.27) are accessible for measurement in the laboratory. In this respect, three-level model, consisting only of one term, proposes an elegant solution for this problem. Linear dependence of two-photon cross section

obtained above validates the use of three-level model to describe two-photon transitions of porphyrins in the near-UV region of spectrum. We use this fact to estimate σ_2 of one of the studied porphyrins in the framework of this model, i.e. we use equation (2.36). We choose ZnOEP because its transient absorption spectrum is known from literature [134].

Since the exact polarization of the $f \leftarrow m$ transition is not known, we assume for simplicity that $\boldsymbol{\mu}_{mg}$ and $\boldsymbol{\mu}_{fm}$ are parallel and use equation (2.37) instead:

$$\sigma_{fg}^{(2)}(\nu) = \frac{2}{5}\frac{(2\pi)^4 \nu^2 L^4}{h^2 n^2 c^2}\frac{\left|\boldsymbol{\mu}_{fm}\right|^2 \left|\boldsymbol{\mu}_{mg}\right|^2}{(\nu_{mg}-\nu)^2 + \Gamma_m^2(\nu)} g(2\nu)\,. \tag{2.37}$$

This will give us an upper estimation of σ_2. We calculate $L^4 = 3.0$ for $n = 1.4$ in CH_2Cl_2, and $L^4 / n^2 = 1.5$. The $\left|\boldsymbol{\mu}_{mg}\right|^2$ was found according to the following equation (see Appendix C, equation (C.13)):

$$\left|\boldsymbol{\mu}_{mg}\right|^2 = \frac{1}{1.07\cdot 10^{38}\bar{\nu}_{mg}}\frac{1}{2}\sqrt{\frac{\pi}{ln2}}\varepsilon_{\max}(\bar{\nu}_{mg})\Delta\bar{\nu}_{mg}\,. \tag{3.9}$$

From independently measured linear absorption parameters (see Table 3.2, last row) we obtained $\left|\boldsymbol{\mu}_{mg}\right|^2 = 4.1\cdot 10^{-36}$ [e.s.u.]. The product $\left|\boldsymbol{\mu}_{fm}\right|^2 g(2\nu)$ can be calculated using equation (C.10). The only unknown value of the singlet excited state extinction $\varepsilon_{fm}(2\bar{\nu} - \bar{\nu}_{mg})$ was obtained by extrapolating the dependence $\varepsilon_{fm}(\bar{\nu})$ [134] to the working frequency $2\bar{\nu} - \bar{\nu}_{mg} = 8000$ cm^{-1}, which gives $\varepsilon_{fm}(2\bar{\nu} - \bar{\nu}_{mg}) \approx 2\cdot 10^3 M^{-1}cm^{-1}$. Substituting all the parameters into equation (2.37), we obtain $\sigma_2 = 5.5$ GM. Taking into account simplifications made during the calculations, the agreement with the measured value of 4.4 GM is very good. Therefore, the single intermediate state approximation gives

quantitatively good estimation of TPA cross section of the studied porphyrins in near-UV.

We conclude that for the compounds shown in Figure 3.11(a-c) and tetrabenzoporphyrins the enhancement of TPA in Soret-band region is due to near-by intermediate first Q-band transition. For other molecules, however, the intermediate Q-band resonance cannot be singled out as the predominant mechanism. For them additional mechanisms should be considered as is discussed in the next sections.

Enhancement of TPA due to *g*-*g* transitions

One can see from Figure 3.11(d-f) that the calculated value of ν_{mg} is notably lower than the frequency of the first Q-band transition in $(NO_2Ph)_8TAP$, H_2TPP, and ZnOEP. Since the first Q-band is the lowest excited singlet electronic state in porphyrins, resonance enhancement cannot be the only factor responsible for strong TPA. In fact, this observation suggests that there are one-photon forbidden but two-photon allowed transitions in the Soret band region, which are not visible in the linear absorption spectrum. We are going to analyze this possibility by reevaluating an assumption made earlier that function $g(2\nu)$ is constant. In Figure 3.14 we plot the quantity $\sigma_2[(\nu_{mg}-\nu)^2+\Gamma_m^2(\nu)]/\nu^2$ as a function of 2ν for six different porphyrins. According to equation (2.36), if the above assumption is correct, then this plot should yield a horizontal straight line. If the opposite is true, then this plot should give effective spectrum of the line shape function, $g(2\nu)$, i.e. shape of pure two-photon allowed $g \leftarrow g$ transitions.

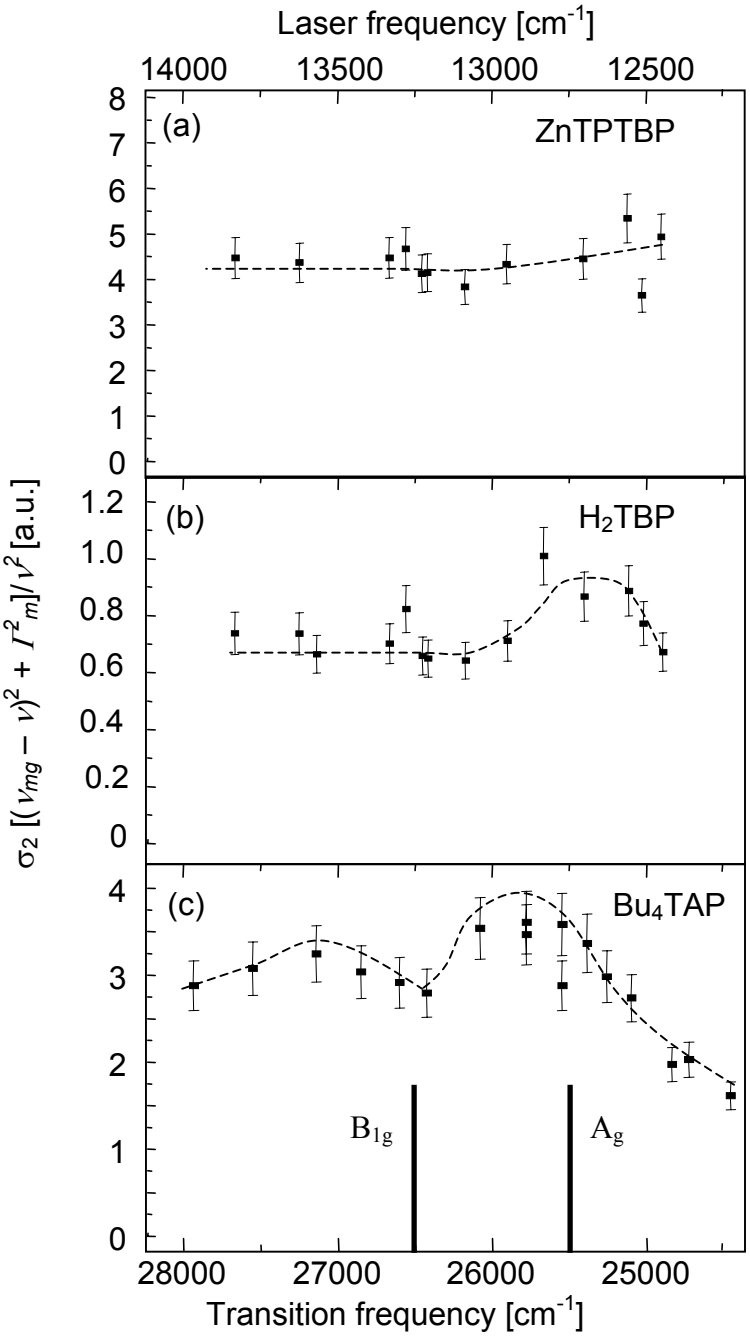

Figure 3.14 (a-c) Quantity $\sigma_2((\nu_{mg}-\nu)^2+\Gamma_m^2(\nu))/\nu^2$ plotted as a function of 2ν for the same molecules as in Figure 3.11(a-c). The dashed lines are drawn as a guide for the eye. Deviation from straight horizontal line represents the spectral profile of $g \leftarrow g$ transitions. Vertical lines in (c) represent positions of the two-photon allowed $g \leftarrow g$ transitions calculated for free-base tetraazaporphine (TAP) in [122].

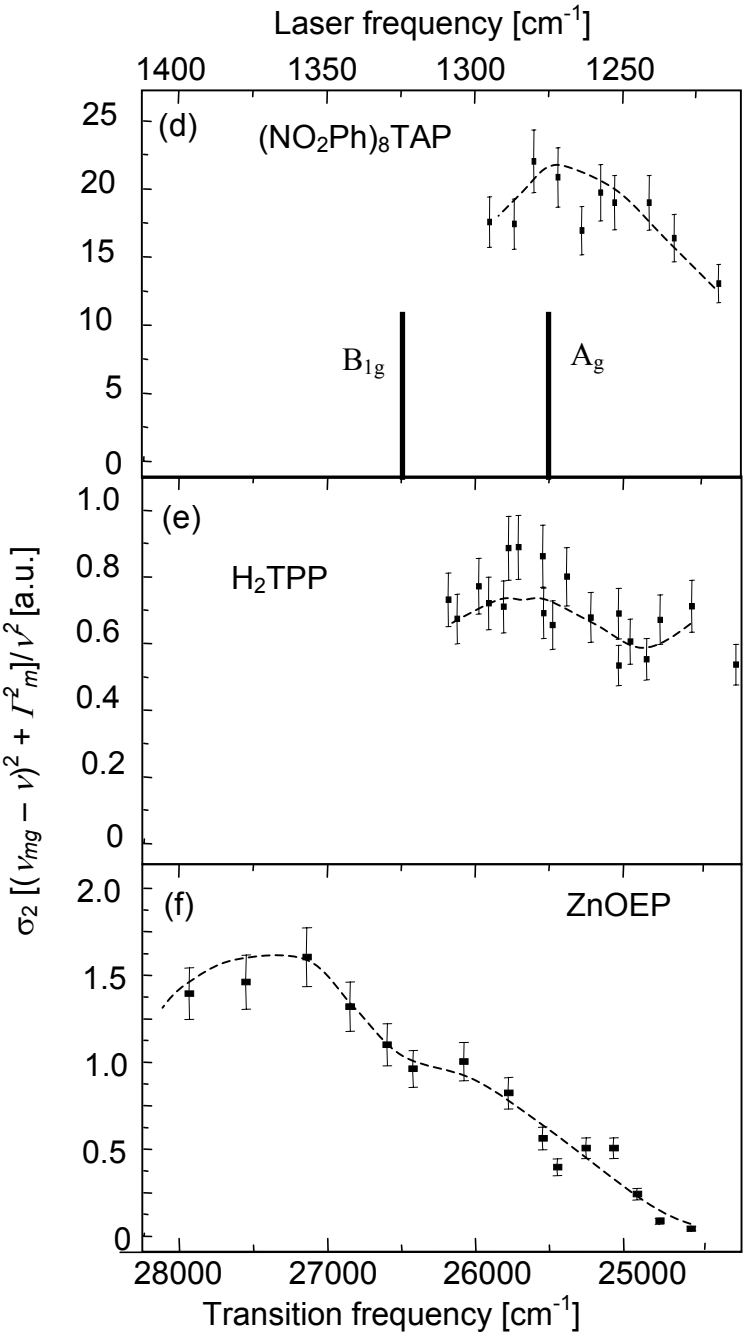

Figure 3.14 (d-f) Quantity $\sigma_2((\nu_{mg}-\nu)^2+\Gamma_m^2(\nu))/\nu^2$ plotted as a function of 2ν for the same molecules as in Figure 3.11(d-f). The dashed lines are drawn as a guide for the eye. Deviation from straight horizontal line represents the spectral profile of $g \leftarrow g$ transitions. Vertical lines in (d) represent positions of the two-photon allowed $g \leftarrow g$ transitions calculated for free-base tetraazaporphine (TAP) in [122].

For ZnTPTBP the dependence is nearly constant (Figure 3.14a), which is in accord with the previous section. It indicates that one still far off from the $g \leftarrow g$ transition peak in this molecule and strong enhancement of TPA cross section in near-UV is solely attributed to resonance enhancement mechanism. For H_2TBP and Bu_4TAP, the plots show some structure at the low frequencies, turning into rather flat spectrum at higher frequencies. Note that in the calculation of ν_{mg} presented above, we used only the nearly constant part of $g(2\nu)$. In case of H_2TBP the peak at low frequencies is very uncertain and might be caused by experimental errors. It is clear from flatness of the $g(2\nu)$ function that resonance enhancement is the main mechanism responsible for TPA enhancement of the molecule. For Bu_4TAP, however, the $g(2\nu)$ shows a clearly visible structure, which is, apparently, created by several overlapping bands.

The plots for $(NO_2Ph)_8$TAP and H_2TPP are not entirely flat and also indicate some structure with $(NO_2Ph)_8$TAP showing rather distinctive peak centered around 25500 cm^{-1}. Finally, line shape function of ZnOEP is the most detailed. Among all the studied molecules, the frequency detuning between laser photons and first one-photon absorption band is largest for ZnOEP, resulting in rather minor role of resonance enhancement. The resonance factor, $1/[(\bar{\nu}_{mg} - \bar{\nu})^2 + \Gamma_m^2(\bar{\nu})]$, at low and high frequency borders of the measured TPA spectrum contributed by the lowest one-photon band values to $3.5 \cdot 10^{-8}$ cm^2 and $7.9 \cdot 10^{-8}$ cm^2 for 12225 cm^{-1} and 14000 cm^{-1} correspondingly. The resonance enhancement is equal to only factor of 2.3 compared to ten-fold increase of TPA cross section. Evidently, strong increase of TPA cross section of ZnOEP when moving to higher frequencies is conditioned by some $g \leftarrow g$ transition or transitions.

There are two types of the two-photon transitions commonly observed in TPA experiments: (1) vibrationally-induced $u \leftarrow g$ transitions, which were described in TPA Properties of Tetrapyrrolic Molecules in the Transitions Spectral Region Corresponding to the Q-bands, and (2) $g \leftarrow g$ transitions. The importance of the $g \leftarrow g$ transitions is conditioned by the fact that they are two-photon allowed (see Appendix A), which leads to their large two-photon cross sections. An estimation made in ref. [4] shows that the ratio between values of two-photon cross sections of the first and second types of TPA is

$$\sigma_2^{u \leftarrow g} / \sigma_2^{g \leftarrow g} \approx \bar{\nu}_{vib} / \bar{\nu}_{el}, \tag{3.10}$$

where $\bar{\nu}_{vib}$ and $\bar{\nu}_{el}$ are typical wavenumbers of the vibrational and electronic transitions of the studied molecules. For porphyrins ($\bar{\nu}_{vib}$ ~ 1000 cm^{-1} , $\bar{\nu}_{el}$ ~ 20000 cm^{-1}) this ratio is about 1/20, which means that two-photon cross sections of the $g \leftarrow g$ transitions should be on the order of $10^2 - 10^3$ GM.

The $g \leftarrow g$ transitions are also of broad importance for molecular spectroscopy, allowing better understanding of the molecular electronic structure as compared to consideration of only *u*-parity levels [6,163]. In general, two-photon spectroscopy provides more information than its one-photon counterpart by utilizing nontrivial dependence of TPA on excitation light polarization. The ordinary (linear) absorption spectroscopy of liquids and gases is not sensitive to polarization state of the excitation light. In contrast, even in isotropic media TPA depends on the polarization state of the excitation light and symmetry of the involved energy levels.

Many efforts have been devoted to theoretical calculations of *g*-levels structure in different compounds (see [6] for some of the references). Calculations of the electronic

structure of porphyrins [107,119-133] support our experimental findings, that *g*-parity levels are situated in Soret band region of spectrum. In particular, calculations predict that for free-base tetraazaporphine (TAP) the first gerade level of A_g symmetry is at 25500 cm^{-1} and the next one, of B_{1g} symmetry, is at 26500 cm^{-1} [122]. Both these calculated frequencies fall within the broad peak obtained in our experiment in Bu_4TAP (Figure 3.14c). Another calculation gives 27700 cm^{-1} for the first $g \leftarrow g$ transition in TAP [127], which is close to our experimental data. Dvornikov et al. [122] suggested that the absence of distinct Soret band in linear absorption spectrum of TAP could be due to overlap of many vibronic transitions into *g*-parity $\pi\pi^*$ state. For $(NO_2Ph)_8TAP$ (Figure 3.14d) we observe about the same broad peak as for Bu_4TAP with maximum frequency (25000 – 26000 cm^{-1}) in good agreement with quantum-mechanical calculations for TAP. Recently, calculation performed by our collaborators [107] showed that the first *g*-parity levels of H_2TPP are situated at 28600 cm^{-1} and 28700 cm^{-1}. It is about 2600 cm^{-1} off from the spectral region that we probed in our experiments, but it indicates that the influence of $g \leftarrow g$ transitions on the obtained $g(2\nu)$ function is possible. We also note that theoretical calculations predicted a large value of σ_2 = 590 GM for free base porphyrins [124] and carbaporphyrins $\sigma_2 \sim 10^3$ GM [133]. This corresponds well to our experimental observation that TPA cross section in Soret region is by one-two orders of magnitude larger than that in the Q-region.

Furthermore, experiments performed on time-resolved stepwise absorption in several porphyrins, including ZnTPTBP [162], H_2TPP [134], and ZnOEP [134] have revealed that $S_n \leftarrow S_1$ transitions into Soret region show a smooth absorption tail,

monotonically increasing towards higher energies. Since selection rules for the stepwise absorption are the same as for the simultaneous TPA, this absorption tail can be attributed to the overlapping of several spectrally broad $g \leftarrow g$ transitions.

All these considerations suggest the importance of $g \leftarrow g$ transitions for the porphyrins in Soret band region of the spectrum. The most notable example is provided by ZnOEP in which we observe dramatic ten-fold increase of the value of TPA cross section, when going from 12225 cm^{-1} to 14000 cm^{-1}, even though the contribution from the resonance enhancement is small. In the case of tetraazaporphyrins, Bu_4TAP and $(NO_2Ph)_8TAP$, both the resonance enhancement effect and the $g \leftarrow g$ transitions are equally important to the TPA.

Other Approaches to the TPA Enhancement

The maximum value of TPA cross section of $(NO_2Ph)_8TAP$ measured in our experiment amounts to 1600 GM at 12990 cm^{-1} (770 nm) excitation laser wavenumber (Figure 3.11d). This constitutes one of the highest intrinsic two-photon cross section values ever reported for a tetrapyrrolic molecule. Although both previously described mechanisms of two-photon cross section enhancement, resonance enhancement and $g \leftarrow g$ transitions, contribute to TPA of $(NO_2Ph)_8TAP$, the value of σ_2 is so large that it cannot be explained solely by them. For Bu_4TAP both mechanisms are also equally important, nevertheless its TPA cross section does not exceed 90 GM. The only difference between two molecules is in the nature of their substituents. In case of $(NO_2Ph)_8TAP$ the

substituent represents very strong electron acceptors, while for Bu_4TAP they are weak (Figire 3.4h,j).

Since the late 1990s it has been noticed that attaching one or more chemical substituents with large electron-accepting ability increases the TPA cross-section of some organic molecules. In particular, such trend was noted previously for some stilbene derivatives with A-D-A (acceptor-donor-acceptor) linear structure and it was thoroughly investigated [86]. Theoretical considerations for linear quadrupolar centrosymmetrical molecules [164,165] and for three-branch octupolar molecules with C_3 symmetry [166] have predicted that σ_2 increases monotonically with the substituents' capability to accept or donate electrons. In particular, Lee et al. [166] predicted a linear correlation between TPA cross-section at the maximum of $g \leftarrow g$ transition and Hammett constant, characterizing electron-accepting or donating ability of the substituent group.

Since the maxima of $g \leftarrow g$ transitions ($\bar{\nu} \cong 25500$ cm^{-1}) of both tetraazaporphyrins were defined in the previous section, one can conduct a quantitative comparison of the influence of substituent electron accepting ability on TPA cross section. To make the comparison more viable we also measured TPA cross section of the similar porphyrin $(BrPh)_8TAP$ (Figure 3.4i) in the same spectral region and obtained value of 380 GM.

Figure 3.15 presents the dependence of TPA cross-section in the maximum of the $g \leftarrow g$ transition on the substituent's Hammett constant for three tetraazaporphyrin molecules, Bu_4TAP, $(BrPh)_8TAP$, and $(NO_2Ph)_8TAP$, and shows that, indeed, σ_2

increases linearly with the acceptor strength. For example, by going from Bu_4TAP to $(NO_2Ph)_8TAP$, the cross-section increases by ~ 37 times.

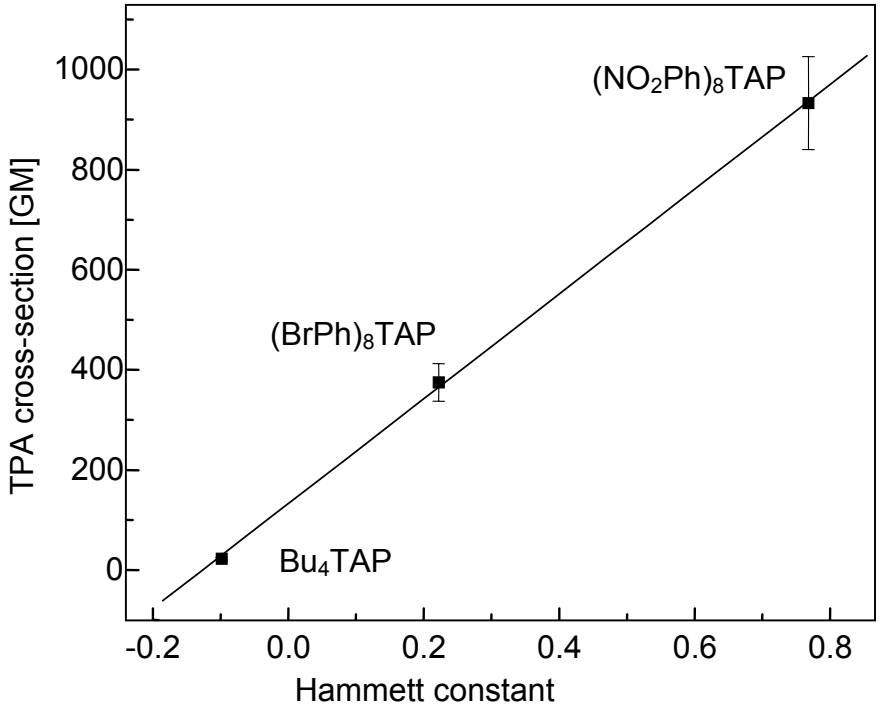

Figure 3.15 Dependence of TPA cross-section (measured in the maximum of *g*-*g* transition) on the substituent Hammett constant for three tetraazaporphyrins. Linear increase of two-photon cross section clearly indicates importance of electron accepting substituents for TPA enhancement.

From the linear absorption (Figure 3.11(c,d)) spectra we find that the corresponding change of $\left|\boldsymbol{\mu}_{mg}\right|^2$ is about 1.5 times. At the same time, the resonance factor, $1/[(\bar{\nu}_{mg}-\bar{\nu})^2+\Gamma_m^2(\bar{\nu})]$, increases by a factor of ~ 3. Evidently, the remaining 8-fold increase is due to $\left|\boldsymbol{\mu}_{fm}\right|^2 g(2\nu)$ (see equation (2.37)) conditioned by stronger electron accepting ability of $(NO_2Ph)_8TAP$ substituent. The last manifests itself in increased coupling between the intermediate state and the final state, i.e. increase of the transition dipole moment, $\boldsymbol{\mu}_{fm}$. Also, adding electron accepting substituents may shift the

intermediate energy level closer to the resonance with the near-IR photons [80,164-166]. As a result, adding electron acceptors to the periphery of the tetrapyrrolic molecules increases all the factors involved in equation (2.37) resulting in strongly enhanced TPA.

Another approach to the TPA enhancement is a so called extension of π-conjugation. It was first established in the 1990-s and was very extensively used since then. During past several years few papers appeared dealing with porphyrin oligomers, i.e. one-dimensional chain structures consisting of several chemically connected porphyrin units. Some porphyrin oligomers demonstrate extended π-conjugation between porphyrin units resulting in a strong increase of their nonlinear properties [101,167,168]. This suggests that TPA enhancement in porphyrin oligomers is also possible. Preliminary studies conducted in ref. [101] show that, indeed, two-photon cross section of such molecular complexes strongly increases. To gain a better understanding of effect of the π-conjugation on two-photon cross section of porphyrins we study TPA properties of a porphyrin dimer (Figure 3.4p) and corresponding monomer (Figure 3.4n) in near-resonance conditions.

Linear absorption and fluorescence spectra of studied monomer and dimer in PVB film are presented in Figure 3.16. Absorption and fluorescence bands of dimer are strongly shifted to the red part of the spectrum in comparison to monomer which testifies that both porphyrin units in the dimer are π-conjugated.

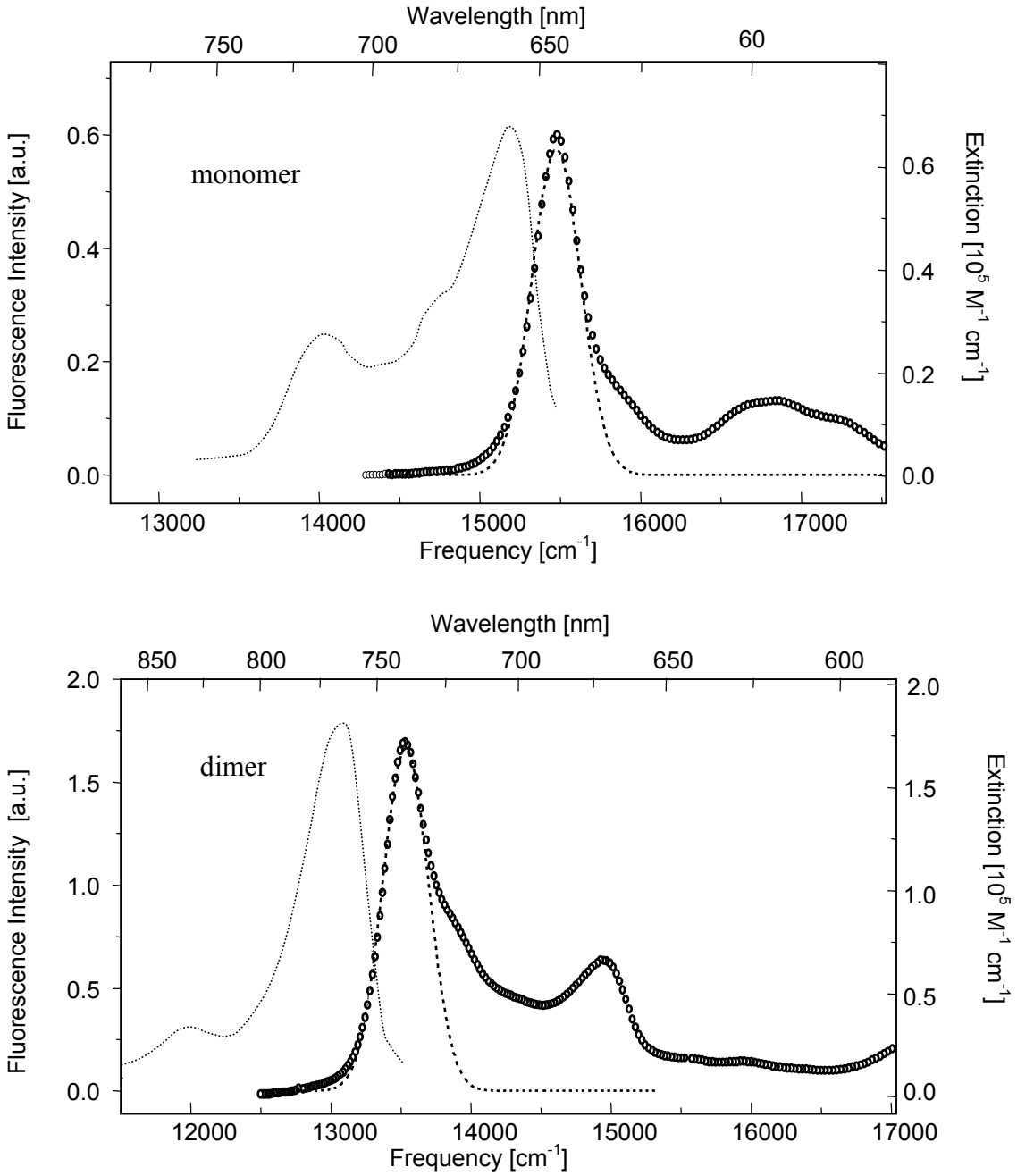

Figure 3.16 Linear absorption (open circles) and fluorescence (dotted line) spectra of monomer, top, and dimer, bottom. Fitting of the first absorption band to Gaussian is shown by dashed line. This function is used to the ratio of the transition dipole moments of monomer and dimer (see (3.12)).

Two-photon cross sections of the both molecules were measured at excitation wavelength λ_{ex} = 860 nm: σ_2 (monomer) = 20 GM, σ_2 (dimer) = 7000 GM. The π-

conjugation, indeed, leads to very strong, 350 times, TPA enhancement. In fact, two-photon cross section of the dimer is the largest so far measured for any tetrapyrrolic molecule. Moreover, there is only one molecule, stilbene-based dendrimer, which TPA cross section is known to be marginally larger [85].

We employ three level model for centrosymmetrical molecule to clarify physical origin of such drastic enhancement. By applying equation (2.37) to both dimer and monomer, the ratio of their TPA cross sections can be written as follows:

$$\frac{\sigma_2^{(D)}}{\sigma_2^{(M)}} = \frac{\left[(\nu_{mg}^{(M)} - \nu)^2 + \Gamma_m^{(M)2}\right]}{\left[(\nu_{mg}^{(D)} - \nu)^2 + \Gamma_m^{(D)2}\right]} \times \frac{\left|\boldsymbol{\mu}_{mg}^{(D)}\right|^2}{\left|\boldsymbol{\mu}_{mg}^{(M)}\right|^2} \times \frac{\left|\boldsymbol{\mu}_{fm}^{(D)}\right|^2 g^{(D)}(2\nu)}{\left|\boldsymbol{\mu}_{fm}^{(M)}\right|^2 g^{(M)}(2\nu)}, \tag{3.11}$$

where, superscripts *D* and *M* refer to the dimer and the monomer, respectively. The three main factors contributing to the large TPA cross section of the dimer are the resonance enhancement, $\left[(\nu_{mg} - \nu)^2 + \Gamma_m^2\right]^{-1}$, the $m \leftarrow g$ transition dipole moment squared, $\left|\boldsymbol{\mu}_{mg}\right|^2$, and the product of the $f \leftarrow m$ transition dipole moment squared and the normalized lineshape function, $\left|\boldsymbol{\mu}_{fm}\right|^2 g(2\nu)$.

At 860-nm excitation wavelength the resonance enhancement factor for dimer is about 4 times larger than that for monomer. If the two porphyrin units forming the dimer were not coupled, then we could assume that each unit absorbs independently. Excluding the above resonance enhancement factor, the resulting dimer TPA cross section would be just two times as large as that of monomer. However, our experiment gives 350/4 ≈ 90 times enhancement, which serves as an additional evidence of strong electronic coupling

between the two units. It also clearly indicates that cooperative enhancement of TPA takes place upon transition from monomer to dimer.

The further enhancement has to come from the product $\left|\boldsymbol{\mu}_{mg}\right|^2 \left|\boldsymbol{\mu}_{fm}\right|^2 g(2\nu)$. The ratio of the $m \leftarrow g$ transition dipole moments squared can be obtained from the linear absorption spectra (see equation (C.13)).

$$\frac{\left|\boldsymbol{\mu}_{mg}^{(D)}\right|^2}{\left|\boldsymbol{\mu}_{mg}^{(M)}\right|^2} \propto \frac{\varepsilon_{\max}^{(D)}(\bar{\nu}_{mg})\Delta\bar{\nu}_{mg}^{(D)}}{\bar{\nu}_{mg}^{(D)}} : \frac{\varepsilon_{\max}^{(D)}(\bar{\nu}_{mg})\Delta\bar{\nu}_{mg}^{(D)}}{\bar{\nu}_{mg}^{(M)}} = 2.6\,. \tag{3.12}$$

The last remaining factor in the equation (3.11) consists of the product of the $f \leftarrow m$ transition dipole moment squared and the normalized lineshape function. In this case, however, we know neither the dipole moment $\boldsymbol{\mu}_{fm}$ nor the TPA spectral shape $g(2\nu)$. On the other hand, since we know the TPA cross sections we can calculate the ratio:

$$\frac{\left|\boldsymbol{\mu}_{fm}^{(D)}\right|^2 g^{(D)}(2\nu)}{\left|\boldsymbol{\mu}_{fm}^{(M)}\right|^2 g^{(M)}(2\nu)} = \frac{1}{4} \times \frac{1}{2.6} \times \frac{\sigma_2^{(D)}}{\sigma_2^{(M)}} = 34\,. \tag{3.13}$$

Since the product $\left|\boldsymbol{\mu}_{fm}\right|^2 g(2\nu)$ is proportional to the excited state OPA, $\varepsilon_{fm}(2\nu - \nu_{mg})$, (see equation (C.10)), expression (3.13) gives the ratio of the excited state extinction coefficients of dimer and monomer, $\varepsilon_{fm}^{(D)}(2\nu - \nu_{mg}) / \varepsilon_{fm}^{(M)}(2\nu - \nu_{mg})$. Singlet-singlet excited-state absorption spectra of related monomer and dimer systems were calculated in [169] and are in good qualitative agreement with our experiment. In particular, a dimer with cumulenic structure of butadiene linker in the first singlet excited

state exhibits an order of magnitude enhancement in $\varepsilon_{fm}(2\nu - \nu_{mg})$, as compared to monomer.

Therefore, the extremely large two-photon cross section of the dimer can be explained by very favorable position of its energy levels. The strong conjugation between porphyrin units in dimer brings first one-photon transition closer to one-half of one of the strong two-photon transitions, giving rise to nearly double resonance enhancement. The porphyrin dimer molecule, presented here, holds a record large σ_2 for tetrapyrrolic molecules. Its σ_2 = 7000 GM is the second largest two-photon cross section obtained so far for any organic chromophore.

New Method for Measuring Absolute TPA Cross Section

The occurrence of residual OPA into the read "tail" of the lowest Q-band can be a serious limiting factor in measuring TPA cross sections in tetrapyrroles (Figure 3.11). We developed a new method of TPA cross section measurement, which allows, at least in part, overcome this problem. Moreover, this new method takes advantage of the presence of OPA, and works in the border spectral region where both OPA and TPA are present.

Consider short laser pulses illuminating a solution of fluorescing molecules at a frequency ν, less than the frequency of the first pure electronic transition. At low pulse intensity, the probability of the TPA is much less than the probability of OPA. However, at higher illumination intensity, because TPA increases quadratically with the incident power, both processes can have a comparable probability. In this case, the intensity of the excited fluorescence can be described as a sum of two contributions:

$$F = K\sigma_1(\nu)\int I(t)dt + \frac{1}{2}K\sigma_2(\nu)\int I^2(t)dt\,, \tag{3.14}$$

Here constant *K* includes fluorescence light collection and photodetection efficiency, fluorescence quantum yield and molecular concentration. Because the one- and two-photon excitation is carried out under identical conditions, *K* is the same for one- and two-photon terms. *I(t)* designates the instantaneous photon flux (in photons s^{-1} cm^{-2}) in a laser pulse. Small aperture is placed in front of the sample so that only central part of the laser beam is used for excitation. This provides for a constant intensity along the excitation beam cross section (see Chapter 3 Experimental). An instantaneous photon flux is related to an average (measured) photon flux *P* as follows: $\int I(t)dt = \frac{P}{r}$, where *r* is the pulse repetition rate. Integration here as well as in equation (3.14) is carried out over the time period of one single pulse. For the Gaussian temporal pulse profile, $\int I^2(t)dt = 0.66\frac{P^2}{r^2\tau}$, where τ is the pulse duration (FWHM). Therefore,

$$F(P) = K'\sigma_1(\nu)P + 0.33K'\frac{\sigma_2(\nu)}{r\tau}P^2 = aP + bP^2\,, \tag{3.15}$$

where *K*' = *K*/*r*. Note that the ratio, *a*/*b,* corresponds to a particular average photon flux, *P**, at which the one- and two-photon absorption have equal probability:

$$P^* = \frac{a}{b} = \frac{\sigma_1(\nu)r\tau}{0.33\sigma_2(\nu)}\,. \tag{3.16}$$

From the latter relation we can express the TPA cross section as follows:

$$\sigma_2(\nu) = \frac{\sigma_1(\nu)r\tau}{0.33(a/b)}\,. \tag{3.17}$$

Here the molecular linear, σ_1, and nonlinear, σ_2, absorption cross sections are measured at the same frequency, ν. The ratio *a/b* can be found from experimental power dependence measurement. Then, in principle, equation (3.17) can produce the TPA cross section. Unfortunately, such experiments require that linear absorption is rather weak, which makes direct measurement of σ_1 difficult.

However, if the linear absorption takes place from vibrationally-excited ground state, then the cross section of such hot-band absorption can be easily evaluated as a probability of vibronic transition at frequency ν:

$$\sigma_1(\nu) = \sigma_1(\nu_{\max}) \exp\left(-\frac{\nu_{\max} - \nu}{kT}\right) \frac{FC(\nu)}{FC(\nu_{\max})}, \tag{3.18}$$

where $\sigma_1(\nu_{\max})$ is the cross section at the band maximum (which, in the case of porphyrins, corresponds to the 0-0 transition maximum), $FC(\nu)$ and $FC(\nu_{\max})$ are the Franck-Condon factors for vibronic and 0-0 transitions, respectively. The ratio $FC(\nu)/FC(\nu_{\max})$ can be independently measured either from fluorescence spectrum, as the ratio of intensities at ν and at fluorescence maximum (if the Stokes shift between absorption coefficients and fluorescence 0-0 transitions is small), or from absorption spectrum as the ratio of absorption at $2\nu_{\max} - \nu$ and at $\nu_{\max}$. Consequently, σ_2 value can be evaluated from equations (3.17) and (3.18).

To verify the new method, we performed experiments with H_2-TTIPS porphyrin (Figure 3.4 (o)). Figure 3.17 shows the linear absorption spectrum. In comparison to other porphyrins studied so far, the first Q-band of H_2-TTIPS is shifted to the red with maximum at 714 nm.

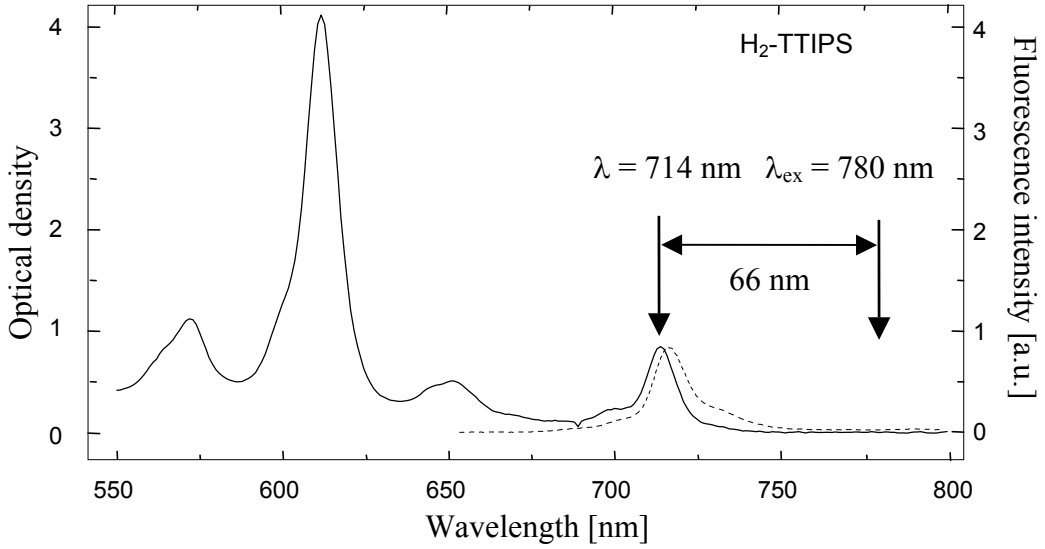

Figure 3.17 Absorption (solid) and fluorescence (dashed) spectra of H_2-TTIPS. The arrow on the right correspond to the wavelength at which two-photon cross section was measured (λ_{ex} = 780 nm). The arrow on the left shows the first Q-band maximum (λ = 714 nm).

Although the excitation wavelength, λ_{ex} = 780 nm, was shifted 66 nm from the first linear absorption spectrum maximum, the dependence of the fluorescence on excitation intensity at room temperature was still linear, revealing presence of strong OPA. In fact, even after tuning regenerative amplifier further to the λ_{ex} = 810 nm the power dependence stayed almost linear. This can be explained by a domination of one-photon hot-band transition (see below) from vibronic manifold of the ground state.

To reduce OPA H_2-TTIPS was embedded into PVB film and into a variable-temperature cryostat. Figure 3.18 shows the excitation power dependence of the fluorescence at two selected temperatures, 180 K (a,b) and 200K (c,d). The graphs (a) and (c) present power dependence in the linear scale, while (b) and (d) present power dependence in the double logarithmic scale. The exponent of the power dependence is equal to 1.25 at T = 200 K and 1.95 at T = 180 K turning from linear to quadratic upon

lowering the temperature. This is in accord with OPA from thermally populated vibronic levels, which efficiency reduces with lower temperature. At T < 180 K, the dependencies are described by quadratic function, i.e. the TPA dominates. In the temperature range 180 – 250 K, the power dependence has an exponent lying in between 1 and 2 and is well described by equation (3.15) in all the cases.

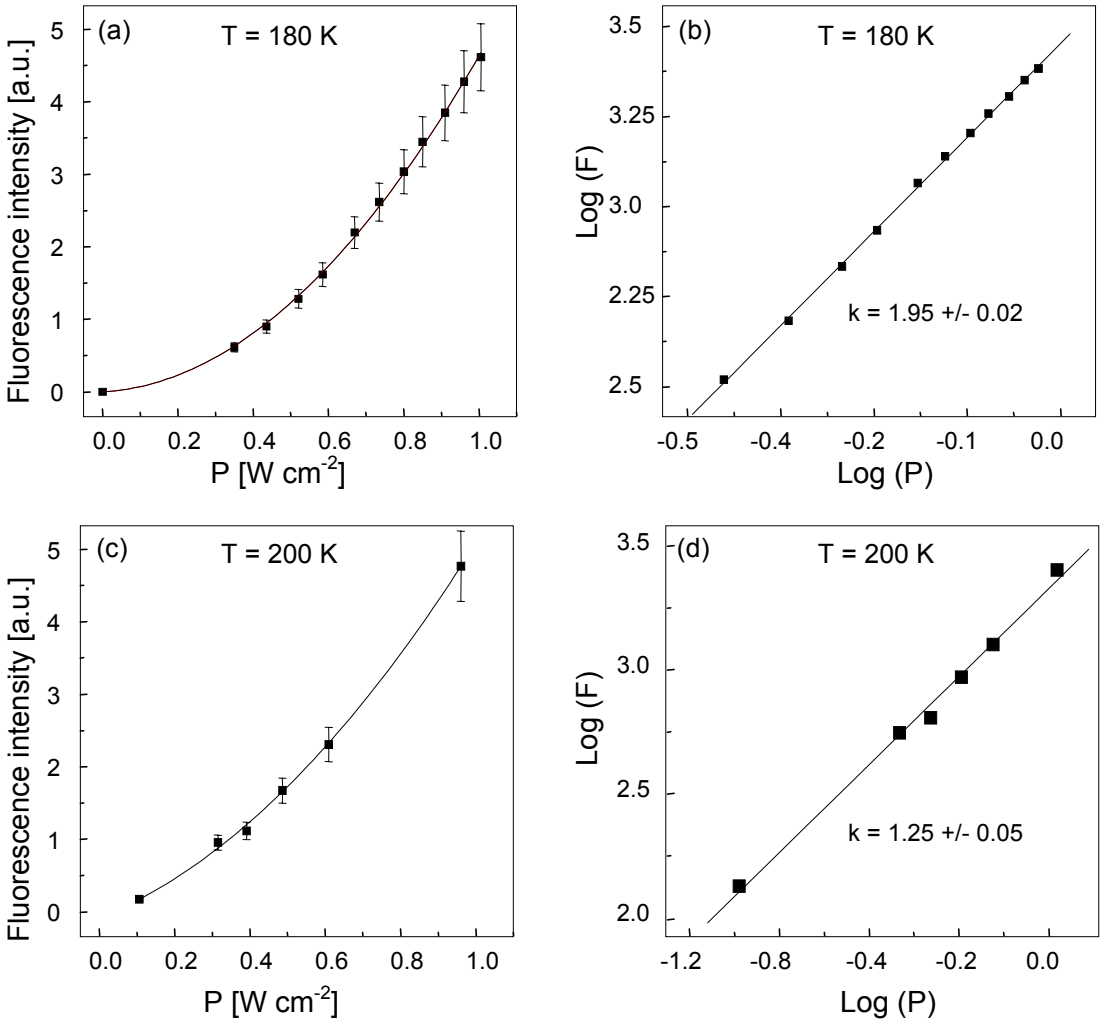

Figure 3.18 Power dependence of fluorescence intensity of H_2-TTIPS in PVB-film upon anti-Stokes excitation at 780 nm at 180 K (a,b) and 200 K (c,d) presented in linear (a,c) and double logarithmic scale (b,d). The latter graphs also show the exponent of the power dependence *k*.

Relative one-photon absorption cross section, proportional to coefficient *a* in (3.15), is plotted in Figure 3.19 as a function of temperature. Continuous line presents the best fit of experimental data with Boltzmann function, $C \exp(-\Delta\nu / kT)$, where only *C* was adjusted, and $\Delta\nu = 1170$ cm^{-1} is taken equal to the difference between the frequencies of the first Q-band maximum and the laser. Excellent agreement between the experimental data and fitting function confirms our assumptions that the one-photon absorption of H_2-TTIPS at 780 nm is due to transitions from thermally-populated vibrational level (or levels) in the ground electronic state.

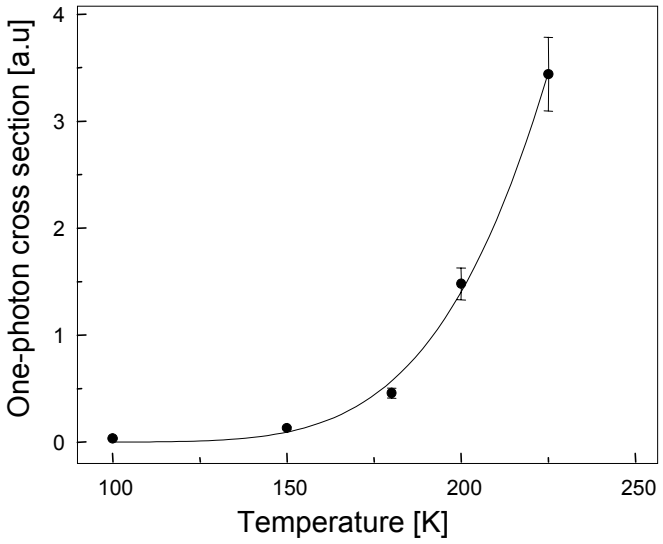

Figure 3.19 Temperature dependence of one-photon absorption cross-section of H_2-TTIPS in PVB-film at 780 nm. Continuous line shows the best fit to the Boltzmann function with frequency detuning from 0-0 transition, $\Delta\nu = 1170$ cm^{-1}.

Table 3.3, lines 3 and 4, presents the values of σ_2 for H_2TTIPS in PVB film calculated according to equations (3.17) and (3.18) by using the fitting parameters *a* and *b*, obtained at each temperature, and Franck-Condon factors, determined from the corrected fluorescence spectrum. The same Table presents also the σ_2 values obtained by

standard procedure (lines 1 and 2). One can see that in contrast to one-photon absorption, the two-photon absorption cross section of H_2TTIPS in PVB film does not strongly depend on temperature. To make sure that the results provided by this method are reliable, we have also measured σ_2 value with the standard fluorescence procedure (see Chapter 3 Experimental). In this case, the one-photon transition at 388 nm was excited in the same sample, but at 77 K, i.e. where TPA completely dominates. As is evident from Table 3.3, (cf. line 2 with lines 3 and 4) the results obtained by these two methods indeed coincide within experimental error.

Table 3.3 Two-photon absorption cross sections of H_2-TTIPS at different experimental conditions.

Exp. No.	*Molecule*	*λ, nm*	*T, K*	*matrix*	*σ_2, GM*
1	H_2-TTIPS	903	300	toluene	40 ± 10
2	H_2-TTIPS	782	77	PVB-film	22 ± 5
3	H_2-TTIPS	782	200	PVB-film	20 ± 5
4	H_2-TTIPS	782	225	PVB-film	17 ± 5
5	H_2-TTIPS	782	77-225	PVB-film	20 ± 3 average

To make still another check, we excited H_2-TTIPS at 903 nm (second harmonic of the optical parametric amplifier idler) and obtained quadratic dependence of the fluorescence at room temperature. This confirms that OPA is not present at this wavelength. Next, we measured σ_2 at this wavelength with the standard method, and obtained σ_2 = 40 ± 10 GM (Table 3.3 line 1). Since we compare two-photon cross sections at different wavelengths, 780 and 903 nm, they are not supposed to be the same. Nevertheless, we expected some similarity in the results. The comparison of the two

values of σ_2 (Table 3.3 line 5 and 1) confirms the validity of the new method for TPA cross section measurement.

In conclusion, the new method of TPA cross section measurement proposed and experimentally validated. It is particularly useful for investigation of the TPA properties of tetrapyrroles near Soret band transition wavelengths. The studies described in this chapter show that two-photon cross section of the porphyrins there is greatly enhanced due to resonance effect and the presence of the $g \leftarrow g$ transitions. The $g \leftarrow g$ transitions of many tetrapyrroles are situated above Soret band, so that only their long wavelength tails can be seen in the investigated spectral range (see Figure 3.14). Note, that the most pronounced spectrum of two-photon $g \leftarrow g$ transitions was observed in ZnOEP (Figure 3.14f), which TPA spectrum was measured further into UV (λ_{tr} = 350 nm) than for most other compounds. In this respect it is highly desirable to probe TPA properties of the tetrapyrrolic molecules further in the UV. As a result of such study, much larger TPA cross sections can be expected and better understanding of the physics of $g \leftarrow g$ transitions in tetrapyrroles can be achieved. The demonstrated here method of TPA cross section measurements allows to perform such investigation.

CHAPTER 4

TPA-INDUCED FREQUECY DOMAIN COHERENCE GRATINGS

Study of coherent transient effects such as time-and-space-domain holography, photon echo, electromagnetically induced transparency, stopping (and accelerating) of light pulses, etc., gives valuable insights into the physics of the interaction between atoms (or molecules) and light. This research is also paving a road for future advances in technology, especially in high-speed high-capacity data storage, ultra stable frequency- and time standards, coherent control of atomic and molecular systems, as well as new ways of performing computations [70-76,170-180].

In the past, coherent transients have been studied traditionally in the situation, where the ground electronic state is coupled to an excited electronic state via resonant one-photon transition. Time-and-space-domain holography and its particular case frequency-domain interference gratings have been demonstrated previously by means of direct one-photon excitation of the lowest singlet-singlet transition in organic molecules in polymer matrices at low temperature [77,181]. Time-and-space-domain holography is a coherent transient technique where frequency-domain interference occurs due to the coherence excited in an absorbing medium by mutually time-delayed object and reference pulses [70-77]. Depending on the relative phase between different components of the complex field of the pulses, either constructive or destructive interference may take place, thus enhancing or suppressing transition probability at particular instants of time and (or) at a particular frequencies. In particular, if a sequence of pairs of identical short phase-locked pulses is employed, then an interference grating in frequency will be

created, with a period equal inverse value of delay between the pulses, provided that the duration of the sequence does not exceed the homogenous dephasing time, $\Delta\tau < T_2$. The resulting spatial-spectral interference pattern is recorded by means of persistent SHB in broad inhomogeneous absorption bands at organic molecules. So far, all the time-and-space-domain holography studies employed one-photon excitation. It may be expected that by using two-photon coherent processes one can greatly increase the variety of nonlinear optical effects useful for optical storage and processing of information.

Coherent interference has been recently observed in two-photon transitions in atomic systems in gas phase [182-187]. In particular, B. Girard et al. have demonstrated coherent control of two-photon transition in atomic cesium vapor with pairs of ultrashort pulses by adjusting the time delay (phase difference) between them, but keeping carrier frequency in resonance with a particular transition [182]. Other examples of two-photon coherent manipulation of light-matter interaction include ultrahigh resolution spectroscopy with short pulses [182-185], forcing or inhibition of two-photon absorption [182-184,186-189] or ionization [190], selective molecular excitation [185], and control of chemical reactions [191-193].

It should be emphasized that, because the phase is given as the product of time and frequency variables, a particular interference condition, e.g. $\Delta\phi = \pi$ or 2π, can be attained in both time and frequency domains, with the complementary variable being fixed. So far, the vast majority of studies have addressed the multi-photon coherence interference in time domain, and neglected interference in frequency domain. This is because most experiments use spectrally narrow atomic or molecular transitions, which,

even in case of broadband pulse excitation, select a particular resonance frequency from the laser spectrum. In our experiments, we utilize organic molecules embedded in solid matrix with broad inhomogeneous absorption bands. This allows us to study, for the first time, interference in the frequency domain produced by simultaneous absorption of two photons.

The SHB allows high-resolution spectral measurements to be performed without limitations due to inhomogeneous broadening [63-69]. So far, most of the experiments concerning site selective spectroscopy of inhomogeneously broadened organic systems used ZPL originating in one-photon transitions. Only a few experiments were performed on two-photon transitions [194-202]. The first observations of energy-selective two-photon excitation of organic molecule were reported by the groups of Hochstrasser [194,195], Mikami [196], and Kohler [197]. In ref. [201], Small and co-authors burned a hole by usual one-photon excitation mechanism, and detected it in TPA fluorescence excitation spectrum. Recently Takeda et al. [202] demonstrated two-photon excited fluorescence line narrowing for several dyes with no inversion symmetry. TPA-induced SHB has never been demonstrated before. By using ultrafast two-photon spectroscopy, new information can be obtained about molecular properties and guest-host interactions in solids that is not accessible by one-photon transitions. In addition, SHB can be used to provide a frequency dimension for the optical data storage, increasing its density by a factor of 10^4 and more. Combination of SHB with TPA 3D optical storage can substantially increase the storage capacity.

In this chapter we describe our experiments where we study two-photon excited coherence gratings in inhomogeneously broadened medium, where the last is consisting of organic dye-doped polymer at low temperature. The following objectives are addressed:

1. Demonstrate persistent SHB by means of two-photon excitation of a visible transition with near-IR pulses.
2. Demonstrate possibility of creation and detection of spectral interference gratings by means of two-photon excitation with phase-locked pairs of ultrashort near-IR laser pulses.
3. Develop a theoretical model describing the observed properties of two-photon-induced spectral gratings, including determination of electron-phonon interaction parameters.

The chapter starts by giving a brief theoretical description of coherence excited by simultaneous absorption of two photons. Next, experiments are described in which the spectral gratings are created at visible wavelengths by illuminating the sample with phase-locked pairs of 100-fs near-IR laser pulses with center wavelength equal to two times the transition wavelength. The two-photon excited coherence is detected in two independent ways – either by measuring the spectrum of fluorescence or, after prolonged illumination, by observing spectrally-modulated persistent spectral holes. The spectral shape of the gratings at different temperatures is analyzed. It is shown that by modeling the spectral grating we can deduce the key electron-phonon interaction parameters such as Debye-Waller factor and phonon spectrum, which are otherwise difficult to access for

two-photon transitions, especially in the presence of large inhomogeneous broadening. The results from this chapter were reported in the following publications [203-211].

Theoretical Description of Coherence Grating Excited by TPA in Inhomogeneously Broadened Medium

Previous treatments of coherent interaction of a sequence of short pulses with a two-photon absorbing medium [182,186] have been based on an assumption that the duration of each illuminating pulse is much shorter than inverse homogeneous- and inhomogeneous line width of the medium, $\tau_p < \Gamma^{-1}$. Since, under such condition, the observation of frequency-domain interference was impossible because of narrow bandwidth of the TPA medium, in previous approaches the interference was observed only by varying the time delay between the pulses. Here we analyze the case of a strongly inhomogeneously broadened medium, such that the overall width of the TPA band is larger than the inverse duration of each pulse. The distinctive property of our approach is that the delay is constant, and the interference occurs directly in the frequency dimension.

Consider a sequence of two linearly polarized, temporally non-overlapping laser pulses, described by electric field:

$$E(t) = E_1(t)e^{-i2\pi\nu_L t} + E_2(t-\Delta\tau)e^{-i2\pi\nu_L(t-\Delta\tau)}, \tag{4.1}$$

where $E_i(t)$ (i = 1,2) is the pulse envelope, ν_L is the carrier frequency of the pulse, and $\Delta\tau$ is the delay of the second pulse. In the one-photon case of holographic recording, one of the pulses serves as an object pulse and the other as a reference pulse [76]. If all molecules are in the ground electronic state before the pulses are applied, then after one-

photon resonance excitation by the field (4.1), the probability of finding molecule with transition frequency ν_k in the excited state is proportional to the intensity of the spectral component of the incident light at this frequency:

$$P(\nu_k) \propto \left|\hat{E}(\nu_k)\right|^2, \tag{4.2}$$

where $\hat{E}(\nu)$ is Fourier transform of the electric field:

$$\hat{E}(\nu) = \int E(t) e^{i2\pi\nu t} dt\,. \tag{4.3}$$

By choosing a suitable reference pulse shape, power spectrum (4.3) contains all necessary information about the object pulse. In the case of two-photon absorption, however, there is no such linear correspondence of the excitation probability and the power spectrum of the electric field. To find this relation for TPA we need to consider the process of absorption in some more detail.

As a result of light-matter interaction during time *t*, the wave function $\left|\Psi_k(t,\nu_k)\right\rangle$ of a particular molecule *k* with transition frequency ν_k will be:

$$\left|\Psi_k(t,\nu_k)\right\rangle = \left|g\right\rangle + a_k(t,\nu_k)\left|e_k\right\rangle, \tag{4.4}$$

where, *g* and e_k denote the ground and excited states, respectively. According to the perturbation theory, the amplitude $a_k(\nu_k)$ is proportional to [187]

$$a_k(\nu_k) \sim \int_{-\infty}^{\infty} E^2(t) exp[2\pi i \nu_k t] dt\,. \tag{4.5}$$

After the first pulse passes through the medium, one will have:

$$a_k(\nu_k) \sim \int_{-\infty}^{\infty} E_1^2(t) \exp[2\pi i(\nu_k - 2\nu_L)t] dt = \hat{E}^2(\nu_k - 2\nu_L)\,, \tag{4.6}$$

where, $\hat{E}^2(\nu_k - 2\nu_L)$ is the Fourier transform of the square of electric field pulse envelope. Excited state population is proportional to the modulus squared of the amplitude a_k:

$$|a_k|^2 \propto \left|\hat{E}_1^2(\nu_k - 2\nu_L)\right|^2 . \tag{4.7}$$

Note the difference with one-photon excitation (see equation (4.2)). The probability is determined by the Fourier transform of the square of the electric field.

If the time delay $\Delta\tau$ between the first and second pulses is less than the homogeneous optical dephasing time T_2, then interference between polarizations induced by the two pulses will occur. If we consider a simplified situation, where the two temporarily non-overlapping pulses have identical envelopes, $E_1(t) = E_2(t - \Delta\tau) = E_0(t)$, then the probability amplitude after two pulses is:

$$\begin{aligned} a_k(\nu_k) \sim & \int_{-\infty}^{\infty} E_0^2(t)\exp[2\pi i(\nu_k - 2\nu_L)]dt + \\ & + \exp[2\pi i 2\nu_L\Delta\tau]\int_{-\infty}^{\infty} E_0^2(t-\tau)\exp[2\pi i(\nu_k - 2\nu_L)]dt + \\ & + \exp[2\pi i\nu_L\Delta\tau]\int_{-\infty}^{\infty} E_0(t)E_0(t-\tau)\exp[2\pi i(\nu_k - 2\nu_L)]dt \end{aligned} . \tag{4.8}$$

$$\begin{aligned} a_k(\nu_k) \sim & \hat{E}_0^2(\nu_k - 2\nu_L) + \hat{E}_0^2(\nu_k - 2\nu_L)\exp[2\pi i\nu_k\Delta\tau] + \\ & + \exp[2\pi i\nu_L\Delta\tau]\int_{-\infty}^{\infty} E_0(t)E_0(t-\tau)\exp[2\pi i(\nu_k - 2\nu_L)]dt \end{aligned} . \tag{4.9}$$

These three terms account for all possible quantum paths leading to TPA. The first and second terms correspond to the case when both photons are absorbed either from the first pulse or from the second pulse. The third term describes the situation when one photon is

absorbed from the first pulse and another from the second. This term crucially depends on the pulse overlap and vanishes if the two pulses do not overlap in time. This corresponds to our experimental conditions and we neglect it.

The probability of finding a molecule in the excited state is proportional to $|a_k|^2$

$$\begin{aligned} |a_k(\nu_k)|^2 &\sim \left|\hat{E}_0^2(\nu_k - 2\nu_L)\right|^2 \left|(1+\exp[2\pi i \nu_k \Delta\tau])\right|^2 \sim \\ &\sim \left|\hat{E}_0^2(\nu_k - 2\nu_L)\right|^2 (1+\cos[2\pi i \nu_k \tau]) \end{aligned} \quad . \tag{4.10}$$

Thus, spectral grating is created, modulated by the following function:

$$f(\nu_k) = (1+\cos[2\pi\nu_k\tau]) \, . \tag{4.11}$$

This result demonstrates that for a fixed $\Delta\tau$ value, the constructive or destructive interference conditions can be obeyed for a predetermined set of transition frequencies within inhomogeneous band. Namely, in case of constructive interference $\nu_k = n/\Delta\tau$, (n = 0, ±1, ±2, …). In time domain language, this means that if the second pulse arrives with a phase delay $\Delta\varphi = 2\pi\nu_k\Delta\tau$ exactly equal to $2\pi n$ for a particular frequency ν_k, one will have a constructive interference of this pulse with a polarization induced by the first pulse at this frequency.

Experimentally, one should observe a spectral grating in inhomogeneously broadened medium with a period of $\Delta\nu = 1/\Delta\tau$. Note that the period of modulation turns out to be the same as in the case of one-photon excitation with the pair of pulses, also delayed by $\Delta\tau$. We underline, however, that the grating is created around an optical frequency, which is double the actual carrier frequency of the pulses illuminating the medium.

Experimental

Figure 4.1 shows experimental setups used for detection of two-photon excited spectral gratings by means of fluorescence (Figure 4.1a) and SHB (Figure 4.1b). The laser system consisting of Ti:sapphire regenerative amplifier and optical parametric amplifier is described in detail in Chapter 3 Experimental. A stack of IR filters was used to cut off any residual visible light from the optical parametric amplifier. A Michelson interferometer, constructed from two mirrors with one of them on the moving stage, divided the optical parametric amplifier beam into two spatially overlapped but time-delayed beams. The time delay between the two pulses was in the range $\Delta\tau \approx$ 100 - 1000 fs, and was adjusted by translating one of the mirrors in the interferometer. Typical spectra of the laser radiation from the optical parametric amplifier before and after the Michelson interferometer are shown in Figure 4.2. The pulses were focused with an f = 500 mm lens onto a sample positioned inside a variable-temperature helium bath cryostat (T = 2 – 300 K). Laser spot size was estimated to be about $2.5 \cdot 10^{-3}$ cm^2. The pulse peak intensity at the sample was varied from 20 to 80 GW/cm^2 by neutral density filters. In the hole burning experiment, a mask with 1 × 0.6 mm opening was placed just before the sample to ensure that the same exact spot was irradiated and probed.

In the fluorescence-based detection scheme, (Figure 4.1a), two-photon excited fluorescence was collected with a spherical mirror and focused on the entrance slit of a Jobin-Yvon TRIAX 550 Jobin Yvon/Spex spectrometer equipped with a N_2-cooled CCD array detector (Jobin Yvon/Spex CCD-3000).

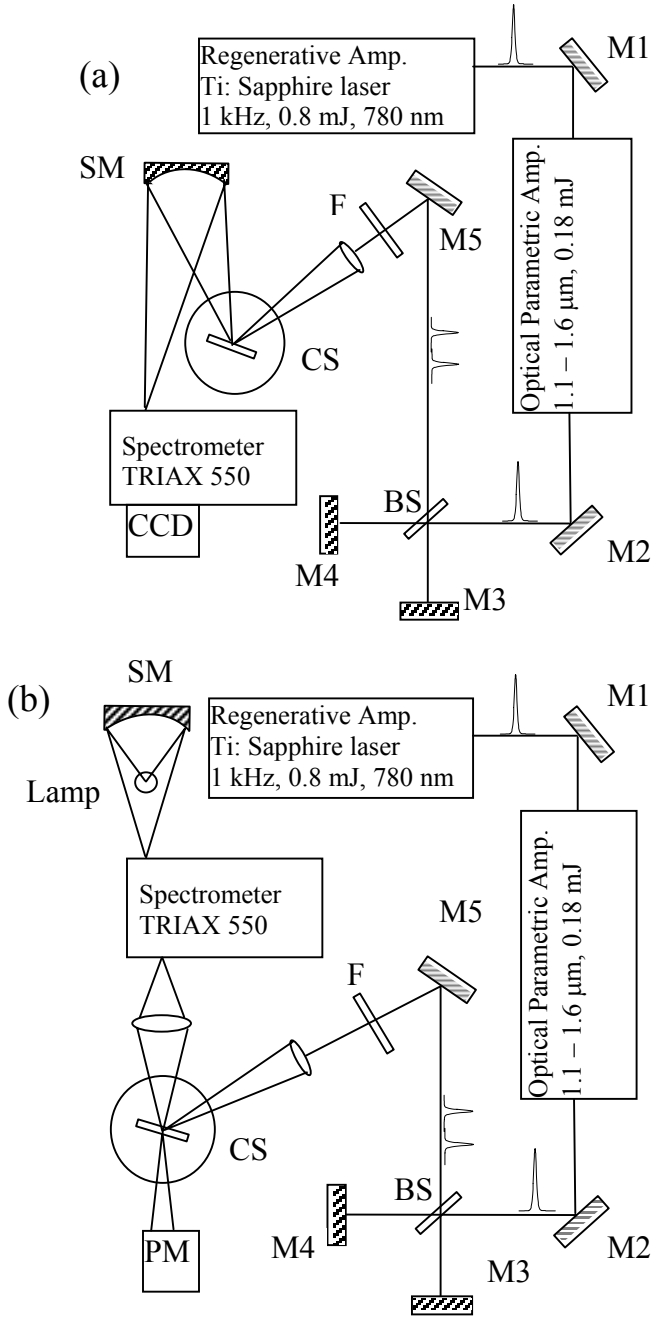

Figure 4.1 Schematic of experimental setup for (a) two-photon excited fluorescence measurements (b) two-photon hole burning. Lamp – filament lamp; PM – photomultiplier; F – set of infrared filters; BS – beam splitter; CS – cryostat with the sample; M1 – M5 mirrors; SM – spherical mirror (f = 50 cm); mirrors M3 and M4 together with beamsplitter BS constitute Michelson interferometer.

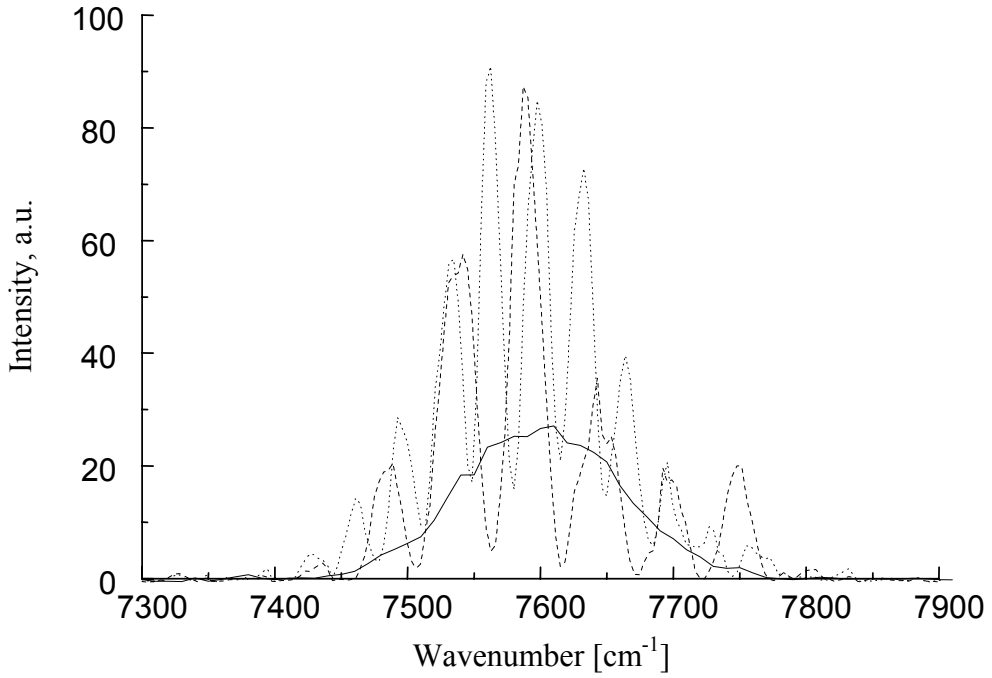

Figure 4.2 Typical example of power spectrum of the optical parametric amplifier radiation before and after Michelson interferometer. Solid line – laser spectrum before the interferometer; dashed and doted lines – laser spectra after the interferometer for corresponding to the pulses with different time delay. The time delay between pulses is determined by the following relation: $\Delta\nu\Delta\tau = 1$, where $\Delta\nu$ is the period of the frequency grating [Hz] and $\Delta\tau$ is the time delay between pulses [s]. In this particular example, the time delay is equal to 1 ps for dotted line and 636 fs for dashed line.

In case of SHB, (Figure 4.1b), spectral holes were registered by measuring transmittance one-photon spectrum of the sample before and after its irradiation with near-IR light. For measurement of the transmission spectra a chopper-modulated light from a filament lamp was dispersed in a TRIAX 550 spectrometer and then focused onto the sample. The intensity transmitted through the sample was recorded with a Hamamatsu photomultiplier (HC120-05) and lock-in amplifier (Stanford Research Systems, SR830 DSP) synchronized with the chopper.

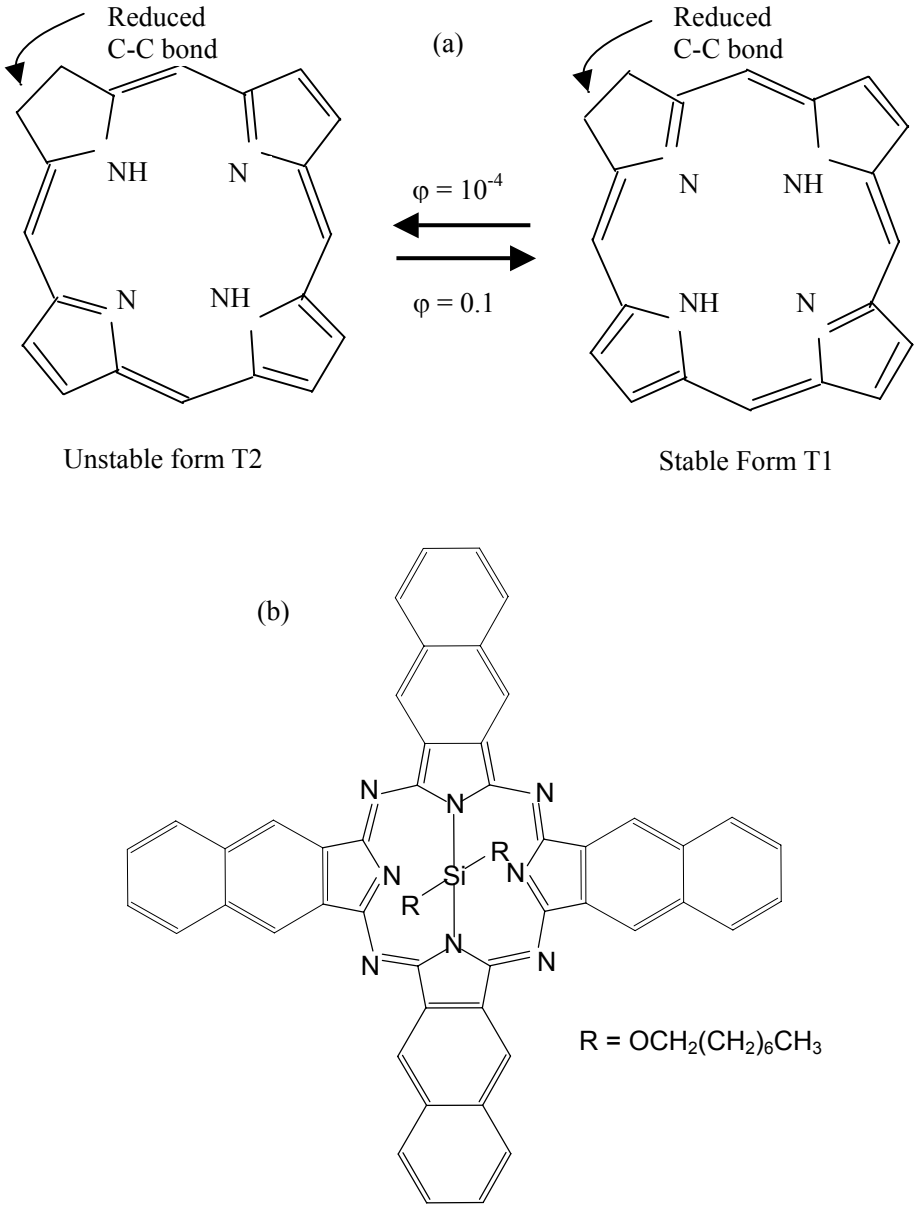

Figure 4.3 Chemical structures of the compounds: (a) 7,8-dihydroporphyrin (chlorin), (b) Silicon-2,3-naphthalocyanine dioctyloxide (SiNc). Two tautomers of chlorin T1 and T2 are shown. The tautomers differ by positions of two protons in the center of the macrocycle. In T1, NH…NH axis is parallel to reduced C-C bond, while in T2 it is perpendicular. Only T1 tautomer is stable at room temperature. T2 tautomer is metastable at liquid helium temperature. The numbers at the arrows show quantum efficiency of the phototransformation T1 $\rightarrow$ T2 (10^{-4}) and T2 $\rightarrow$ T1 (0.1). Reduced C-C bond that makes chlorin non-centrosymmetrical is also shown. In contrast, SiNc is a centrosymmetrical molecule.

The samples we used represented 0.2 mm thick PVB films activated with 7,8-dihydroporphyrin (chlorin) or Silicon-2,3-naphthalocyanine dioctyloxide (SiNc) molecules (Figure 4.3) at a concentration of about 10^{-4} M. SiNc was purchased from Aldrich. Linear absorption spectra were measured with Lambda 900 Perkin Elmer spectrophotometer.

Ti:sapphire oscillator (Coherent, Mira 900) in cw mode at $\lambda = 785$ nm was used for conventional one-photon hole burning in SiNc. He-Ne laser (JDS Uniphase, 1137P) working at $\lambda = 633$ nm was used for one-photon hole burning in chlorin.

Two-Photon-Excited Coherence Gratings Detected by SHB

To demonstrate two-photon-excited coherence gratings by means of SHB one has to find a material suitable for the task. To do that, some conditions should be defined that must be met to perform a successful experiment. This is complicated by the fact that SHB by means of simultaneous TPA has never been achieved before representing complicated problem in itself. Generally, one can identify the following key conditions, which need to be fulfilled to perform one-photon SHB: (1) the lowest purely electronic transition should be spectrally-selective; i.e. the homogeneous spectrum (zero-phonon line plus phonon side-band) should be at least 10 times narrower than inhomogeneous distribution; (2) quantum efficiency of photochemical transformation has to be sufficiently large for spectral changes to be observable at reasonable irradiation times; (3) the product absorption spectrum should be far enough detuned from the excitation light frequency so that reverse photochemical reaction does not take place.

In case of two-photon excitation all the conditions described above become more restrictive. Since the selection rules for one- and two-photon excitation are mutually exclusive for centrosymmetrical molecules, simultaneous excitation of the lowest pure electronic transitions by both OPA and TPA is impossible. Since we are going to excite a molecule with two photons and detect the resulting grating with one-photon process (transmittance spectrum or fluorescence), this rules out centrosymmetrical molecules as potential candidates for TPA-based SHB experiments. It was shown in Chapter 3 (see TPA Properties of Tetrapyrrolic Molecules in the Transitions Spectral Region Corresponding to the Q-bands) that for some centrosymmetrical molecules two-photon excitation into first pure electronic transition might be weakly allowed due to distortion of molecular symmetry. This can be achieved by introducing bulky substituents and/or by stresses induced in the molecule by its environment (PVB film). The influence of these mechanisms on SHB by means of TPA is not very clear by now. Therefore, we decide to make initial experiments with non-centrosymmetrical molecules so that both OPA and TPA are allowed to excite a particular electronic transition.

The quantum efficiency of phototransformation should not be very different for both modes of excitation. In particular, since one excites the same transition in both cases, namely the first pure electronic transition, the quantum efficiency of phototransformation should be the same. On the other hand, the efficiency of two-photon excitation is very low in comparison to its one-photon counterpart. This limits possible materials to the ones with the largest values of quantum yield of phototransformation so that efficient photochemistry can partly overcome low efficiency of TPA.

The condition of non-overlapping frequencies of excitation and photoproduct absorption is more restrictive in the case of TPA because femtosecond pulses are typically required for efficient two-photon excitation. The spectral bandwidth of such pulses is rather large, requiring particularly large separation between absorption bands of original molecule and its photoproduct. In our case the time duration of the laser pulses used for two-photon excitation is τ_{FWHM} = 100 fs. For Gaussian Fourier transform limited pulse it corresponds to spectral width of $\nu_{FWHM} = 4.5 \cdot 10^{12}$ Hz or 5 nm in the used wavelength range ($\lambda \sim 570$ nm).

Of all the molecules whose two-photon spectra in the Q-bands region have been studied in Chapter 3 only chlorin does not possess the center of inversion because of the reduced C-C bond (Figure 4.3a). Its TPA spectrally coincides with the one-photon spectrum in the first electronic Q-band region, confirming that the first pure electronic transition is accessible for both OPA and TPA. It is also well known that chlorin molecule can exist in two different isomeric forms [212,213]. They are called tautomers T1 and T2 (Figure 4.3a). In T1, the NH…NH axis is parallel to the reduced C-C bond. In T2, two protons in the center of chlorin macrocycle occupy different positions so that the NH…NH axis becomes perpendicular to the reduced C-C bond. At room temperature only T1 form exists. At liquid helium temperatures T1 form can undergo photoinduced tautomerization yielding T2. Moreover, absorption spectra of the tautomers are very different (see Figure 4.4). The first absorption band of the T2 shifts about 50 nm to the blue part of the spectrum as compared to T1, providing a good possibility for their independent excitation with femtosecond pulses.

Not surprisingly, one-photon-based SHB in T1 tautomer, based on T1 → T2 phototransformation has been shown before in Shpolskii matrices [213] and polymer films [213,214]. Nevertheless, our attempts to induce a detectable change in T1 absorption by means of its two-photon excitation failed even for irradiation times as large as several hours. The main reason is a very small quantum efficiency of phototautomerization ~ 10^{-4} – 10^{-3} [214,215].

Fortunately, there is another opportunity of using a reverse photoreaction T2 → T1. As compared to T1 → T2 phototransformation, a drastic increase of the rate of back T2 → T1 process has been observed upon one-photon excitation [213-215], giving rise to up to 10% quantum efficiency of this process in polymer matrices. Moreover, all the advantages of the main T1 form of chlorin for TPA-based SHB also apply for its unstable form T2. One disadvantage is that T2 tautomer has a low Debye - Waller factor in polymer matrices [214,215]. Nevertheless, it is known that its inhomogeneous band has a certain degree of spectral selectivity. Therefore, we turn to the metastable (at low temperatures) T2 tautomer to demonstrate the effect of two-photon SHB.

Initial absorption spectrum of stable T1 form of chlorin at 4 K is shown in Figure 4.4, dotted line. This figure also shows the spectrum of the sample after its illumination (20 min) with 633-nm pulses (second harmonic of OPA tuned to 1265 nm), solid line. One can see the strong band appearing at 567 nm, which has been observed earlier at low temperatures in the same system [215] and attributed to the chlorin T2 tautomer.

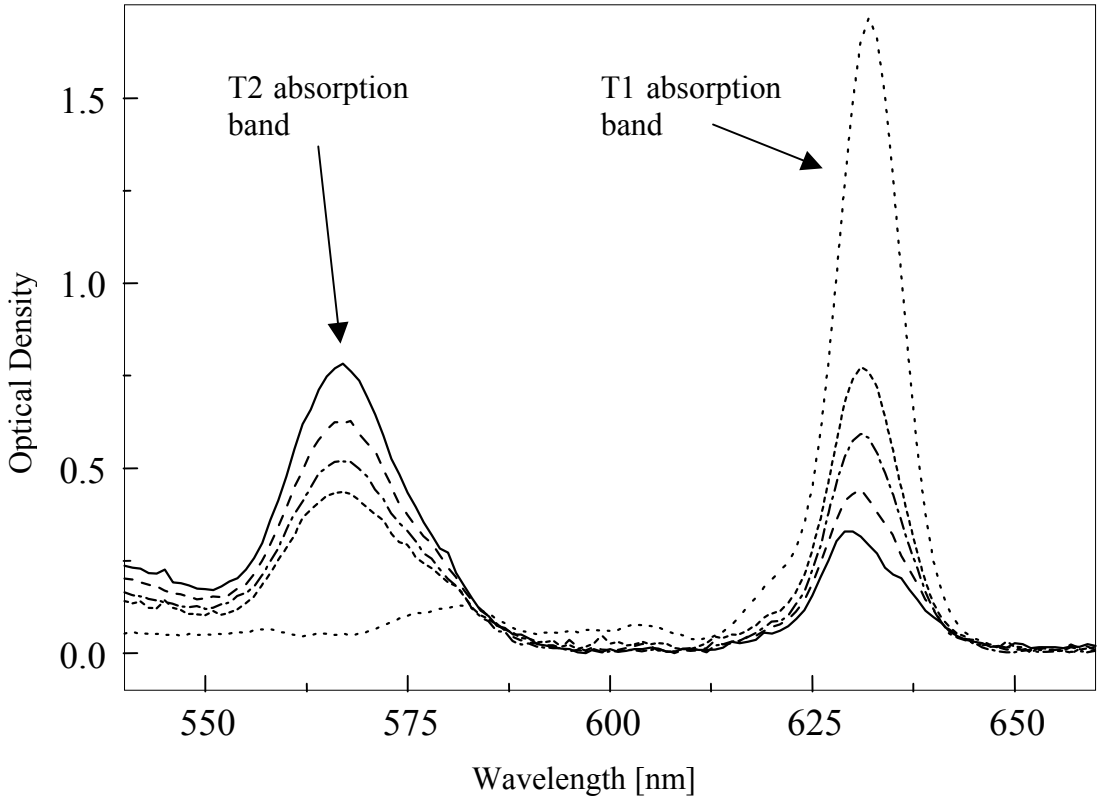

Figure 4.4 Absorption spectrum of the stable chlorin tautomer T1 in PVB film at 4K, dotted line. Spectrum of the sample after illumination with second harmonic of OPA (633 nm, 1 W/cm^2 average power density) for 20 min, solid line. The band at 567 nm corresponds to unstable tautomer T2. Dashed, dash-dotted, and short dashed lines correspond to spectra after illumination of T2 form with 3.6, 4.7, and 6.1-kJ/cm^2 total fluence of 1134-nm OPA pulses, respectively.

Excitation of the sample now with 1134-nm pulses yields an orange fluorescence. Prolonged illumination results in a decrease of absorption at 567 nm and simultaneous increase of the initial band at 633 nm (dash, dot-dash, and short dash lines in figure 3.3). These facts confirm that the TPA of the photoproduct T2 takes place and leads to T2 $\rightarrow$ T1 back transformation. As can be seen from Figure 4.4, the changes in T2 spectrum are non-selective, i.e. absorption band goes down as a whole, without SHB. This is due to the fact that the laser spectrum in this particular experiment has almost the same width and maximum as the inhomogeneous absorption band.

To obtain the frequency-selective SHB, we used Michelson interferometer with a time delay of ~ 180 fs between two pulses. This resulted in a spectral modulation with $\Delta\nu = 180 \pm 20$ cm^{-1}. Figure 4.5 demonstrates the changes in T2 absorption band of chlorin as a result of irradiation of sample with pairs of pulses.

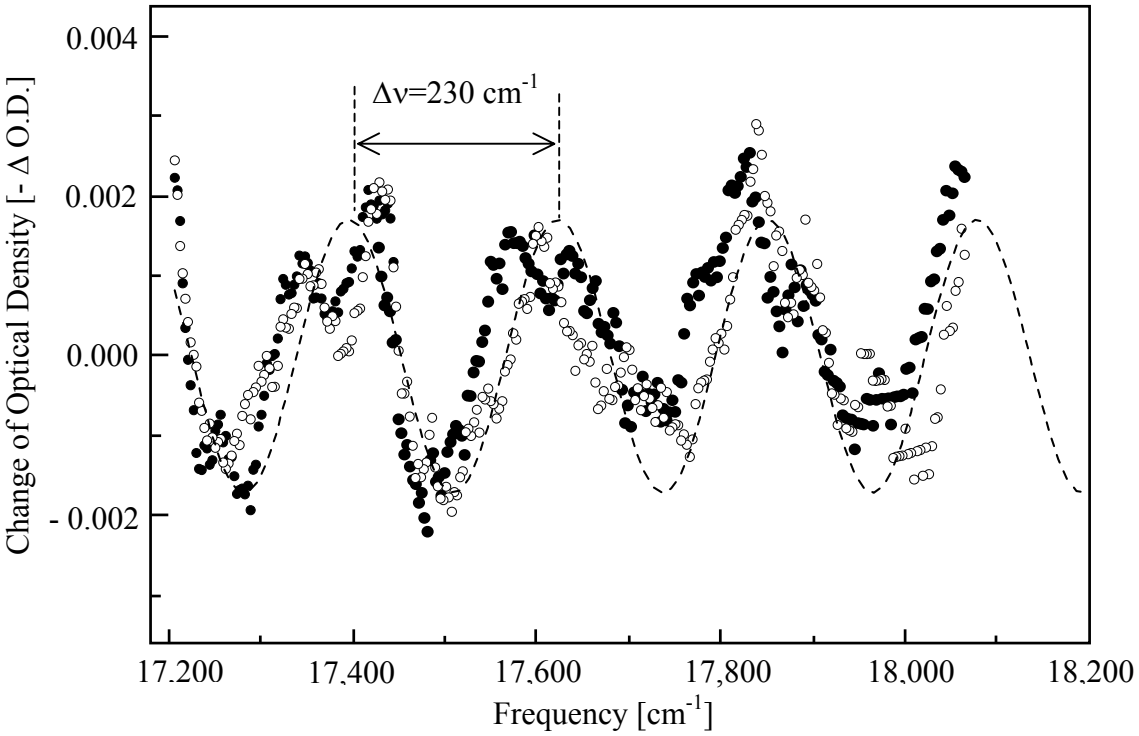

Figure 4.5 Spectral modulation in the T2 absorption band induced by two-photon absorption from pairs of pulses with 180-fs time delay between them after irradiation time of 45 (closed dots) and 285 s (open dots), I = 3 W/cm^2. Dashed line represents a cosine function with a period of 230 cm^{-1}.

Experimental dots (closed and open) were obtained as follows. Absorption spectrum before burning was subtracted from that after burning. Then, this differential spectrum was approximated with a Gaussian envelope function. Finally, the Gaussian fit was subtracted from experimental differential spectrum and the result was smoothed with standard method using 10 adjacent points. The closed and open dots correspond to the 45

s and 285 s irradiation times, respectively. The experimental results show modulation period of the holes of 230 ± 30 cm^{-1}. This value coincides with expected period within experimental error.

A poor contrast of the holes occurs because of low Debye - Waller factor (< 0.1) [214,215], which was mentioned above. However, it is known that for a broad inhomogeneous distribution function, exceeding both the phonon wing of homogeneous spectrum and laser spectrum, one can still observe the spectral selectivity [216,217]. At low irradiation fluence, a relatively broad hole will appear exactly at laser maximum frequency. During the burning process the hole will broaden and shift towards the maximum of inhomogeneous distribution to coincide with it when almost all the centers will be burnt. We can use this effect here as another convincing demonstration of SHB via simultaneous TPA. Successive changes of the hole shape as a function of irradiation time are shown in Figure 4.6. One can definitely see that at the earlier stages the maximum of the broad envelope continuously shifts to the center of inhomogeneous distribution (567 nm). This is depicted in Figure 4.6, inset. This experiment shows that during the burning process molecules with different transition frequencies become involved in photoinduced reaction, which means that the system is spectrally selective.

Note that the effect of SHB via non-resonant TPA differs radically from the well-known photon-gated SHB [63]. The latter implies sequential absorption of two photons with the first one in resonance with molecule absorption.

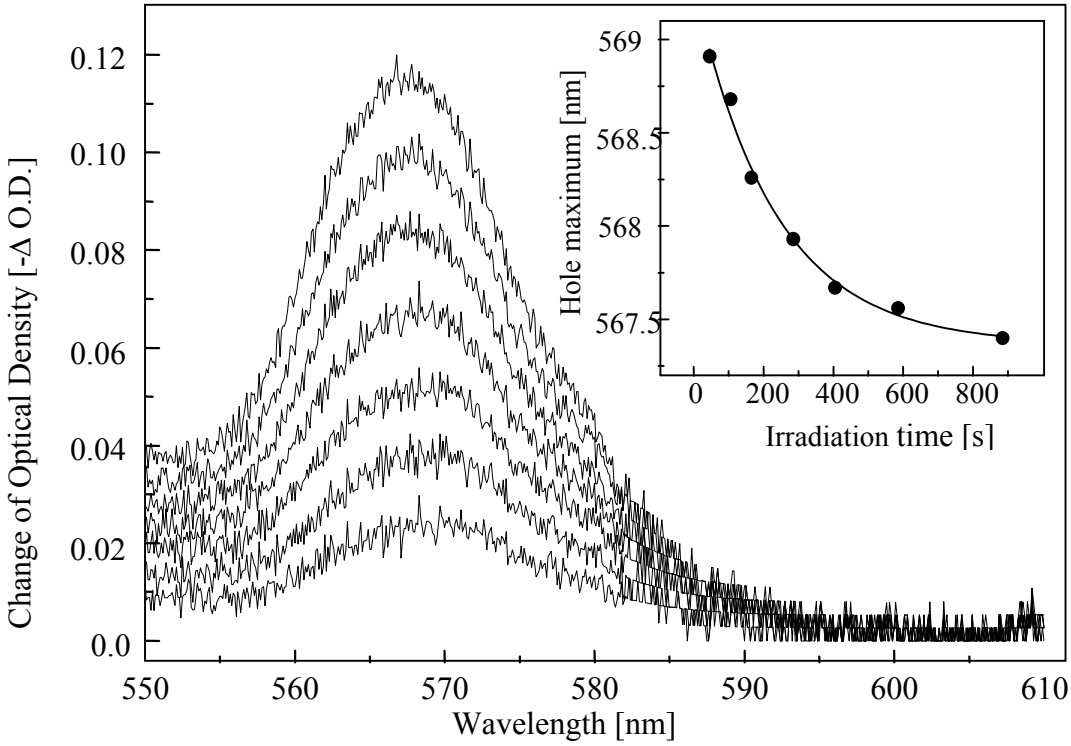

Figure 4.6 Spectral changes in T2 absorption band upon successive irradiation with pairs of pulses with carrier wavelength at 1138 nm, I = 3 W/cm^2. Curves from bottom to top correspond to increasing irradiation time. Inset shows the position of spectral envelope maximum of each curve as a function of that time (points) with exponential decay fit (solid line).

Two-Photon Excited Coherence Gratings Detected by Fluorescence

To observe the spectral modulation, we first recorded a spectrum of resonance fluorescence of a chlorin-doped polymer film (stable T1 tautomer), kept at 4 K, in the region of inhomogeneously broadened 0-0 transition near 630 nm, Figure 4.7, solid line. Excitation was carried out with pairs of infrared pulses with 670 fs time delay at carrier wavelength of 1270 nm. The period of fluorescence intensity modulation is 50 cm^{-1}, which is exactly equal to the period of laser spectrum modulation. For comparison, the power spectrum of second harmonic of the excitation light (dashed line) obtained with nonlinear crystal is also presented at Figure 4.7.

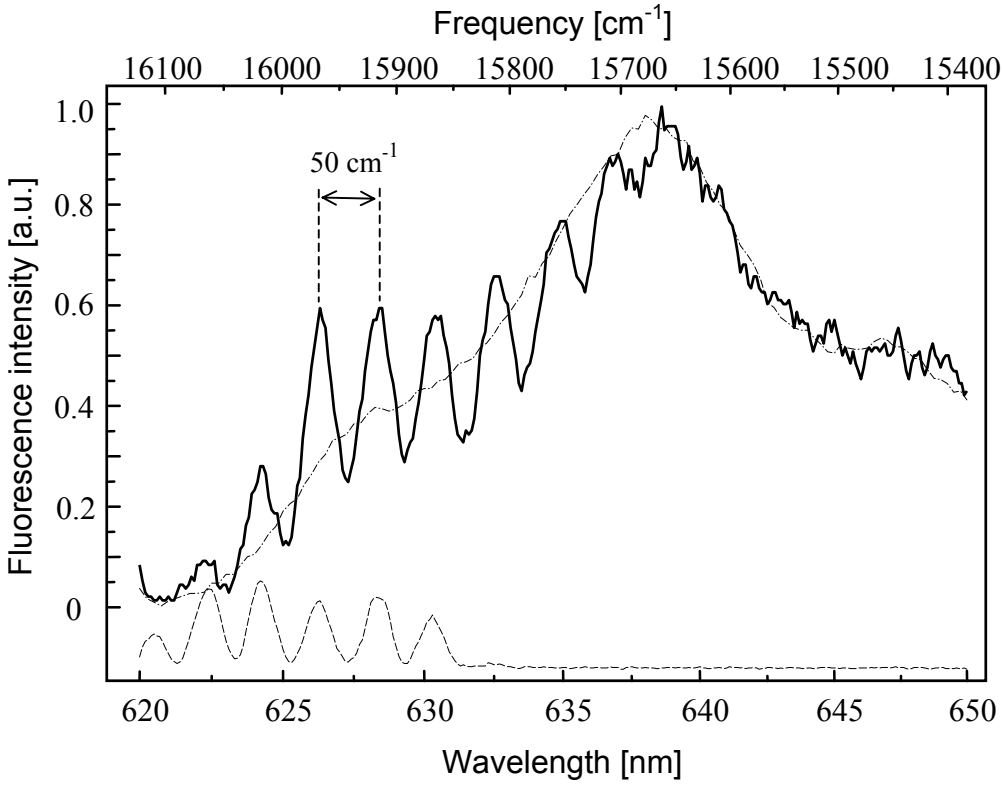

Figure 4.7 Frequency-domain modulated ($\Delta\nu$ = 50 cm^{-1}) fluorescence spectrum of chlorin in PVB film (solid line). Two-photon excitation is performed with pairs of femtosecond pulses at 1270 nm. The spectrum obtained with one closed arm of Michelson interferometer (dote-dashed line) is normalized with respect to the previous one. The spectrum of laser second harmonics is presented for comparison (dashed line).

The long wavelength side of the spectrum is distorted due to narrow synchronism bandwidth of our thick nonlinear crystal. We checked that a change of delay time between infrared pulses resulted in corresponding change in fluorescence modulation period. Note that the excitation light reaching the sample contained no second harmonic. In all the cases the period (measured in wavenumbers) of fluorescence modulation was equal to that of the laser spectrum. The modulation in fluorescence spectrum disappeared (Figure 4.7, dash-dotted line) when one of the arms of Michelson interferometer was blocked. Although power spectrum of the laser second harmonic approximately

corresponds to the TPA-induced fluorescence spectrum we underline that one cannot deduce the whole modulation structure in the fluorescence signal from that in the power spectrum.

Note that the Debye – Waller factor is larger for the stable form of chlorin T1 (α_{T1} = 0.55) [215] in comparison to its unstable counterpart T2 ($\alpha_{T2} < 0.1$) [214,215] resulting in a much deeper modulation than the one observed in SHB experiment. Also the quantum yield of fluorescence of the stable form is much larger than its quantum yield of phototransformation making observation of spectral gratings via fluorescence detection technique possible. In fact, it is much easier to find molecule with large quantum yield of fluorescence (> 0.1) than large quantum efficiency of phototransformation so that the second condition described in the previous paragraph is less restrictive for the fluorescence-based measurements.

Next, we applied the same method for two-photon excitation of fluorescence of centrosymmetrical molecule SiNc in PVB film at T = 4 K. The wavelength of the laser pulses is 1570 nm so that excitation takes place into the first OPA band situated around 785 nm (Figure 4.8). Although the two-photon transition to the one-photon band is prohibited for centrosymmetrical molecules by symmetry, we were able to observe the fluorescence signal modulated similarly to chlorin. The only difference is that for SiNc the modulation depth of the fluorescence spectrum is smaller than that for chlorin. At first sight this behavior seems very unusual because the Debye – Waller factor of SiNc ($\alpha_{SiNc} \approx 1.0$) [218]is even larger than that of chlorine.

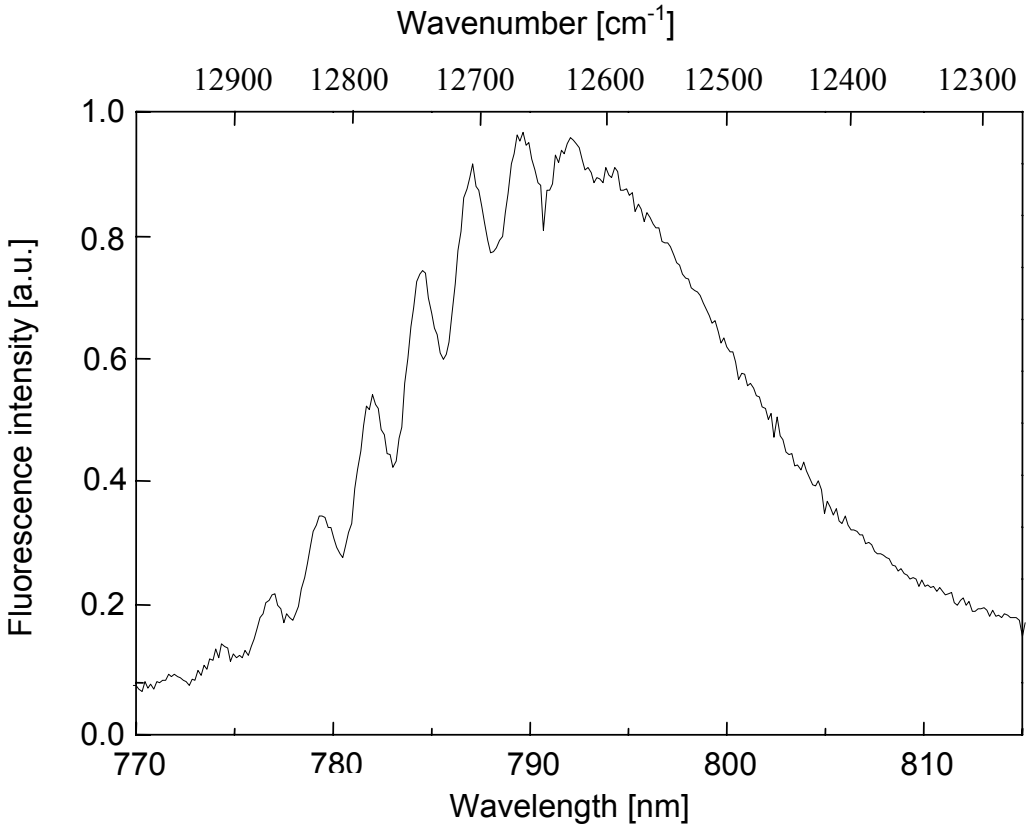

Figure 4.8 Frequency-domain modulated fluorescence spectrum of SiNc. Two-photon excitation is performed with pairs of femtosecond pulses at 1570 nm. Note, that the depth of modulation is smaller than that for chlorin.

The effect can be explained by considering molecular symmetry and its effect on the one- and two-photon transitions. For SiNc, two-photon transition into the first pure electronic transition is prohibited by symmetry. Nevertheless, one still can induce some TPA through creation of phonons in the PVB matrix. The resulting two-photon electron-phonon transition can be partially allowed through the Herzberg-Teller mechanism. In this case one can suppose that the zero phonon line in the homogeneous TPA spectrum of SiNc is either absent or very weak. All the absorption takes place through the phonon wing (PW), making the Debye – Waller factor effectively equal to zero. This remarkable difference between the one- and two-photon homogeneous spectra of centrosymmetrical

molecules explains a shallow modulation of the spectral grating. In the case of chlorin, TPA is allowed into the first pure electronic transition so that the zero photon line is present in the homogeneous TPA spectrum. As a result, the modulation depth of the spectral grating of non-centrosymmetrical molecule is larger than that of centrosymmetrical molecule.

Temperature Dependence of Spectral Gratings

To get more insight into the role of molecular symmetry in homogeneous TPA spectrum, we measured the temperature dependence of TPA fringes in non-centrosymmetrical chlorin and centrosymmetrical SiNc. The results are presented in Figure 4.9. In both cases, an increase of temperature results in diminishing contrast of the fringes. The striking difference between the two systems is that in chlorin the fringes shift to the red with increasing temperature, whereas in SiNc this shift is much less pronounced. Indeed, for chlorin the observed shift of the grating constitutes a half of its period upon increasing temperature from 4 to 60K. We checked that this shift was completely reversible when temperature was lowered down to 4K again, thus ensuring that it is the inherent property of the sample.

Theoretical Model

In order to simulate quantitatively the temperature dependence of TPA-induced gratings, presented in Figure 4.9, we have elaborated the following model. Fluorescence spectrum of inhomogeneously broadened ensemble of molecules, each of which possesses homogeneous TPA spectrum $g_2(\nu-\nu_0,T)$, homogeneous one-photon

fluorescence spectrum $g_1(\nu-\nu_0,T)$, where ν_0 is the ZPL frequency, and excited by excitation spectrum $E(\nu")$, is given by

$$F(\nu,T)=K(\nu)\int_{-\infty}^{\infty} g_1(\nu-\nu_0,T)\,d\nu_0 \int_{-\infty}^{\infty} g_2(\nu"-\nu_0,T)E(\nu")d\nu", \qquad (4.12)$$

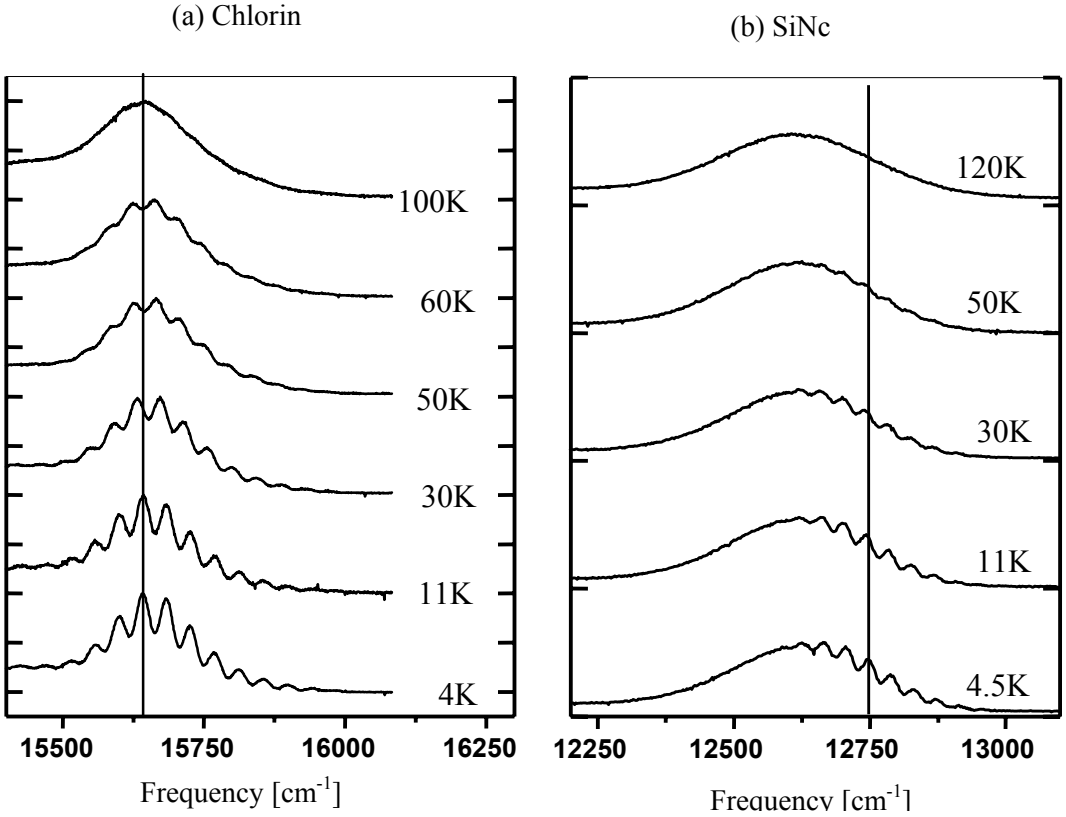

Figure 4.9 (a) $S_1 \rightarrow S_0$ fluorescence emission spectra of a chlorin-doped polymer film obtained at different temperatures upon illumination with pairs of 1280-nm pulses. At low temperatures, one can clearly see a modulation with a period of 45 cm^{-1}, which corresponds exactly to the inverse time delay between the pulses. With increasing temperature, the grating shifts to longer wavelengths and the depth (contrast) of the modulation decreases. (b) $S_1 \rightarrow S_0$ fluorescence spectra of a SiNc-doped polymer film obtained at different temperatures upon illumination with pairs of 1585-nm pulses. As compared to chlorin, there is almost no spectral shift of the grating, but only decrease of modulation depth.

where $K(\nu)$ is a slowly varying spectral function, including excitation spectrum envelope and inhomogeneous distribution function, which are both much broader than the grating period, ZPL, and PW. The excitation spectrum $E(\nu'')$ is described by the equation (4.11).

The homogeneous TPA and one-photon fluorescence spectra are represented as a sum of ZPL and PW:

$$g_{1,2}(\nu-\nu_0,T)=\alpha_{1,2}(T)\delta(\nu-\nu_0)+[1-\alpha_{1,2}(T)]p_{1,2}(\nu-\nu_0)\,, \tag{4.13}$$

where $\alpha_{1,2}(T)$ is the Debye –Waller factor, indexes 1 and 2 designate fluorescence and absorption, respectively, ZPL is represented by delta-function, and $p_{1,2}(\nu-\nu_0)$ describes PW.

To find out a model function PW we performed a standard one-photon hole burning experiment with both chlorin and SiNc in PVB films. The Ti:sapphire laser working in cw mode at λ = 785 nm, was used for one-photon hole burning in SiNc. The He-Ne laser (λ = 633 nm) was used for one-photon excitation of chlorin.

Figure 4.10 demonstrates the profiles of the resulting spectral holes. Both figures were obtained by subtracting absorption spectrum after irradiation from that before irradiation. Note that a ratio of integrated ZPL and PW does not reflect the real Debye – Waller factor, since zero-phonon hole is already saturated. However, pseudophonon sideband reasonably reflects the PW profile. The dashed line shows a fit of the PW profile with the following function:

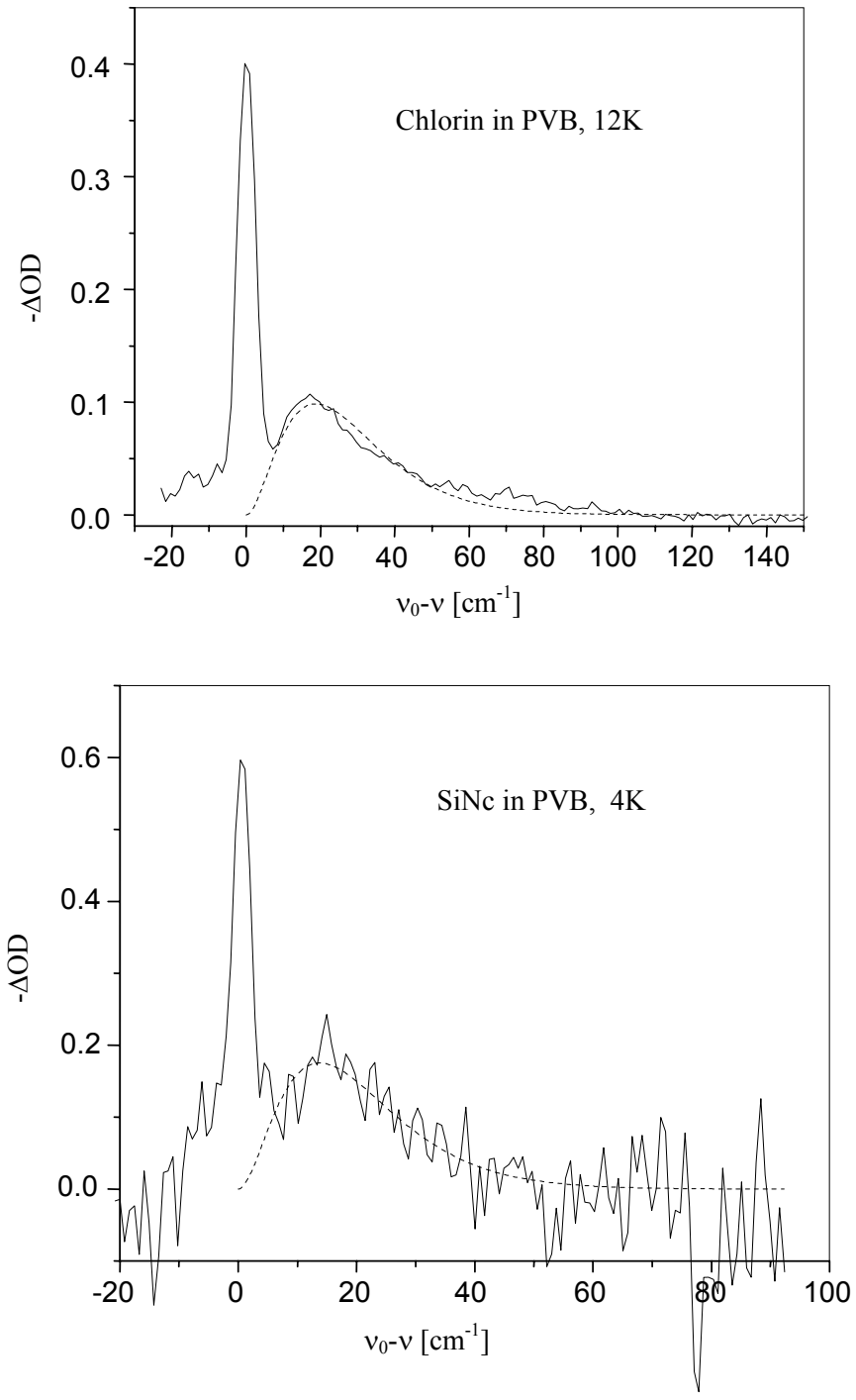

Figure 4.10 Spectral hole profiles for chlorin (a) and SiNc (b) in PVB. A ratio of integrated ZPL and PW does not reflect the Debye-Waller factor, since zero-phonon hole is already saturated. However, pseudophonon sideband (to the right of ZPL) reasonably reflects the PW profile. A fit of PW profile to function (4.14) is shown by dashed line on each plot.

$$p(\nu-\nu_0)=\frac{Const}{\nu_{\max}^3}(\nu_0-\nu)^2\exp[-\tfrac{2}{\nu_{\max}}(\nu_0-\nu)], \tag{4.14}$$

where ν_{max} is the maximum of spectral distribution of PW and *Const* is some constant. The only adjustable parameters in equation (4.14) are *Const* and ν_{max}. The best fit gives ν_{max} = 18 cm^{-1} for chlorin and ν_{max} = 14 cm^{-1} for SiNc, which agrees well with previous hole burning [214,219] and Raman scattering [220] results for PVB. We assume the effect of temperature broadening of PW is negligible, which is justified experimentally [221] in the same temperature range (4 – 100 K) as in our experiments. Since function (4.14) satisfactory fits experimental data in Figure 4.10 we use it as a shape function describing homogeneous PW. Namely,

$$p_{1,2}(\nu-\nu_0)=\begin{cases}\dfrac{4}{\nu_{1,2}^3}(\nu_0-\nu)^2\exp[\mp\tfrac{2}{\nu_{1,2}}(\nu_0-\nu)], & \mp(\nu_0-\nu)>0\\ 0, & \pm(\nu_0-\nu)\le 0\end{cases}, \tag{4.15}$$

where the upper sign is for fluorescence and the lower sign is for absorption, $\nu_{1,2}$ is the maximum of spectral distribution of PW. Coefficient 4 in front of the equation (4.15) is placed for normalization reason so that the integral $\int_0^\infty p(\nu-\nu_0)d\nu$ is equal to unity.

All the temperature dependence of the homogeneous spectrum is contained in Debye – Waller factor, which we describe in one-oscillator approximation as

$$\alpha_{1,2}(T)=\exp\left(-\xi_{1,2}\ cth\left(\frac{h\nu_{1,2}}{2kT}\right)\right), \tag{4.16}$$

where ξ is the electron-phonon coupling strength.

By substituting all the equations into (4.12) and performing integration, one gets the following expression for fluorescence spectrum (see Appendix D for details):

$$F(\nu,T) = K(\nu)[1 + M(T)\cos(2\pi\Delta\tau\nu + \Delta\varphi(T))]\,. \tag{4.17}$$

The oscillating part of this function demonstrates that the spectral grating is indeed must be observed in fluorescence spectrum. The amplitude $M(T)$ and the phase shift $\Delta\varphi(T)$ of the grating are given by the following expressions:

$$\begin{aligned} M(T) = \beta\{&[A(T) + B(T)\cos\delta_2 + C(T)\cos\delta_1 + D(T)\cos(\delta_1+\delta_2)]^2 \\ &+ [B(T)\sin\delta_2 + C(T)\sin\delta_1 + D(T)\sin(\delta_1+\delta_2)]^2\}^{1/2} \end{aligned}, \tag{4.18}$$

$$\Delta\varphi(T) = arctg\frac{B(T)\sin\delta_2 + C(T)\sin\delta_1 + D(T)\sin(\delta_1+\delta_2)}{A(T) + B(T)\cos\delta_2 + C(T)\cos\delta_1 + D(T)\cos(\delta_1+\delta_2)}, \tag{4.19}$$

where the functions $A(T)$, $B(T)$, $C(T)$, $D(T)$, and δ are equal to:

$$A(T) = \alpha_1(T)\alpha_2(T)\,, \tag{4.20}$$

$$B(T) = [1-\alpha_1(T)]\alpha_2(T)\{1 + (\pi\Delta\tau\nu_2)^2\}^{-3/2}\,, \tag{4.21}$$

$$C(T) = \alpha_1(T)[1-\alpha_2(T)]\{1 + (\pi\Delta\tau\nu_1)^2\}^{-3/2}\,, \tag{4.22}$$

$$D(T) = [1-\alpha_1(T)][1-\alpha_2(T)]\{[1 + (\pi\Delta\tau\nu_2)^2][1 + (\pi\Delta\tau\nu_1)^2]\}^{-3/2}\,, \tag{4.23}$$

$$\delta_{1,2} = 3arctg(\pi\Delta\tau\nu_{1,2})\,. \tag{4.24}$$

Equation (4.19), describing the phase shift, is physically meaningful only in some limiting cases. For example, if PW is absent, i.e. the Debye – Waller factor is equal to one, then no phase shift should take place, because ZPL is the same for both absorption and fluorescence homogeneous spectra. Indeed, for $\alpha_1(0) = \alpha_2(0) = 1$, equation (4.19) gives quantitatively correct result: $\Delta\varphi(0) = 0$. On the other hand if ZPL is missing in both spectra, i.e. $\alpha_1(0) = \alpha_2(0) = 0$, then

$$\Delta\varphi = 3(arctg(\pi\Delta\tau\nu_1) + arctg(\pi\Delta\tau\nu_2)). \quad (4.25)$$

If $\pi\Delta\tau\nu_{1,2} \ll 1$, expression (4.25) can be approximated by:

$$\Delta\varphi = 3\pi\Delta\tau(\nu_1 + \nu_2). \quad (4.26)$$

The fluorescence spectrum (see equation (4.17)) then turns into:

$$F(\nu,T) = K(\nu)[1 + M(T)\cos\{2\pi\Delta\tau(\nu + \frac{3}{2}(\nu_1 + \nu_2))\}]. \quad (4.27)$$

An additional frequency shift, $\Delta\nu = \frac{3}{2}(\nu_1 + \nu_2)$, corresponds to the Stokes shift, equal to a difference between centers of gravity of PWs (see equation (4.15)) in absorption and fluorescence. In general case, the values of $\Delta\varphi$ allowed by (4.19) are restricted by definition of function *arctg*(*x*), and, therefore, equation (4.19) is unable to describe a wide range of other real sets of parameters. In our approach, we use equation (4.18) for the simulation of the temperature dependence of the amplitude (contrast) of the fringes, but we resort to a simpler model for the simulation of the temperature dependence of the phase. Namely, we consider the Stokes shift as a difference between the first moments (centers of gravity) of absorption and fluorescence spectra,

$$\Delta\nu(T) = (1 - \alpha_2(T))\nu_2 + (1 - \alpha_1(T))\nu_1, \quad (4.28)$$

and, therefore,

$$\Delta\varphi(T) = 2\pi\Delta\tau[(1 - \alpha_2(T))\nu_2 + (1 - \alpha_1(T))\nu_1]. \quad (4.29)$$

Simulation and Discussion

First, we simulated the temperature dependence of the fringes in chlorin in PVB by using symmetrical model with $\xi_1 = \xi_2 = \xi$ and $\nu_1 = \nu_2 = \nu_m$, i.e. we suppose that

homogeneous TPA and homogeneous one-photon fluorescence spectra have mirror symmetry. Symmetrical model can be a reasonable approximation for chlorin because both one- and two-photon transitions are simultaneously allowed. Therefore, one expects one- and two-photon homogeneous spectra to be similar. By varying two adjustable parameters, ξ and ν_m, we obtain the best fit, shown in Figure 4.11a, at ξ=0.36, (i.e. $\alpha_1(0) = \alpha_2(0) = 0.70$) and $\nu_m = 25$ cm^{-1}. Substitution of these parameters into equation (4.29) without any further fitting gives a phase shift, shown in Figure 4.11b by solid line. One can conclude that the model fits well to experimental data in this case and the obtained parameters are reasonable. The value of ν_m is slightly larger than the maximum phonon frequency (18 cm^{-1}), but it is very close to a center of gravity of PW distribution, which can be a real effective frequency entering equation (4.16). The limiting Debye-Waller factor $\alpha_1(0)$ agrees well with the value measured at 7 K ($\alpha_1 = 0.55$) in [215].

We then performed the fit procedure of the same data but using an asymmetrical model, where all four parameters ξ_1, ξ_2, ν_1, and ν_2 were varied independently. The best fit of $M(T)$ (Figure 4.12a), and $\Delta\varphi(T)$ (Figure 4.12b), do, in fact, describe the experiment quite well, but the limiting Debye-Waller factor $\alpha_1(0) = 0.86$ comes out much larger than the literature data, cited before. The main conclusion that can be drawn from the simulation obtained for chlorin in PVB, is that the symmetrical model works quite well for this system, indicating that homogeneous TPA spectrum contains ZPLs.

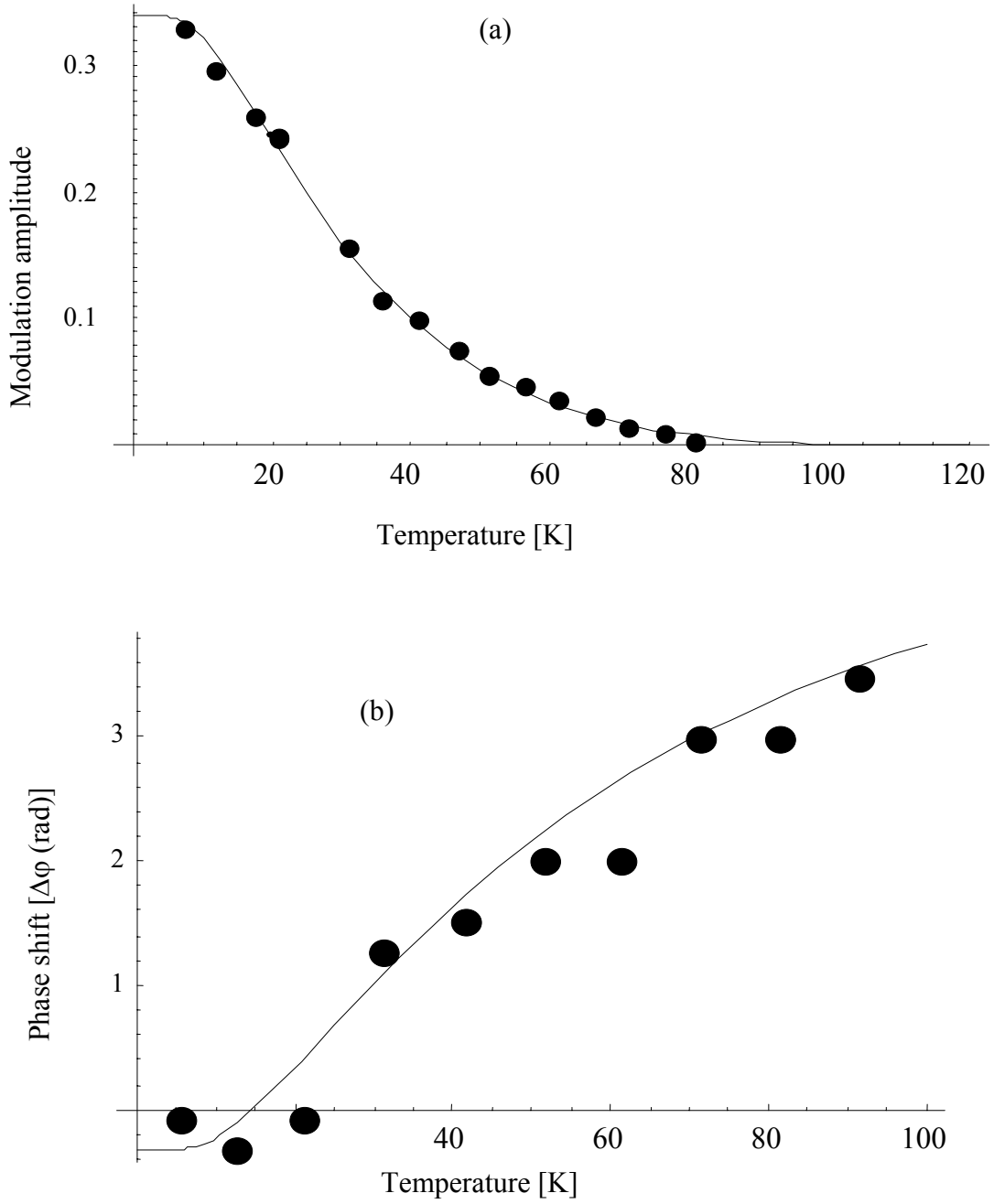

Figure 4.11 Temperature dependence of amplitude M (a) and phase shift $\Delta\varphi$ (b) of the spectral grating observed in chlorin and corresponding fits of these data to equations (4.18) and (4.29) within mirror-symmetrical model.

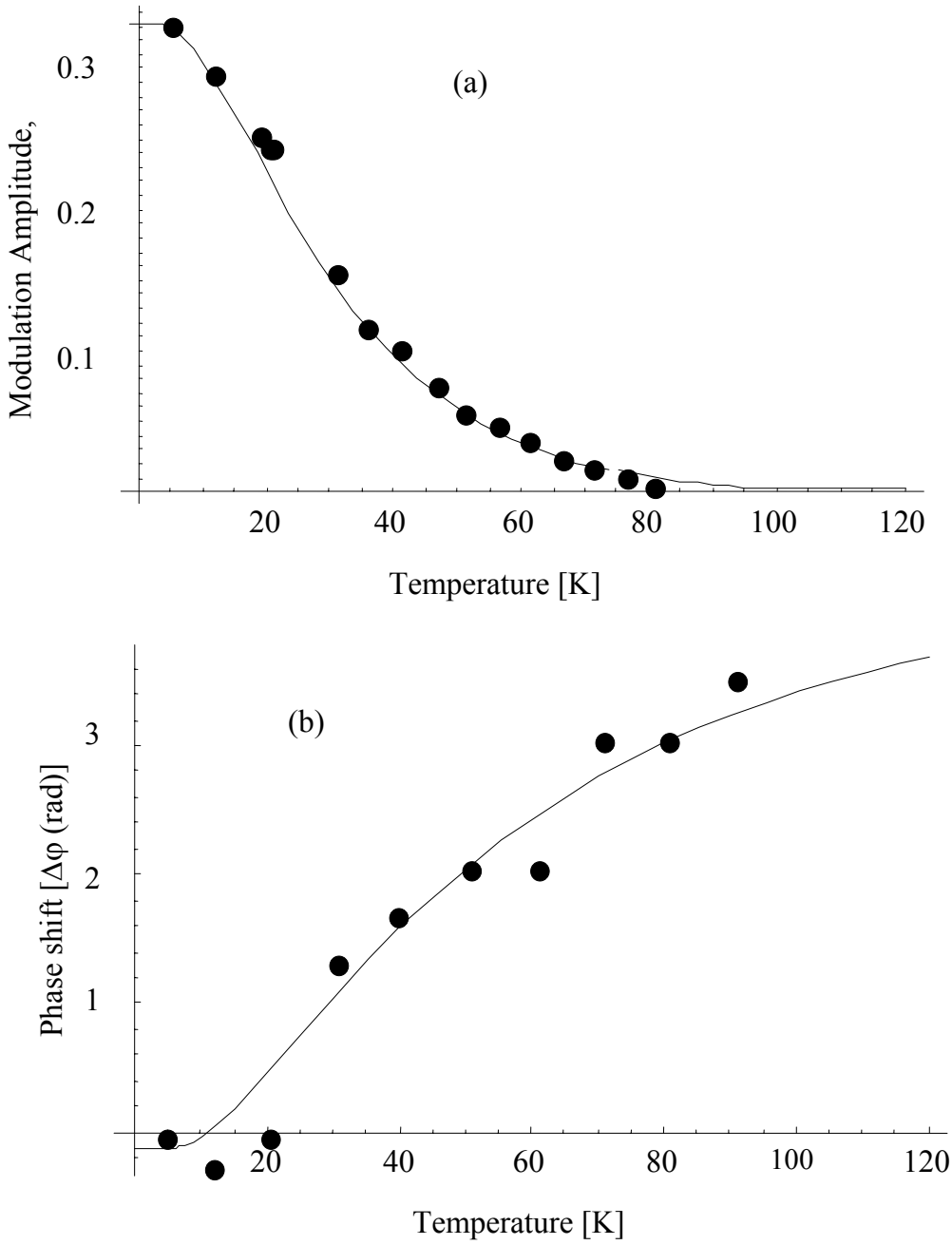

Figure 4.12 Temperature dependence of amplitude M (a) and phase shift $\Delta\varphi$ (b) of the spectral grating observed in chlorin and corresponding fits of these data to equations (4.18) and (4.29) within non-mirror-symmetrical model.

The simulation of experimental data for SiNc:PVB with mirror-symmetrical model is shown in Figure 4.13. Again, the fit procedure was first accomplished for the

amplitude and then the best parameters were introduced into equation (4.29) to describe the phase shift. The main inconsistency between the simulation and experiment is observed in the phase behavior, because the model tends to overestimate the rate of the shift with temperature. The obtained best fit parameters also differ considerably from literature data: the limiting value of Debye-Waller factor $(\alpha_1(0) = 0.56)$ is way too small as compared to that reported previously $(\alpha_1 = 1.0$ at 1.5 K) [218] and the characteristic phonon frequency $\nu_m = 39$ cm^{-1} seems to be overestimated.

Our next attempt was to simulate the data with asymmetrical model with four independent parameters (Figure 4.14). One-photon parameters were fixed to the values, known from hole-burning spectroscopy: α_1 (0) = 0.9 and $\nu_1 = 17$ cm^{-1}, and ξ_2 and ν_2 were varied. The best fitting values obtained for these parameters are $\xi_2 = 1.0$ ($\alpha_2(0) = 0.37$) and $\nu_2 = 56$ cm^{-1}. It is obvious that this fit fails again in describing the phase shift of Figure 4.14b.

The only reasonably good fit could be obtained if α_2 was artificially set to zero, $\alpha_2(T) = 0$ $(\xi_2 = 10000)$, and other three parameters were varied independently (Figure 4.15). It implies no ZPL in TPA spectrum even at the lowest temperature. For the emission spectrum we obtain reasonable $\xi_1 = 0.46$ and $\nu_1 = 27$ cm^{-1}, while the Debye-Waller factor again occurs smaller than measured in [218] (0.63 vs. 1.0). Note that the homogeneous TPA spectrum turns out to be strongly asymmetric with respect to homogeneous one-photon emission spectrum. Not only does this absorption contain no ZPL ($\alpha_2(0) = 0$), but its PW is shifted by only $\nu_2 = 10$ cm^{-1} from the zero-phonon origin.

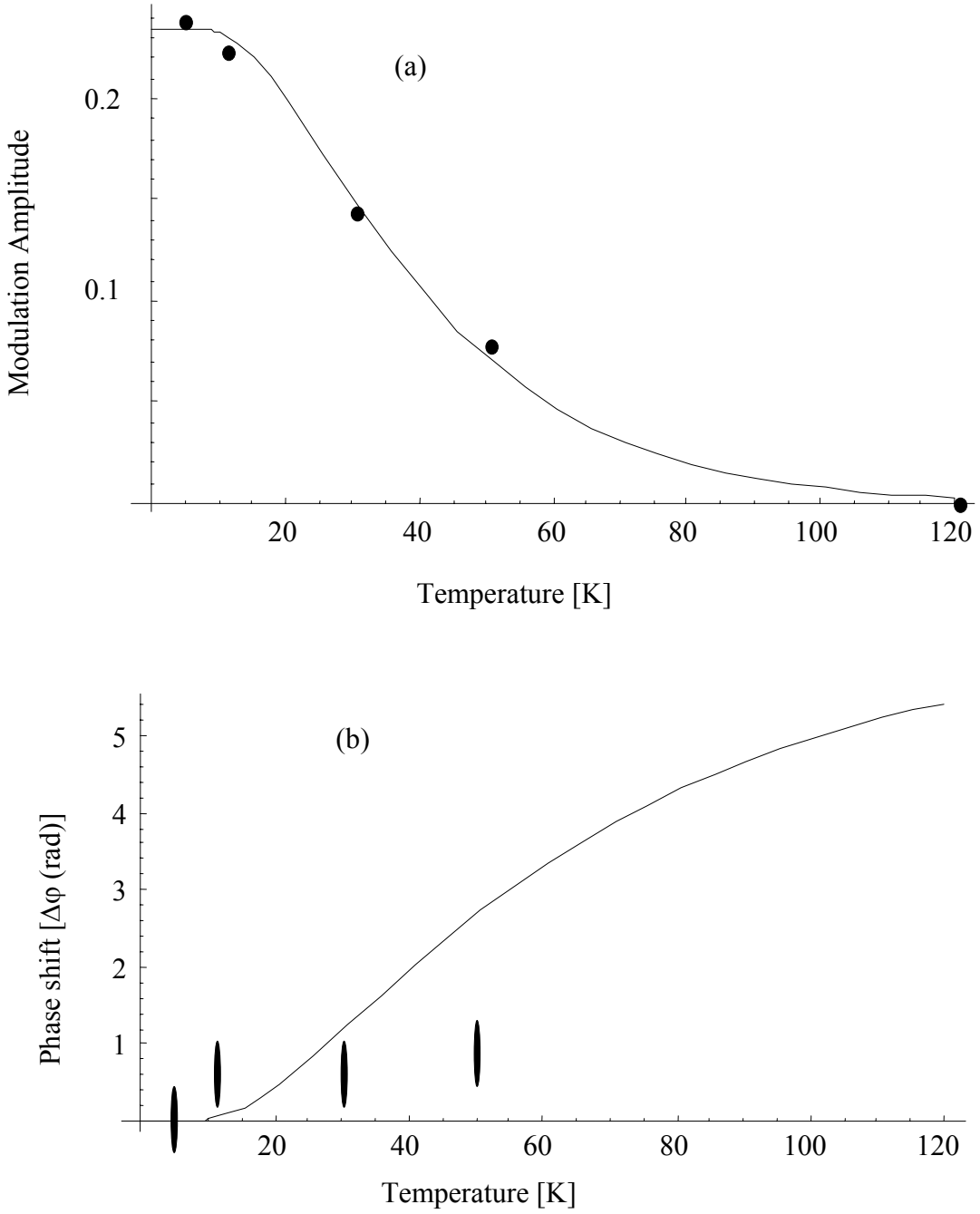

Figure 4.13 Temperature dependence of amplitude M (a) and phase shift $\Delta\varphi$ (b) of the spectral grating observed in SiNc and corresponding fits of these data to equations (4.18) and (4.29) within mirror-symmetrical model.

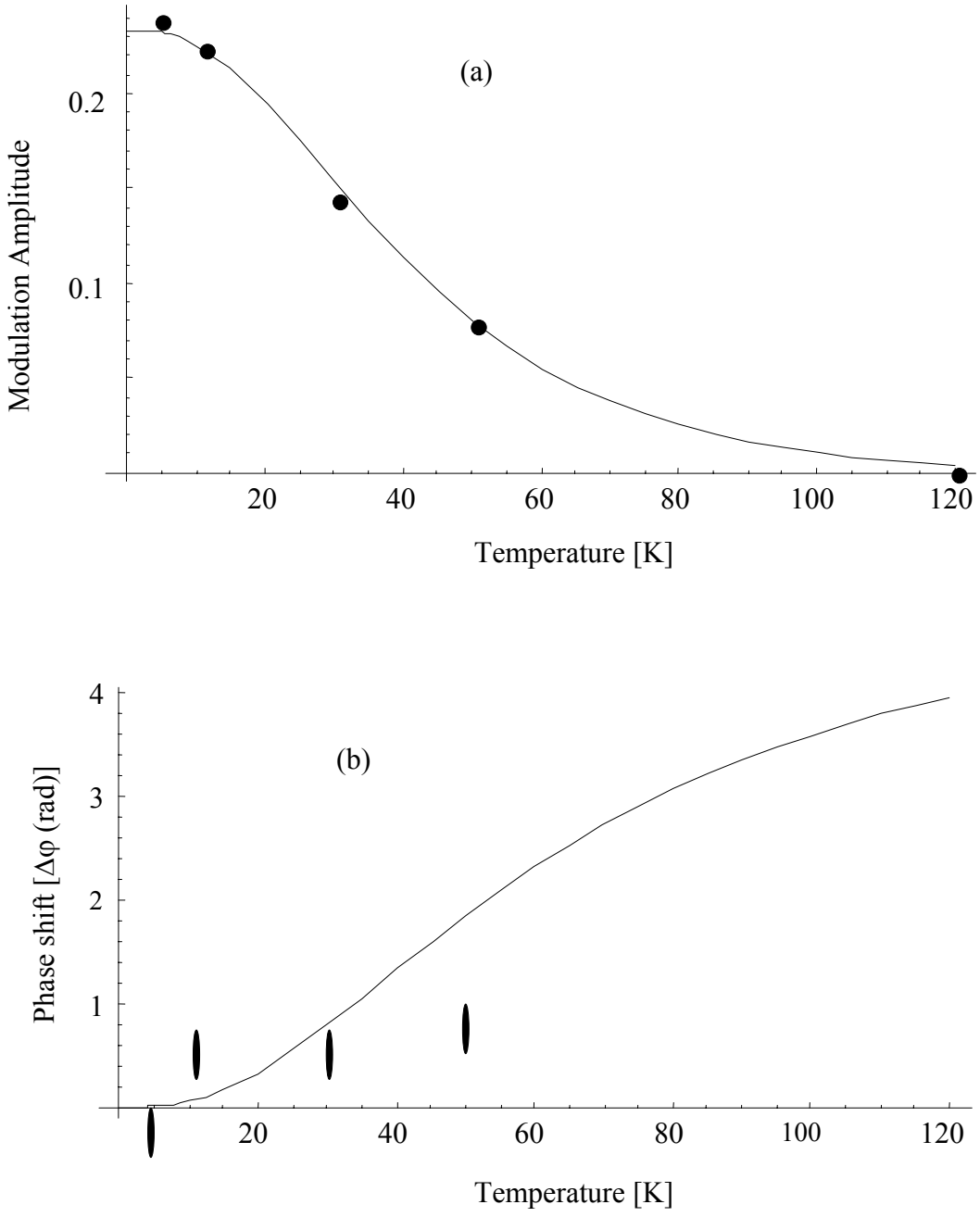

Figure 4.14 Temperature dependence of amplitude M (a) and phase shift $\Delta\varphi$ (b) of the spectral grating observed in SiNc and corresponding fits of these data to equations (4.18) and (4.29) within non-mirror-symmetrical model.

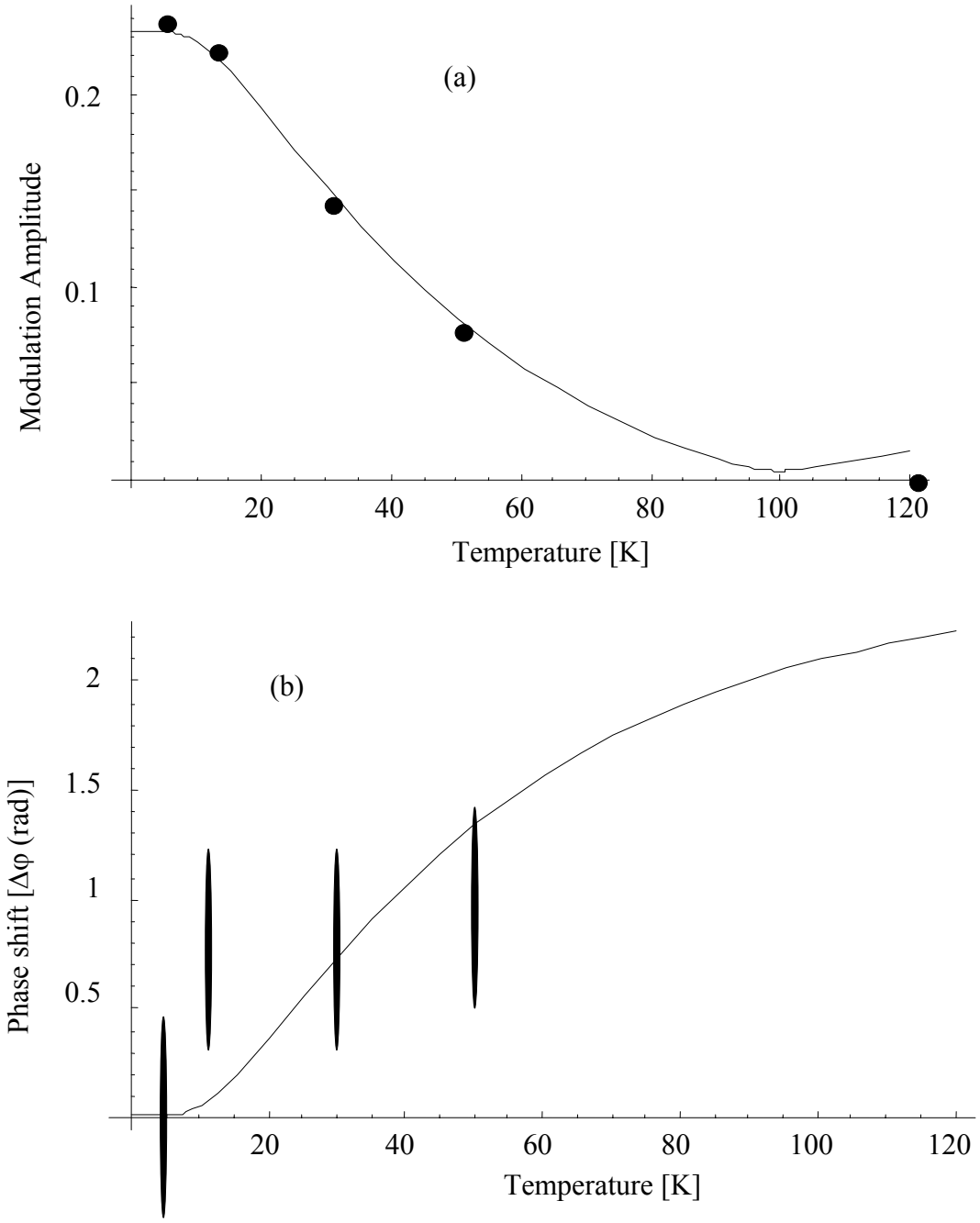

Figure 4.15 Temperature dependence of amplitude M (a) and phase shift $\Delta\varphi$ (b) of the spectral grating observed in SiNc and corresponding fits of these data to equations (4.18) and (4.29) within non-mirror-symmetrical model, where the Debye-Waller factor for TPA (α_2) was set to zero.

Several important conclusions can be drawn from these observations. First of all, mirror-symmetric spectral model works well for chlorin. This is not very surprising result because this molecule does not possesses the center of inversion, and, therefore, selection rules for one- and two-photon transitions should be the same. On the other hand, TPA-gratings in SiNc:PVB system are best described by strongly asymmetrical model in which ZPL of TPA is completely missing. This fact can be explained if we consider selection rules for pure electronic transition in this centrosymmetrical molecule. Since we are dealing with *gerade* ↔ *ungerade,* $S_0 \leftrightarrow S_1$ one-photon transition, it must be strongly forbidden for pure electronic TPA. However, TPA with creation of phonons (electron-phonon transition, building up PW in homogeneous TPA spectrum) can be allowed through Herzberg-Teller mechanism. In this case, TPA grating can be created on pure phonon coherences. It is, of course, evident that for observation of the fringes, the phonon coherence time, T_2, must be comparable or longer than the time delay between pulses, $\Delta\tau$. It is known from femtosecond photon echo experiments [220,221] that the phonon coherence time in polymer matrices at low temperatures ranges from several hundred of fs to 1 ps. In our experiments we use $\Delta\tau = 700$ fs, which is a sufficiently small value to produce spectral interference on phonon coherences, at least in SiNc:PVB system. From the other side, one cannot reduce $\Delta\tau$ to an arbitrarily small value, since it is limited from below by inverse inhomogeneous width, which is of the order of 100 fs. Therefore, there exists a limited range of delays ($\Delta\tau \sim 100 - 1000$ fs), where TPA-gratings can be observed in the case of absence of ZPLs in a system.

CHAPTER 5

PHOTOSENSITIZATION OF SINGLET MOLECULAR OXYGEN BY MEANS OF TWO-PHOTON EXCITATION AND ITS APPLICATION FOR PDT

A long-standing dream in the field of cancer therapy is the ability to treat subcutaneous tumors non-invasively, while at the same time eliminating the adverse physical discomfort associated with traditional chemotherapy, and the debilitating effects of actinic radiation treatments. PDT is gaining acceptance worldwide as an alternative treatment, which is devoid most of the drawbacks mentioned above.

One-photon PDT was initially developed in 1970s [94,95,222,223] by T. J. Dougherty. His early setup was primitive. To obtain a red light needed to excite photodynamic agent he passed a white light from an old slide projector through 35mm slide colored red. Currently PDT is a sophisticated technique which is either used or in trials for different types of cancer and several other illnesses. As for the moment, two drugs are approved by Food and Drug Administration (FDA). Porfimer sodium (Photofrin®) is used to treat esophageal, bladder, head and neck, and skin cancers and some stages of lung cancer [223]. Verteporfin (Visudyne®) treats age-related macular degeneration, which is the most common cause of legal blindness in elderly Western population [224]. Several more compounds are in the last phase of their trials.

Despite several successes PDT has its own disadvantages. The main problem is a very limited penetration depth into a human tissue of light, used for PDT drug excitation, which severely limits PDT treatment efficiency. Fortunately, there is a so called “tissue transparency window” in the near-IR (~ 750 – 1000 nm). The penetration depth of

excitation light with wavelengths falling into the “tissue transparency window” is strongly increased owing to decreased absorption and scattering. The use of near-IR light for PDT agents excitation would greatly enhance its efficiency except that current photosensitizers do not absorb in this spectral range. One way to overcome this problem is to use TPA for drug excitation. Owing to the fast development of and large interest to nonlinear absorption, this idea was examined several times during recent years [57-60]. Nevertheless its success was rather modest because of small efficiency of two-photon excitation. In particular, one of the ways to confirm that photodynamic agent produces enough singlet oxygen to be used in PDT is to register luminescence spectrum of the oxygen. So far it has never been done upon two-photon excitation. The main reason for that is very low TPA cross sections of currently used photosensitizers.

In this respect, our group is uniquely suited to resolve this problem. Since most of the photosensitizers are based on tetrapyrrolic compounds we can use our expertise in synthesizing new molecules with strongly enhanced two-photon cross sections. It already has been discussed in Chapter 3 how one can strongly increase TPA cross section of tetrapyrrolic molecules upon excitation in near-IR by fine-tuning their properties. In this particular case we use our new approach, which is based on synthesis of new molecules consisting of porphyrin as core and two-photon absorbing chromophore as its “tail”.

The main goal of experiments described in this chapter is to study TPA properties of such molecules and to show the ability to generate singlet molecular oxygen upon their two-photon excitation. The following objectives are addressed:

1. Test some of the currently used one-photon photosensitizers with respect to two-photon excitation.
2. Perform reliable measurements of TPA cross sections of the new two-photon photosensitizers and elucidate the mechanism of TPA enhancement in them.
3. Prove ability to produce large quantities of photosensitized singlet oxygen by means of two-photon excitation of the new compounds.

The chapter starts by introducing main concepts of PDT. Advantages of the two-photon PDT over one-photon PDT are discussed. Next, TPA properties of some currently used one-photon photosensitizers are investigated. Finally, TPA properties of new two-photon photosensitizers with greatly enhanced two-photon cross section are investigated. Efficient generation of singlet molecular oxygen with these photosensitizers upon their two-photon excitation is demonstrated. The work described in this chapter was reported in the following publications [105,206,225-232].

What is PDT

PDT employs special ability of some porphyrin photosensitizers to accumulate in pathologic cells, and to transfer absorbed photon energy efficiently to extremely active singlet oxygen molecules, which then wipe out the surrounding tumor. Injecting a porphyrin photosensitizer into patient's blood stream commences a typical PDT procedure. After an appropriate time interval (usually tens of hours) the photosensitizer is activated by shining a visible light, usually a red color laser beam, at the tumor's location. Photophysical processes constituting PDT are summarized in the energy level diagram shown in Figure 5.1.

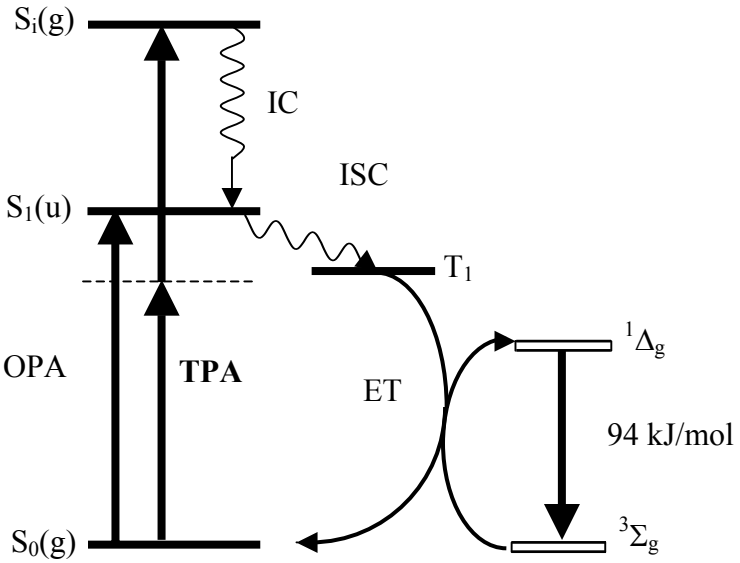

Figure 5.1 Schematic of the energy levels for porphyrin photosensitizer (solid bars) and molecular oxygen (open bars). $S_0(g)$, $S_1(u)$, $S_i(g)$, and T_1 represent, respectively, ground, first singlet, i^{th} excited singlet, and lowest triplet states of the photosensitizer. The symbols in the parenthesises denote *gerade* (g) and *ungerade* (u) symmetry of the corresponding states. $^3\Sigma_g^-$ and $^1\Delta_g$ denote the ground and the first excited singlet states of molecular oxygen. Upon one-photon excitation (OPA) the lowest singlet state S_1 of photosensitizer is populated. Thereafter the radiationless intersystem crossing (ISC) $S_1 \sim > T_1$ takes place. This is followed by energy transfer (ET) between photosensitizer and oxygen $T_1 + {}^3\Sigma_g^- \rightarrow S_0(g) + {}^1\Delta_g$ (semicircle arrows). Upon two-photon excitation (TPA), a transition occurs to one of the higher excited states $S_i(g)$. In this case the energy of the excitation photon is much lower than that used in OPA and falls into the "tissue transparency window". Because of the internal conversion (IC) the $S_1(u)$ state is ultimately populated. All the following processes are the same as in the one-photon case.

In its classical implementation, absorption of one visible photon (OPA) brings a photosensitizer molecule into a short-living excited state, S_1, with energy of 170 - 190 kJ mol^{-1}, which corresponds to an illumination wavelength of λ = 620 - 690 nm. After few nanoseconds, the porphyrin undergoes intersystem crossing (ISC) to the triplet state, T_1, with energy of 110 - 130 kJ mol^{-1}, and with much longer lifetime (on the order of microseconds). From the triplet state, the energy is transferred (semicircle arrows in Figure 5.1) to omnipresent oxygen molecules by switching them from a triplet ground

state, $^3\Sigma_g^-$, into an excited singlet state, $^1\Delta_g$, with excitation energy of 94 kJ mol^{-1}. Once in the excited singlet state, the oxygen presents an extremely reactive specie capable of damaging surrounding tissue in an irreversible manner.

The radiative transition $^1\Delta_g \rightarrow {}^3\Sigma_g^-$ between the first excited and the ground states of the oxygen is spin and symmetry forbidden which provides for a long lifetime of the singlet state oxygen (for in depth discussion of singlet molecular oxygen photophysics see [233]). A presence of excited singlet oxygen molecules ($^1\Delta_g$) in solution is usually detected by their $^1\Delta_g \rightarrow {}^3\Sigma_g^-$ luminescence at about 1270 nm. Since this radiative transition is forbidden, the detection of singlet molecular oxygen by its luminescence typically implies that large amount of oxygen is photosensitized. For example quantum yield of singlet oxygen luminescence in the water is $7.7 \cdot 10^{-7}$ (see Table 5.1), which means that for every excited oxygen molecule emitting a photon there are more than a million molecules undergoing radiationless transition.

Main advantages of PDT are [234,235]:

1. Patients will not require surgical treatment. Usually patients do not even need to check into a hospital.
2. PDT is selective. The PDT agent mainly accumulates in cancer cells and not in surrounding normal tissue. Upon treatment, healthy cells a left mostly intact.
3. Side effects typical for radiation therapy and chemotherapy (losing hair, suffering nausea, reduced resistance to infections, internal bleeding, diarrhea, vomiting, anemia, and so on) are avoided.

4. PDT works when surgery is not possible, providing the only possible treatment. Surgery may not be possible when tumour lies near or within vital tissue (lung cancer).
5. PDT is a low-cost treatment.
6. PDT can be used many times without accumulation of negative side effects as in radiation therapy. As a result, PDT provides for long-term management of cancer even if complete cure is not possible.

To be effective, photosensitizers have to selectively accumulate in tumour tissue. Serendipitously, tetrapyrrolic molecules possess this rare feature. The problem is that the affinity of porphyrins to tumours is mainly conditioned by fast metabolism of cancer cells. Any rapidly proliferating tissue, including the skin, accumulates large amounts of porphyrins as well. This leads to an important parameter describing PDT agents, namely, how fast photosensitizer is removed from a human body after the treatment. The patient cannot go outside into the sunlight while photosensitizer is present in his or her skin, otherwise burns and skin rashes may result. This constitutes the main drawback of PDT. But while spending several days in a dark room is definitely inconvenient it is not intolerable.

Another critical point for any potential photosensitizer is its quantum yield of singlet oxygen formation. Typically, the crucial step in formation of singlet oxygen is intersystem crossing from the first excited singlet state of a photosensitizer into the triplet state. As long as the triplet state is occupied, energy transfer to the molecular oxygen takes place with high efficiency, often close to unity. Thus, to be efficient,

photosensitizer must have large efficiency of triplet state formation, otherwise most of the excitation energy will be lost to fluorescence and nonradiative decay between S_1 and S_0 levels.

Finally, penetration depth of the excitation laser light without being absorbed or scattered is important issue. Tissue transmittance generally increases upon shifting illumination wavelength from the visible to the red and near-IR part of the spectrum resulting in "tissue transparency window" at $\lambda \sim$ 750-1000 nm [236-239]. Many porphyrins are effective photosensitizers of singlet oxygen, but their linear absorption bands correspond to the blue-green part of the spectrum making them useless for PDT. Porphyrins currently in use for PDT also fall short of the transparency window: their $S_1 \leftarrow S_0$ absorption varies from 620 to 690 nm (Photofrin® λ_{ex} = 630 nm, Visudyne® λ_{ex} = 689 nm), where effective penetration in most tissues is no more than just one millimeter in depth. Many efforts were made to shift one-photon absorption band towards longer wavelengths by chemical modification of the porphyrin structure. Unfortunately, such modifications come into conflict with the fundamental requirement that the excitation energy of singlet oxygen ($^1\Delta_g$ state) is lower than the energy of the T_1 state (Figure 5.1Figure). In addition, long-wavelength shift of porphyrin's energy levels often aggravates the situation by reducing compound's stability.

In the view of the difficulties encountered when trying to achieve singlet oxygen photosensitization upon one-photon excitation with near-IR photons, a proposal to use TPA appears to be the best alternative way to achieve deeper penetration. TPA allows using near-IR photons in the "tissue transparency window" and does not require the red

shift of the lowest electronic transition of the porphyrin (Figure 5.1). Note that even if TPA takes a molecule into one of its' higher excited states, S_i, the lowest S_1 state will be ultimately populated via internal conversion. Once this state is formed, the subsequent events follow the same path as in case of one-photon excitation. In addition, TPA provides two further advantages. First, laser-induced hyperthermia is minimized, since near-IR light has a reduced absorption in tissues. In case of one-photon PDT scattered excitation light might penetrate into healthy cells and excite a photosensitizer accumulated there. For two-photon PDT this is not a problem. Two-photon excitation by scattered light is negligible due to its very low intensity. Second, nonlinear (quadratic) dependence of TPA on laser intensity provides for higher spatial selectivity of treatment by using focused laser light. Nonlinear nature of TPA guarantees that two-photon excitation of a photosensitizer is effectively confined to focal volume where laser light intensity is greatest. The latter is essential for treatment of sensitive tissues.

While PDT has its own problems, the advantages of this method of treatment greatly outweight any drawbacks. In many cases PDT is the only option for patients. All this explains a great interest to PDT from medical and biological sciences.

Experimental

Figure 5.2 presents experimental setup. It is similar to the experimental setup described in Chapter 3, where detailed description of the laser system and methodics of two-photon cross section and spectrum measurements are given (see Chapter 3 Experimental). The only difference is that Ti:sapphire amplifier was used directly to

measure TPA spectra (The amplifier is tunable in the following wavelength range λ = 770 – 815 nm).

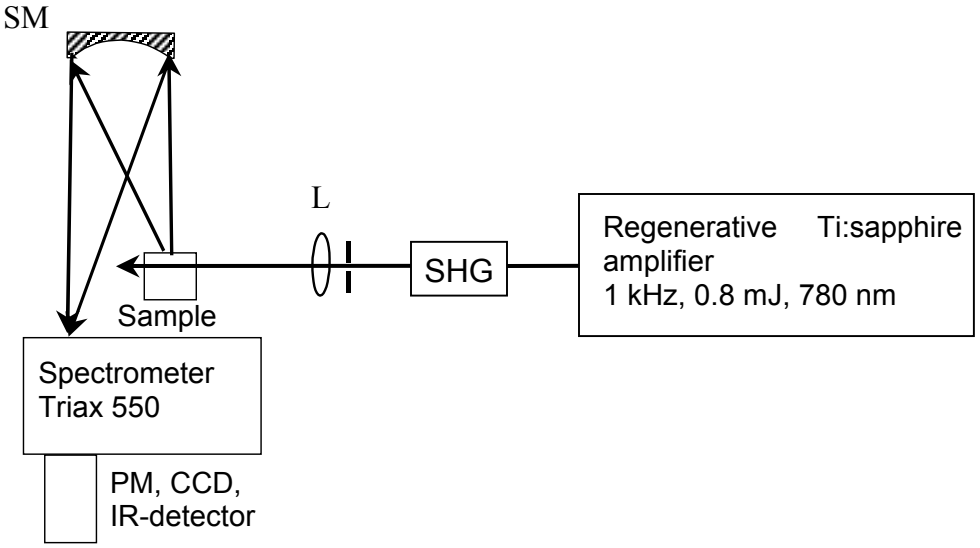

Figure 5.2 Experimental setup. L – lens (f = 20 – 100 cm), SHG – second harmonic generator, SM – spherical mirror (f = 50 cm), PM – photomultiplier.

To measure luminescence of the photosensitized singlet oxygen, a lens (f = 20 – 100 cm) was used to increase efficiency of two-photon excitation of a photosensitizer. Since singlet oxygen luminescence is centered around λ = 1.27 μm, liquid nitrogen cooled Ge IR-detector (Advanced Detectors Corporation) was used for its detection.

Quantum yield of singlet oxygen photosensitization was measured relative to H_2TPP (see Figure 3.4b). Both, the etalon (H_2TPP) and a compound of interest are excited by means of OPA in the same geometry and with the same excitation power. The intensity of the photosensitized singlet oxygen luminescence is measured. Quantum yield is calculated according to the following expression:

$$\Phi_{\Delta} = \Phi_{\Delta}^{etalon} \frac{I_{\Delta}}{I_{\Delta}^{etalon}} \frac{\beta^{etalon}}{\beta} \frac{n^2}{n^{2etalon}}, \qquad (5.1)$$

where the parameter without superscript and with superscript *etalon* refer to the sample and the etalon, respectively. Φ_Δ and I_Δ are quantum yield of singlet oxygen photosensitization and intensity of the singlet oxygen luminescence. For H_2TPP quantum yield is equal to Φ_Δ (H_2TPP) = 0.68 [240]. The n is the refraction index. In our case, all the samples including etalon were dissolved in the same solvent (toluene) so that the ratio $n^2/n^{2etalon}$ is equal to unity. β is the part of the excitation light that is absorbed by the photosensitizer:

$$\beta = 1 - 10^{OD}, \tag{5.2}$$

where *OD* is optical density of the photosensitizer at the excitation wavelength. In our case, excitation was carried out by second harmonic of the Ti:sapphire amplifier at λ_{ex} = 396 nm.

For one-photon excitation of the fluorescence by near-UV light xenon lamp with a set of UV filters was used. Linear absorption spectra of the samples were measured with Lambda 900 Perkin Elmer spectrophotometer. In all the cases, concentration of the samples was around $10^{-4} - 10^{-5}$ M.

Quantum yield of singlet oxygen luminescence crucially depends on the type of the solvent. As a result, singlet oxygen luminescence signal can be substantially increased by changing the solvent. In this work five different solvents have been used, water (H_2O), heavy water (D_2O), toluene (C_7H_8), dichloromethane (CH_2Cl_2), and ethanol (CH_6O).

Table 5.1 summarizes photophysical properties of singlet oxygen in these solutions. Symbols $k_{(S\rightarrow T)}$, τ, and $\Phi_{(S\rightarrow T)}$ represent radiative rate constant of singlet oxygen luminescence from the first singlet level $^1\Delta_g \rightarrow {}^3\Sigma_g^-$, singlet oxygen lifetime, and

quantum yield of luminescence, respectively (Figure 5.1). The quantum yield of luminescence was calculated according to the following expression:

$$\Phi_{(S\to T)} = k_{(S\to T)}\tau \,. \tag{5.3}$$

Table 5.1 Photophysical properties of singlet oxygen in five different solutions used in this work. The radiative rate constants $k_{(S\to T)}$ are taken from ref. [241]. The lifetimes τ represent an average of all the data in the ref. [240].

Solvent	$k_{(S\to T)}$, s^{-1}	τ, μs	$\Phi_{(S\to T)}$
H_2O	0.209	3.7	$7.7 \cdot 10^{-7}$
D_2O	0.206	61	$1.3 \cdot 10^{-5}$
CH_6O	0.55	13	$7.2 \cdot 10^{-6}$
C_7H_8	1.44	27	$3.9 \cdot 10^{-5}$
CH_2Cl_2	0.75	87	$6.5 \cdot 10^{-5}$

Table 5.1 demonstrates that the quantum yield of singlet oxygen luminescence grows about two orders of magnitude when going from water (H_2O) to dichloromethane (CH_2Cl_2). Correspondingly, the total signal of singlet oxygen luminescence also grows by about two orders of magnitude.

For quantum chemical calculations Hyperchem 7 package was used. Geometry optimization was accomplished with AM1 method. Spectral calculations were performed with the ZINDO/S method.

Figure 5.3 shows chemical structures of the two photosensitizers that are approved for one-photon photodynamic therapy. Their TPA properties are studied for comparison with new TPA photosensitizers. Photolon® (Figure 5.3a) and its active derivative chlorin were acquired from Scientific Pharmaceutical Center, JSC

Belmedpreparaty, Minsk, Belarus. Verteporphin (Figure 5.3b) was obtained from QLT Inc.

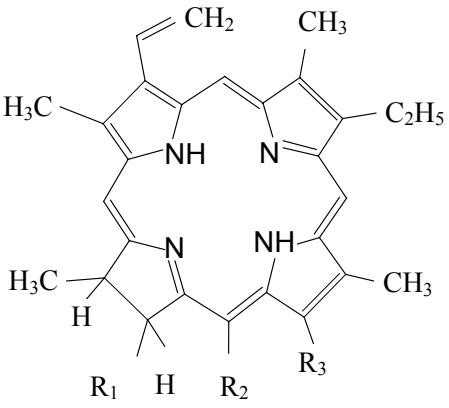

(a) Photolon®

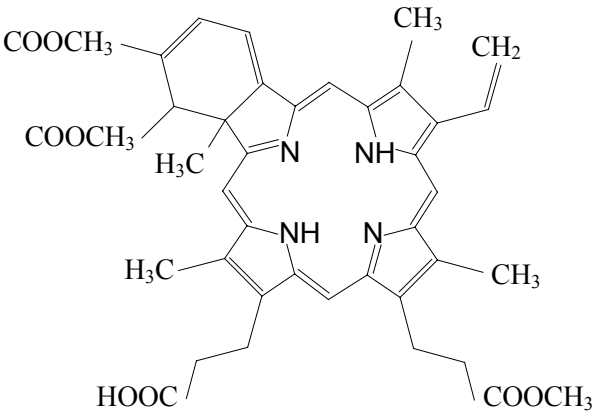

(b) Visudyne®

Figure 5.3 Chemical structures of currently approved one-photon-based photosensitizers that were studied for comparison. (a) Photolon®, chlorin-based - approved for the cancer treatment by Ministry of Health of the Republic of Belarus, R_1=CH_2CH_2COOH, R_2=CH_2COOCH_3, R_3=COOH; (b) Visudyne®, benzoporphine-based - approved for macular degeneration treatment by Food and Drug Administration, USA.

New photosensitizers for the TPA-based PDT are shown in Figure 5.4. They were synthesized by Prof. C. W. Spangler group*.

* Prof. Charles W. Spangler, Department of Chemistry and Biochemistry, Montana State University, Bozeman, MT 59717, USA.

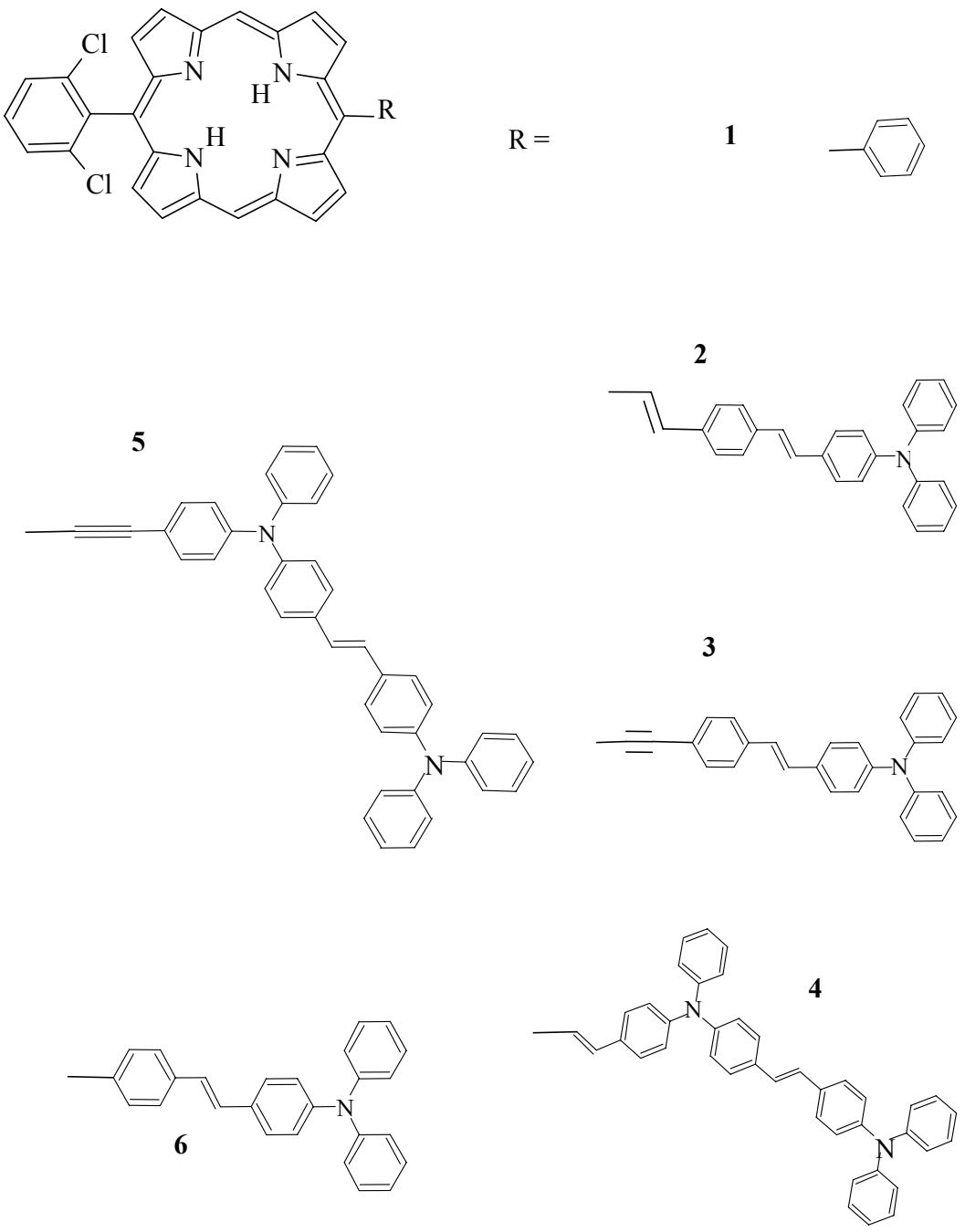

Figure 5.4 (**1-6**) Chemical structures of new TPA-based photosensitizers for PDT. The numbered structures correspond to TPA units that are connected to the porphyrin core (top left corner) to enhance TPA. To determine the best structure different TPA units have been tried (**1-6**), differing by their length and type of the bond with the porphyrin core.

7

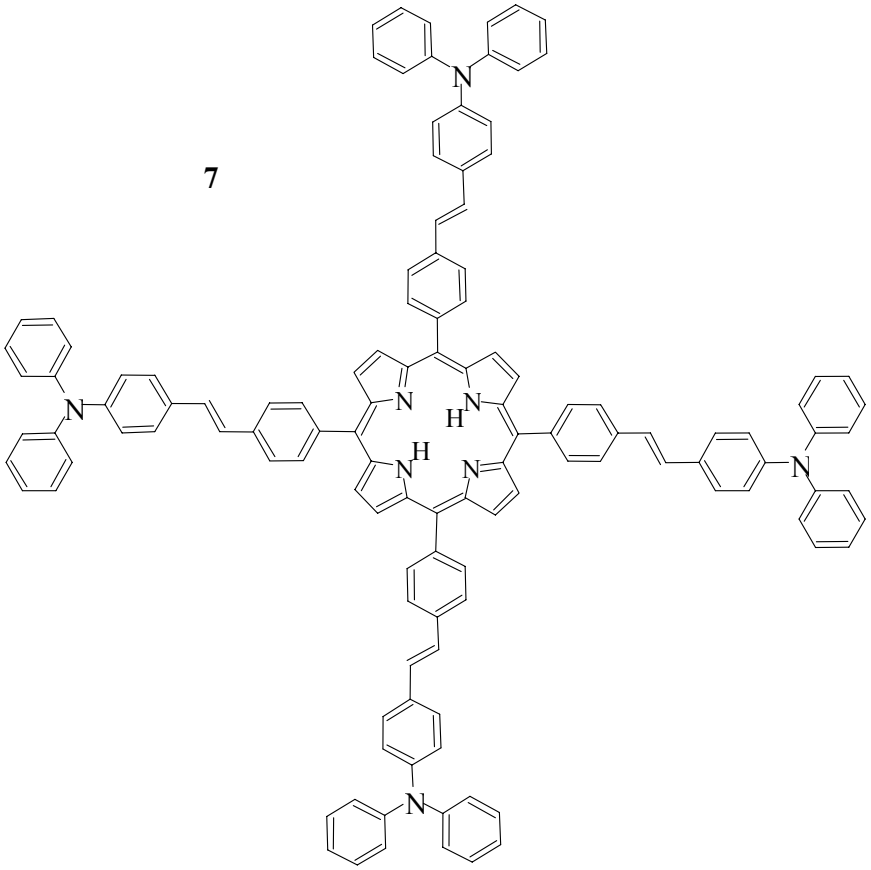

Figure 5.4 (**7**) Chemical structure of the new TPA-based photosensitizer for PDT with four TPA substituents. It can be considered as a core of a dendrimer-like structure.

Two-Photon Excitation of Some Currently Used Photosensitizers

Since any new molecule which potentially can be used as a drug must be approved by FDA or analogous agencies in other countries, it is reasonable to check first the TPA properties of some currently approved photosensitizers. Two drugs have been used Visudyne® (Figure 5.3b) and Photolon® (Figure 5.3a). Visudyne® is approved by FDA for treatment of the age related macular degeneration. Photolon® has been approved for the cancer treatment by Ministry of Health of the Republic of Belarus.

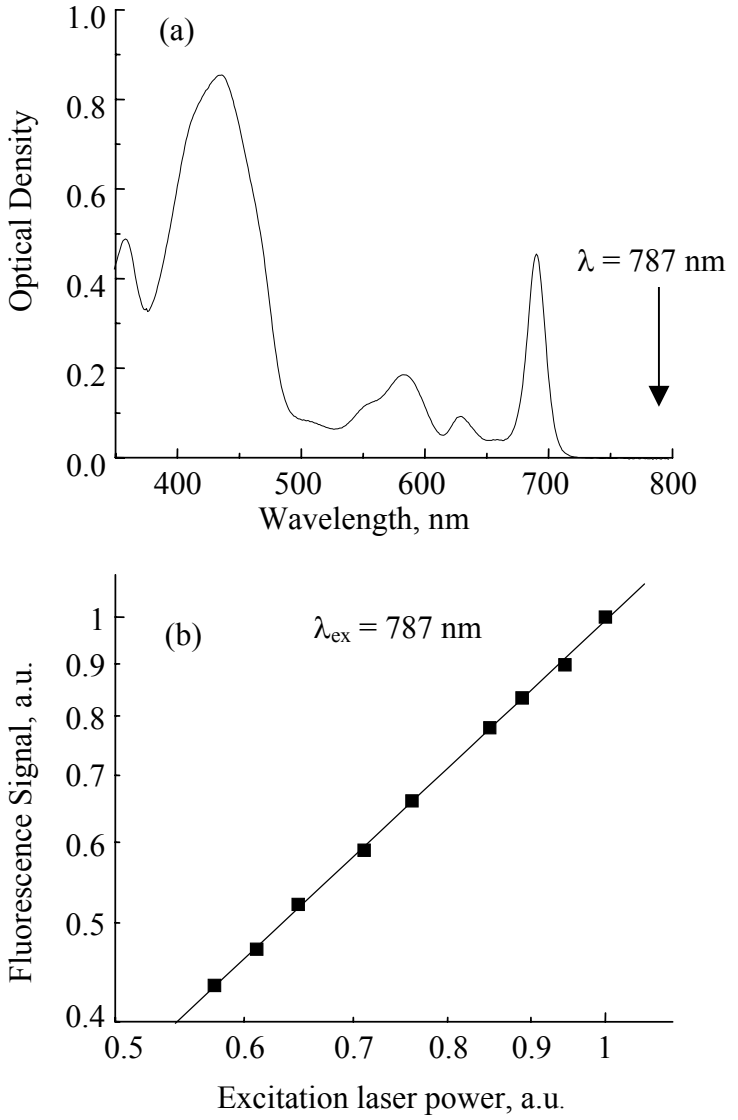

Figure 5.5 (a) Absorption spectrum of the Visudyne® in toluene. The arrow shows λ = 787 nm wavelength. (b) Power dependence of the Visudyne® fluorescence excited at λ_{ex} = 787 nm presented in double logarithmic scale. The exponent of the power dependence is equal to k = 1.50, demonstrating that both OPA and TPA are present. Similar measurements at λ_{ex} = 775 nm (not shown) resulted in the k = 1.36.

Figure 5.5 presents linear absorption spectrum of Visudyne®. Although maximum of the first linear absorption band is situated at λ = 691 nm (Figure 5.5a), an excitation of its fluorescence with the Ti:sapphire amplifier in near-IR wavelength range

revealed that both OPA and TPA are present (Figure 5.5b). The power dependence of the excited fluorescence was measured at two different wavelengths λ_{ex} = 775 nm and λ_{ex} = 787 nm. The linear plot in double logarithmic scale resulted in the following values of the exponent of the power dependence, *k* (775 nm) = 1.36, *k* (787 nm) = 1.50. Upon moving to longer excitation wavelength, contribution from OPA decreases, so that at λ_{ex} = 787 nm both OPA and TPA have about the same efficiency. This kind of anti-Stokes one-photon excitation at the tail of the linear absorption band can be explained by OPA from thermally populated vibrational levels of the ground state (see Chapter 3 New Method for Measuring Absolute TPA Cross Section for details).

We were able to record a luminescence of singlet oxygen, photosensitized by Visudyne® upon its excitation with Ti:sapphire amplifier. Although one-photon excitation provided at least the same contribution to photosensitization of the observed singlet oxygen the result is important because the excitation wavelength falls into the "tissue transparency window". The efficiency of PDT treatment, deep inside of a tissue, with this drug can be substantially increased by applying near-IR excitation light instead of currently used λ_{ex} = 689 nm. From the other hand, to fully exploit advantages provided by "tissue transparency window" one has to use excitation wavelength around 900 nm where the tissue transmittance is largest. Clearly, one-photon excitation at this wavelength is impossible so that TPA must be used. To roughly estimate two-photon cross section of Visudyne® we used our standard method, which compares intensity of one- and two-photon excited fluorescence. The λ_{ex} = 788 nm was used for the molecule excitation. Since contributions from OPA and TPA at this wavelength are about the same

(Figure 5.5b) we estimated that the half of the fluorescence signal comes from TPA and based our calculations on this assumption. The resulting value of two-photon cross section is σ_2 = 100 GM. It is well in the range of the TPA cross sections measured for other tetrapyrrolic molecules in the same wavelength range (see Chapter 3 Resonance Enhancement of TPA in the Spectral Region Corresponding to One-Photon Soret Transition). While this two-photon cross section is enough to generate singlet oxygen, larger values of σ_2 are desirable to improve efficiency of two-photon PDT*.

Photolon® (Figure 5.3a) has been developed by Scientific Pharmaceutical Center of JSC "Belmedpreparaty" on the basis of tetrapyrrolic photosensitizer chlorine e_6 [242]. Photolon® is a pharmaceutical composition of chlorine e_6 and poly-*N*-vinylpyrrolydone (PVP) with a component weight ratio 1:1. Complexation of chlorine e_6 with PVP improves its solubility in water and leads to higher selectivity of Photolon® accumulation in malignant tissues.

Figure 5.6a presents a linear absorption spectrum of Photolon®. Its first linear absorption band (λ_{max} = 663 nm) is shifted to the blue as compared to Visudyne®. This allowed us to perform direct two-photon excitation of this compound with Ti:sapphire amplifier in the near-IR. TPA spectrum of Photolon® in the λ_{ex} = 775 – 810 nm excitation wavelength region is presented at Figure 5.6b. The spectrum is flat with average two-photon cross section equal to ~ 50 GM. Again, as in the case of Visudyne®,

---

* Recently there has been a report (D. T. Cramb and R. L. Goyan, Proceedings SPIE, **4262**, pp. 41-47, 2001) claming that two-photon cross section of Verteporfin is equal to 3300 GM at excitation wavelength λ = 756 nm. It is clear from the discussion in the text that authors mixed OPA from the hot vibronic bands with TPA, which resulted in strongly overestimated value of two-photon cross section.

the value of σ_2 is in the range expected for tetrapyrrolic compounds in this wavelength range.

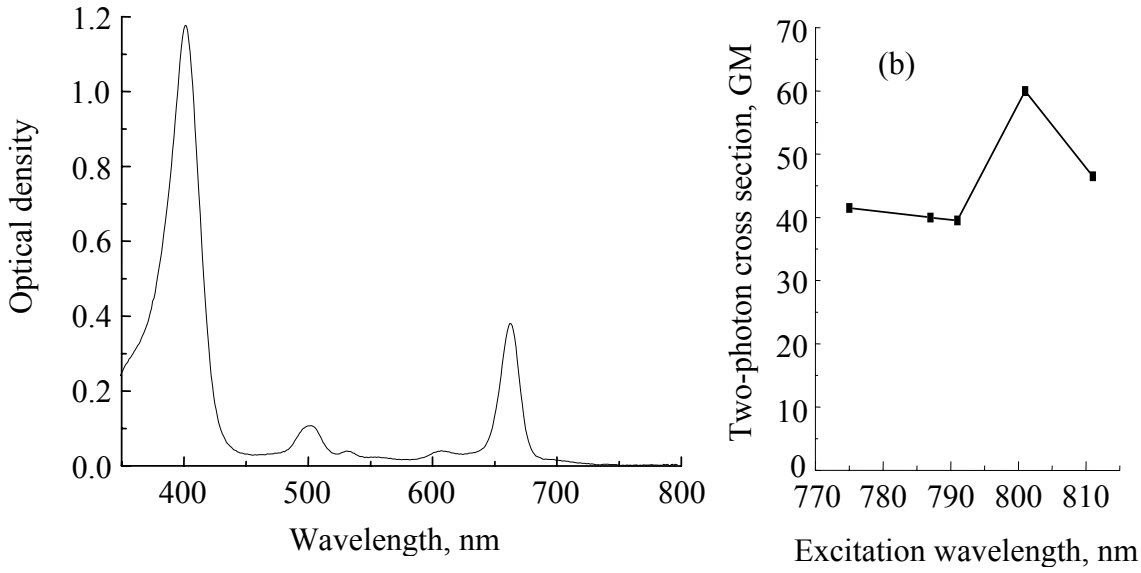

Figure 5.6 (a) Linear absorption spectrum of Photolon® in ethanol. (b) Two-photon absorption spectrum of Photolon® in ethanol.

We were not able to detect singlet oxygen upon two-photon excitation of Photolon® dissolved in water. The probable reason is that quantum yield of singlet oxygen photosensitization by Photolon® is low. The quantum yield was not measured, nevertheless some indirect data allows deducing that it is similar to Φ_Δ of the chlorin e_6. Several values of Φ_Δ for chlorin e_6 were obtained at different conditions, slightly varying between 0.70 and 0.76 [95,243]. Both in polar environment (heavy water) and in less polar (pyridine) the measured figures are practically the same (Φ_Δ is 0.76 and 0.74, respectively). Complexation with liposomes, human serum albuminum (HSA) and surfactant Triton X-100 does not reveal noticeable variation in Φ_Δ value. Thus, in

micelles formed with Triton X-100 quantum yield of the singlet oxygen photosensitization Φ_Δ was found to be 0.70 and being complexed with HSA chlorin e_6 has Φ_Δ value as high as 0.75 [243]. Presence of other chlorin e6 derivatives does not also change this value appreciably. All the investigated structures have Φ_Δ value in the same range, with the maximum value Φ_Δ=0.80 found for mono-L-aspartyl chlorin e_6 (MACE), which is produced by Nippon Petrochemicals, Japan [95]. Therefore one can suggest that quantum yield of singlet oxygen photosensitization Φ_Δ is barely affected by conjugation of chlorin e_6 with PVP and Φ_Δ figure for Photolon® can be taken as that found for the parent chlorin e_6 molecule. This means that the problem is with the low efficiency of two-photon excitation of the drug.

To increase the signal we dissolved Photolon® in ethanol and heavy water. The resulting increase of the quantum yield of singlet oxygen luminescence allowed us to register the luminescence (see Table 5.1). Nevertheless, the signal was just above the noise background. To improve signal to noise ratio and, correspondingly, reliability of our results, we used toluene instead of heavy water. Since Photolon® is specifically made to be solvable in polar solvents (water) it cannot be dissolved in nonpolar solvents like toluene. To overcome this problem we used an active photosensitizing center of Photolon®, namely chlorin e_6 without PVP polymer. The discussion above shows that PVP does not affect the efficiency of singlet oxygen generation by Photolon®. Moreover, the two-photon cross section of chlorin e_6 in ethanol measured at the excitation wavelength of λ_{ex} = 788 nm is equal to 50 GM which corresponds well to that of Photolon®. All the above facts indicate that pure chlorin e_6 constitutes a good model

compound for study of the two-photon excited photosensitization of singlet oxygen by the Photolon®. Because of the improved signal to noise ratio, we were able to reliably detect singlet oxygen luminescence (Figure 5.7a) and prove its TPA nature by measuring power dependence (Figure 5.7b).

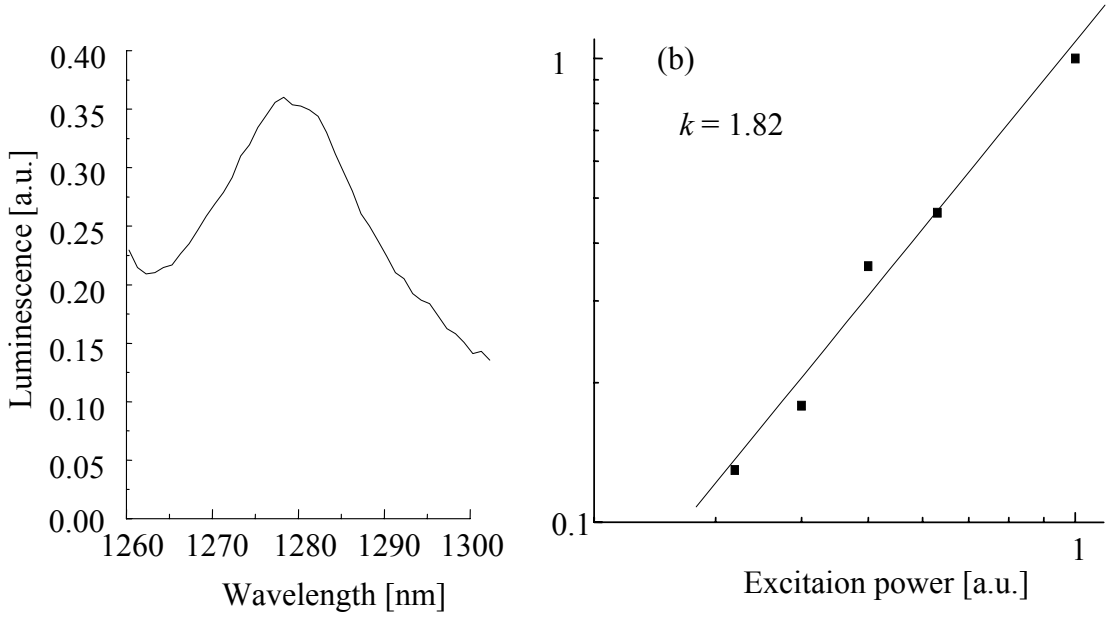

Figure 5.7 (a) Luminescence spectrum of molecular oxygen in air-equilibrated toluene solution of chlorin e_6 upon two-photon excitation. (b) Power dependence of the luminescence intensity is shown in double logarithmic scale. The exponent of the power dependence is equal to $k = 1.82$.

In conclusion, TPA cross sections (σ_2 = 50 -100 GM) of the currently used photosensitizers in near-IR excitation wavelength region are typical for tetrapyrrolic molecules. While two-photon excited photosensitization of singlet oxygen with Visudyne® and Photolon® is possible the efficiency of this process is rather small. New porphyrin photosensitizers with increased two-photon cross sections are required.

New Porphyrin-Based Compounds for PDT with Greatly Enhanced TPA Cross Sections

Compounds with increased two-photon cross sections are required to increase efficiency of singlet oxygen photosensitization. There are few molecules that are known to have $\sigma_2 \sim 10^3$ GM. However, they either lack the vital property to generate singlet oxygen, or their interaction with biological tissue is not known. On the other hand, all previous studies of tetrapyrrolic compounds showed that their two-photon cross sections are very small to be practically useful.

Our approach to this problem lies in special chemical modification of porphyrin molecules, which enhances molecule's TPA cross-section without jeopardizing its ability to generate singlet oxygen. In particular, σ_2 is increased by chemically attaching strong electron donors to porphyrins. It was shown in Chapter 3 (see Other Approaches to the TPA Enhancement) that the attachment of electron acceptor to porphyrin molecule strongly enhances its TPA cross section. Similar effect is expected for electron donors.

Figure 5.8 shows schematic structure of chemically modified molecules that were synthesized by Prof. C. W. Spangler group in Department of Chemistry and Biochemistry, Montana State University, and summarizes photophysical processes that lead to efficient singlet oxygen generation. The new photosensitizer consists of three main parts, a porphyrin, a TPA absorber, and an ISC helper. The TPA absorber represents a strong electron donor that boosts the TPA cross section of the photosensitizer. The ISC helper increases efficiency of intersystem crossing (ISC) in the porphyrin unit so that after excitation most of the photosensitizer molecules end up in their triplet state. Porphyrin unit effectively photosensitizes singlet oxygen.

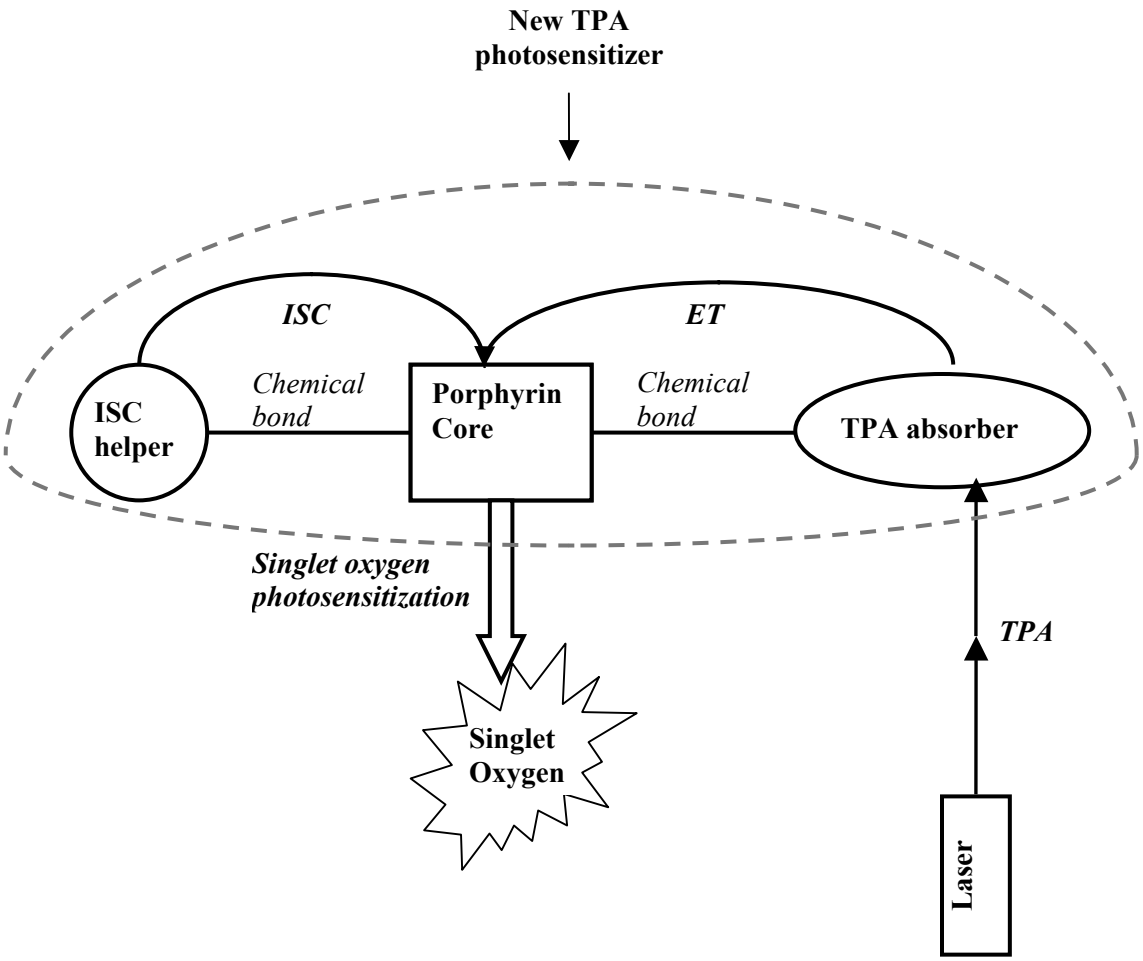

Figure 5.8 Schematic structure of new two-photon-based photosensitizers and photophysical processes leading to efficient singlet oxygen generation. The photosensitizer consists of three main parts: porphyrin, TPA absorber, and ISC helper. TPA absorber is a chromophore with increased two-photon cross section and strong electron donating properties. This part of the molecule is responsible for strong TPA of the photosensitizer. After two-photon excitation the energy is effectively concentrated on the first excited singlet level of the porphyrin core. This concentration of energy is either caused by energy transfer (***ET***) from the TPA absorber to the porphyrin or by intersystem crossing from the higher laying singlet states of the porphyrin excited directly with the help of large static dipole moment created by the TPA absorber (see the text for details). ISC helper increases intersystem crossing efficiency in the porphyrin core so that most of the photosensitizer molecules end up being in its triplet state. Next step is photosensitization of singlet oxygen, which is efficiently performed by the porphyrin.

Figure 5.4 shows chemical structures of the studied molecules. The porphyrin core of the new photosensitizers represents basic porphine unit. In molecules **1**-**6**, 2,6-dichlorophenyl is the ISC helper,

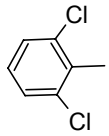

assisting intersystem crossing via an internal heavy atom effect. Molecule **7** does not have this unit. Instead, it has four electron donating groups forming a zeroth order of a porphyrin-based dendrimer. In compounds **1**, **6**, **7** substituents are connected directly to the porphyrin, while in molecules **2**, **4** they are connected through alkene link (double bond) and in molecules **3**, **5** through alkyne link (triple bond). The first molecule can be considered as a parent for the rest of them so that any effect of the electron donating substituents on the photophysical behavior should be evaluated in comparison to compound **1**.

Figure 5.9 presents linear absorption and fluorescence spectra of the molecules under investigation. The main photophysical parameters are summarized in Table 5.2. The linear absorption spectra are typical for porphyrins and show weak Q bands in the visible part of the spectrum and strong Soret band near 400 nm. Absorption spectra of compounds **2**-**5** are more disrupted in comparison to **1**. Number of Q bands is reduced from four to two. Maxima of the first absorption bands of compounds **2**-**5**, **7** are shifted to the red as compared to **1**, indicating that the strong electronic coupling between porphyrin and its electron-donating substituents takes place. Small red shift is also observed for the **6**, indicating that electronic conjugation is not as strong in this case.

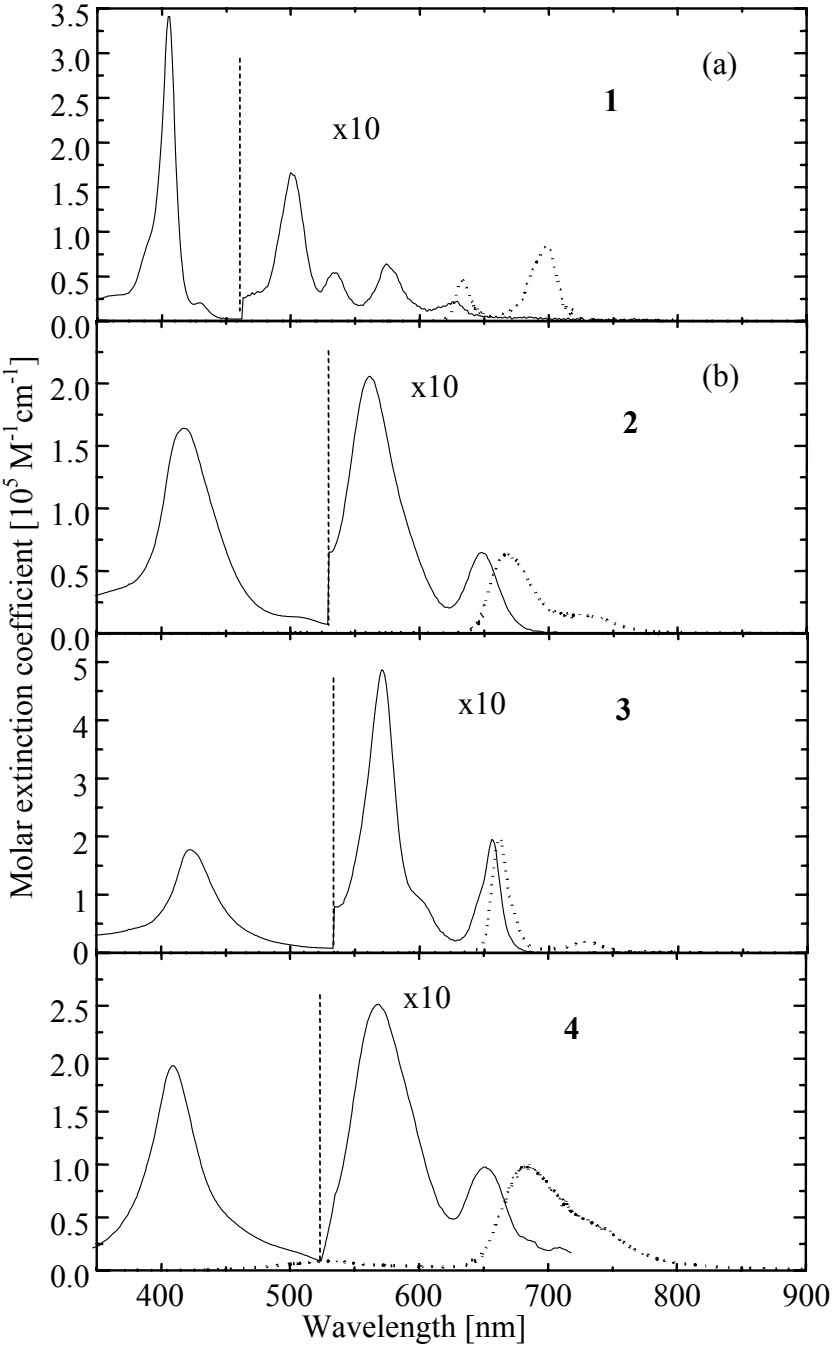

Figure 5.9 (a-d) Linear absorption (solid) and fluorescence (dot) spectra of the compounds **1** – **4**. The region of the spectra corresponding to the Q-bands is multiplied by ten to equalize it with the Soret band region. The fluorescence spectra of the **2** – **4** are normalized with respect to the first lowest absorption band. The fluorescence spectrum of the **1** is shown several times larger because of low intensity of the corresponding absorption band.

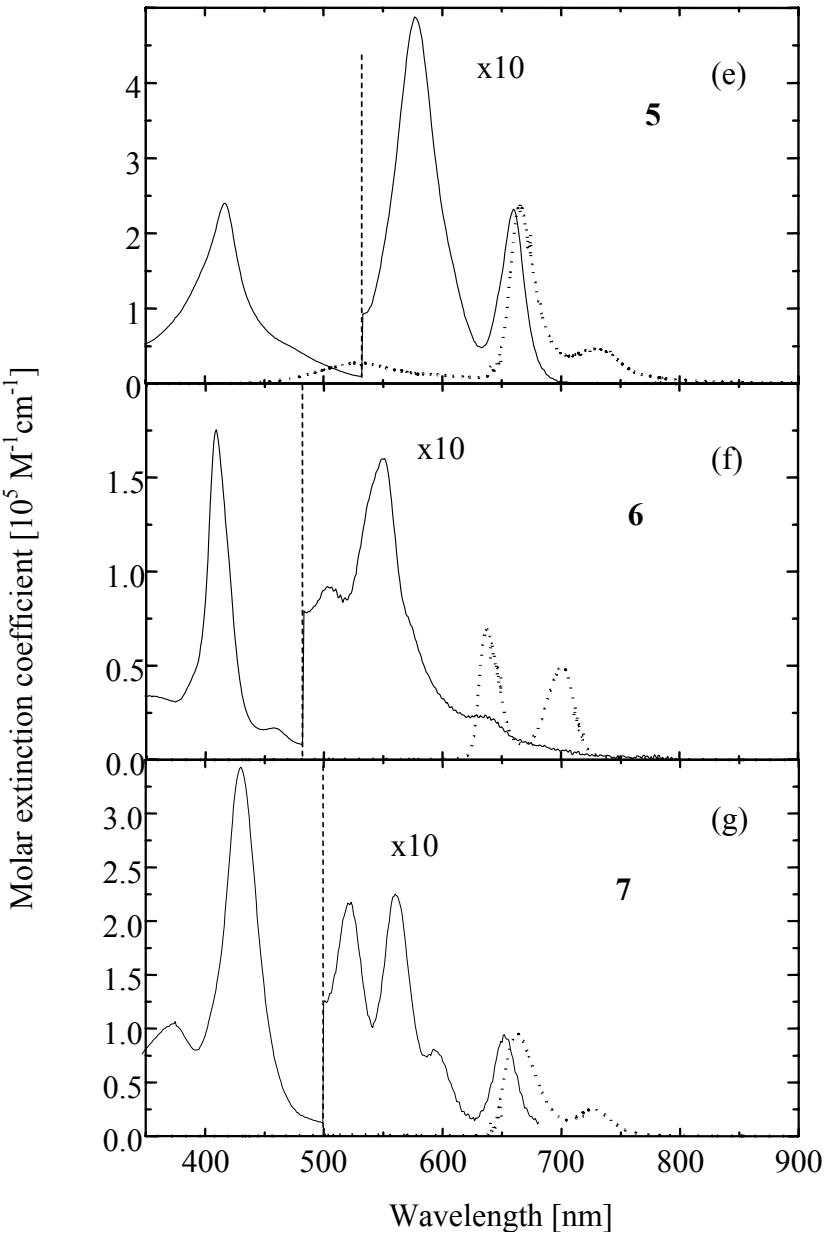

Figure 5.9 (e-g) Linear absorption (solid) and fluorescence (dot) spectra of the compounds **5** – **7**. The region of the spectra corresponding to the Q-bands is multiplied by ten to equalize it with the Soret band region. The fluorescence spectra of the **5** and **7** are normalized with respect to the first lowest absorption band. The fluorescence spectrum of the **6** is shown several times larger because of low intensity of the corresponding absorption band.

When going from the **1** to the **7**, Soret band behavior is similar to that of the first Q band. Strong red shift and broadening are observed for compounds **2**-**5**, **7**. In the case

of **6**, the red shift is rather small. These observations suggest that alkene and alkyne linkers provide for stronger π-conjugation between the porphyrin core and the TPA fragment. When the substituent is connected directly, a certain degree of conjugation is present, but it is not as strong.

Table 5.2 Photophysical properties of the new photosensitizers. All the chemicals are dissolved in CH_2Cl_2.

Molecule No.	Type of chemical bond	Q bands number	First Q band λ_{max}, nm	First Q band $\varepsilon\times10^{-3}$ $M^{-1}cm^{-1}$	Soret Band λ_{max}, nm	Soret Band $\varepsilon\times10^{-5}$ $M^{-1}cm^{-1}$
1	Single	4	628	1.5	405	3.4
2	Double	2	648.5	6.5	417	1.6
3	Triple	2	657	20	422	1.8
4	Double	2	652	9.6	408.5	2.0
5	Triple	2	660.5	23	416.5	2.4
6	Single	4	636	2.3	409	1.8
7	Single (dendritic)	4	651.5	9.4	429	3.4

Fluorescence spectra of the molecules (Figure 5.9) were measured using xenon lamp as an excitation source. A broadband filter with transmittance in the near-UV was placed in front of the sample. The resulting excitation with near-UV light allowed both porphyrin core and TPA fragment to be excited. The fluorescence spectra reveal almost pure porphyrin fluorescence (λ_{max} = 650 – 700 nm) with a rather weak fluorescence from the TPA substituents (λ_{max} = 530 nm). In triple-bond connected molecules **3**, **5** as well as in directly connected **6**, **7** the green peak constitutes less than 1% of the main porphyrin peak. In the double-bond connected molecules **2**, **4** it amounts up to 5%. At this point we

assign this last value to a small percentage of conformers **2** and **4**, where the substituent is not coupled directly to the core. Since quantum yield of fluorescence of the TPA fragments is larger then that of the porphyrin, a very weak fluorescence at 530 nm indicates that very efficient transfer of the excitation energy to the porphyrin first singlet state takes place. This result is important because the porphyrin constitutes a photodynamic agent generating singlet oxygen.

Table 5.3 TPA cross sections, linear absorption parameters that are relevant for two-photon cross section estimate (see pp. 164-165), and quantum yield of singlet oxygen photosensitization. All the values except Φ_Δ correspond to the chemicals dissolved in CH_2Cl_2. Quantum yield of singlet oxygen photosensitization is measured in toluene.

Molecule No.	σ_2, GM	$\varepsilon\times10^{-4}$ $M^{-1}cm^{-1}$ (397 nm)	$\lvert\Delta\mu_{fg}\rvert$ (S_0–S_3), D	$\bar{\nu}_{fg}\times10^{-4}$, (Soret), cm^{-1}	β	Calculated σ_2, GM	Φ_Δ	$\sigma_2\times\Phi_\Delta$, GM
1	7	-	-	-	-	-	-	-
2	440	6.92	9.4	2.40	1°	190	0.80	350
3	520	7.16	10.4	2.37	3°	240	0.89	460
4	520	14.9	9.8	2.45	0°	430	0.76	390
5	880	15.9	5.5	2.40	16°	150	0.82	720
6	110	17.9	9.7	2.44	1°	510	0.75	80
7	740	8.47	0.2	2.33	4°	~ 0	0.53	390

Table 5.3 presents TPA cross sections of the studied molecules measured at 795 nm excitation wavelength. Two-photon spectra of compounds **1**-**3** and **6**,**7** are presented at Figure 5.10. The immediate important result is that the values of two-photon cross sections of the porphyrins with TPA substituents are much larger than the values reported for most of the porphyrins in Chapter 3 and are well above two-photon cross sections of currently used one-photon photosensitizers studied in this chapter (see Two-Photon

Excitation of Some Currently Used Photosensitizers). The largest σ_2 = 880 GM, which is about ~ 100 times larger than parent molecule's two-photon cross section, competes well with the strongest organic TPA chromophores. This corroborates the chosen strategy and substantiates the claim that new molecules can be efficient two-photon photosensitizers.

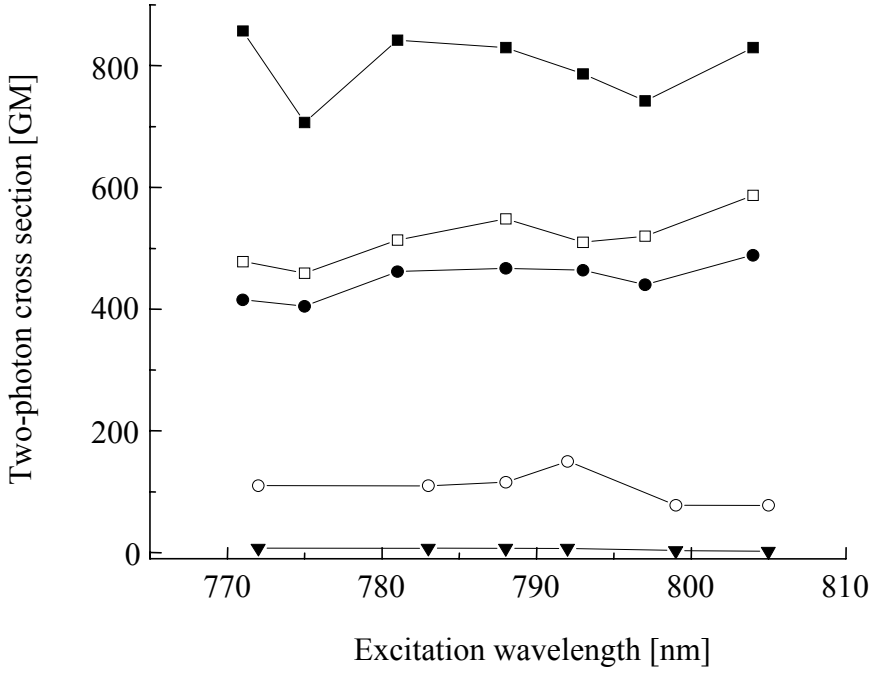

Figure 5.10 Two-photon spectra of the studied compounds in the 770 – 805 nm excitation wavelength range: **1** (triangles), **2** (solid circles), **3** (open squares), **6** (open circles), **7** (solid squares). The spectra of the compounds **2, 3** and **7** are measured in CH_2Cl_2. Spectra of the **1** and **6** are measured in toluene.

The molecules with the triple chemical bond linker (**3** and **5**) possess the largest TPA cross sections 880 and 520 GM followed by the double-bond linked compounds (**2** and **4**) 520 and 440 GM. Although TPA cross section of the single-bond linked molecule **6** is much larger than that of the parent compound **1**, it is rather small in comparison to the rest of the compounds. This behavior is in accord with the previous discussion of the π-conjugation efficiency in the new photosensitizers based on their linear absorption

spectra and our finding, described in Chapter 3 (see Other Approaches to the TPA Enhancement), that π-conjugation increases σ_2 in porphyrins in the near-IR excitation wavelength spectral range. Compound **7,** which has four TPA units identical to that of **6**, reveals two-photon cross section close to that of much stronger conjugated **2**-**5** compounds. It is clear that simultaneous attachment of the four TPA units (electron donors) to the **7** results in increased number of TPA absorbers leading to large TPA cross section, and, yet, it shows the disadvantage of the single-bond connection. Four TPA units are required to reach the same value of σ_2 that is obtained in the more efficiently conjugated systems with just one substituent. Note that 2,6-dichlorophenyl responsible, for the efficient intersystem crossing has to be sacrificed in **7** in order to obtain large σ_2. Although compounds **6** and **7** are not as efficiently designed as the rest of the molecules, they do show the way to increase TPA cross sections even further. The two-photon cross section of **7** is almost seven times larger than that of **6**, while the number of TPA substituents is increased only by four. Evidently, cooperative enhancement of two-photon cross section takes place upon increasing number of the TPA substituents.

All the studied molecules (except **7**) are non-centrosymmetrical. In general case, TPA probability in non-centrosymmetrical porphyrins is proportional to a modulus squared of the sum of probability amplitudes of two quantum TPA pathways (see Chapter 2 Three-Level Model for Non-Centrosymmetrical Molecule):

$$\sigma_{fg}^{(2)}(\omega) = 2\frac{(2\pi)^3\omega^2 L^4}{\hbar^2 n^2 c^2}\left|\frac{(\boldsymbol{e}\cdot\boldsymbol{\mu}_{fm})(\boldsymbol{e}\cdot\boldsymbol{\mu}_{mg})}{\omega_{mg}-\omega+i\Gamma_m(\omega)}+\frac{(\boldsymbol{e}\cdot\boldsymbol{\mu}_{fg})(\boldsymbol{e}\cdot\Delta\boldsymbol{\mu}_{fg})}{\omega}\right|^2 g(2\omega) \qquad (2.40)$$

(1) transition in a three-level system (*f*, *m*, *g*) with the real intermediate state; (2) transition in a two-level system (*f*, *g*) with a large change in the permanent dipole moment between these states. If the change of the static dipole moment between the ground and excited states is large, then the main contribution to the two-photon cross section may be caused by the second term containing the change of the dipole moment squared. In our case introduction of the TPA substituents with strong electron donating ability should induce permanent dipole moment.

The first Q-band represents a real intermediate level in equation (2.40). The nature of the excited state is not as clear. Since all the molecules except **7** are non-centrosymmetrical, both one- and two-photon transitions are allowed between any energy levels. The TPA spectra presented in Figure 5.10 do not possess any structure and cover only small wavelength range. Although the obtained TPA spectra are not very informative by themselves they do overlap with their one-photon counterparts in the studied wavelength range. By this means we suppose that both one- and two-photon excitation at $\lambda \sim 400$ nm transition wavelength populate the same energy levels. In the case of OPA, $\lambda = 400$ nm corresponds to the Soret band, which means that two-photon excitation also populates the Soret band making it an excited state.

To determine which mechanism (term) is responsible for the strong TPA enhancement in the new photosensitizers we use equation (2.46) to estimate the contribution of the change of the static dipole moment $\Delta\boldsymbol{\mu}_{fg}$ into σ_2.

$$\sigma_{fg}^{(2)}(\nu) = \frac{2}{5}\frac{(2\pi)^4 L^4}{h^2 n^2 c^2}\left|\boldsymbol{\mu}_{fg}\right|^2 \left|\Delta\boldsymbol{\mu}_{fg}\right|^2 g(2\nu) \qquad (2.46)$$

The angle β between vectors $\Delta\boldsymbol{\mu}_{fg}$ and $\boldsymbol{\mu}_{fg}$ is not taken into account because it is close to zero for all the studied molecules (Table 5.3). The change of the static dipole moment was obtained by means of quantum chemical calculations with Hyperchem 7 package. Product of the transition dipole moment squared from the ground state to the excited state with the line shape function $\left|\boldsymbol{\mu}_{fg}\right|^2 g(2\nu)$ was found from the linear absorption spectra using calculations similar to the ones described in Appendix C (see equation (C.10)):

$$\left|\boldsymbol{\mu}_{fg}\right|^2 g_{TPA}(2\nu) = \frac{\varepsilon_{fg}(2\bar{\nu})}{1.07\cdot 10^{38}\bar{\nu}_{fg}c}, \tag{5.4}$$

where $\bar{\nu}_{fg}$ is the mean frequency of the Soret transition [cm^{-1}], $\varepsilon_{fg}(2\nu)$ is the molar extinction coefficient [$M^{-1}cm^{-1}$] at twice the laser frequency, i.e. 25190 cm^{-1} (397 nm), c is the speed of light.

Table 5.3 presents the calculated change of the static dipole moment $\left|\Delta\boldsymbol{\mu}_{fg}\right|^2$ along with the rest of parameters entering equations (2.46) and (5.4). The $\left|\Delta\boldsymbol{\mu}_{fg}\right|^2$ is large for all the unsymmetrically substituted molecules peaking for compound **3**, $\left|\Delta\boldsymbol{\mu}_{fg}\right| = 10.4\cdot 10^{-18}$ e.s.u. = 10.4 D. The estimated value of two-photon cross section is also shown in the table. Taking into account approximations used in this estimate the order of magnitude coincidence between experimentally measured and theoretically estimated values of σ_2 for compounds **2**-**6** is remarkable. The large increase of TPA cross sections of these molecules is indeed partially due to the static dipole moment induced by the substituents. For compound **5**, the measured value of σ_2 is about 6 times larger than the estimated one. Although the difference might look large, the theoretical estimation gives the same order

of magnitude for two-photon cross section value as experimental result. Both values are in agreement with each other in the sense that they are much larger than that measured for the parent molecule **1**. The difference between experimental and theoretical values may be caused by the rough approximations that have been made and/or by the errors introduced by quantum mechanical calculations with Hyperchem. Note, that the angle, β, between $\Delta\boldsymbol{\mu}_{fg}$ and $\boldsymbol{\mu}_{fg}$ calculated for the **5** is markedly different from the rest of the compounds. It gives ground to the last assumption that the Hyperchem calculations for this molecule might be somewhat erroneous. An underestimated value of the change of the static dipole moment for **5** (Table 5.3) can easily explain rather large difference between experimental on theoretical two-photon cross sections.

The rest of the σ_2 for the compounds **2-5** is clearly contributed by the resonance enhancement (see the first term in equation (2.40)). Indeed, the first Q-band in the **2-5** is moved 20-32 nm to the red being closer to the excitation laser wavelength. The extinction coefficient increases by a factor of 4 ÷ 15 also contributing to the resonance enhancement. Note, that the largest red shift and extinction coefficient increase is observed for the compounds with triple bonds (**3** and **5**) resulting in larger two-photon cross sections as compared the compounds with double bonds (**2** and **4**).

Molecule **6** shows several times lower TPA cross section than molecules **2-5**. The σ_2 is also about five times smaller than can be expected from the estimation (Table 5.3). Taking into account rather weak electronic conjugation between the porphyrin core and the substituent in **6** and small TPA cross section (σ_2 = 7 GM) of the parent molecule **1**, one can suppose that the main TPA absorber in this case is the substituent itself.

However, an excitation at 395 nm does not result in any significant green fluorescence of **6** that could be associated with the substituent. This can imply that very efficient energy transfer from the substituent to the porphyrin core occurs after initial excitation. The same mechanism is most likely true also for dendritic compound **7**. In this case, a rather small change of permanent dipole moment, $\Delta\boldsymbol{\mu}_{fg}$ = 0.2 D, (molecule is centrosymmetrical) cannot be responsible for such a large value of σ_2 = 740 GM, observed experimentally. The estimated value of TPA cross section is less than 1 GM. The σ_2 of compound **7** is rather determined by a combination of absorptions of its four substituents (dendrons). Since this value increases by almost seven times as compared to the mono-substituted molecule **6**, we can assume that there could be a slight cooperativity in TPA response of dendrons.

The very significant fact is that the excitation wavelength region λ_{ex} ~ 750 – 800 nm, used in these experiments, falls well into the "tissue transparency window". Figure 5.11 demonstrates that we were able to detect directly production of singlet oxygen upon two-photon excitation (λ_{ex} ~ 800 nm) of the compounds **2**-**7**. Figure 5.11a shows two luminescence spectra obtained upon one- (dash) or two-photon (solid) excitation of **6**, both normalized to unity. Note that the two spectra coincide well within experimental error, and show a characteristic peak near 1276 nm, which undoubtedly corresponds to singlet oxygen luminescence spectrum. Figure 5.11b shows that the intensity of luminescence upon two-photon excitation increases as a square of the illumination intensity, which proves that the porphyrin is indeed excited by absorbing two near-IR photons simultaneously.

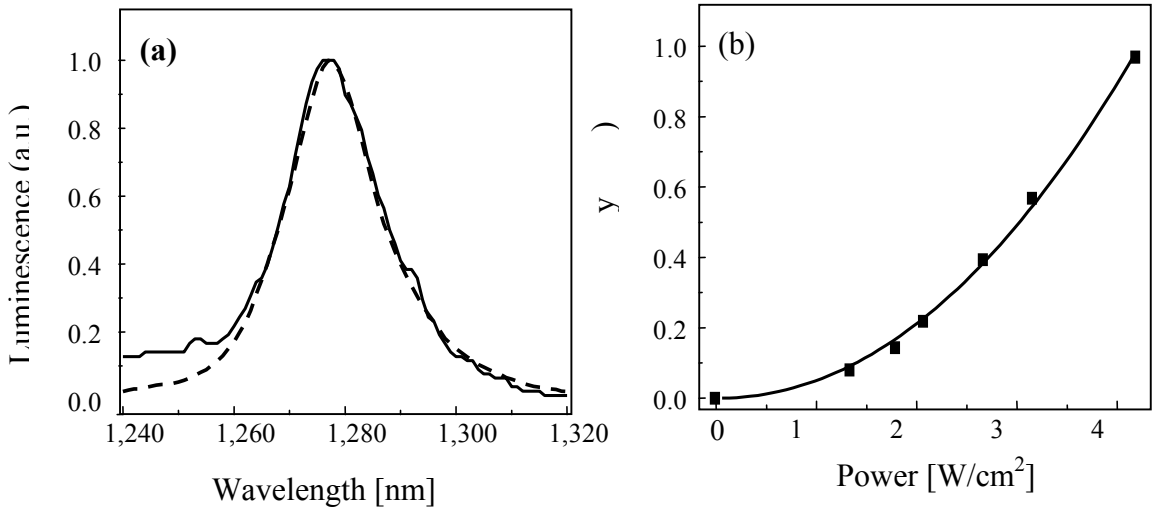

Figure 5.11 (a) The $^1\Delta_g \rightarrow {}^3\Sigma_g^-$ luminescence spectra of molecular oxygen in air-saturated toluene solution of the compound **6**. Dashed and solid curves represent, respectively, the spectra measured with one- and two-photon excitation. Both spectra are normalized to unity. The spectra obtained with the rest of the porphyrins are not shown because they look the same (singlet oxygen luminescence spectrum does not depend on the excitation process bringing the oxygen to its $^1\Delta_g$ state, i.e it does not depend on the type of the used photosensitizer). Thus the spectrum obtained with the photosensitizer with the lowest value of the product $\sigma_2 \times \Phi_\Delta$ is shown. (b) The dependence of the $^1\Delta_g \rightarrow {}^3\Sigma_g^-$ luminescence intensity I_Δ on the average illumination intensity, P, upon two-photon excitation. Experimental data are shown by black squares. Solid curve is the best power-law fit $I_\Delta = aP^n$ with $n = 2.1 \pm 0.1$.

If the solution was purged with nitrogen gas, the intensity of luminescence decreased because of the decreased oxygen concentration indicating that the obtained signal is not caused by the porphyrin phosphorescence. Furthermore, the pure solvent without porphyrin photosensitizer does not produce luminescence signal shown at Figure 5.11a proving that we do not excite oxygen in the solvent directly. The singlet oxygen luminescence could be reliably detected only upon two-photon excitation of the compounds with strongly enhanced TPA cross sections, namely **2**-**7**. In the case of the parent molecule, while strong oxygen luminescence could be obtained upon one-photon excitation, the TPA cross section was too low to observe it with two-photon excitation.

For all efficient two-photon photosensitizers we measured quantum efficiency of singlet oxygen generation Φ_Δ. The corresponding values are presented in Table 5.3. The quantum yield for all the molecules is close to unity, indicating that efficient singlet $\rightarrow$ triplet intersystem crossing takes place. The only exception is the dendritic photosensitizer, **7**, whose quantum yield of singlet oxygen generation ($\Phi_\Delta = 0.53$) is about 1.5 times lower than that of the rest of the molecules. A possible reason for that is the lack of the ISC-helping substituent 2,6-dichlorophenyl. Table 5.3 also presents an important for two-photon photodynamic therapy parameter, $\sigma_2 \times \Phi_\Delta$, which can be considered as a figure of merit. First, it shows that among all the studied photosensitizers **5** is the most efficient. Second, it demonstrates the importance of the efficient intersystem crossing. Although the dendritic molecule **7** has the second largest TPA cross section (σ_2 = 740 GM) its low yield of singlet oxygen generation makes it less efficient than, for example, compound **3** whose TPA cross section is only 520 GM.

In conclusion, an introduction of strong electron donating groups to the porphyrin core results in strong, 10 – 100 fold, increase of porphyrin TPA cross section. The substituents connected by means of double and triple chemical bonds, **2**-**5**, show the strongest degree of electronic conjugation with the porphyrin core, and correspondingly, the largest increase of two-photon cross sections. The largest measured value of σ_2 in this series is equal to 880 GM. It competes well with the strongest organic TPA chromophores. The mechanism of TPA enhancement in these compounds is accounted for the combination of two effects: (1) the large change of permanent dipole moment and (2) resonance enhancement. Substituents connected by single chemical bonds, **6**,**7**, are

less conjugated with porphyrin core. The enhancement of their TPA properties is not as large, indicating that this design strategy is less efficient. The mechanism of TPA enhancement in this case is connected to TPA by the substituent and consecutive energy transfer to the porphyrin core. The dendritic porphyrin with four substituents shows slight cooperative enhancement of TPA in comparison with the mono-substituted compound. Two-photon excited photosensitization of singlet molecular oxygen by all the compounds (except parent) was observed. Quantum yield of singlet oxygen photosensitization was measured. The resulting values $\Phi_\Delta = 0.75 – 0.89$ are rather large for compounds **2**-**6**. For **7**, the quantum yield is reduced to $\Phi_\Delta = 0.53$ possibly due to lack of 2,6-dichlorophenyl substituent, demonstrating importance of ISC helper for efficient singlet oxygen photosensitization. The efferent generation of singlet oxygen by means of two-photon excitation of the new photosensitizers opens up new perspectives for two-photon-based photodynamic therapy.

CHAPTER 6

SUMMARY AND CONCLUSION

This chapter summarizes the work done in the thesis and presents conclusions for three main areas of research, TPA properties of tetrapyrrolic molecules, TPA-based spectral gratings, and TPA-based PDT. Future research directions are also given.

TPA Properties of Tetrapyrrolic Compounds and Methods of Enhancement of Two-Photon Cross Section (Chapter 3)

For the first time TPA properties of the tetrapyrrolic molecules are investigated in rigorous manner. Two different spectral regions are probed, λ = 550 – 700 nm transition wavelength (near Q-bands) and λ = 350 – 410 nm transition wavelength (near Soret band). It is found that the spectra and absolute cross sections of TPA of tetrapyrroles these regions are remarkably different.

In the Q-bands region (transition wavelength), TPA is weak so that two-photon cross section does not exceed 10 GM and TPA spectra show the same transitions as the corresponding linear absorption spectra. These observations are explained by the fact that there are no *g* – parity electronic states in this spectral region. Although most of the studied molecules are centrosymmetrical both one- and two-photon transitions are allowed between the same energy levels. Apparent violation of parity selections rules is due to symmetry breaking caused, most likely, by substituents and/or solvent effect. Another mechanism, which may lead to $u \leftarrow g$ type two-photon transitions is the coupling between vibronic and electronic levels (Herzberg-Teller mechanism). This

results in strong enhancement of vibronic $S_1 \leftarrow S_0$ two-photon transition in comparison to pure electronic $S_1 \leftarrow S_0$ transition. Electronic-vibronic coupling also explains somewhat different shape of vibronic $S_1 \leftarrow S_0$ transition in case of one- and two-photon excitation because different vibrations are active in both cases.

The fact that for some of the studied molecules TPA is allowed in the purely electronic $S_1 \leftarrow S_0$ transition indicates that the corresponding TPA band may possess ZPL at low temperature. Later on, we use these molecules to study SHB and coherence phenomena.

In Soret band region (transition wavelength) TPA of tetrapyrroles is strongly enhanced in comparison to the Q-bands region with two-photon cross section as large as $10^3 - 10^4$ GM. The shape of the TPA spectra is distinctively different from the linear absorption for the most of the molecules and show large increase of the two-photon cross section upon moving to higher frequencies. Two main mechanisms that lead to the TPA enhancement in this spectral region are identified: resonance enhancement and $g \leftarrow g$ transitions.

The resonance enhancement mechanism is caused by the lowest singlet – singlet electronic transition, $S_1 \leftarrow S_0$ (I-st Q-band), which lies slightly above half-way between the ground state and Soret band. Two factors, increase of the intensity and redshift closer to the excitation laser wavelength, lead to the enhancement of the TPA cross section, as confirmed by studding a series of tetrabenzoporphyrins. Large resonance enhancement effect justifies application of three-level model with a single intermediate level three-level model for description of the TPA properties of tetrapyrroles in this spectral region.

Presence of the strong two-photon allowed $g \leftarrow g$ transitions near and above Soret band in the tetrapyrrolic molecules is established. These transitions account for additional increase of the two-photon cross section as compared to the Q-bands region.

Two other mechanisms leading to TPA enhancement in some tetrapyrroles are also established and discussed. These are (a) electron-donating and/or electron-accepting substitution and (b) electronic conjugation (π-conjugation). As a result, we report a record large two-photon cross section for tetrapyrrolic molecule, porphyrin dimer synthesized by Prof. H. L. Anderson group, University of Oxford, amounting to 7000 GM.

Finally, a new method of measuring absolute TPA cross section is proposed and tested. This method is most useful in the border between spectral regions where OPA and TPA dominate. It consists in comparison of the efficiency of OPA and TPA excited at the same wavelength. In our experiments, we were able to extend the TPA cross section measurements further into UV spectral region, where regular fluorescence method fails.

There are two directions where future research may concentrate. First, it is important to find molecules with larger TPA cross sections in the purely electronic $S_1 \leftarrow S_0$ transition. Low TPA efficiency of ZPLs is currently an obstacle in extending study of TPA-based coherence phenomena. New porphyrin-based photosensitizers described in the Chapter 5 may resolve this problem. The two-photon cross section of these molecules corresponding to the transitions in the near-UV are large, $\sigma_2 \sim 10^2 - 10^3$ GM. Most of them represent non-centrosymmetrical molecules, which means that both one- and two-photon transitions are simultaneously allowed into the first absorption band, $S_1 \leftarrow S_0$.

Since much of their two-photon cross section is due to large change of permanent dipole moment, it can be expected that they have large σ_2 of the $S_1 \leftarrow S_0$ transition as well.

Second, we have not been able to study intermediate spectral region, λ = 410 – 550 nm (transition wavelength), λ = 820 – 1100 nm (excitation wavelength) due to limitations of our current laser system. This "blind spot" represents an interesting spectral region for future studies. It is predicted that some tetrapyrrolic compounds may have $g \leftarrow g$ transitions in this spectral region. This would allow studying $g \leftarrow g$ transitions without interference with OPA. Furthermore, the "tissue transparency window" also corresponds to this spectral region. Studying TPA properties of tetrapyrroles there will allow their better characterization for two-photon PDT.

TPA-Induced Frequency Domain Coherence Gratings (Chapter 4)

The information obtained in Chapter 3 about TPA properties of the first singlet – singlet electronic transition obtained in the Chapter 3 is used here to study coherence gratings induced in two-photon transitions of tetrapyrrolic molecules in solid matrix at low temperature. For the first time such experiments are performed in frequency domain. The interference grating is created by illuminating the sample with phase-locked pairs of 100-fs near-IR laser pulses, whereas the transition takes place at a two times shorter wavelength in the visible spectrum. The two-photon excited coherence grating is detected in two independent ways, by measuring the fluorescence spectrum and by measuring persistent spectral holes structure in the absorption spectrum at low temperature, T = 4 – 60 K

In the first experiment, a spectral grating is created by means of SHB in the inhomogeneously broadened absorption spectrum of $S_1 \leftarrow S_0$ transition in chlorin. This experiment constitutes the first demonstration of SHB by means of TPA. We overcome the low efficiency of TPA ($\sigma_2 \sim 1$ GM) by using less stable tautomer form of chlorin, which has a larger quantum efficiency of phototransformation ($\varphi \sim 0.1$).

Next, spectral grating is created in the fluorescence spectrum of two different molecules, centrosymmetrical SiNc and non-centrosymmetrical chlorin. By varying the sample temperature, T = 4 – 120 K, we show that for chlorin the shape of the grating dramatically depends on temperature, whereas for SiNc the dependence on temperature is much less. The exact shape of the fluorescence grating is analyzed at different temperatures. We use this data to deduce key parameters such as Debye-Waller factor and phonon frequency for the two-photon transition. We note that in the presence of large inhomogeneous broadening these parameters are difficult to obtain for two-photon transitions. A quantitative model is developed, describing the observed spectral temperature-dependent peculiarities.

The temperature dependence of the spectral grating can be used for easy determination of the presence/absence of the ZPL in TPA spectrum of different molecules. This is particularly remarkable because short 100-fs time duration pulses are used for two-photon excitation. The spectral width ($\Delta\nu \sim 10^{13}$ Hz) of such pulses precludes direct observation of ZPL by means of fluorescence line narrowing, while still takes advantage of high peak intensity of femtosecond pulses.

Future research in this area may concentrate on the study of TPA analogs of transient coherent phenomena such as photon echo, optical nutation, etc. known from one-photon spectroscopy. As it was mentioned above, low TPA efficiency ($\sigma_2 \sim 1$ GM) is inherently the main limiting factor. New porphyrins with much larger σ_2 value described in the Chapter 5 may resolve this problem.

Photosensitization of Singlet Molecular Oxygen by Means Of Two-Photon Excitation and Its Application for PDT (Chapter 5)

The information about properties of TPA transitions in the tetrapyrrolic molecules near Soret band spectral region (near-IR excitation wavelength) obtained in the Chapter 3 is used here to demonstrate feasibility of two-photon photosensitization of singlet molecular oxygen. The "tissue transparency window" in the near-IR corresponds well to the excitation wavelength region where two-photon cross sections of tetrapyrrolic molecules are enhanced. Since tetrapyrroles are already used as "classical" one-photon photosensitizers for treatment of cancer and some other illnesses, this motivated us to study possibility of two-photon initiated PDT.

First, TPA properties and generation of singlet molecular oxygen upon two-photon excitation of some currently used photosensitizers, Visudyne® and Photolon®, are studied. The main conclusion is that because of small TPA cross sections of these photosensitizers, $\sigma_2 \sim 50 - 100$ GM, the efficiency of singlet oxygen generation in near-IR is rather small. New photosensitizers with enhanced two-photon cross sections are required.

Next, we study new two-photon-based photosensitizers, consisting of porphyrin core, TPA unit, and ISC helper, which were synthesized by C. W. Spangler group, Montana State University. The combinations of the TPA enhancement mechanisms studied in Chapter 3 accounts for increase of the value of two-photon cross section up to about 10^3 GM. In particular, it is shown that structures with the strongest electronic conjugation between the porphyrin core and the TPA unit demonstrate the largest TPA cross sections. By using new photosensitizers we show, for the first time, efficient generation of singlet oxygen upon two-photon excitation of a photosensitizer in toluene solution.

All the studies so far were performed *in vitro*. Future research may concentrate on characterization of the new photosensitizers *in vivo* (in living tissue). In particular, the evaluation of the efficient penetration depth of ultrashort laser pulses into the tissue is of great importance. It is known that strongly scattering media elongates pulse duration. The efficiency of the singlet oxygen generation deep inside of the tissue by such laser pulses is critical issue for two-photon-based PDT. Also, future research may be directed to the development of new, even more efficient, two-photon photosensitizers.

REFERENCES CITED

1. W. Kaiser and C. G. Garrett, "Two-Photon Excitation in $CaF_2:Eu^{2+}$," Phys. Rev. Lett. **7**, pp. 229-231, 1961.

2. P. A. Franken, A. E. Hill, C. W. Peters, and G. Weinreich, "Generation of Optical Harmonics," Phys. Rev. Lett. **7**, pp. 118-119, 1961.

3. G. Eckhardt, R. W. Hellwarth, F. J. McClung, S. E. Schwarz, D. Weiner, and E. J. Woodbury, "Stimulated Raman Scattering From Organic Liquids," *Phys. Rev. Lett.* **9**, pp. 455-457, 1962.

4. V. I. Bredikhin, M. D. Galanin, and V. N. Genkin, "Two-photon absorption and Spectroscopy," *Sov. Phys.-Usp.* **16**, pp. 299-321, 1973.

5. D. M. Friedrich and W. M. McClain, "Two-Photon Molecular Electronic Spectroscopy," *Ann. Rev. Phys. Chem.* **31**, pp. 559-577, 1980.

6. P. R. Callis, "Two-Photon-Induced Fluorescence," *Ann. Rev. Phys. Chem.* **48**, pp. 271-297, 1997.

7. O. Lammel and A. Penzkofer, "Femtosecond Pulse Duration Measurement by Two-Photon Fluorescence Detection," *Opt. Quant. Electr.* **32**, pp. 1147-1160, 2000.

8. M. Müller, J. Squier, and G. J. Brakenhoff, "Measurement of Femtosecond Pulses in the Focal Point of a High-Numerical-Aperture Lens by Two-Photon Absorption," *Opt. Lett.* **20**, pp. 1038-1040, 1995.

9. W. Schade, J. Preusser, D. L. Osborn, Y. Y. Lee, J. deGouw, S. R. Leone, "Spatially Resolved Femtosecond Time Correlation Measurements on a GaAsP Photodiode," *Opt. Commun.* **162**, pp. 200-204, 1999.

10. J. A. Giordmaine, P. M. Rentzepis, S. L. Shapiro, and K. W. Wecht, "Two-Photon Excitation of Fluorescence by Picosecond Light Pulses," *Appl. Phys. Lett.* **11**, pp. 216-218, 1967.

11. F. G. Omenetto, W. A. Schroeder, K. Boyer, J. W. Longworth, A. McPherson, and C. K. Rhodes, "Measurement of 160-fs, 248-nm Pulses by Two-Photon Fluorescence in Fused-Silica Crystals," *Appl. Opt.* **36**, pp. 3421-3424, 1997.

12. A. Tünnermann, H. Eichmann, R. Henking, K. Mossavi, and B. Wellegehausen, "Single-Shot Autocorrelator for KrF Subpicosecond Pulses Based on Two-Photon Fluorescence of Cadmium Vapor at $\lambda = 508$ nm," *Opt. Lett.* **16**, pp. 402-404, 1991.

13. B. Luther-Davies, M. Samoc, J. Swiatkiewicza, A. Samoc, M. Woodruff, R. Trebino, and K. W. Delong, "Diagnostics of Femtosecond Laser Pulses Using Films of Poly(*p*-phenylenevinylene)," *Opt. Commun.* **131**, pp. 301-306, 1996.

14. A. Reuther, A. Laubereau, and D. N. Nikogosyan, "A Simple Method for the in Situ Analysis of Femtosecond UV Pulses in the Pump-Probe Spectroscopy of Solutions," *Opt. Commun.* **141**, pp. 180-184, 1997.

15. M. Rasmusson, A. N. Tarnovsky, E. Åkesson, and V. Sundström, "On the Use of Two-Photon Absorption for Determination of Femtosecond Pump-Probe Cross-Correlation Functions," *Chem. Phys. Lett.* **335**, pp. 201-208, 2001.

16. J. I. Dadap, G. B. Focht, D. H. Reitze, and M. C. Downer, "Two-Photon Absorption in Diamond and Its Application to Ultraviolet Femtosecond Pulse-Width Measurement," *Opt. Lett.* **16**, pp. 499-501, 1991.

17. I.G. Cormack, W. Sibbett, and D.T. Reid, "Practical Measurement of Femtosecond Optical Pulses Using Time-Resolved Optical Gating," *Opt. Commun.* **194**, pp. 415-424, 2001.

18. K. Ogawa, "Real-Time Spectrogram Measurement of Ultrashort Optical Pulses Using Two-Photon Absorption in Semiconductor," *Opt. Exp.* **10**, pp. 262-267, 2002.

19. T. Sekikawa, T. Kanai, and S. Watanabe, "Frequency-Resolved Optical Gating of Femtosecond Pulses in the Extreme Ultraviolet," *Phys. Rev. Lett.* **91**, pp. 103902-1 – 103902-4, 2003.

20. G. S. He, R. Signorini, and P. N. Prasad, "Two-Photon-Pumped Frequency-Upconverted Blue Lasing in Coumarin Dye Solution," *Appl. Opt.* **37**, pp. 5720-5726, 1998.

21. G. S. He, P. P. Markowicz, T.-C. Lin, and P. N. Prasad, "Observation of Stimulated Emission by Direct Three-Photon Excitation," *Nature* **415**, pp. 767-770, 2002.

22. A. Mukherjee, "Two-Photon Pumped Upconverted Lasing in Dye Doped Polymer waveguides," *Appl. Phys. Lett.* **62**, pp. 3423-3425, 1993.

23. W. Denk, J. H. Strickler, and W. W. Webb, "Two-Photon Laser Scanning Fluorescence Microscopy," *Science* **248**, pp. 73-76, 1990.

24. R. M. Williams, D. W. Piston, and W. W. Webb, "Two-Photon Molecular Excitation Provides Intrinsic 3-Dimensional Resolution for Laser-Based Microscopy and Microphotochemistry," *FASEB J.* **8**, pp. 804-813, 1994.

25. W. Denk and K. Svoboda, "Photon Upmanship: Why Multiphoton Imaging is More Than a Gimmick," *Neuron* **18**, pp. 351-357, 1997.

26. B. R. Masters, P. T. C. So, K. H. Kim, C. Buehler, and E. Gratton, "Multiphoton Excitation Microscopy, Confocal Microscopy, and Spectroscopy of Living Cells

and Tissues; Functional Metabolic Imaging of Human Skin *in Vivo*," in *Methods of Enzymology: Confocal Microscopy*, Academic Press, San Diego, ed. P. M. Conn, **307**, pp. 513-536, 1999.

27. J. B. Shear, "Multiphoton-Excited Fluorescence in Bioanalytical Chemistry," *Anal. Chem.* **71**, pp. 598A-605A, 1999.

28. R. M. Williams, W. R. Zipfel, and W. W. Webb, "Multiphoton Microscopy in Biological Research," *Curr. Opin. Chem. Biol.* **5**, pp. 603-608, 2001.

29. D. R. Larson, W. R. Zipfel, R. W. Williams, S. W. Clark, M. P. Bruchez, F. W. Wise, W. W. Webb, "Water-Soluble Quantum Dots for Multiphoton Fluorescence Imaging in Vivo," *Science* **300**, pp. 1434-1436, 2003.

30. D. A. Parthenopoulos and P. M. Rentzepis, "Three-Dimensional Optical Storage Memory," *Science* **245**, pp. 843-845, 1989.

31. A. Toriumi, J. M. Herrmann, and S. Kawata, "Nondestructive Readout of a Three-Dimensional Photochromic Optical Memory with a Near-Infrared Differential Phase-Contrast Microscope," *Opt. Lett.* **22**, pp. 555-557, 1997.

32. A. Toriumi, S. Kawata, and M. Gu "Reflection Confocal Microscope Readout System for Three-Dimensional Photochromic Optical Data Storage," *Opt. Lett.* **23**, pp. 1924-1926, 1998.

33. A. S. Dvornikov, C. M. Taylor, Y. C. Liang, and P. M. Rentzepis, "Photorearrangement Mechanism of 1-Nitro-Naphthaldehyde and Application to Three-Dimensional Optical Storage Devices," *J. Photoch. Photobiol. A* **112**, pp. 39-46, 1998.

34. H. E. Pudavar, M. P. Joshi, P. N. Prasad, and B. A. Reinhardt, "High-Density Three-Dimensional Optical Data Storage in a Stacked Compact Disk Format with Two-Photon Writing and Single Photon Readout," *Appl. Phys. Lett.* **74**, pp. 1338-1340, 1999.

35. M. Gu, J. O. Amistoso, A. Toriumi, M. Irie, and S. Kawata, "Effect of Saturable Response to Two-Photon Absorption on the Readout Signal Level of Three-Dimensional Bit Optical Data Storage in a Photochromic Polymer," *Appl. Phys. Lett.* **79**, pp. 148-150, 2001.

36. J. H. Strickler and W. W. Webb, "Three-Dimensional Optical Data Storage in Refractive Media by Two-Photon Point Excitation," *Opt. Lett.* **16**, pp. 1780-1782, 1991.

37. B. H. Cumpston, S. P. Ananthavel, S. Barlow, D. L. Dyer, J. E. Ehrlich, L. L. Erskine, A. A. Heikal, S. M. Kuebler, I.-Y. S. Lee, D. McCord-Maughon, J. Qin, H.

Röckel, M. Rumi, X.-L. Wu, S. R. Marder, and J. W. Perry, "Two-Photon Polymerization Initiators for Three-Dimensional Optical Data Storage and Microfabrication," *Nature* **398**, pp. 51-54, 1999.

38. M. Gu and D. Day, "Use of Continuous-Wave Illumination for Two-Photon Three-Dimensional Optical Bit Data Storage in Photobleaching Polymer," *Opt. Lett.* **24**, pp. 288-290, 1999.

39. Y. Kawata, H. Ishitobi, and S. Kawata, "Use of Two-Photon Absorption in a Photorefractive Crystal for Three-Dimensional Optical Memory," *Opt. Lett.* **23**, pp. 756-758, 1998.

40. E. N. Glezer, M. Milosavljevic, L. Huang, R. J. Finlay, T.-H. Her, J. P. Callan, and E. Mazur, "Three-Dimensional Optical Storage Inside Transparent Materials," *Opt. Lett.* **21**, pp. 2023-2025, 1996.

41. M. Watanabe, S. Juodkazis, H.-B. Sun, S. Matsuo, H. Misawa, M. Miwa, and R. Kaneko, "Transmission and Photoluminescence Images of Three-Dimensional Memory in Vitreous Silica," *Appl. Phys. Lett.* **74**, pp. 3957-3959, 1999.

42. J.-A. Reyes-Esqueda, L. Vabre, R. Lecaque, F. Ramaz, B. C. Forget, A. Dubois, B. Briat, C. Boccara, G. Roger, M. Canva, Y. Levy, F. Chaput, J.-P. Boilot, "Optical 3D-Storage in Sol-Gel Materials with a Reading by Optical Coherence Tomography-Technique," *Opt. Commun.* **220**, pp. 59-66, 2003.

43. S. Maruo and S. Kawata, "Two-Photon-Absorbed Near-Infrared Photopolymerization for Three-Dimensional Microfabrication," *J. Microelectromech. Syst.* **7**, pp. 411-415, 1998.

44. H.-B. Sun, T. Kawakami, Y. Xu, J.-Y. Ye, S. Matuso, H. Misawa, M. Miwa, and R. Kaneko, "Real Three-Dimensional Microstructures Fabricated by Photopolymerization of Resins Through Two-Photon Absorption," *Opt. Lett.* **25**, pp. 1110-1112, 2000.

45. S. Kawata, H.-B. Sun, T. Tanaka, and K. Takada, "Finer Features for Functional Microdevices," *Nature* **412**, pp. 697-698, 2001.

46. W. Zhou, S. M. Kuebler, K. L. Braun, T. Yu, J. K. Cammack, C. K. Ober, J. W. Perry, and S. R. Marder, "An Efficient Two-Photon-Generated Photoacid Applied to Positive-Tone 3D Microfabrication," *Science* **296**, pp. 1106-1109, 2002.

47. T. Yu, C. K. Ober, S. M. Kuebler, W. Zhou, S. R. Marder, and J. W. Perry, "Chemically Amplified Positive Resists for Two-Photon Three-Dimensional Microfabrication," *Adv. Mater.* **15**, pp. 517-521, 2003.

48. H.-B. Sun and S. Kawata, "Two-Photon Laser Precision Microfabrication and Its Applications to Micro-Nano Devices and Systems," *J. Lightw. Tech.* **21**, pp. 624-633, 2003.

49. S. Maruo, K. Ikuta, and H. Korogi, "Submicron Manipulation Tools Driven by Light in a Liquid," *Appl. Phys. Lett.* **82**, pp. 133-135, 2003.

50. H.-B. Sun, Y. Xu, S. Juodkazis, K. Sun, M. Watanabe, S. Matsuo, H. Misawa, and J. Nishii, "Arbitrary-Lattice Photonic Crystals Created by Multiphoton Microfabrication," *Opt. Lett.* **26**, pp. 325-327, 2001.

51. H.-B. Sun, V. Mizeikis, Y. Xu, S. Juodkazis, J.-Y. Ye, S. Matsuo, and H. Misawa, "Microcavities in Polymeric Photonic Crystals," *Appl. Phys. Lett.* **79**, pp. 1-3, 2001.

52. I. Wang, M. Bouriau, P. L. Baldeck, C. Martineau, and C. Andraud, "Three-Dimensional Microfabrication by Two-Photon-Initiated Polymerization with a Low-Cost Microlaser," *Opt. Lett.* **27**, pp. 1348-1350, 2002.

53. C. W. Spangler, "Recent Development in the Design of Organic Materials for Optical Power Limiting," *J. Mater. Chem.* **9**, pp. 2013-2020, 1999.

54. G. Zhou, X. Wang, D. Wang, Z. Shao, and M. Jiang, "Upconversion Fluorescence and Optical Power Limiting Effects Based on the Two- and Three-Photon Absorption Process of a New Organic Dye BPAS," *Appl. Opt.* **41**, pp. 1120-1123, 2002.

55. C. Desroches, S. Parola, F. Vocanson, N. Ehlinger, P. Miele, R. Lamartine, J. Bouix, A. Eriksson, M. Lindgren, and C. Lopes, "Synthesis, Characterization and Optical Power Limiting Behavior of Phenylazo- and 4-Nitrophenylazo-Tetrahydroxytetrathiacalix[4]arene," *J. Mater. Chem.* **11**, pp. 3014-3017, 2001.

56. M. G. Silly, L. Porrès, O. Mongin, P.-A. Chollet, and M. Blanchard-Desce, "Optical Limiting in the Red-NIR Range with Soluble Two-Photon Absorbing Molecules," *Chem. Phys. Lett.* **379**, pp. 74-80, 2003.

57. W. G. Fisher, W. R. Partridge, Jr., C. Dees, and E. A. Wachter, "Simultaneous Two-Photon Activation of Type-I Photodynamic Therapy Agents," *Photoch. Photob.* **66**, pp. 141-1455, 1997.

58. J. D. Bhawalkar, N. D. Kumar, C.-F. Zhao, and P. N. Prasad, "Two-Photon Photodynamic Therapy," *J. Clin. Lasers Med. Surg.* **15**, pp. 201-204, 1997.

59. P. K. Frederiksen and O. P. R. Jørgensen, "Two-Photon Photosensitized Production of Singlet Oxygen," *J. Am. Chem. Soc.* **123**, pp. 1215-1221, 2001.

60. J. Liu, Y. W. Zhao, J. Q. Zhao, A. D. Xia, L. J. Jiang, S. Wu, L. Ma, Y. Q. Dong, Y. H. Gu, "Two-Photon Excitation Studies of Hypocrellins for Photodynamic Therapy," *J. Photoch. Photob. B: Biol.* **68**, pp. 156-164, 2002.

61. Yu. P. Meshalkin, E. E. Alfimov, N. E. Vasil'ev, A. N. Denisov, V. K. Makukha, and A. P. Ogirenko, "Two-Photon Excitation of Aluminium Phthalocyanines," *Quant. Electron.* **29**, pp. 1066-1068, 1999.

62. N. N. Vsevolodov, L. P. Kostikov, L. P. Kayushin, and V. I. Gorbatenkov, "Two-Photon Absorption of Laser Radiation by Chlorophyll *a* and Some Organic Dyes," *Biophysics (USSR)* **18**, pp. 755-757, 1973.

63. *Persistent Spectral Hole Burning: Science and Applications*, ed. W. E. Moerner, Springer-Verlag, Berlin, 1988.

64. B. M. Kharlamov, R. I. Personov, and L. A. Bykovskaya, "Stable Gap in Absorpiton Spectra of Solid Solutions of Organic Molecules by Laser Irradiation," *Opt. Commun.* **12**, pp. 191-193, 1974.

65. A. A. Gorokhovskii, R. K. Kaarli, and L. A. Rebane, "Hole Burning in Contour of a Pure Electronic Line in a Shpolskii System," *JETP Lett.* **20**, pp. 216-218, 1974.

66. L. A. Rebane, A. A. Gorokhovskii, and J. V. Kikas, "Low-Temperature Spectroscopy of Organic-Molecules in Solids by Photochemical Hole Burning," *Appl. Phys. B* **29**, pp. 235-250, 1982.

67. J. Friedrich and D. Haarer, "Photochemical Hole Burning – A Spectroscopic Study of Relaxation in Polymers and Glasses," *Ang. Chem. Int. Edit.* **23**, pp. 113-140, 1984.

68. K. Holliday and U. P. Wild, "Spectral Hole-Burning," in *Molecular Luminescence Spectroscopy: Methods and Applications Part III*, ed. S. Schulman, Wiley, New York, pp. 149-228, 1993.

69. *Zero-Phonon Lines and Spectral Hole Burning in Spectroscopy and Photochemistry*, eds. O. Sild and K. Haller, Springer-Verlag, Berlin, 1988.

70. A. Rebane and J. Feinberg, "Time-Resolved Holography," *Nature* **351**, pp. 378-380, 1991.

71. A. Rebane, R. Kaarli, P. Saari, A. Anijalg, and K. Timpmann, "Photochemical Time-Domain Holography of Weak Picosecond Pulses," *Opt. Commun.* **47**, pp. 173-176, 1983.

72. T. W. Mossberg, "Time-Domain Frequency-Selective Optical-Data Storage," *Opt. Lett.* **7**, pp. 77-79, 1982.

73. A. Rebane, "Femtosecond Time-and-Space Domain Holography," in *Trends in Optics, Research, Developments and Applications*, ed. A. Consortini, Academic Press, San Diego, pp. 165-188, 1996.

74. K. K. Rebane, "Spectral Hole Burning and Optical Information Processing in *Current Trends in Optics*, ed. J. C. Dainty, Academic Press, London, p. 177-194, 1994.

75. A. Rebane, M. Drobizhev, and C. Sigel, "Single Femtosecond Exposure Recording of an Image Hologram by Spectral Hole Burning in an Unstable Tautomer of a Phthalocyanine Derivative," *Opt. Lett.* **25**, pp. 1633-1635, 2000.

76. H. Schwoerer, D. Erni, and A. Rebane, "Holography in Frequency-Selective Media. 3. Spectral-Synthesis of Arbitrary Time-Domain Pulse Shapes," *J. Opt. Soc. Am. B* **12**, pp. 1083-1093, 1995.

77. M. Drobizhev, C. Sigel, and A. Rebane, "Photo-tautomer of Br-porphyrin: a new frequency-selective material for ultrafast time-space holographic storage," *J. Lumin.* **86**, pp. 391-397, 2000.

78. M. Göppert-Mayer, "Elementartakte mit zwei Quanten-sprungen," *Ann. Phys.* **9**, pp. 273-294, 1931.

79. R. W. Boyd, *Nonlinear Optics*, Academic Press, Amsterdam, Netherlands, 2003.

80. E. Zojer, D. Beljonne, T. Kogej, H. Vogel, S. R. Marder, J. W. Perry, and J. L. Brédas, "Tuning the Two-Photon Absorption Response of Quadrupolar Organic Molecules," *J. Chem. Phys.* **116**, pp. 3646-3658, 2002.

81. S. H. Lin, Y. Fujimura, H. J. Neusser, E. W. Schlag, "Multiphoton Spectroscopy of Molecules" in *Quantum Electronics – Principles and Applications*, Academic press, Orlando, 1984. (p. 21).

82. R. H. Pantell and H. E. Puthoff, *Fundamentals of Quantum Electronics*, Wiley, New York, 1969 (p. 67).

83. R. R. Birge, J. A. Bennett, B. M. Pierce, and T. M. Thomas, "Two-Photon Spectroscopy of the Visual Chromophores. Evidence for a Lowest Excited $^1A_g^-$ - Like $\pi\pi^*$ State in *all-trans*-Retinol (Vitamin A)," *J. Am. Chem. Soc.* **100**, pp. 1533-1539, 1978.

84. W. J. Meath and E. A. Power, "On the Importance of Permanent Moments in Multiphoton Absorption Using Perturbation Theory," *J. Phys. B: At. Mol. Phys.* **17**, pp. 763-781, 1984.

85. M. Drobizhev, A. Karotki, A. Rebane, and C.W. Spangler, "Dendrimer molecules with record large two-photon absorption cross section," *Opt. Lett.* **26**, pp. 1081-1083, 2001.

86. M. Albota, D. Beljonne, J.-L. Brédas, J. E. Ehrlich, J.-Y. Fu, A. A. Heikal, S. E. Hess, T. Kogej, M. D. Levin, S. R. Marder, D. McCord-Maughon, J. W. Perry, H. Röckel, M. Rumi, G. Subramaniam, W. W. Webb, X.-L. Wu, and C. Xu, "Design of Organic Molecules with Large Two-Photon Cross Sections," *Science* **281**, pp. 1653-1656, 1998.

87. V. S.-Y. Lin, S. G. DiMagno, and M. J. Therien, "Highly Conjugated, Acetylenyl Bridged Porphyrins: New Molecules for Light-Harvesting Antenna Systems," *Science* **264**, pp. 1105-1111, 1994.

88. M. S. Choi, T. Aida, T. Yamazaki, I. Yamazaki, "Dendritic multiporphyrin arrays as light-harvesting antennae: Effects of generation number and morphology on intramolecular energy transfer," *Chem.-Eur. J.* **8**, pp. 2668-2678, 2002.

89. H. Imahori, Y. Mori, and Y. Matano, "Nanostructured Artificial Photosynthesis," *J. Photoch. Photob. C: Photoch. Rev.* **4,** pp. 51-83, 2003.

90. M. P. O'Neil, M. P. Niemczyk, W. A. Svec, D. Gosztola, G. L. Gaines III, M. R. Wasielewski, "Picosecond Optical Switching Based on Biphotonic Excitation of an Electron Donor-Acceptor-Donor Molecule," *Science* **257**, pp. 63-65, 1992.

91. R. W. Wagner, J. S. Lindsey, J. Seth, V. Palaniappan, and D. F. Bocian, "Molecular Optoelectronic Gates," *J. Am. Chem. Soc.* **118**, pp. 3996-3997, 1996.

92. D. Holten, D. F. Bocian, and J. S. Lindsey, "Probing Electronic Communication in Covalently Linked Multiporphyrin Arrays. A Guide to the Rational Design of Molecular Photonic Devices," *Acc. Chem. Res.* **35**, pp. 57-69, 2002.

93. C. M. Drain, "Self-Organization of Self-Assembled Photonic Materials into Functional Devices: Photo-Switched Conductors," *Proc. Nat. Ac. Sc.* **99**, pp. 5178-5182, 2002.

94. B. W. Henderson and T. J. Dougherty, "How does Photodynamic Therapy work?," *Photoch. Photob.* **55**, pp. 147-157, 1992.

95. R. Bonnett, *Chemical Aspects of Photodynamic Therapy,* Gordon and Breach Science Publishers, Amsterdam, Netherlands, 2000.

96. R. K. Pandey and G. Zheng, "Porphyrins as Photosensitizers in Photodynamic Therapy," in *The Porphyrin Handbook: Applications: Past, Present and Future*, eds. K. M. Kadish, K. M. Smith, and R. Guilard, **6,** Academic Press, 2000.

97. K. J. McEwan, G. Bourhill, J. M. Robertson, and H. L. Anderson, "The Nonlinear Optical Characterization of Meso-Substituted Porphyrin Dyes" *J. Nonlinear Opt. Phys. Mater.* **9**, pp. 451-468, 2000.

98. K. S. Suslick, C.-T. Chen, G. R. Meredith, and L.-T. Cheng, "Push-Pull Porphyrins as Nonlinear Optical Materials," *J. Am. Chem. Soc.* **114**, pp. 6928-6930, 1992.

99. S. Guha, K. Kang, P. Porter, J. F. Roach, D. E. Remy, F. J. Aranda, and D. V. G. L. N. Rao, "Third-Order Optical Nonlinearities of Metallotetrabenzoporphyrins and a Platinum Poly-ene," *Opt. Lett.* **17**, pp. 264-266, 1992.

100. H. L. Anderson, "Building Molecular Wires from the Colours of Life: Conjugated Porphyrin Oligomers," *Chem. Comm.* pp. 2323-2330, 1999.

101. T. E. O. Screen, J. R. G. Thorne, R. G. Denning, D. G. Bucknall, and H. L. Anderson, "Amplified Optical Nonlinearity in a Self-Assembled Double-Strand Conjugated Porphyrin Polymer Ladder," *J. Am. Chem. Soc.* **124**, p. 9713, 2002.

102. H. S. Nalwa, "Organic Materials for Third-Order Nonlinear Optics," in *Nonlinear Optics of Organic Molecules and Polymers*, eds. H. S. Nalwa and S. Miyata, CRC Press, Boca Raton, pp. 611-797, 1997.

103. M. Drobizhev, A. Karotki, M. Kruk, and A. Rebane, "Resonance enhancement of two-photon absorption in porphyrins," *Chem. Phys. Lett.* **355**, pp. 175-182, 2002.

104. M. Drobizhev, A. Karotki, M. Kruk, N.Zh. Mamardashvili, and A. Rebane, "Drastic enhancement of two-photon absorption in porphyrins associated with symmetrical electron-accepting substitution," *Chem. Phys. Lett.* **361,** pp. 504-512, 2002.

105. A. Karotki, M. Drobizhev, M. Kruk, C. Spangler, E. Nickel, N. Mamardashvili, and A. Rebane, "Enhancement of two-photon absorption in tetrapyrrolic compounds," *J. Opt. Soc. Am. B* **20,** pp. 321-332, 2003.

106. M. Drobizhev, A. Karotki, M. Kruk, A. Krivokapic, H. L. Anderson, and A. Rebane, "Photon energy upconversion in porphyrins: one-photon hot-band absorption versus two-photon absorption," *Chem. Phys. Lett.* **370**, pp. 690- 699, 2003.

107. M. Kruk, A. Karotki, M. Drobizhev, V. Kuzmitsky, V. Gael, and A. Rebane, "Two-Photon absorption of tetraphenylporphin free base," *J. Lumin.* **105**, pp. 45-55, 2003.

108. A. Karotki, M. Drobizhev, Yu. Dzenis, P. N. Taylor, H. L. Anderson, and A. Rebane, "Dramatic Enhancement of Intrinsic Two-Photon Absorption in a Conjugated Porphryin Dimer," *PhysChemChemPhys* (submitted).

109. M. Drobizhev, M. Kruk, A. Karotki, and A. Rebane, "Resonance Enhancement of Two-Photon Absorption in Porphyrins," in *Technical Digest of Qunatum Electronics ans Laser Science Conference*, Long Beach, CA, pp. 52-53, 2002.

110. M. Drobizhev, A. Karotki, A. Rebane, M. Kruk, and N.Zh. Mamardashvili, "Drastic Enhancement of Two-Photon Absorption in Porphyrins by Optimizing resonance Conditions in Three-Level System," in *Technical Digest International Quantum Electronics Conference,* Moscow, Russia, p. 87, 2002.

111. M. Drobizhev, A. Karotki, M. Kruk, A. Rebane, E. Nickel, and C.W. Spangler, "Mechanisms of enhanced two-photon absorption in porphyrins," in *Proceedings of the SPIE* **4797,** pp. 152-162, 2002.

112. M. Drobizhev, A. Karotki, H.L. Anderson, and A. Rebane, "Very Efficient Multi-Photon Absorption in Porphyrins with Extended π-Conjugation," in *Technical Digest of Quantum Electronics and Laser Science Conference*, Baltimore, MD, pp. QML4, 2003.

113. M. Kruk, A. Karotki, M. Drobizhev, A. Rebane, V. Kuzmitsky, V. Gael, C. Spangler, R. Meng, E. Nickel, N. Mamardashvili, "Two-Photon Absorption in Tetrapyrrolic Compounds," in *Proceedings of IX International Conference on Chemistry of Porphyrins and Their Analogs*, Ivanovo, Russia, pp. 160-162, 2003.

114. L. R. Milgrom, *The Colours of Life: An Introduction to the Chemistry of Porphyrins and Related Compounds*, Oxford Univ. Press, 1997.

115. R. L. Goyan and D. T. Gramb, "Near-Infrared Two-Photon Excitation of Protoporphyrin IX: Photodynamics and Photoproduct Generation," *Photochem. Photobiol.* **72**, pp. 821-827, 2000.

116. T. C. Wen, L. C. Hwang, W. Y. Lin, C. H. Chen, and C. H. Wu, "Nonlinear Absorption of Light: Two-Photon Absorption and Optical Saturation in Metalloporphyrin-Doped Boric Acid Glass," *Chem. Phys.* **286**, pp. 293-302, 2003.

117. E. A. Wachter, W. P. Partridge, W. E. G. Fisher, H. C. Dees, and M. G. Petersen, "Simultaneous Two-Photon Excitation of Photodynamic Therapy Agents," in *Proceedings of the SPIE* **3269**, pp. 68-75, 1998.

118. I. Suzuka, M. Kozawa, and Y. Numata, "Two-Photon Absorption Spectra of Porphyrins – First Observation of the Hidden *g*-Excited State," presented at the XVIII International Union of Pure and Applied Chemistry Simposium on Photochemistry, Dresden, Germany, July 19-22, 2000.

119. V. A. Kuz'mitsii and K. N. Solov'ev, "Calculation of the Electronic Spectra of Porphin Molecules in the CNDO/S Approximation," *J. Appl. Spectr.* **27**, pp. 1341-1345, 1977.

120. V. I. Gael', V. A. Kuz'mitskii, and K. N. Solov'yov, "All-Valence Calculation by Fragments of Electronic Spectrum of Mg-Tetraphenylporphyrin Molecule," *J. Appl. Spectr.* **63**, pp. 790-798, 1996.

121. V. A. Kuz'mitskii, "Excited Even-Symmetry States of Metallocomplexes of Porphin and its Derivatives," *J. Appl. Spectr.* **68**, 758-765, 2001.

122. S. S. Dvornikov, V. N. Knyukshto, V. A. Kuzmitsky, A. M. Shulga, and K. N. Solovyov, "Spectral-Luminescent and Quantum-Mechanical Study of Azaroporphyrin Molecules," *J. Lumin.* **23**, pp. 373-392, 1981.

123. V. G. Maslov, "Calculations of Electronic Spectra of Mg-P, Mg-Pc and Their Ionic Forms by the CNDO/S Method," *Theor. Exp. Chem.* **20**, pp. 271-280, 1984.

124. M. B. Masthay, L. A. Findsen, B. M. Pierce, D. F. Bocian, J. S. Lindsey, and R. R. Birge, "A Theoretical Investigation of the One- and Two-Photon Properties of Porphyrins," *J. Chem. Phys.* **84**, pp. 3901-3915, 1986.

125. H. Nakatsuji, J. Hasegawa, and M. Hado, "Excited and Ionized States of Free Base Porphin Studied by Symmetry Adapted Cluster-Configuration Interaction (SAC-CI) Method," *J. Chem. Phys.* **104**, pp. 2321-2329, 1996.

126. D. Sundholm, "Density Functional Theory Study of the Electronic Absorption Spectrum of Mg-Porphyrin and Mg-Etioporphyrin," *Chem. Phys. Lett.* **317**, pp. 392-399, 2000.

127. E. Orti, M. C. Piqueras, R. Crespo, and J. L. Bredas, "Influence of Annelation on the Electronic-Properties of Phthalocyanine Macrocycles," *Chem. Mater.* **2**, pp. 110-116, 1990.

128. V. A. Kuz'mitskii, K. N. Solov'ev, V. N. Knyukshto, I. K. Shushkevich, V. N. Korpanenkov, and A. M. Vorotnikov, "Annelation of Aromatic Rings to the Porphyrin Ring and its Effect on the Electronic Structure and Electronic Spectra," *Theor. Exp. Chem.* **19**, pp. 604-611, 1983.

129. V. A. Kuz'mitskii, K. N. Solov'ev, and V. N. Korpanenkov, "Quantum-Chemical Electronic-Structure and Electronic-Spectrum Calculations for Tetrabenzoporphyrin N-Heteroanalogs," *J. Appl. Spectr.* **49**, pp. 1165-1171, 1988.

130. V. I. Gael', V. A. Kuz'mitskii, and K. N. Solov'ev, "Quantum-Chemical Characteristics of the Ground and Excited Electronic States of Isomeric Porphrycene and Porphin Molecules," *J. Appl. Spectr.* **55**, pp. 813-820, 1991.

131. K. A. Kon'kov, G. M. Zhidomirov, V. I. Khleskov, V. N. Kopranenkov, and Yu. V. Ivanov, "Quantum-Chemical Analysis of the Spectra of Metal Complexes of Azaporphyrins by the INDO/S Method," *Theor. Exp. Chem.* **25**, pp. 436-440, 1989.

132. K. Toyota, J. Hasegawa, and H. Nakatsuji, "SAC-CI Study of the Excited States of Free Base tetraazaporphin," *Chem. Phys. Lett.* **250**, pp. 437-442, 1996.

133. X.-J. Liu, J.-K. Feng, A.-M. Ren, X. Zhou, "Theoretical Studies of the Spectra and Two-Photon Absorption Cross Sections for Porphyrin and Carbaporphyrins," *Chem. Phys. Lett.* **373**, pp. 197-206, 2003.

134. J. Rodriguez, C. Kirmaier, D. Holten, "Optical properties of metalloporphyrin excited states," *J. Am. Chem. Soc.* **111**, pp. 6500-6506, 1989.

135. H. Gratz and A. Penzkofer, "Singlet-Singlet Excited-State Absorption and Triplet-Triplet Absorption of *Meso*-Tetraphenylporphine," *Chem. Phys.* **254**, pp. 363-374, 2000.

136. N.V. Chizhova and V.D. Berezin, "Nitration of Octaphenyl-Meso-Tetraazaporphine," *Zh. Org. Khim*+ **30,** pp. 1678-1680, 1994.

137. N. V. Chizhova, O. G. Khelevina, and V. D. Berezin, "Bromation of Porphyrins," *Izv. Vuz. Khim. Kh. Tekh.* **37,** pp. 20-23, 1994.

138. P. N. Taylor, J. Huuskonen, G. Rumbles, R. T. Aplin, E. Williams, and H. L. Anderson, "Conjugated Porphyrin Oligomers from Monomer to Hexamer," *Chem. Commun.* pp. 909-910,1998.

139. P. N. Taylor and H. L. Anderson, "Cooperative Self-Assembly of Double-Strand Conjugated Porphyrin Ladders," *J. Am. Chem. Soc.* **121**, pp. 11538-11545, 1999.

140. R. DeSalvo, M. Sheik-Bahae, A. A. Said, D. J. Hagan, and E. W. Van Stryland, "Z-Scan Measurements of the Anisotropy of Nonlinear Refraction and Absorption in Crystals," *Opt. Lett.* **18**, pp. 194-196, 1993.

141. G. P. Das, R. Vaia, A. T. Yeates, and D. S. Dudis, "A Theoretical Model for Excited State Absorption," *Synthetic Metals* **116,** pp. 281-283, 2001.

142. D. A. Oulianov, I. V. Tomov, A. S. Dvornikov, and P. M. Rentzepis, "Observation on the Measurement of Two-Photon Absorption Cross-Section," *Opt. Commun.* **191**, pp. 235-243, 2001.

143. M. D. Galanin and Z. A. Chizhikova, "Effective Cross Sections of Two-Photon Absorption in Organic Molecules," *JETP Lett.* **4**, pp. 27-28, 1966.

144. J. P. Hermann and J. Ducuing, "Absolute Measurement of Two-Photon Cross Sections," *Phys. Rev. A* **5**, pp. 2557-2568, 1972.

145. J. M. Song, T. Inoue, H. Kawazumi, and T. Ogawa, "Determination of Two-Photon Absorption Cross Section of Fluorescein Using a Mode locked Titanium Sapphire Laser," *Anal. Sci.* **15**, pp. 601-603, 1999.

146. W. L. Peticolas, J. P. Goldsborough, and K. E. Rieckhoff, "Double Photon Excitation in Organic Crystals," *Phys. Rev. Lett.* **10**, pp. 43-45, 1963.

147. S. Singh and B. P. Stoicheff, "Double-Photon Excitation in Anthracene Single Crystals," *J. Chem. Phys.* **38**, pp. 2032-2033, 1963.

148. R. Pariser, "Theory of Electronic Spectra and Structure of the Polyacenes and of Alternant Hydrocarbons," *J. Chem. Phys.* **24**, pp. 250-268, 1956.

149. R. Pantell, F. Pradere, J. Hanus, M. Schott, and H. Puthoff, "Theoretical and Experimental Values for Two-, Three-, and Four-Photon Absorptions," *J. Chem. Phys.* **46**, pp. 3507-3511, 1967.

150. Honig, J. Jortner, and A. Szöke, "Theoretical Studies of Two-Photon Absorption Processes. I. Molecular Benzene," *J. Chem. Phys.* **46**, pp. 2714-2727, 1967.

151. M. Iannuzzi and E. Polacco, "Double-Photon Excitation of Fluorescence in Anthracene," *Phys. Rev. Lett.* **13**, pp. 371-372, 1964.

152. M. Iannuzzi and E. Polacco, "Polarization Dependence of Laser-Induced Fluorescence in Anthracene," *Phys. Rev.* **138**, pp. A806-A808, 1965.

153. W. L. Peticolas, R. Norris, and K. E. Rieckhoff, "Polarization Effects in the Two-Photon Excitation of Anthracene Fluorescence," *J. Chem. Phys.* **42**, pp. 4164-4169, 1965.

154. F. C. Strome, Jr. and J. S. Hayward, "Fluorescence Ratio in Anthracene Melt and Solution with Circular and Linear Polarization of Ruby-Laser Excitation," *J. Chem. Phys.* **45**, pp. 4356-4357, 1966.

155. R. Guccione and J. Van Kranendonk, "Theory of Higher Multipole Contributions to Two-Photon Absorption Processes," *Phys. Rev. Lett.* **14**, pp. 583-584, 1965.

156. M. W. Dowley, K. B. Eisenthal, and W. L. Peticolas, "Two-Photon Laser Excitation of Polycyclic Molecules," *J. Chem. Phys.* **47**, pp. 1609-1619, 1967.

157. A. P. Aleksandrov, V. P. Bredikhin, and V. N. Genkin, "Electron-Vibrational Nature of Two-Quantum Absorption in Centrally-Symmetrical Organic Molecules," *JETP Lett.* **10**, pp. 117-119, 1969.

158. A. P. Aleksandrov, V. P. Bredikhin, and V. N. Genkin, "Two-Photon Absorption by Centrally Symmetric Organic Molecules," *JETP* **60**, pp. 1078-1082, 1971.

159. P. R. Monson and W. M. McClain, "Complete Polarization Study of the Two-Photon Absorption of Liquid 1-Chloronaphthalene," *J. Chem. Phys.* **56**, pp. 4817-4825, 1972.

160. W. Blau, H. Byrne, W.M. Dennis, J.M. Kelly, "Reverse Saturable Absorption in Tetraphenylporphyrins," *Opt. Commun.* **56,** pp. 25- 29, 1985.

161. H. Stiel, A. Volkmer, I. Rückmann, A. Zeug, B. Ehrenberg, B. Röder, "Non-linear and transient absorption spectroscopy of magnesium(II)-tetrabenzoporphyrin in solution," *Opt. Commun.* **155,** pp. 135-143, 1998.

162. P. Chen, I.V. Tomov, A.S. Dvornikov, M. Nakashima, J.F. Roach, D.M. Alabran, P.M. Rentzepis, **"**Picosecond Kinetics and Reverse Saturable Absorption of Meso-Substituted Tetrabenzoporphyrins,*" J. Phys. Chem.* **100**, pp. 17507-17512, 1996.

163. D. M. Friedrich, "Two-Photon Molecular Spectroscopy," *J. Chem. Ed.* **59**, pp. 472-481, 1982.

164. W.-H. Lee, M. Cho, S.-J. Jeon, and B. R. Cho, "Two-Photon Absorption and Second Hyperpolarizability of the Linear Quadrupolar Molecule," *J. Phys. Chem. A* **104**, pp. 11033-11040, 2000.

165. M. Barzoukas and M. Blanchard-Desce, "Molecular Engineering of Push-Pull Dipolar and Quadrupolar Molecules for Two-Photon Absorption: A Multivalence-Bond States Approach," *J. Chem. Phys.* **113**, pp. 3951-3959, 2000.

166. W.-H. Lee, H. Lee, J.-A. Kim, J.-H. Choi, M. Cho, S.-J. Jeon, B. R. Cho, "Two-Photon Absorption and Nonlinear Optical Properties of Octupolar Molecules," *J. Am. Chem. Soc.* **123**, pp. 10658-10667, 2001.

167. K. Ogawa, T. Zhang, K. Keitaro, and Y. Kobuke, "Large Third-Order Optical Nonlinearity of Self-Assembled Porphyrin Oligomers," *J. Am. Chem. Soc.* **124**, pp. 22-23, 2002.

168. A. Tsuda and A. Osuka, "Fully Conjugated Porphyrin Tapes with Electronic Absorption Bands That Reach into Infrared," *Science* **293**, pp. 79-82, 2001.

169. D. Beljonne, G. E. O'Keefe, P. J. Hamer, R. H. Friend, H. L. Anderson, and J. L. Brédas, "Investigation of the linear and nonlinear optical response of edge-linked conjugated zinc porphyrin oligomers by optical spectroscopy and configuration interaction techniques," *J. Chem. Phys.* **106**, pp. 9439-9460, 1997.

170. T. Bottger, G. J. Pryde, and R. L. Cone, 'Programmable Laser Frequency Stabilization at 1523 nm by Use of Persistent Spectral Hole Burning," *Opt. Lett.* **28**, pp. 200-202, 2003.

171. K. D. Merkel and W. R. Babbitt, "Optical Coherent-Transient True-Time-Delay Regenerator," *Opt. Lett.* **21**, pp. 1102-1104, 1996.

172. R. Reibel, Z. Barber, M. Tian, and W. R. Babbitt, "High Bandwidth Spectral Gratings Programmed with Linear Frequency Chirps," *J. Lumin.* **98**, pp. 355-365, 2002.

173. Z. Cole, T. Böttger, R. K. Mohan, R. Reibel, W. R. Babbitt, R. L. Cone, and K. D. Merkel, "Coherent Integration of 0.5 GHz Spectral Holograms at 1536 nm Using Dynamic Biphase Codes," *Appl. Phys. Lett.* **81**, pp. 3525-3527, 2002.

174. G. J. Pryde, T. Böttger, R. L. Cone, and R. C. C. Ward, "Semiconductor Lasers Stabilized to Spectral Holes in Rare Earth Crystals to a Part in 10^{13} and their Application to Devices and Spectroscopy," *J. Lumin.* **98**, pp. 309-315, 2002.

175. K. D. Merkel, W. R. Babbitt, K. E. Anderson, and K. H. Wagner, "Variable-Time-Delay Optical Coherent Transient Signal Processing," *Opt. Lett.* **24**, pp. 1386-1388, 1999.

176. C. Liu, Z. Dutton, C. H. Behroozi, and L. V. Hau, "Observation of Coherent Optical Information Storage in an Atomic Medium Using Halted Light Pulses," *Nature* **409**, pp. 490-493, 2001.

177. M. D. Lukin and A. Imamoğlu, "Controling Photons Using Electromagnetically Induced Transparency," *Nature* **413**, pp. 273-276, 2001.

178. N. F. Scherer, R. J. Carlson, A. Matro, M. Du, A. J. Ruggiero, V. Romero-Rochin, J. A. Cina, G. R. Fleming, and S. A. Rice, "Fluorescence-Detected Wave Packet Interferometry – Time Resolved Molecular-Spectroscopy with Sequences of Femtosecond Phase-Locked Pulses," *J. Chem. Phys.* **95**, pp. 1487-1511, 1991.

179. W. S. Warren, H. Rabitz, and M. Dahleh, "Coherent Control of Quantum Dynamics – The Dream is Alive," *Science* **259**, pp. 1581-1589, 1993.

180. R. J. Gordon and S. A. Rice, "Active Control of the Dynamics of Atoms and Molecules," *Annu. Rev. Phys. Chem.* **48**, pp. 601-641, 1997.

181. P. M. Saari, R. K. Kaarli, and A. K. Rebane, "Holography of Spatial-Temporal Events," *Sov. J. Quantum Electron.* **15**, pp. 443-449, 1985.

182. V. Blanchet, C. Nicole, M.-A. Bouchene, and B. Girard, "Temporal Coherent Control in Two-Photon Transitions: From Optical Interferences to Quantum Interferences," *Phys. Rev. Lett.* **78**, pp. 2716-2719, 1997.

183. R. Teets, J. Eckstein, and T. W. Hänsch, "Coherent 2-photon Excitation by Multiple Light Pulses," *Phys. Rev. Lett.* **38**, pp. 760-764, 1977.

184. T. H. Yoon, A. Marian, J. L. Hall, and J. Ye, "Phase-Coherent Multilevel Two-Photon Transitions in Cold Rb Atoms: Ultrahigh-Resolution Spectroscopy via Frequency-Stabilized Femtosecond Laser," *Phys. Rev. A* **63**, pp. 011402-1 – 011402-4, 2000.

185. R. R. Jones, "Multiphoton Ionization Enhancement Using 2 Phase-Coherent Laser-Pulses," *Phys. Rev. Lett.* **75**, pp. 1491-1494, 1995.

186. D. Meshulach and Y. Silberberg, "Coherent Quantum Control of Two-Photon Transitions by a Femtosecond Laser Pulse," *Nature* **396**, pp. 239-242, 1998.

187. D. Meshulach and Y. Silberberg, "Coherent Quantum Control of Multiphoton Transitions by Shaped Ultrashort Optical Pulses," *Phys. Rev. A* **60**, pp. 1287-1292, 1999.

188. K. A. Walowicz, I. Pastirk, V. V. Lozovoy, and M. Dantus, "Multiphoton Intrapulse Interference. 1. Control of Multiphoton Processes in Condensed Phases," *J. Phys. Chem. A* **106**, pp. 9369-9373, 2002.

189. V. V. Lozovoy, I. Pastirk, K. A. Walowicz, and M. Dantus, "Multiphoton Intrapulse Interference. II. Control of Two- and Three-Photon Laser Induced Fluorescence with Shaped Pulses," *J. Chem. Phys.* **118**, pp. 3187-3196, 2003.

190. T. Brixner, N. H. Damrauer, P. Niklaus, and G. Gerber, "Photoselective Adaptive Femtosecond Quantum Control in the Liquid Phase," *Nature* **414**, pp. 57-60, 2001.

191. A. Assion, T. Baumert, M. Bergt, T. Brixner, B. Kiefer, V. Seyfried, M. Strehle, and G. Gerber, "Control of Chemical Reactions by Feeadback-Optimized Phase-Shaped Femtosecond Laser Pulses," *Science* **282**, pp. 919-922, 1998.

192. R. J. Levis, G. M. Menkir, and H. Rabitz, "Selective Bond Dissociation and Rearrangement with Optimally Tailored, Strong-Field Laser Pulses," *Science* **292**, pp. 709-713, 2001.

193. T. Brixner and G. Gerber, "Quantum Control of Gas-Phase and Liquid-Phase femtochemistry," *ChemPhysChem* **4**, pp. 418-438, 2003.

194. R. M. Hochstrasser and H. N. Sung, "Electronic and Vibrational States of Biphenyl Crystals Using Two-Photon Excitation Spectroscopy," *J. Chem. Phys.* **66**, pp. 3265-3275, 1977.

195. R. M. Hochstrasser and H. N. Sung, "Vibronic Spectra of the Naphthalene Crystal at 1.6 K Using Two-Photon Fluorescence Excitation," *J. Chem. Phys.* **66**, pp. 3276-3296, 1977.

196. N. Mikami and M. Ito, "Two-Photon Excitation Spectra of Naphthalene-h_8 and $-d_8$: Vibronic Coupling Involving the Ground State," *Chem. Phys.* **23**, pp. 141-152, 1977.

197. M. F. Granville, G. R. Holtom, B. E. Kohler, R. L. Christensen, K. L. D'Amico, "Experimental Confirmation of the Dipole Forbidden Character of the Lowest Excited Singlet-State in 1,3,5,7-octatetraene," *J. Chem. Phys.* **70**, pp. 593-594, 1979.

198. M. Gutman, P.-F. Schönzart, and G. Hohlneicher, "High-Resolution One- and Two-Photon Spectroscopy of Matrix-Isolated Molecules. II. Investigation of Naphthalene and Octadeuteronaphthalene," *Chem. Phys.* **140**, pp. 107-131, 1990.

199. T. Plakhotnik, D. Walser, A. Renn, and U. P. Wild, "Two Shpol'skii Sites of All-Trans-1,8-Diphenyloctatetraene in n-Tetradecane," *Chem. Phys. Lett.* **262**, pp. 379-383, 1996.

200. D. Walser, G. Zumofen, and T. Plakhotnik, "Symmetry Breaking and Spectra of Diphenyloctatetraene in *n*-Alkanes," *J. Chem. Phys.* **113**, pp. 8047-8058, 2000.

201. M. C. Edelson, J. M. Hayes, G. J. Small, "Application of Non-Photochemical Hole Burning to the 2-Photon Spectroscopy of Impurity Molecules in Low-Temperature Glasses," *Chem. Phys. Lett.* **60**, pp. 307-309, 1979.

202. M. Takeda, K. Matsuda, C. Suzuki, S. Saikan, "Two-Photon Excited Fluorescence Line Narrowing Spectroscopy in Dyes Without Inversion Symmetry," *J. Lumin.* **86**, pp. 285-288, 2000.

203. M. Drobizhev, A. Karotki, and A. Rebane, "Persistent Spectral Hole Burning by Simultaneous Two-Photon Absorption," *Chem. Phys. Lett.* **334**, pp. 76-82, 2001.

204. A. Karotki, M. Kruk, M. Drobizhev, and A. Rebane, "Two-Photon Excited Coherence Gratings in Inhomogeneously Broadened Organic Solid," *J. Mod. Opt.* **49**, pp. 379-390, 2002.

205. A. Rebane, M. Drobizhev, and A. Karotki, "Frequency-Domain Gratings by Simultaneous Absorption of Two Photons," *J. Lumin.* **98,** pp. 341-353, 2002.

206. M. Drobizhev, A. Rebane, A. Karotki, C.W. Spangler, "New Two-Photon Absorbing Organic Molecules and Macromolecules for Photonic Applications," in *Recent Research and Development in Applied Physics*, ed. S. G. Pandalai, Transworld Research Network, Trivandrum, India, **4**, pp. 197-222, 2001.

207. M. Drobizhev, Yu. Dzenis, A. Karotki, and A. Rebane, "Electron-Phonon Coupling in Two-Photon Spectral Gratings: Role of Molecular Symmetry," *J. Lumin.* (accepted).

208. A. Karotki, M. Drobizhev, and A. Rebane, "Femtosecond Hole Burning Storage by Two-Photon Absorption," in *Technical Digest of Conference on Lasers and Electro-Optics*, Baltimore, MD, pp.373-374, 2001.

209. M. Drobizhev, A. Karotki, M. Kruk, and A. Rebane, "Spectral Gratings Created in Organic Film upon Two-Photon Absorption from Femtosecond Pulses," in *Book of Abstracts OSA Annual Meeting and Exhibit 2001, 17th Interdisciplinary Laser Science Conference*, Long Beach, CA, p.129, 2001.

210. M. Drobizhev, A. Karotki, A. Rebane, "Phonon-Induced Phase Shift of Spectral Gratings Created upon Two-Photon Excitation in Inhomogeneously Broadened Organic System," in *Technical Digest of Conference on Lasers and Electro-Optics*, Long Beach, CA, pp. 38-39, 2002.

211. M. Drobizhev, A. Karotki, Yu. Dzenis, and A. Rebane, "Electron-Phonon Coupling in Selectively-Excited Two-Photon Transition: Role of Molecular Symmetry," in *Proceedings of 8th International Meeting on Hole Burning, Single Molecule, and Related Spectroscopies: Science and Applications*, Bozeman, MT, p. 48, 2003.

212. C. B. Storm and Y. Teklu, "Nitrogen-Hydrogen Tautomerism in Porphyrins and Chlorins," *J. Am. Chem. Soc.* **94**, pp. 1745-1747, 1972.

213. S. Völker and R. M. Macfarlane, "Laser Photochemistry and Hole-Burning of Chlorin in Crystalline Normal-Alkanes at Low-Temperature," *J. Chem. Phys.* **73**, pp. 4476-4482, 1980.

214. I. Renge, H. Wolleb, H. Spahni, and U. P. Wild, "Phthalonaphthalocyanines: New Far-Red Dyes for Spectral Hole Burning," *J. Phys. Chem. A* **101**, pp. 6202-6213, 1997.

215. H.-Y. Huang, A. Rebane, U. P. Wild, and L. W. Johnson, "Total Fluorescence Spectra of Free Base Chlorin and Its Photo-Product in Polyvinylbutyral at Liquid Helium Temperatures," *J. Lumin.* **71**, pp. 237-243, 1997.

216. J. Friedrich, J. D. Swalen, and D. Haarer, "Electron-Phonon Coupling in Amorphous Organic Host Materials as Investigated by Photochemical Hole Burning," *J. Chem. Phys.* **73**, pp. 705-711, 1980.

217. M. A. Drobizhev, M. N. Sapozhnikov, and V. M. Kobrianski, "Exciton Localization in Thin Polymer Films Probed by Selective Fluorescence Spectroscopy," *J. Lumin.* **72-74**, pp. 490-493, 1997.

218. A. V. Turukhin, A. A. Gorokhovsky, C. Moser, I. V. Solomatin, and D. Psaltis, *J. Lumin*. "Spectral Hole Burning in Naphthalocyanines Derivatives in the Region 800 nm for Holographic Storage Applications," **86**, pp. 399-405, 2000.

219. I. Renge, "Spectral Hole Burning Study of Electron-Phonon Coupling in Polymers," *J. Chem. Phys*. **106**, pp. 5835-5849, 1997.

220. S. Saikan, "Linear Electron Phonon Coupling in Dye Polymer Systems – In Search of Weakly Coupled Systems," *J. Lumin*. **53**, pp. 147-152, 1992.

221. A. Rebane, J. Gallus, and O. Ollikainen, "Femtosecond Photon Echo Spectroscopy in Single Laser Shot," *Laser Phys*. **12**, pp. 1126-1134, 2002.

222. T. J. Dougherty, G. B. Grindey, R. Fiel, K. R. Weishaupt, and D. G. Boyle, "Photoradiation Therapy. 2. Cure of Animal Tumors with Hematoporphyrin and Light," *J. Natl. Cancer* **55**, pp. 115-121, 1975.

223. N. Lane, "New Light on Medicine," *Sci. Am.*, #1, pp. 38-45, 2003.

224. N. M. Bressler and J. P. Gills, "Age Related Macular Degeneration," *Brit. Med. J.* **321**, pp. 1425-1427, 2000.

225. A. Karotki, M. Kruk, M. Drobizhev, A. Rebane, E. Nickel, and C.W. Spangler, "Efficient Singlet Oxygen Generation Upon Two-Photon Excitation of New Porphyrin with Enhanced Nonlinear Absorption," *IEEE J. Sel. Top. Quant. Electron.* **7**, pp. 971-975, 2001

226. A. Karotki, M. Drobizhev, M. Kruk, A. Rebane, E. Nickel, and C.W. Spangler, "Strong two-photon absorption and singlet oxygen photogeneration in near-IR with new porphyrin molecule," in *Proceedings of the SPIE* **4612**, pp. 143-151, 2002.

227. A. Karotki, M. Drobizhev, A. Rebane, M. Kruk, E. Nickel, and C.W. Spangler, "Efficient Singlet Oxygen Photosensitization Upon Two-Photon Excitation of Porphyrins," in *Technical Digest of Conference on Lasers and Electro-Optics*, Long Beach, CA, pp. 589-590, 2002.

228. M. Kruk, A. Karotki, M. Drobizhev, and A. Rebane, "First observation of two-photon photosensitization of singlet molecular oxygen by porphyrin in aqueous solution," in *Conference Digest of IX International Conference on Laser Applications in Life Sciences*, Vilnius, Lithuania, p. 92, 2002.

229. M. Drobizhev, A. Karotki, A. Rebane, C.W. Spangler, M. Kruk, N.V. Chizhova, G.M. Mamardashvili, and E. Nickel, "Efficient generation of singlet oxygen by two-photon excited porphyrins," in *Technical Digest of Conference on Lasers, Applications and Technologies*, Moscow, Russia, p. 158, 2002.

230. M. Kruk, A. Karotki, M. Drobizhev, A. Rebane, P. Petrov, G. Isakov, "Two-Photon Absorption in Photodynamic Therapy," in *Book of Abstracts of International Conference "Laser Physics and Applications" ICLPA*, Minsk, Belarus, pp. III-23-Y, 2003.

231. M. Kruk, A. Karotki, M. Drobizhev, A. Rebane, G. Isakov, P. Petrov, "Photodynamic Therapy with Two-Photon Excitation of Tetrapyrrolic Sensitizers," in *Proceedings of IX International Conference on Chemistry of Porphyrins and Their Analogs*, Ivanovo, Russia, pp. 318-320, 2003.

232. M. Kruk, A. Karotki, M. Drobizhev, A. Rebane, G. Isakov, and P. Petrov, "Application of Two-Photon Absorption in Photodynamic Therapy," in *Proceedings of III International Conference of Young Scientists*, Sankt-Peterburg, Russia, p. 285, 2003.

233. C. Schweitzer and R. Schmidt, "Physical Mechanisms of Generation and Deactivation of Singlet Oxygen," *Chem. Rev.* **103**, pp. 1685-1757, 2003.

234. "Advantages of Photodynamic Therapy," Oregon Meical Laser Center, http://omlc.ogi.edu/pdt/articles/PDTadvantages.html

235. "Photodynamic Therapy," RadaPharma http://www.radapharma.ru/eng/pdt/comparison/index.php

236. S. WanJ. A. Parrish, R. R. Anderson, and M. Madden, "Transmittance of Nonionizing Radiation in Human Tissues," *Photochem. Photobiol.* **34**, pp. 679-681, 1981.

237. W.-F. Cheong, S. A. Prahl, and A. J. Welch, "A Review of the Optical Properties of Biological Tissues," *IEEE J. Quantum Electr.* **26**, pp. 2166-2185, 1990.

238. S. Stolik, J. A. Delgado, A. Pérez, and L. Anasagasti, "Measurement of the Penetration Depths of Red and Near Infrared Light in Human "Ex Vivo" Tissues," *J. Photoch. Photob. B: Bilology* **57**, pp. 90-93, 2000.

239. J.-P. Ritz, A. Roggan, C. Isbert, G. Müller, H. J. Buhr, and C.-T. Germer, "Optical Properties of Native and Coagulated Porcine Liver Tissue Between 400 and 2400 nm," *Laser. Surg. Med.* **29**, pp. 205-212, 2001.

240. F. Wilkinson, W. P. Helman, and A. B. Ross, "Rate Constants for the Decay and Reactions of the Lowest Electronically Excited Singlet State of Molecular Oxygen in Solution. An Expanded and Revised Compilation," *J. Phys. Chem. Ref. Data.* **24**, pp. 663-1021, 1995.

241. M. Hild and R. Schmidt, "The Mechanism of the Collision-Induced Enhancement of the $a^1\Delta_g \rightarrow X^3\Sigma_g^-$ and $b^1\Sigma_g^+ \rightarrow a^1\Delta_g$ Radiative Transitions of O_2," *J. Phys. Chem. A* **103**, pp. 6091-6096, 1999.

242. O. N. Albitskaya, I. N. Zhuravkin, M. A. Kaplan, N. D. Kochubeeva, A. L. Mescherjakova, P. T. Petrov, et. al. "Agent for Photodynamical Diagnostics and

Therapy of oncological Diseases," Russian Federation Patent #2152790 on 05.12.1999.

243. G. A. Kochubeev, A. A. Frolov, G. P. Gurinovich, "Chlorin e6. Spectral-Energetic Characteristics and Generation of Singlet Molecular Oxygen in Some Homogeneous and Heterogeneous Systems," *Khimicheskaja Fizika* **8**, pp. 1184-1190, 1989 (in Russian).

244. D. M. Friedrich, "Tensor Pattern and Polarization Ratios for Three-Photon Transitions in Fluid Media," *J. Chem. Phys.* **75**, pp. 3258-3268, 1981.

APPENDICES

APPENDIX A

PARITY SELECTION RULES FOR THE TWO-PHOTON TRANSITIONS

According to the electric dipole approximation, the intensity of TPA between the ground state $|0\rangle$ and some upper final state $|2\rangle$ is determined by the following expression (see equations (2.14) and (2.25)):

$$\sum_i \langle 2|e\boldsymbol{r}\cdot\boldsymbol{E}|i\rangle\langle i|e\boldsymbol{r}\cdot\boldsymbol{E}|0\rangle, \tag{A.1}$$

where $|i\rangle$ is any energy eigenstate that plays a role of intermediate level and $e\boldsymbol{r}\cdot\boldsymbol{E}$ is the electric-dipole energy in the field $\boldsymbol{E}$. If the molecule is centrally-symmetric then the wavefunctions corresponding to different energy levels also possess some degree of symmetry which limits the number of radiation transitions between the energy levels. In particular wavefunctions ψ of centrosymmetrical molecules can have either even (gerade parity) or odd symmetry (ungerade parity) in which case the following relations are obeyed:

$$\begin{cases} \psi_g(\boldsymbol{r}) = \psi_g(-\boldsymbol{r}) & gerade \\ \psi_u(\boldsymbol{r}) = -\psi_u(-\boldsymbol{r}) & ungerade \end{cases}. \tag{A.2}$$

Two different cases are possible: 1) ground and final levels have different parity 2) ground and final levels have the same parity. In the first case no matter what the parity of the intermediate level *m* is one of the multipliers always will be equal to zero. In the second case if symmetry of the intermediate level is different from the symmetry of the ground and final excited levels then both multipliers are different from zero. Correspondingly, in centrally-symmetric molecules, TPA can take place only if the initial and final levels have the same parity, i.e. $g \leftarrow g$ (*gerade* ← *gerade*) or $u \leftarrow u$ (*ungerade* ← *ungerade*) transitions. Two-photon transitions between levels with different parity are prohibited in the dipole approximation.

Since the ground level typically has *gerade* parity the two-photon transitions from the ground levels are allowed only into other gerade parity levels. Since allowed transitions are always much stronger than the prohibited transitions (prohibited transition always can be slightly allowed for example through quadrupole approximation) $g \leftarrow g$ TPA bands have large two-photon cross sections.

Note that selection rules for OPA are opposite, namely $g \leftarrow u$ (*gerade* $\leftarrow$ *ungerade*) or $u \leftarrow g$ (*ungerade* $\leftarrow$ *gerade*). Thus the two-photon spectroscopy is complimentary to one-photon spectroscopy allowing to investigate otherwise inaccessible energy levels. If molecule does not have a center of symmetry then the symmetry of its energy levels cannot be precisely defined and both types of transition are allowed between different levels. Nevertheless, there tend to be transitions that are weak for OPA but strong for TPA and vice versa. While parity selection rules for three-photon absorption are the same as for OPA, three-photon spectroscopy can still reveal even more information about molecules. There are $g \leftarrow u$ transitions in centrally-symmetric molecules that are parity allowed for OPA but still forbidden for one-photon spectroscopy by other symmetry considerations. In that case these transitions become allowed for higher order absorption, like simultaneous absorption of three photons [6,163,244]. Three-photon spectroscopy also permits observation of a greater manifold of vibronic transitions than are accessible to one-photon spectroscopy [244].

APPENDIX B

EVALUATION OF THE ABSOLUTE TPA CROSS SECTION

Consider a homogeneous two-photon absorbing medium of length L and molecular density n irradiated by a laser pulse of intensity $I_0(r,t)$, were r is the distance from the geometrical center of the pulse to the observation point, and t is the time. The intensity just after the sample will be

$$I(r,t) = \frac{I_0(r,t)}{1+\sigma_2 nLI_0(r,t)}. \tag{B.1}$$

If the TPA is weak, i.e. if $\sigma_2 nLI_0(r,t) \ll 1$, which is the case in our experiments, then

$$I(r,t) \simeq I_0(r,t)(1-\sigma_2 nLI_0(r,t)). \tag{B.2}$$

The total energy absorbed by the medium from the pulse can be found integrating over the pulse duration and its cross section:

$$\Delta E_{TPA} = \sigma_2 nL\int_0^\infty 2\pi r dr \int_{-\infty}^{\infty} I_0^2(r,t)dt. \tag{B.3}$$

In our experiment we used a pinhole of radius, $r_0 < r_L$, in front of the sample (r_L is the radius of the laser beam), and in a good approximation we can neglect variation of the intensity within r. In the time domain, the pulse intensity has nearly Gaussian shape:

$$I_0(r,t) = I_{0i} Exp[-\frac{4t^2 ln2}{\tau^2}], \tag{B.4}$$

where I_{0i} is the pulse intensity at its maximum, τ is a time duration of the pulse (FWHM).

$$\Delta E_{TPA} = \frac{\sigma_2 nL\pi^{3/2} r_0^2 I_{oi}^2 \tau}{\sqrt{8ln2}}. \tag{B.5}$$

From the experimental point of view it is much easier to operate with average intensity of the excitation light, which is easy to measure, then its peak intensity. To make the

transition to the average intensity we initially derive expression for the total energy of the laser pulse used for two-photon excitation in terms of the peak intensity.

$$E_{TPA} = \int_0^{r_0} 2\pi r dr \int_{-\infty}^{\infty} dt I_{0i} Exp[-\frac{4t^2 ln2}{\tau^2}] = \frac{\pi^{3/2}\tau r_0^2 I_{oi}}{2\sqrt{ln2}}. \quad \text{(B.6)}$$

Then the following expression for the absorbed energy can be obtained:

$$\Delta E_{TPA} = \frac{\sqrt{2ln2}\sigma_2 nLE_{iTPA}^2}{\pi^{3/2}\tau r_0^2}. \quad \text{(B.7)}$$

Since the total energy of one pulse is equal to the average intensity of the excitation light divided by the repetition rate of the laser expression (B.7) can be rewritten in the following form:

$$\Delta E_{TPA} = \frac{\sqrt{2ln2}\sigma_2 nL\left\langle I_{TPA}\right\rangle^2}{\pi^{3/2}\tau^3 r_0^2 g^2}, \quad \text{(B.8)}$$

where $\left\langle I_{TPA}\right\rangle$ is the average intensity of the laser light used for two-photon excitation and g is the repetition rate of the laser. The number of the molecules in the sample excited during one second is:

$$N_{TPA} = \frac{\Delta E_{TPA} g}{2h\nu_{TPA}} = \frac{\sqrt{2Ln2}\sigma_2 nL\left\langle I_{TPA}\right\rangle^2}{2h\nu_{TPA}\pi^{3/2}\tau r_0^2 g}, \quad \text{(B.9)}$$

where h is the Plank constant, ν_{TPA} is the frequency of the two-photon excitation light. Note that two photons are required to excite one molecule. In the case of one-photon excitation, the energy absorbed by the same sample form one pulse is:

$$\Delta E_{OPA} = E_{OPA}(1 - Exp[-\sigma_1 nL]) \simeq E_{OPA}\sigma_1 nL, \quad \text{(B.10)}$$

where E_{OPA} is the energy of laser pulse and σ_1 is the one-photon (linear) absorption cross-section. The number of excited molecules excited during one second is:

$$N_{OPA} = \frac{\Delta E_{OPA} g}{h\nu_{OPA}} = \frac{\sigma_1 n L E_{OPA} g}{h\nu_{OPA}} = \frac{\sigma_1 n L \left\langle I_{OPA} \right\rangle}{h\nu_{OPA}}, \tag{B.11}$$

where ν_{OPA} and $\left\langle I_{OPA} \right\rangle$ are the frequency and average intensity of the laser light used for one-photon excitation. If the geometry of one- and two-photon excitation is the same, then the corresponding fluorescence intensity, F_{TPA} and F_{OPA}, should be proportional to the number of excited molecules in each case. We also suppose that quantum yield of the fluorescence does not depend on the mode of excitation. The ratio of the fluorescence intensities is:

$$\frac{F_{TPA}}{F_{OPA}} = \frac{\sqrt{2\ln 2}\sigma_2 \left\langle I_{TPA} \right\rangle^2 \nu_{OPA}}{2\nu_{OPA}\pi^{3/2} g\tau r_0^2 \sigma_1 \left\langle I_{OPA} \right\rangle}, \tag{B.12}$$

which leads to the final expression for the TPA cross section:

$$\sigma_2 = \sqrt{\frac{2\pi^3}{\ln(2)}} \frac{F_{TPA}\nu_{TPA} g\tau r_0^2 \left\langle I_{OPA} \right\rangle}{F_{OPA}\nu_{OPA} \left\langle I_{TPA} \right\rangle^2} \sigma_1 . \tag{B.13}$$

It was supposed everywhere that the same sample was used for both one- and two-photon excitation. If two-photon excited fluorescence is too weak then one can improve signal to noise ratio by dissolving more studied compound. In this case, expression (B.13) turns into following:

$$\sigma_2(cm^4 s/W) = \sqrt{\frac{2\pi^3}{\ln(2)}} \frac{F_{TPA}\nu_{TPA} g\tau r_0^2 \left\langle I_{OPA} \right\rangle}{pF_{OPA}\nu_{OPA} \left\langle I_{TPA} \right\rangle^2} \sigma_1 , \tag{B.14}$$

where p is the coefficient taking into account different density of the samples. It is equal to the ratio of the optical density of the two-photon sample at some wavelength to the optical density of the one-photon sample at the same wavelength. The two-photon cross section is typically quoted with intensities measured in $photon/cm^2 s$. To obtain TPA cross section in these units, expression (B.14) should be multiplied by an energy of one excitation photon $h\nu_{TPA}$:

$$\sigma_2(cm^4 s/photon) = \sqrt{\frac{2\pi^3}{\ln(2)}} \frac{F_{TPA} h\nu_{TPA}^2 g\tau r_0^2 \langle I_{OPA} \rangle}{pF_{OPA}\nu_{OPA} \langle I_{TPA} \rangle^2} \sigma_1 . \qquad \text{(B.15)}$$

APPENDIX C

RELATIONS BETWEEN TRANSITION DIPOLE MOMENT, OSCILLATOR STRENGTH, LINE SHAPE FUNCTION, AND MOLAR EXTINCTION COEFFICIENT

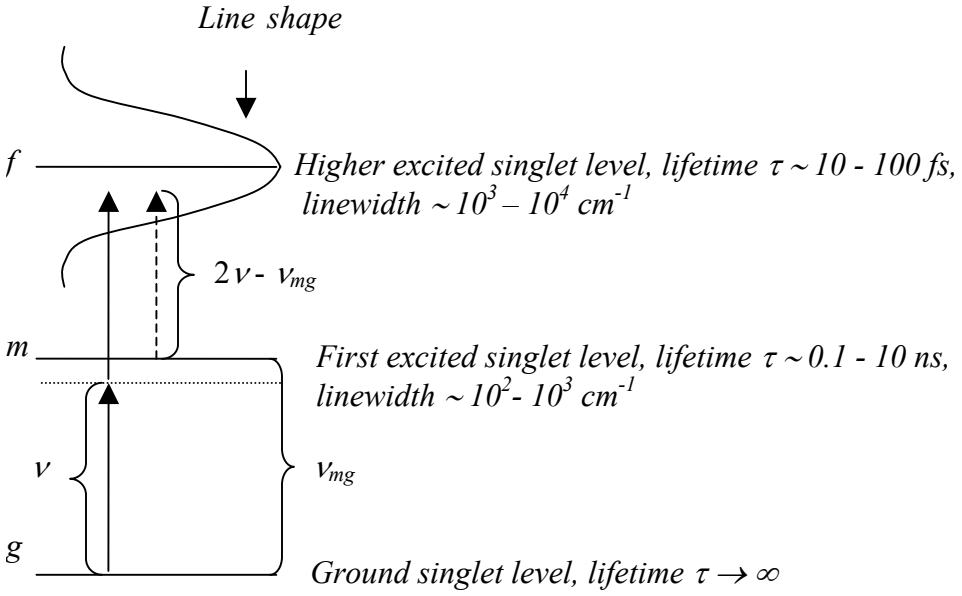

Figure C.1 Comparison of two-photon excitation $f \leftarrow g$ (solid arrows) from the ground state g and one-photon excitation $f \leftarrow m$ (dashed arrow) from the intermediate level m.

Figure C.1 presents three energy levels, ground g, intermediate m, and final excited f, used in the three-level model. The text in italic near every level shows typical lifetime of the levels and thee linewidth corresponding to the transition from the ground level. The broadening of the level f is much larger than the broadening of the levels m and g due to the short lifetime of f. Simple estimate shows that finite lifetime contribution to the broadening of the level f is about $1/\tau \sim 1/10\text{fs} \approx 3000\ \text{cm}^{-1}$. As a result, the line shape functions of the two-photon transition $f \leftarrow g$, $g^{TPA}_{f \leftarrow g}(2\nu)$, and one-photon transition $f \leftarrow m$, $g^{OPA}_{f \leftarrow m}(2\nu - \nu_{mg})$, are mainly determined by the broadening of the level f. Therefore, the line shape functions $g_{TPA}(2\nu)$ and $g_{OPA}(2\nu - \nu_{mg})$ are equal in the first approximation:

$$g^{TPA}_{f \leftarrow g}(2\nu) = g^{OPA}_{f \leftarrow m}(2\nu - \nu_{mg}). \qquad \text{(C.1)}$$

The oscillator strength f of an electronic transition is defined as

$$f = 4.39 \cdot 10^{-9} \int \varepsilon(\bar{\nu}) d\bar{\nu}, \tag{C.2}$$

where the bar on top of the ν means that wavenumbers [cm^{-1}] are used instead of frequencies [Hz], $\varepsilon(\bar{\nu})$ is the extinction coefficient of the transition as a function of wavenumber [$M^{-1}cm^{-1}$]. The oscillator strength is also defined through the transition dipole moment $\boldsymbol{\mu}_{trans}$ [e.s.u.] as

$$f = 4.70 \cdot 10^{29} \bar{\nu}_{trans} G \left| \boldsymbol{\mu}_{trans} \right|^2, \tag{C.3}$$

where $\bar{\nu}_{trans}$ is the mean wavenumber of the transition [cm^{-1}] and G is the degeneracy of the transition (in our case G is equal to one and will be omitted). Combining equations (C.2) and (C.3) the following equation is obtained:

$$\int \varepsilon(\bar{\nu}) d\bar{\nu} = 1.07 \cdot 10^{38} \bar{\nu}_{trans} \left| \boldsymbol{\mu}_{trans} \right|^2. \tag{C.4}$$

The value of the extinction coefficient at some particular wavenumber $\bar{\nu}$ is equal to:

$$\begin{cases} \varepsilon(\bar{\nu}) = A g(\bar{\nu}) \\ A = \int \varepsilon(\bar{\nu}') d\bar{\nu}' \end{cases}, \tag{C.5}$$

where $g(\bar{\nu})$ is the line shape function of the transition. By comparing equations (C.4) and (C.5) it is clear that extinction coefficient is equal to

$$\varepsilon(\bar{\nu}) = 1.07 \cdot 10^{38} \bar{\nu}_{trans} \left| \boldsymbol{\mu}_{trans} \right|^2 g(\bar{\nu}). \tag{C.6}$$

In our particular case, we compare TPA, $f \leftarrow g$, with wavenumber $\bar{\nu}$ with OPA, $f \leftarrow m$, with wavenumber $2\bar{\nu} - \bar{\nu}_{mg}$ (see Figure C.1).

$$\varepsilon_{fm}(2\bar{\nu} - \bar{\nu}_{mg}) = 1.07 \cdot 10^{38} \bar{\nu}_{fm} \left| \boldsymbol{\mu}_{fm} \right|^2 g^{OPA}_{f \leftarrow m}(2\bar{\nu} - \bar{\nu}_{mg}), \tag{C.7}$$

where subscript *OPA* means that, it is a one-photon transition. Since

$$g^{OPA}_{f\leftarrow m}(2\bar{\nu}-\bar{\nu}_{mg}) = g^{TPA}_{f\leftarrow g}(2\bar{\nu}), \tag{C.1}$$

$$\Downarrow$$

$$\varepsilon_{fm}(2\bar{\nu}-\bar{\nu}_{mg}) = 1.07\cdot 10^{38}\bar{\nu}_{fm}\left|\boldsymbol{\mu}_{fm}\right|^2 g_{TPA}(2\bar{\nu}). \tag{C.8}$$

By substituting $\nu / c = \bar{\nu}$, where c is the speed of light, into expression (2.28) for the line shape function the following transformation can be made:

$$g_{TPA}(2\bar{\nu}) = cg_{TPA}(2\nu). \tag{C.9}$$

$$\Downarrow$$

$$\left|\boldsymbol{\mu}_{fm}\right|^2 g_{TPA}(2\nu) = \frac{\varepsilon_{fm}(2\bar{\nu}-\bar{\nu}_{mg})}{1.07\cdot 10^{38}\bar{\nu}_{fm}c}. \tag{C.10}$$

The expression (3.8) is used as a variable for the Figure 3.13.

$$\sigma_2 \sim \frac{\left|\boldsymbol{\mu}_{mg}\right|^2}{(\nu_{mg}-\nu)^2}. \tag{3.8}$$

Let us modify this expression, so that only easily measurable OPA parameters are left. From equation (C.4) the modulus squared of the transition dipole moment is equal to:

$$\left|\boldsymbol{\mu}_{trans}\right|^2 = \frac{\int \varepsilon(\bar{\nu})d\bar{\nu}}{1.07\cdot 10^{38}\bar{\nu}_{trans}}. \tag{C.11}$$

For the Gaussian absorption band

$$\int \varepsilon(\bar{\nu})d\bar{\nu} = \frac{1}{2}\sqrt{\frac{\pi}{ln2}}\varepsilon_{\max}(\bar{\nu}_{trans})\Delta\bar{\nu}_{trans}, \tag{C.12}$$

where $\varepsilon_{\max}(\bar{\nu}_{trans})$ and $\Delta\bar{\nu}_{trans}$ are the maximum extinction coefficient [$M^{-1}cm^{-1}$] and halfwidth [cm^{-1}] of the transition.

$$\Downarrow$$

$$\left|\boldsymbol{\mu}_{trans}\right|^2 = \frac{1}{1.07 \cdot 10^{38} \bar{\nu}_{trans}} \frac{1}{2} \sqrt{\frac{\pi}{ln2}} \varepsilon_{\max}(\bar{\nu}_{trans}) \Delta \bar{\nu}_{trans} . \tag{C.13}$$

By combining equations (3.8) and (C.13) the following expression is obtained:

$$\sigma_2 \sim \frac{\left|\boldsymbol{\mu}_{mg}\right|^2}{(\nu_{mg} - \nu)^2} \sim \frac{\varepsilon_{\max}(\bar{\nu}_{mg}) \Delta \bar{\nu}_{mg}}{\bar{\nu}_{mg} (\bar{\nu}_{mg} - \bar{\nu})^2}, \tag{C.14}$$

where $\varepsilon_{\max}(\bar{\nu}_{mg})$ and $\Delta \bar{\nu}_{mg}$ are the maximum extinction coefficient [$M^{-1}cm^{-1}$] and halfwidth [cm^{-1}] of the transition $m \leftarrow g$.

APPENDIX D

DERIVATION OF THE EXPRESSION DESRIBING FREQUENCY GRATING IN THE FLUORESCENCE SPECTRUM CREATED WITH TWO-PHOTON EXCITATION

Substitution of the equation (4.15) into equation (4.13) leads to the following expression for the homogeneous (one-photon) fluorescence spectrum:

$$\begin{cases} g_1(\nu-\nu_0,T)=\alpha_1(T)\delta(\nu-\nu_0)+ \\ +(1-\alpha_1(T))\dfrac{4}{\nu_1^3}(\nu-\nu_0)^2\exp[\dfrac{2}{\nu_1}(\nu-\nu_0)], \quad (\nu_0-\nu)>0 \\ \alpha_1(T)\delta(\nu-\nu_0), \quad (\nu_0-\nu)\le 0 \end{cases} \tag{D.1}$$

and (two-photon) absorption spectrum:

$$\begin{cases} g_2(\nu-\nu_0,T)=\alpha_2(T)\delta(\nu-\nu_0)+ \\ +(1-\alpha_2(T))\dfrac{4}{\nu_2^3}(\nu-\nu_0)^2\exp[-\dfrac{2}{\nu_2}(\nu-\nu_0)], \quad -(\nu_0-\nu)>0\,. \\ \alpha_2(T)\delta(\nu-\nu_0), \quad -(\nu_0-\nu)\le 0 \end{cases} \tag{D.2}$$

Now one has to substitute the expressions describing homogeneous (one-photon) fluorescence spectrum (D.1), homogeneous (two-photon) absorption spectrum (D.2), and effective laser power spectrum (4.10) into the general equation for fluorescence spectrum (4.12). The following form of the effective laser power spectrum is used:

$$f(\omega_k)=\beta(1+cos[2\pi\nu_k\Delta\tau])\,, \tag{D.3}$$

where coefficient β accounts for non one hundred percent modulation depth of the efficient laser power spectrum if two laser pulses are not exactly the same. Let us initially calculate the right hand side integral in (4.12).

$$\int_{-\infty}^{\infty} g_2(\nu"-\nu_0,T)E(\nu")d\nu" = \beta[\int_{-\infty}^{\infty}\alpha_2(T)(1+cos[2\pi\nu"\Delta\tau])\delta(\nu"-\nu_0)d\nu" +$$

$$+\int_{\nu_0}^{\infty}(1-\alpha_2(T))\frac{4}{\nu_2^3}(\nu"-\nu_0)^2\exp[-\frac{2}{\nu_2}(\nu"-\nu_0)](1+cos[2\pi\nu"\Delta\tau])d\nu"] =$$

$$= \beta[\alpha_2(T)(1+cos[2\pi\nu_0\Delta\tau]) + (1-\alpha_2(T)) +$$
$$+(1-\alpha_2(T))\frac{\cos(2\pi\nu_0\Delta\tau + 3arctg(\pi\Delta\tau\nu_2))}{(1+\pi^2\Delta\tau^2\nu_2^2)^{3/2}}] = \tag{D.4}$$
$$= \beta[1+\alpha_2(T)cos[2\pi\nu_0\Delta\tau] + (1-\alpha_2(T))\frac{\cos(2\pi\nu_0\Delta\tau + 3arctg(\pi\Delta\tau\nu_2))}{(1+\pi^2\Delta\tau^2\nu_2^2)^{3/2}}]$$

Substitution of (D.4) into (4.12) and integration of the left hand side gives:

$$\beta[\int_{-\infty}^{\infty}\alpha_1(T)\delta(\nu-\nu_0)d\nu_0 + \int_{-\infty}^{\infty}\alpha_1(T)\delta(\nu-\nu_0)\alpha_2(T)cos[2\pi\nu_0\Delta\tau]d\nu_0 +$$
$$+\int_{-\infty}^{\infty}\alpha_1(T)\delta(\nu-\nu_0)(1-\alpha_2(T))\frac{\cos(2\pi\nu_0\Delta\tau + 3arctg(\pi\Delta\tau\nu_2))}{(1+\pi^2\Delta\tau^2\nu_2^2)^{3/2}}d\nu_0 +$$
$$+\int_{\nu}^{\infty}(1-\alpha_1(T))\frac{4}{\nu_1^3}(\nu-\nu_0)^2\exp[\frac{2}{\nu_1}(\nu-\nu_0)]d\nu_0 +$$
$$+\int_{\nu}^{\infty}(1-\alpha_1(T))\frac{4}{\nu_1^3}(\nu-\nu_0)^2\exp[\frac{2}{\nu_1}(\nu-\nu_0)]\alpha_2(T)cos[2\pi\nu_0\Delta\tau]d\nu_0 +$$
$$+\int_{\nu}^{\infty}(1-\alpha_1(T))\frac{4}{\nu_1^3}(\nu-\nu_0)^2\exp[\frac{2}{\nu_1}(\nu-\nu_0)](1-\alpha_2(T))\times$$
$$\times\frac{\cos(2\pi\nu_0\Delta\tau + 3arctg(\pi\Delta\tau\nu_2))}{(1+\pi^2\Delta\tau^2\nu_2^2)^{3/2}}d\nu_0]$$
$$= \beta[\alpha_1(T) + \alpha_1(T)\alpha_2(T)cos(2\pi\nu\Delta\tau) +$$
$$+\alpha_1(T)(1-\alpha_2(T))\frac{\cos(2\pi\nu\Delta\tau + 3arctg(\pi\Delta\tau\nu_2))}{(1+\pi^2\Delta\tau^2\nu_2^2)^{3/2}} +$$
$$+(1-\alpha_1(T)) + (1-\alpha_1(T))\alpha_2(T)\frac{\cos(2\pi\nu\Delta\tau + 3arctg(\pi\Delta\tau\nu_1))}{(1+\pi^2\Delta\tau^2\nu_1^2)^{3/2}} + \tag{D.5}$$
$$+(1-\alpha_1(T))(1-\alpha_2(T))\frac{\cos(2\pi\nu\Delta\tau + 3arctg(\pi\Delta\tau\nu_1) + 3arctg(\pi\Delta\tau\nu_2))}{(1+\pi^2\Delta\tau^2\nu_1^2)^{3/2}(1+\pi^2\Delta\tau^2\nu_2^2)^{3/2}}]$$

To simplify further calculations the following variables are introduced:

$$A(T) = \alpha_1(T)\alpha_2(T), \tag{D.6}$$

$$B(T) = [1-\alpha_1(T)]\alpha_2(T)\{1+(\pi\Delta\tau\nu_2)^2\}^{-3/2}, \tag{D.7}$$

$$C(T) = \alpha_1(T)[1-\alpha_2(T)]\{1+(\pi\Delta\tau\nu_1)^2\}^{-3/2}, \tag{D.8}$$

$$D(T) = [1-\alpha_1(T)][1-\alpha_2(T)]\{[1+(\pi\Delta\tau\nu_2)^2][1+(\pi\Delta\tau\nu_1)^2]\}^{-3/2}, \tag{D.9}$$

$$\delta_{1,2} = 3arctg(\pi\Delta\tau\nu_{1,2}\tilde{)} \tag{D.10}$$

Equation (D.5) turns into:

$$\begin{aligned} F(\nu,T) = K(\nu)\beta[1 + Acos(2\pi\nu\Delta\tau) + C\cos(2\pi\nu\Delta\tau+\delta_2) + \\ + B\cos(2\pi\nu\Delta\tau+\delta_1) + D\cos(2\pi\nu\Delta\tau+\delta_1+\delta_2)] \end{aligned}. \tag{D.11}$$

The following trigonometric manipulations with this equation lead to the final result:

$$\begin{aligned} F(\nu,T) = K(\nu)\beta[1+\cos(2\pi\nu\Delta\tau)(A + B\cos(\delta_2 + C\cos(\delta_1) + \\ D\cos(\delta_1+\delta_2)) - \sin(2\pi\nu\Delta\tau)(C\sin(\delta_1) + B\sin(\delta_2) + D\cos(\delta_1+3\delta_2))] \end{aligned} \tag{D.12}$$

$$\Downarrow$$

$$F(\nu,T) = K(\nu)(1 + M(T)\cos(2\pi\nu\Delta\tau + \Delta\varphi(T))), \tag{D.13}$$

where

$$\begin{aligned} M(T) = \beta[(A + B\cos(\delta_2 + C\cos(\delta_1) + D\cos(\delta_1+\delta_2))^2 + \\ +(C\sin(\delta_1) + B\sin(\delta_2) + D\cos(\delta_1+3\delta_2))^2]^{1/2} \end{aligned}, \tag{D.14}$$

$$\Delta\varphi(T) = arctg\frac{B(T)\sin\delta_2 + C(T)\sin\delta_1 + D(T)\sin(\delta_1+\delta_2)}{A(T) + B(T)\cos\delta_2 + C(T)\cos\delta_1 + D(T)\cos(\delta_1+\delta_2)}. \tag{D.15}$$